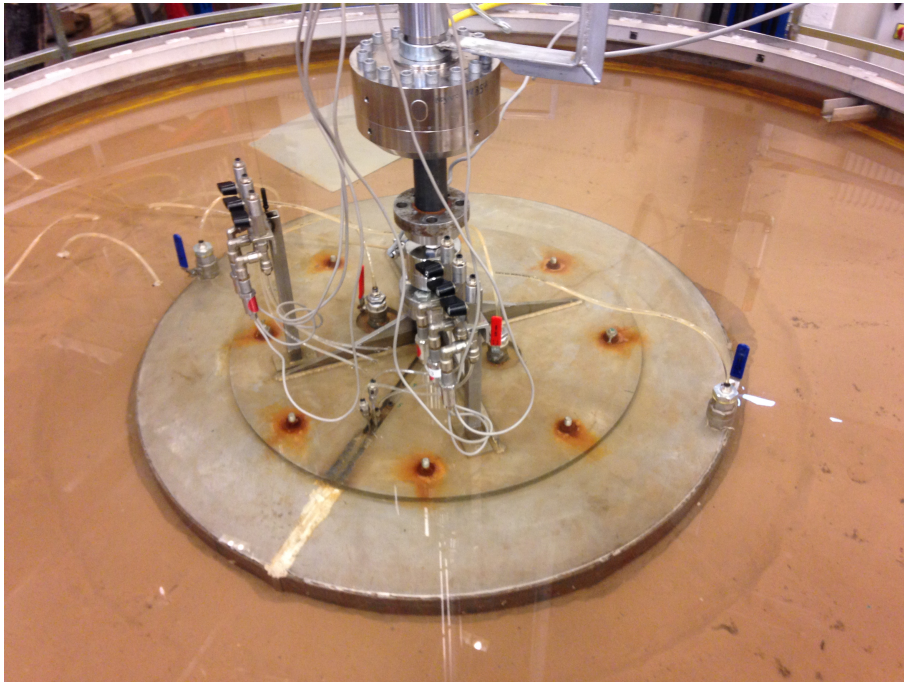


AALBORG UNIVERSITY

MASTER THESIS

Installation of Suction Bucket Foundations in Sand



Authors:

Thomas Gitsas

Hector Pandiella Martinez

Georgios Nektarios Sgourakis

Supervisor:

Lars Bo Ibsen

Structural and Civil Engineering
School of Civil Engineering and Science
June 9, 2016



AALBORG UNIVERSITY
DENMARK

School of Engineering and Science

Fredrik Bajers Vej 5, P. O. Box 159
DK-9100 Aalborg, Denmark
Tel.: (45)99409940
E-mail: aau@aaau.dk
<http://www.ses.aau.dk>

Title: Installation of Suction Bucket Foundations in Sand

Theme: Master Thesis

Project period: 01.09.2015 - 09.06.2016

Participants:

Thomas Gitsas

Hector Pandiella Martinez

Georgios Nektarios Sgourakis

Supervisor:

Professor Lars Bo Ibsen

Issues: 6

Pages: 124

Appendix: 57

Annex-CD: 3

Delivery Date: 09.06.2016

Abstract:

The main focus of this project is the interaction of the bucket foundation with the surrounding soil (saturated sand) during installation and uninstallation procedure. In order to achieve that, experimental tests were performed in the laboratory facilities of Aalborg University. Installation tests were separated in two categories, installation by force and installation by suction. Uninstallation was performed by inducing water pressure under the lid of the bucket. Displacement and pore pressures were measured during the whole procedure. Results were resembled in the finite element software Plaxis 2D in order to investigate the seepage around the bucket during suction installation and uninstallation. Furthermore, based on CPT results the empirical coefficients k_p and k_f associated with tip resistance and skirt friction of the bucket respectively, were calculated and compared with the ones proposed by other studies. Finally, beta factor values that illustrate the differences in soil penetration resistance during installation by suction and installation by force, were proposed. Three research articles were conducted with respect to the above mentioned analysis. This project will be considered to be a step forward in the development of an improved model of the soil penetration resistance based on CPT results.

PREFACE

The current report is the Master Thesis for the M.Sc. in Structural and Civil Engineering at the School of Engineering and Science at Aalborg University. It is denoted as "Long Master Thesis" of 45 ECTS and it has been conducted from 1st of September 2015 to 9th of June 2016. The project has involved laboratory work at the Laboratory facilities of Aalborg University. Regarding the work performed at the laboratory, the authors would like to thank the technical staff, especially Kim Borup, for his valuable help during the whole procedure. Most tests have been conducted in cooperation with Ph.D. fellow Aleksandra Koteras, whose help and guidance is highly appreciated.

The authors would like to show gratitude to Professor Lars Bo Ibsen for his guidance, assistance and advice during the course of the Master Thesis.

Reading guide

References during the main report are collected in a Bibliography located in the end of the thesis. In the main report, the references are listed by the Harvard Method, so a reference in the text appears as [Last name, Year] when used passively and as Last name [Year] when used actively in the text. If the reference contains more than one author, then it is specified by the last name of the first author followed by "et al.". In the bibliography, books are specified by author, title, edition and possibly publisher. Websites are specified by author. References for the articles are collected in the same manner as in the main report, however they are only listed in the end of the relevant article. Figures and tables made by the authors themselves, no reference is specified.

Figures and tables are numbered according to the chapter where are located. Therefore, the first figure in chapter 3 has number 3.1, the second figure 3.2 and so on. Captions are placed beneath the corresponding figures and tables. Equations are specified by a number inside bracket, thus the first equation in chapter 2 has number (2.1), the second equation (2.2), etc.

Appendices are divided in accordance to letters of the alphabet and they are placed after the bibliography. Finally, the annexes will be available on CD in the report's rear side. The CD is referred as "Annex-CD" and contains all the calculations underlying the contents of the report.

SUMMARY

Suction bucket foundations have been used for many years in offshore industry, to support oil and gas platforms. Recently, they are considered an attractive and cost effective way of supporting offshore wind turbines. Its effectiveness derives from the fact that suction, which is applied under the lid of the bucket, make installation an easier and more quiet process. When suction is applied, the downward force, due to pressure differential under the lid, increases gradually. However, in sandy soils (high coefficient of permeability) a flow between the voids of the soil is developed, called seepage flow. Moreover, excess pore pressure of the soil increases with the applied suction, leading to a decrement of the penetration resistance, making the installation of the bucket easier. Although, many studies have proposed design methods for suction buckets installation in sand, only few of them focus on the interaction between the sand and the skirt of the bucket during penetration. The scope of this thesis is to analyse the seepage flow during installation by suction and uninstillation by induced water pressure of a medium scale model of a bucket foundation. Furthermore, the interaction between soil and bucket is investigated by calculating the empirical coefficients k_p and k_f associated to tip resistance and skirt friction of the bucket respectively. Results are being compared and empirical β factors are acquired with respect to the AAU CPT-based method. The document consists of 3 research articles regarding the above mentioned analysis.

Firstly, the procedure of the experimental tests followed in the laboratory is being explained. Tests consisted of suction installation, force installation and induced water pressure uninstillation of a bucket foundation model in homogeneous sand. Results from specific tests are given as an example, in order to investigate all the data acquired during the experiments. Next step was to resemble the laboratory tests in the finite element software Plaxis 2D. A complete numerical analysis of the seepage flow around the bucket was conducted for both installation and uninstillation, along with calculations for the pore pressure factor and the critical pressure. In both chapters, a detailed procedure, on how the values used in the research articles were obtained, is described.

In the first article, only suction installation and induced water pressure uninstillation of the bucket is considered. A numerical analysis of seepage length, pore pressure factor and critical pressure of the real experiments is presented. In order to achieve that, installation and uninstillation procedure of the bucket in homogeneous sand, was resembled in the finite element software Plaxis 2D in discrete steps, by applying the real pressure measured in the experiments. Research proved that values of the hydraulic gradient at the tip are much higher compared to the ones inside and at the exit of the bucket skirt. As a result, the soil resistance at the tip is the one that shows larger reduction. Furthermore, during the installation procedure in all the experiments, the theoretical critical suction pressure was exceeded by the applied suction, but piping phenomena were not observed. Additionally, during the uninstillation, values of critical pressure were not exceeded. All results show

high correlation with solutions from other studies for homogeneous sand.

In the second article, only installation by force and induced water pressure uninstillation of the bucket is considered. DNV (1992) proposed that soil penetration resistance can be calculated based on CPT results. Based on DNV (1992) theoretical model, calculations of the empirical coefficients k_p and k_f , associated to the tip and skirt friction resistance of the bucket respectively, were performed for the experiments presented in the current study and the ones conducted by Vaitkunaite et al. [2015]. Results found to follow a similar trend for most of the tests, along with other known studies using the same method . However, due to the abstract nature of the theory used, some of the results illustrate high deviations from each other.

In the last article, k_p and k_f coefficients were found for all the experiments conducted for the purpose of this study. Comparing the results from suction to force installation procedure, β factors were obtained. Those factors show the reduction in penetration resistance at the tip and at the skirt of the bucket during suction installation. It is very important to mention that there has not been any study that tries to calculate experimental values of β factors and compare them to the theoretical ones, thus results are inconclusive and need to be verified by further investigation.

The analysis presented in this document will considered to be a step forward in the development of an improved model of soil penetration resistance based on CPT results.

CONTENTS

Preface	v
Summary	vii
1 Introduction to Bucket Foundations	1
1.1 Classification of Offshore Structures according to the Function	1
1.2 Classification of Offshore Foundations for Wind Turbines	2
1.3 Monopile Foundations in comparison to Suction Bucket Foundations	4
1.4 Suction Bucket Foundations	5
2 Literature Review	9
2.1 Literature for seepage	9
2.2 Literature for empirical coefficients k_p , k_f and β factors	12
3 Experimental Analysis	15
3.1 Test N_o 3	17
3.2 Test N_o 5	28
3.3 Test N_o 8	35
4 Numerical Analysis	43
4.1 Dimensions of the Bucket Foundation and Model Properties	44
4.2 Calculation Model and Soil Parameters	45
4.3 Boundary Conditions	45
4.4 Convergence Analysis and Mesh	46
4.5 Calculation Phases-Steps of the Installation	48
4.6 Results	48
5 Article I: Seepage analysis for suction installation and uninstallation of bucket foundations in sand	65
6 Article II: Calculation of empirical coefficients associated with tip resistance and skirt friction of a bucket foundation	79
7 Article III: Calculation of β factors from installation of a medium-scale model of bucket foundation in dense sand	91
8 Conclusions and Discussion	107
Bibliography	108
A Appendix: Laboratory	111
A.1 Laboratory Guide	111

B Appendix: Skirt friction coefficient (k_f), tip resistance coefficient (k_p)	139
B.1 Calculation of k_f and k_p	139
B.2 Experiments from Vaitkunaite et al. [2015]	140
B.3 Experiments from Laboratory	147
C Appendix: Numerical Analysis	161
C.1 Installation Tests	161
C.2 Uninstallation Test	197
D Attached CD	217

INTRODUCTION TO BUCKET FOUNDATIONS

1

The main purpose of the introduction is to present different types of offshore foundations, with a special emphasis on the suction caisson, also called suction bucket foundation. Due to expansion of the renewable energy industry, the need of creating wind farms in more challenging offshore sites has grown. These sites concern both different soil conditions and water depths [Koterak et al. 2016]. Furthermore, offshore locations can allow bigger capacity wind turbines, maximizing the potential of each wind farm, without raising any objections for aesthetic reasons [Byrne and Houlsby 2003]. One of the biggest problems confronting the renewable energy industry is the installation of wind turbines in sea water, which is a much more complicated procedure than onshore. A proper and feasible installation can lead to higher levels of energy production along with lower costs and smaller impact on the environment [Lian et al. 2014].

1.1 Classification of Offshore Structures according to the Function

Firstly, classification of structures by function is presented in order to have an overview of the main offshore structures that use bucket foundation technology. There are 3 main different offshore structures that require bucket foundations [Andersen 2015]. First group consists of drilling rigs, used for oil and gas exploration, which stay in a place temporarily, normally a few months. Secondly, there are platforms, used for production of oil and gas, which stay permanently in a place, usually between 20 and 30 years, before demolition. Last but not least, the wind turbines used for the production of electricity, stay also permanently in a place, for around 20 years before uninstillation. The different modifications of each structure depending on the water depth are presented as:

- Drilling Rigs
 - Jack-up drilling rig (Shallow water)
 - Mobile Offshore Drilling Unit (MODU) (Deep water)
- Production Platforms
 - Ground-based structure (depth < 500-800 m)
 - Floating Structures (depth > 800 m)
- Wind Turbines
 - Round based, typically monopile foundations (depth < 40 m, but increasing)
 - Floating structures, still in development (Deep water)

1.2 Classification of Offshore Foundations for Wind Turbines

In this section, the classification of offshore foundations for wind turbines is presented. Below, the most important and commonly used offshore foundations for wind turbines are presented and illustrated in Figure 1.1.

- Monopile foundation
- Gravity based foundation
- Monopod foundation (suction bucket foundation)
- Tripod/quadripod foundation
 - Connection of piles
 - Connection of suction buckets
- Jacket structure foundation
- Floating foundation

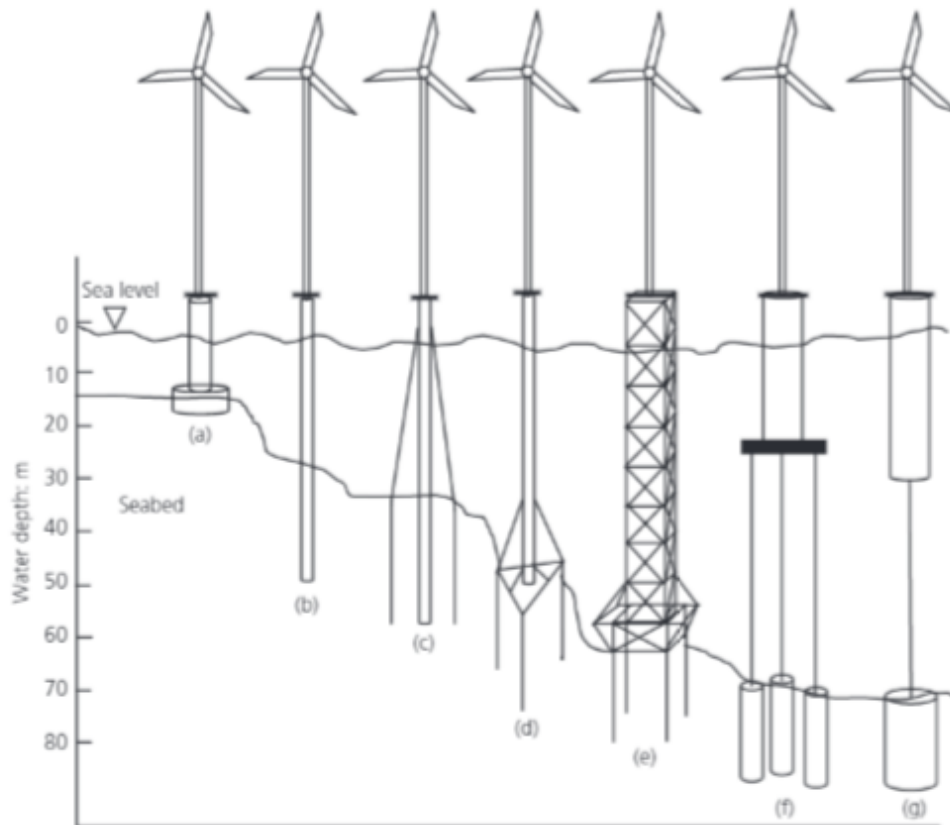


Figure 1.1: Types of wind turbines foundations: a) Gravity based foundation, b) Monopile foundation, c) Monopile foundation with guy wire, d) Tripod foundation, e) Jacket foundation, f) Tension leg with suction buckets, g) Buoy with suction anchor [Arshad and O'Kelly 2015].

For wind farms located in shallow waters, the most widely adopted foundation system is the monopile. Monopile transfers the vertical and lateral loading deep into the seabed. The loading is resisted by the horizontal earth pressure of the surrounding soil around the embedded length of the monopile.



Figure 1.2: Installation process of a monopile [DONG a].

Braced support structures, such as tripods and jacket foundations are more suitable for heavier structures or for deeper water. With these kind of foundations, the loads are transferred axially to the seabed through the braces of the foundation.

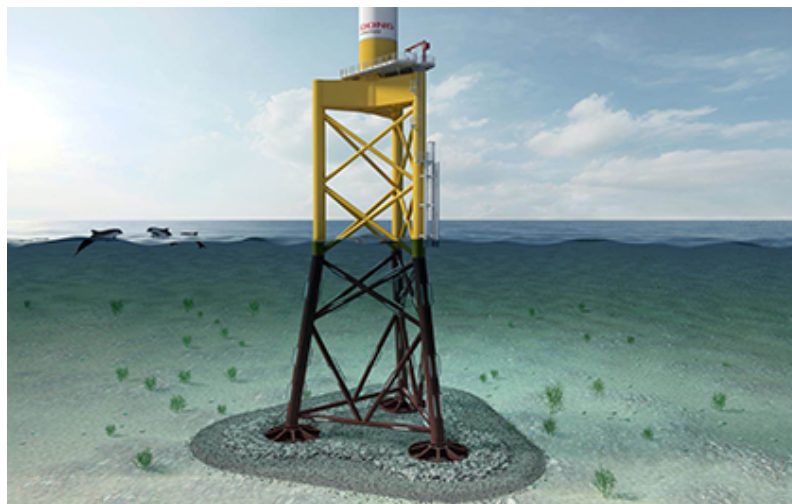


Figure 1.3: Suction bucket jacket structure [DONG b].

The floating structures are currently under development and they will be used in the future in deep waters.



Figure 1.4: Floating structures [Gicon].

1.3 Monopile Foundations in comparison to Suction Bucket Foundations

In this section a comparison between monopile and suction bucket foundations is presented. Monopile foundations have dominated the offshore wind market for years, however wind industry is moving towards larger capacity wind turbines that require stronger foundation structures. In such cases monopile has proven to be not cost effective any longer. While monopile foundations remain as an attractive solution for the industry, bucket foundations usage have start being increased due to their lightness and adaptability in different locations.

Sea-bed conditions and manufacturing capacity of the most active European offshore industries are in favor of the monopile. Monopile is currently, the most used solution worldwide with almost 75% share of the market. Jacket and tripod foundations are responsible for only 5% of the current offshore structures [Energy 2015]. In Europe, monopile foundation represent 91% of the installed offshore wind capacity, while buckets represent only 8% [Association 2014]. However, with projects moving towards larger offshore turbines, there will be an increase in the use of bucket foundations as opposed to monopile.

Bucket foundations have the advantage of an easier installation compared to the monopile. From economic point of view the transportation of larger monopile foundations has proven to be a big disadvantage. However, the limited manufacturing capacity for suction buckets in Europe compared to the well-established supply chain for monopile, is considered a disadvantage for the second category.

The operational foundation types by capacity of the wind turbines are illustrated in Figure 1.5.

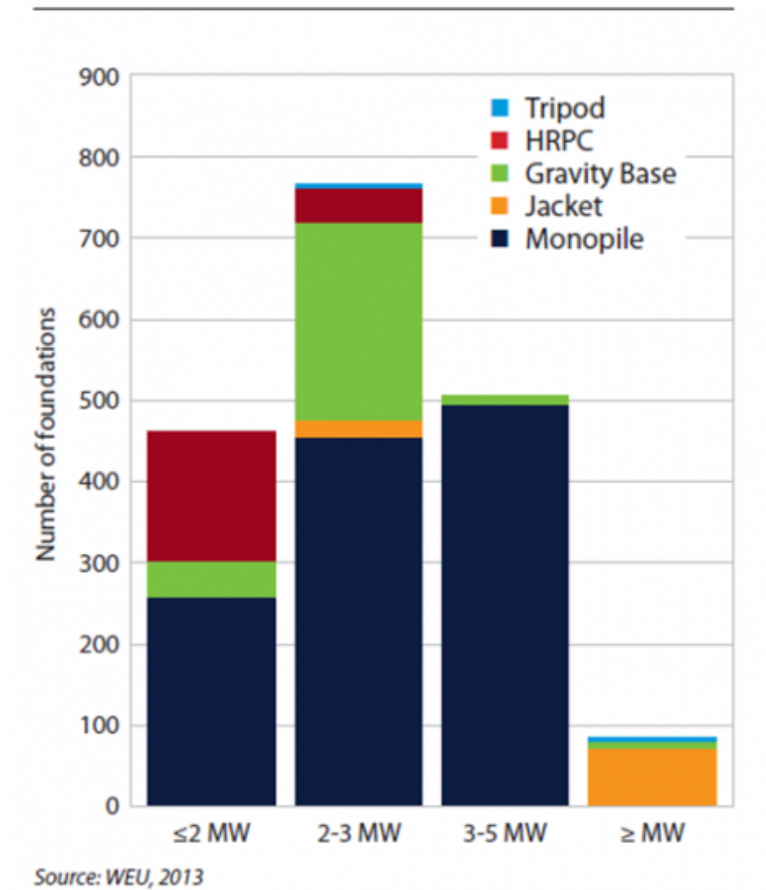


Figure 1.5: Operational Foundation Types by Capacity [WEU 2000].

Figure 1.5 depicts a trend of turbines over 5 MW, using alternative types of foundation compared to the monopile. It is concluded that for the largest wind turbines, buckets are mostly used as a foundation solution.

1.4 Suction Bucket Foundations

1.4.1 Introduction to the suction bucket foundations

The installation process of bucket foundations is quieter and more simple compared to the monopile one. Steps of suction installation are presented as follows:

- The bucket is lowered to the seabed.
- First part of the bucket penetrates in the soil due to self-weight, in order to ensure a seal component between the soil and the bucket's skirt [Houlsby and Byrne 2005].
- Suction is applied inside the bucket's skirt by using pumps, creating a pressure differential inside the bucket, where the pressure is lower than outside.
- The pressure differential causes the downward movement of the bucket.
- Holes in the buckets are sealed to obtain total impermeability.

- A thin layer of concrete or ballast can be injected between seabed and the bucket lid, for protection against scour and other types of soil erosion.

In Figure 1.6 an outline of the suction bucket with the different variables is illustrated.

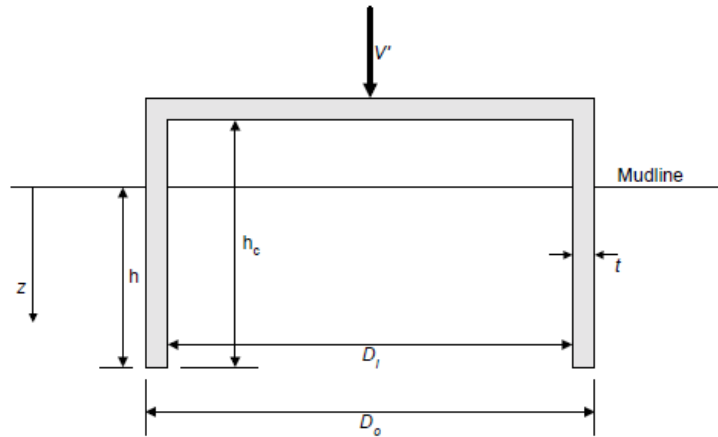


Figure 1.6: Outline of suction bucket [Houlsby and Byrne 2005].

Where,

V'	Applied installation force, including suction and buoyancy
h	Height of the embedded bucket
h_c	Height of the bucket
t	Thickness of the bucket skirt
D_I	Inner diameter of the bucket
D_O	Outer diameter of the bucket

1.4.2 Advantages of the suction bucket foundations

There are two main advantages for the suction bucket foundations. First one is the silent installation process, which enables to operate in noise regulated projects and also saves money from the associated noise mitigation costs. The installation of a monopile can be achieved either by the use of drilling or hammering methods, which are both noisy. The second advantage is related to the fact that suction bucket foundations can be used in deep waters and there is a large cost reduction compared to the current foundation technology.

Figure 1.7 depicts the moment of a tripod suction bucket installation.



Figure 1.7: Installation of a real tripod model of suction bucket [DONG c].

Summarizing, the suction bucket foundations are more cost-effective and quieter procedure than the monopile, the solution most commonly used in the wind turbine industry. That is the reason that analysis of the interaction between the skirt of the bucket and the surrounding soil will be performed in this report. The work presented here, will be considered a step forward to a proposed solution of suction bucket foundations installation and uninstillation in sand soil profiles.

LITERATURE REVIEW 2

2.1 Literature for seepage

Installation standards of bucket foundations are usually based on theories regarding pile foundations. It can be assumed that the bucket works as an open ended pile. The most common one was proposed by American Petroleum Institute (API) [2000] concerning open ended pile foundations. Soil resistance is assumed to be the sum of the external shaft friction, the end bearing on the pile wall annulus and the total internal shaft friction or the end bearing of the plug. Additionally, the unit end bearing is dependent on the dimensionless bearing capacity factor, N_q and on the effective overburden pressure, p_o .

Det Norske Veritas Institution, also called DNV, presented a study in 1992 about penetration resistance of skirts. DNV suggests that penetration resistance of the steel skirts is the sum of friction resistance, inside, outside and at the tip of the bucket skirt, where calculations should be based on the results of in-situ testing supported by laboratory tests. For the field tests CPT data was used, since it gives a continuous record of the cone penetration resistance over the depth.

DNV method for calculating the penetration resistance based on results from CPT tests, is presented in the following equation as:

$$R = A_{tip}k_pk_c(z) + \pi D_I k_f \int_0^z q_c(l)dz + \pi D_O k_f \int_0^z q_c(l)dz \quad (2.1)$$

Where,

A_{tip}	Area of the tip of the bucket
z	Penetration depth
k_p	Empirical coefficient related to the tip resistance
k_f	Empirical coefficient related to the skirt friction
q_c	Cone resistance
D_I	Inner diameter of the bucket
D_O	Outer diameter of the bucket

From both of the above mentioned theories, several uncertainties remain regarding the conversion from one type of penetration resistance to another. As an example, the excess pore pressures along with the seepage flow effects are not being investigated regarding the reduction of penetration resistance. Houlsby and Byrne [2005] proposed a method based on numerical calculations, assuming that the distribution of pore pressure on the inside

and outside the skirt of the bucket varies linearly with depth. Pore pressure factor, α , was calculated relating the excess pore pressure at the tip of the bucket skirt, Δu_{tip} , with the applied suction, p as:

$$\alpha = \frac{\Delta u_{tip}}{p} \quad (2.2)$$

Theoretically, a value of 0.5 is expected for $h/D = 0$ and a value of 0 when h/D is very large, for uniform permeability soil situation. Numerical analysis performed by Houlsby and Byrne [2005] found a relatively good fit for the results, shown in equation 2.3.

$$\alpha_1 = 0.45 - 0.36 \left[1 - \exp\left(\frac{h}{0.48D}\right) \right] \quad (2.3)$$

Furthermore, rewriting Houlsby and Byrne [2005] calculations in terms of critical suction, which if exceeded can cause piping of the soil, the following equation is proposed:

$$\frac{p_{crit}}{\gamma' D} = \frac{h}{D} \left(1 + \frac{\alpha_1 k_{fac}}{1 - \alpha_1} \right) \quad (2.4)$$

Where, k_{fac} is the ratio k_i/k_o (k_i and k_o is the permeability inside and outside of the bucket respectively and $k_i \geq k_o$) that represent the soil permeability during suction, when the soil inside the bucket loosens, causing a higher permeability coefficient.

A simpler approach based on assumed linear decrease in internal friction and end bearing, as the suction pressure increases from zero up to the critical value causing internal piping, was proposed by Senders and Randolph [2009]. According to their review, the critical hydraulic gradient occurs at the tip of the bucket. However, due to sand constrained by other materials at that point, it was observed that the hydraulic gradient that controls when piping will occur is the exit gradient adjacent to the skirt of the bucket. That gradient was used to estimate the reduction in penetration resistance and presented in the following equation as:

$$i = \frac{p}{\gamma_w s} \quad (2.5)$$

Where, s denoted as the seepage length, γ_w as the unit weight of the water and p as the applied suction.

The critical hydraulic gradient for piping to occur, is given by equation 2.6.

$$i_{crit} = \frac{\gamma'}{\gamma_w} \quad (2.6)$$

Therefore, the critical pressure against piping is defined as:

$$p_{crit} = s\gamma_w i_{crit} = s\gamma' \quad (2.7)$$

Where, γ' is the effective soil unit weight.

Based on numerical calculations performed in finite element software Plaxis and SEEP by Senders and Randolph [2009], a solution for the normalized seepage length was proposed, shown in equation 2.8. The results found to have an excellent fit with centrifuge models for installation of a suction bucket. Moreover, by multiplying the equation with the penetration ratio h/D a solution for the normalized critical suction was found (equation 2.9).

$$\left(\frac{s}{h}\right)_{exit} = \pi - \arctan \left[5 \left(\frac{h}{D}\right)^{0.85} \right] \left(2 - \frac{2}{2\pi}\right) \quad (2.8)$$

$$\frac{p_{crit}}{\gamma' D} = \left(\frac{s}{h}\right)_{exit} \left(\frac{h}{D}\right) \quad (2.9)$$

A study performed by Ibsen and Thilsted [2010], using finite element software FLAC 3D, proposed a similar solution for normalized seepage length and critical suction, as shown in equations 2.10 and 2.11, for homogeneous sand soil profiles. The solution is based on results from installation of a suction bucket in Frederikshavn port.

$$\left(\frac{s}{h}\right)_{ref} = 2.86 - \arctan \left[4.1 \left(\frac{h}{D}\right)^{0.8} \right] \left(2 - \frac{2}{2\pi}\right) \quad (2.10)$$

$$\frac{p_{crit}}{\gamma' D} = \left(\frac{s}{h}\right)_{ref} \left(\frac{h}{D}\right) \quad (2.11)$$

Finally, Feld [2001] performed finite element analysis in SEEP and proposed a solution for the normalized critical suction as following:

$$\frac{p_{crit}}{\gamma' D} = 1.32 \left(\frac{h}{D} \right)^{0.75} \quad (2.12)$$

2.2 Literature for empirical coefficients k_p , k_f and β factors

Det Norske Veritas [1992] proposes reference values for k_p and k_f coefficients for North Sea sand and they are presented in table 2.1.

Empirical coefficients	k_p	k_f
Lowest expected	0.3	0.001
Highest expected	0.6	0.003

Table 2.1: Recommended values from DNV for empirical coefficients k_p and k_f .

A method proposed by Lehane et al. [2007] based on the API (2000) standard called UWA-05 design method, was developed for open and closed ended driven piles in sand. Alternatively to DNV, the UWA-05 method suggests that k_f is a function of the internal and external diameter ratio of the pile. UWA-05 design method is developed for open and closed ended driven piles in sand. The empirical coefficient k_f is calculated with the following equation as:

$$k_f = C \left[1 - \left(\frac{D_I}{D_O} \right)^2 \right]^{0.3} \tan \delta \quad (2.13)$$

Where,

- C Constant, assumed 0.021 in Lehane et al. [2007]
- δ Interface friction angle
- D_I Inner diameter of the bucket
- D_O Outer diameter of the bucket

In addition to DNV (1992) theory, a study conducted by Koteris et al. [2016] presents the AAU CPT-based method, which takes into account the penetration resistance reduction due to suction by introducing the β factors in the equations 2.14, 2.15 and 2.16 as:

$$R_{fI_s} = \pi \beta_{in} D_I k_{fI_f} \int_0^z q_c(l) dz \quad (2.14)$$

$$R_{fO_s} = \pi\beta_{out}Dok_{fO_f} \int_0^z q_c(l)dz \quad (2.15)$$

$$R_{tip_s} = A_{tip}\beta_{tip}k_{pf}q_c(z) \quad (2.16)$$

Where,

$$\beta_{in} = \left(1 - r \frac{p}{p_{crit,avg,in}}\right) \quad (2.17)$$

$$\beta_{out} = \left(1 + r \frac{p}{p_{crit,avg,out}}\right) \quad (2.18)$$

$$\beta_{tip} = \left(1 - r \frac{p}{p_{crit,tip}}\right) \quad (2.19)$$

Where,

p	Applied suction
$p_{crit,avg,in}$	Critical suction, average inside
$p_{crit,avg,out}$	Critical suction, average outside
$p_{crit,avg,tip}$	Critical suction, average at the tip
r	Restriction Factor

The subscript s , denotes the soil penetration resistance that was calculated with respect to suction installation. The subscript f denotes all the values calculated with respect to force installation.

In another study performed by Andersen et al. [2008], results about skirt friction and tip resistance coefficients are presented for prototype models, along with small scale laboratory tests. Calculations in this study, are based on the DNV standard. It has to be mentioned that in our study both tests that the bucket was installed with additional weight and by underpressure application under the lid will be considered. Therefore, the prototype models installed by force in Andersen et al. [2008] study, were denoted as Draupner E and Sleipner T and the ones installed by suction as Hardening A7, A8 and Prototype A. Different values of k_f were assumed in order to calculate k_p . As far as the laboratory tests are concerned, the bucket tested had a diameter, D of 0.557 m, skirt thickness, t of 8 mm,

and 0.32 m skirt height, h . Tests run in a tank with a diameter of 1.6 m . The value for k_f was set to 0.0053 in order to have the best fit with the measured penetration resistance. Tests PEN 1-3 were preceded with installation by force and tests PEN 5, 9 and 12 with installation by suction. In tables 2.2 and 2.3 an overview of Andersen et al. [2008] results for k_p and k_f for suction and force installation are presented.

Case	k_{p_f}	k_{f_f}
Draupner E	0.01 – 0.08	0 – 0.0015
Sleipner T	0.05 – 0.13	0 – 0.0015
PEN 1-3	1.03 – 1.19	0.0053

Table 2.2: Values from Andersen et al. [2008] for empirical coefficients k_p and k_f , for different cases with force installation.

Case	k_{p_s}	k_{f_s}
Hardening A7	0.37 – 0.45	0.001 – 0.0015
Hardening A8	0.55 – 0.60	0.001 – 0.0015
Prototype A	0.13 – 0.15	0.001 – 0.0015
PEN 5	1.24	0 – 0.0053
PEN 9	0.95	0.0053
PEN 12	0.93	0.0053

Table 2.3: Values from Andersen et al. [2008] for empirical coefficients k_{p_s} and k_{f_s} , for different cases with suction installation.

Senders and Randolph [2009] conducted jacked tests (without suction), at a penetration ratio of 0.1 mm/s . Using the UWA-05 method (eq. 2.13), proposed by Lehane et al. [2007], they found a k_f value of 0.0015 for an interface friction angle of 22 degrees (constant C was assumed to be 0.012). The k_p value was assumed to be 0.2 due to the fact that sand used was very dense. For the suction installation tests that Senders and Randolph [2009] conducted, no calculations for empirical coefficients were performed.

Furthermore, Lian et al. [2014] carried out small-scaled tests, without suction to get unreduced penetration resistance under no pore water flow. The penetration resistance was calculated by the CPT-based method using averaged values of q_c . Results show that the best correlation to their calculations are obtained with the values proposed by DNV (1992) (see table 2.1).

EXPERIMENTAL ANALYSIS

3

In the present chapter, tests for installation and uninstallation of a medium-scale model bucket foundation, following different procedures, are presented. The tests conducted in the laboratory facilities of Aalborg University in the period between January and May 2016. The procedures followed are installation with force and suction, also called "Suction + Force", installation with only suction, also called "Pure Suction", installation with only force also called "Pure Force", and its corresponding induced water pressure uninstallation, by simulating different weights of the bucket. 10 different tests have been performed but only 3 of them (one per procedure) are shown in the current chapter. Rest of the tests are presented in Appendix B. The following table shows the characteristics and location of each installation test in the report:

Test Number	Characteristics	Date	Water Level [cm]	Location in the Report
1	Suction+Force	10/03/2016	8	Appendix B
2	Suction+Force	20/06/2016	8	Appendix B
3	Suction+Force	29/03/2016	13	Chapter 3
4	Pure Suction	01/04/2016	11	Appendix B
5	Pure Suction	05/04/2016	11	Chapter 3
6	Pure Force	07/04/2016	10	Appendix B
7	Pure Force	12/04/2016	7	Appendix B
8	Pure Force	14/04/2016	8	Chapter 3
9	Pure Suction	18/04/2016	10	Appendix B
10	Pure Force	25/04/2016	10	Appendix B

Table 3.1: Installation tests.

For each installation test, an uninstallation test was performed. The characteristics of all the uninstallation tests and the location in the report are shown in the following table:

Test Number	Characteristics	Date	Water Level [cm]	Location in the Report
1	Uninstallation without weight	10/03/2016	8	Appendix B
2	Uninstallation without weight	20/06/2016	8	Appendix B
3	Uninstallation without weight	29/03/2016	13	Chapter 3
4	Uninstallation without weight	01/04/2016	11	Appendix B
5	Uninstallation with 201 kg	05/04/2016	11	Chapter 3
6	Uninstallation with 402 kg	07/04/2016	10	Appendix B
7	Uninstallation with 402 kg	12/04/2016	7	Appendix B
8	Uninstallation with 302 kg	14/04/2016	8	Chapter 3
9	Uninstallation with 302 kg	18/04/2016	10	Appendix B
10	Uninstallation with 201 kg	25/04/2016	10	Appendix B

Table 3.2: Uninstallation tests.

The physical model gives the ability to examine the influence of suction during installation and influence of different weights on the bucket during uninstillation. Tests have been conducted with one specimen, which dimensions are shown in Figure 3.1. In Appendix A, the detailed procedure followed for all the different cases is presented.

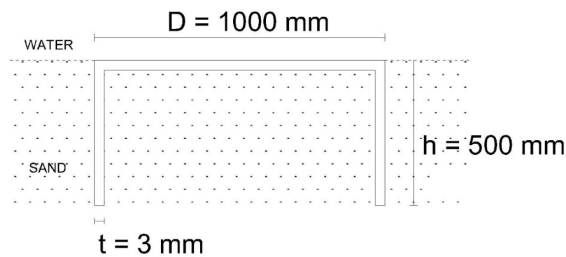


Figure 3.1: Dimensions of the bucket.

From the 10 experiments that have been performed, only 3 of them (the most characteristic ones) are presented in this chapter, where the procedure and results for each test are shown

in the following order:

- A - Test Number 3-Installation with suction and force/ Uninstallation without weight
- B - Test Number 5-Installation with only suction/ Uninstallation with 201 kg
- C - Test Number 8-Installation with only force/ Uninstallation with 302 kg

3.1 Test N_o 3

3.1.1 Cone Penetration Test before Installation of the Bucket

First, soil properties are measured before the installation by performing CPT tests, which are explained in Appendix A. 4 CPTs were conducted before installation, in the positions as shown in Figure 3.2.

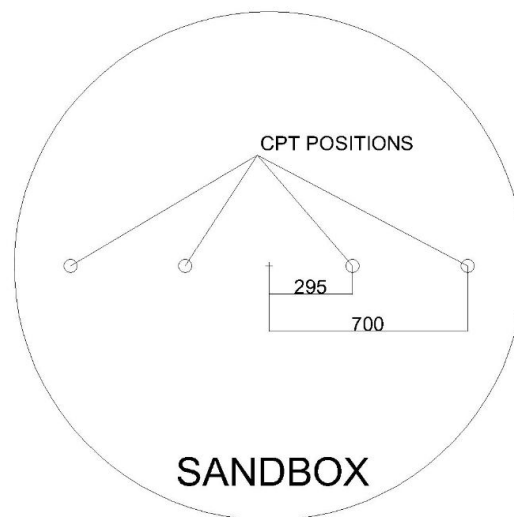


Figure 3.2: Location of CPT tests before installation [mm].

The calculated cone resistance over the depth until 600 mm is shown in Figure 3.3.

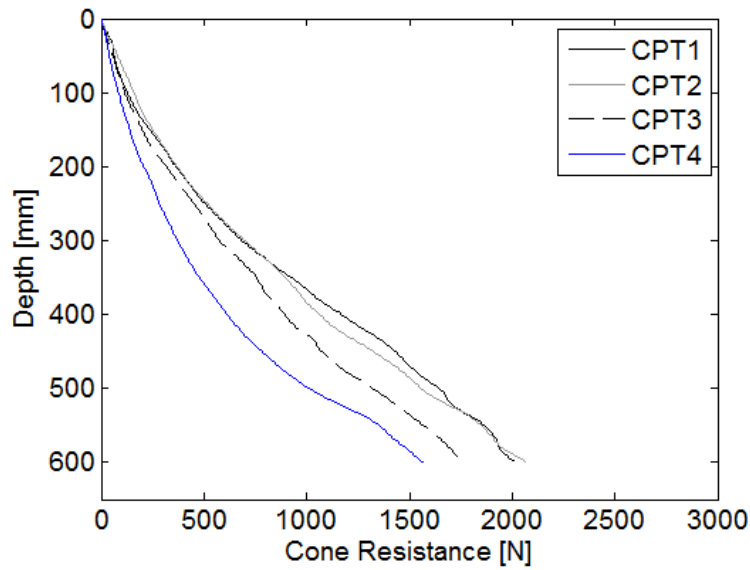


Figure 3.3: Cone resistance, before installation of the bucket.

Furthermore, from the cone resistance, the relative density of the soil is extracted and it is illustrated over the depth in Figure 3.4.

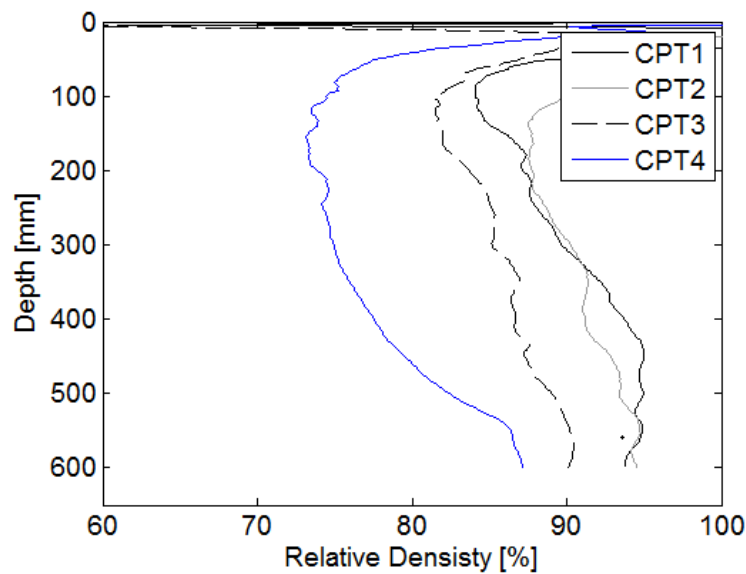


Figure 3.4: Relative density of the soil, before installation of the bucket.

3.1.2 Installation of the Bucket

After measuring the soil properties, the installation of the bucket can begin. There are 3 different steps in the installation procedure. Firstly, installation begins without neither suction nor force, just with the self-weight of the bucket that for this specimen is 201 kg, until no further penetration exists. Secondly, the force starts to act progressively, until the value of 2.01 kN is reached. This value was chosen in order to coincide with the self-weight

of the bucket, until no further penetration exists again. Finally, the suction starts to act jointly with the self-weight of the bucket and the applied force until the bucket is fully installed.

Regarding the pressure transducers, their position and corresponding name are illustrated in Figure 3.5. The purpose of the transducers is to measure the excess pore pressure outside and inside the bucket skirt, which is corrected with the hydrostatic one.

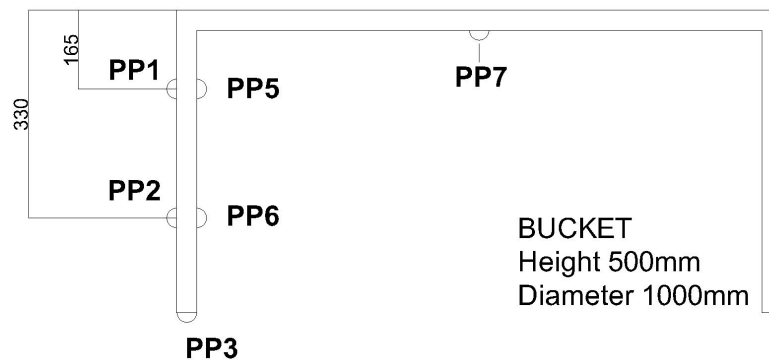


Figure 3.5: Position and name for each pressure transducer.

In table 3.3, the location and name for each pressure transducer placed on the bucket, is explained.

Name	Location
PP1	Outside of the skirt, 335 mm over the tip
PP2	Outside of the skirt, 170 mm over the tip
PP3	At the tip
PP5	Inside of the skirt, 335 mm over the tip
PP6	Inside of the skirt, 170 mm over the tip
PP7	Under the lid, inside

Table 3.3: Description of pressure transducers.

In Figure 3.6, corrected excess pore pressures that were generated during the installation, from all the pressure transducers, is depicted.

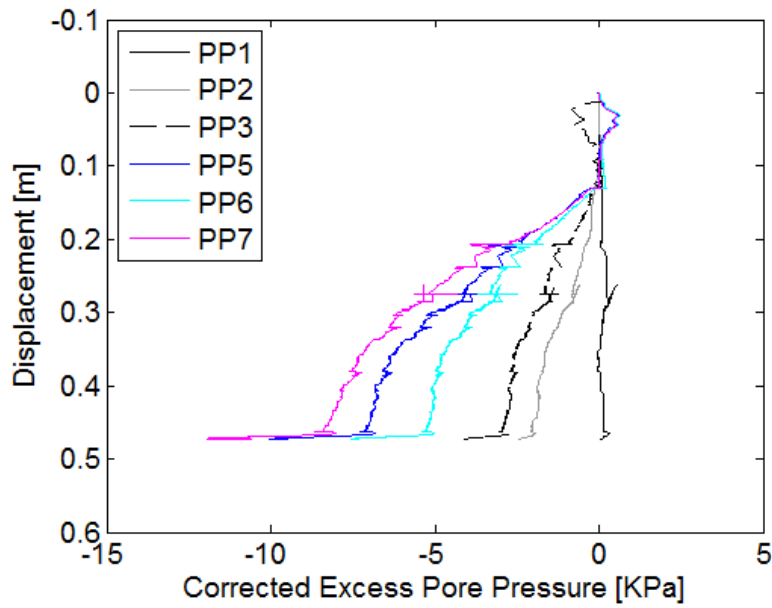
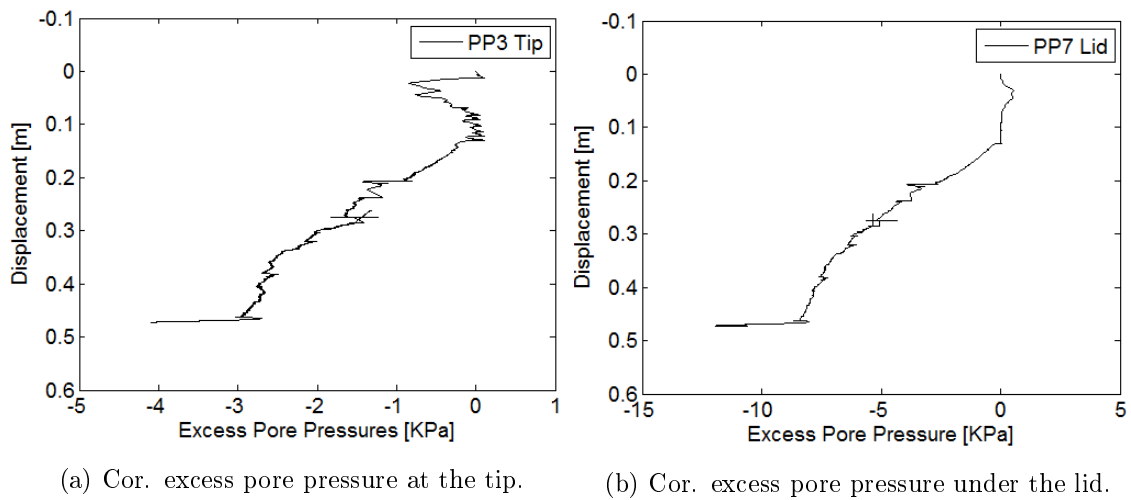


Figure 3.6: Corrected excess pore pressures from all the pressure transducers.

In Figure 3.7, the corrected excess pore pressure at the tip and under the lid of the bucket are illustrated, respectively, in order to have a better understanding of the development of excess pore pressures in the 2 most crucial positions.



(a) Cor. excess pore pressure at the tip. (b) Cor. excess pore pressure under the lid.

Figure 3.7: Corrected excess pore pressures for the tip and under the lid of the bucket.

In the following table, different steps during installation, along with the displacement range for each step, are explained.

Step Number	Description	Displacement Range
1	Loading only with self-weight of the bucket	0 mm-90.4 mm
2	Loading with self-weight of the bucket and increasing force until reach 2.01 kN	90.4 mm-186.2 mm
3	Loading with self-weight of the bucket, 2.01 kN force and suction	186.2 mm-476.5 mm

Table 3.4: Steps during the installation of the bucket.

In addition, the applied suction for 5 different displacement steps is shown in the following table.

Step Number	Suction	Displacement
1	0 kPa	100 mm
2	2.458 kPa	200 mm
3	6.145 kPa	300 mm
4	7.786 kPa	400 mm
5	11.920 kPa	476.5 mm

Table 3.5: Steps during the installation of the bucket.

The maximum suction that was applied found to be around 12 kPa. The installation of this test lasted more than 6 hours and full installation was reached, when 95 % of the skirt length was inside the soil.

3.1.3 Boundary contributions from the tank

Regarding the contributions of the boundaries of the tank during installation, a beam with 3 pressure transducers was placed at the edge of the tank in order to measure disturbances. The beam had 3 pressure transducers on different heights. The first was placed at the tip, the second 250 mm above the tip and the third 500 mm above the tip. The beam is illustrated in Figure 3.8.

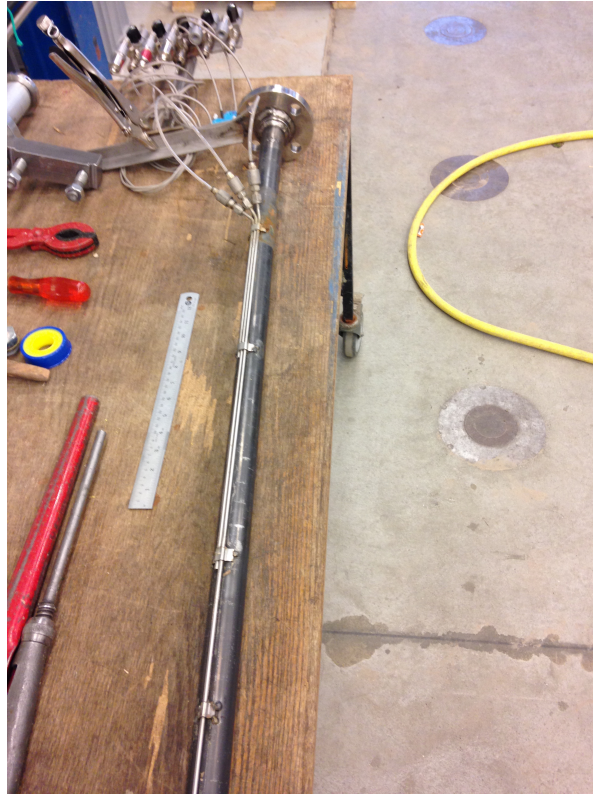


Figure 3.8: Beam used in real experiments.

Figure 3.9 shows the excess pore pressure created at the boundaries during installation.

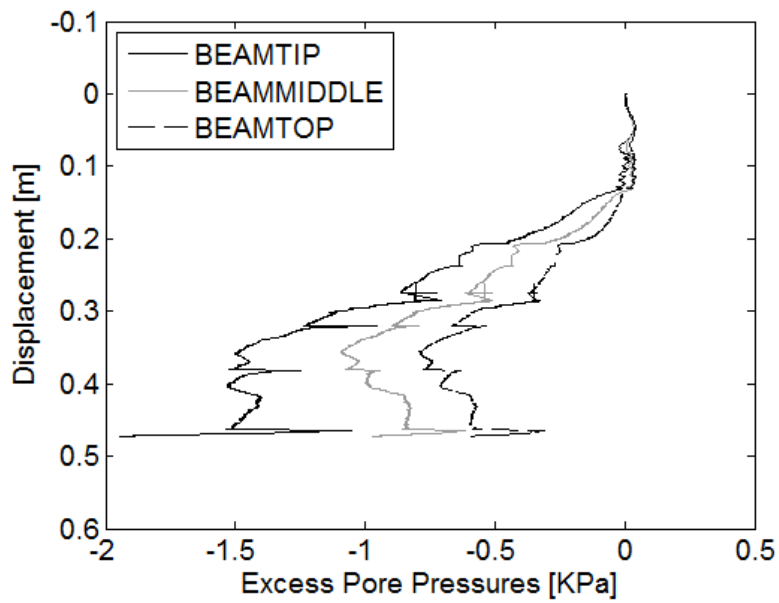


Figure 3.9: Excess of pore pressure created at the boundary during the installation.

Interpreting the measurements obtained from the beam, it can be concluded that the boundaries of the tank, do not affect the results from the installation, because the

disturbances measured, found to be insignificant.

3.1.4 Cone Penetration Tests after Installation of the Bucket

After the end of the installation of the bucket, soil properties were investigated again with the CPT method. In this case, 4 CPTs were performed outside the bucket's skirt and another 4 inside, through the valves used for the suction application. The position of the 8 CPTs are illustrated in Figure 3.10.

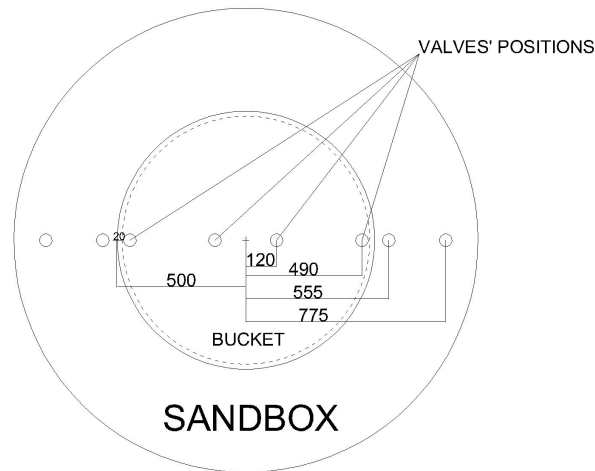


Figure 3.10: Location of CPT tests after installation [mm].

The calculated cone resistance over the depth, for 600 mm is shown in Figure 3.11.

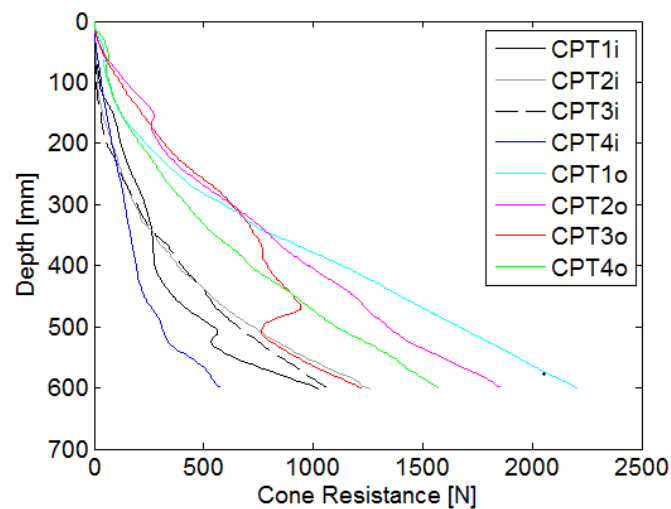


Figure 3.11: Cone resistance after installation of the bucket.

$1o$ is denoted as the first CPT performed from the left side of the tank, outside the bucket skirt. $1i$ is denoted as the first CPT performed from the left side, inside the bucket skirt.

Furthermore, from the cone resistance the relative density of the soil can be extracted and it is shown over the depth in Figure 3.12.

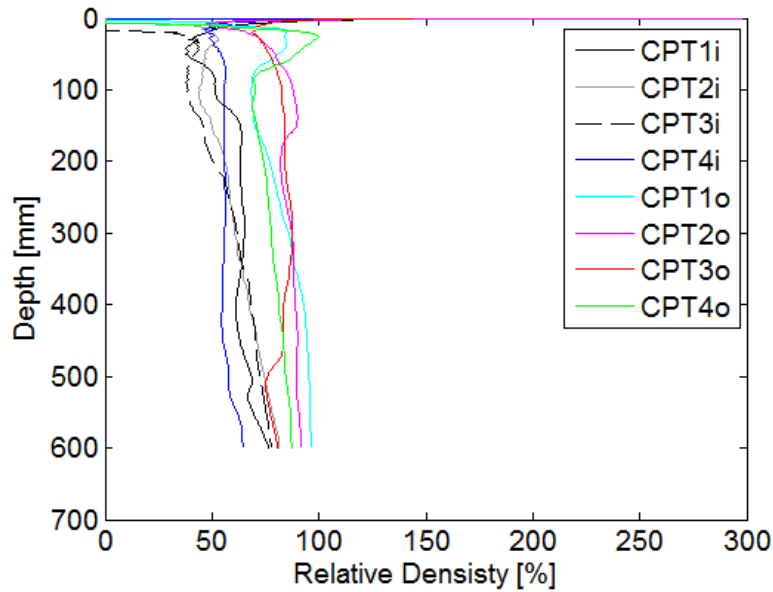


Figure 3.12: Relative density of the soil after installation of the bucket.

From the CPT results, on the one hand, it is possible to conclude that the sand inside the bucket skirt has lost most of its resistance due to the seepage flow, created by the suction application. On the other hand, the soil outside the bucket skirt has barely changed its properties.

3.1.5 Uninstallation of the Bucket

After the installation process by the means of suction, the uninstallation process is ready to begin. In order to carry out the uninstallation, water pressure is applied inside the bucket skirt. Water pressure was induced through one of the valves, which was placed on top of the bucket, while the others remained closed at all times during the whole procedure.

The uninstallation lasts less time than the installation procedure. It takes around 15 minutes for fully uninstalled bucket, compared to the several hours that are used for the installation. Normally, the uninstallation finishes after 35 cm of displacement, so around 65 % of bucket skirt outside the soil. The hydraulic piston was used as an assisting driving tool during the whole procedure.

In Figure 3.13 the corrected excess pore pressures that were generated during the uninstallation in all the pressure transducers are shown.

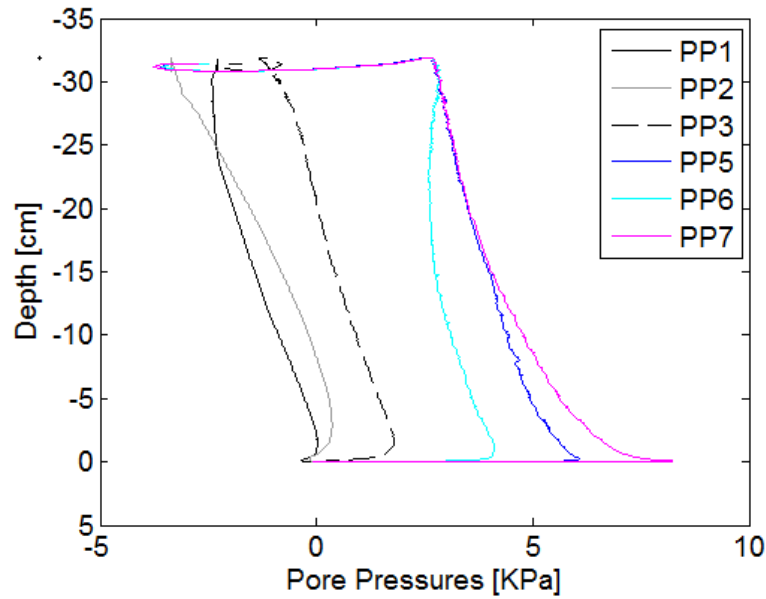
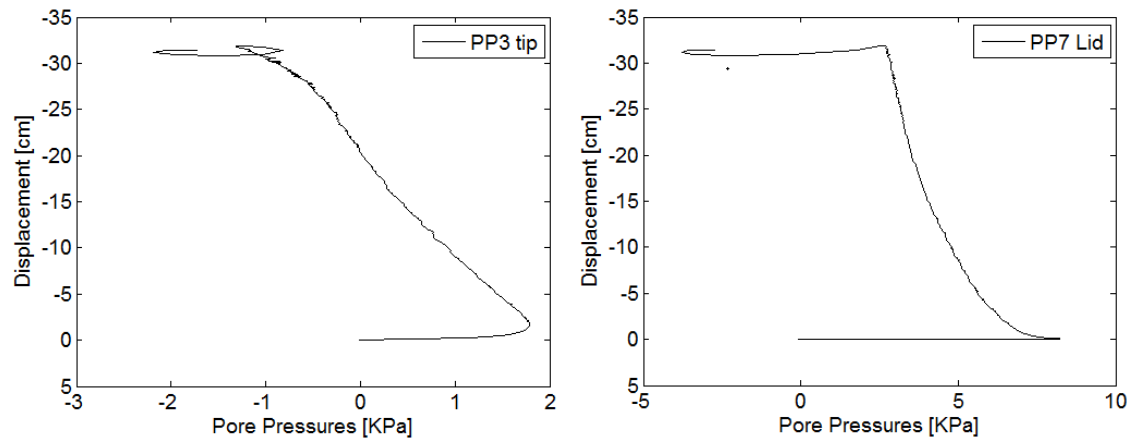


Figure 3.13: Corrected excess pore pressures.

Figure 3.14 illustrates the corrected excess pore pressures at the tip and under the lid of the bucket, respectively.



(a) Cor. excess pore pressure at the tip.

(b) Cor. excess pore pressure under the lid.

Figure 3.14: Corrected excess pore pressures at the tip and under the lid of the bucket.

From the results, it can be seen that 8.22 kPa are needed for the uninstillation to start. In this test, no additional weight was placed on top of the bucket. Regarding the boundary contributions of the tank, Figure 3.15 shows the excess of pore pressure at the boundary during uninstillation. As for the installation, the boundaries do not affect the results for the uninstillation.

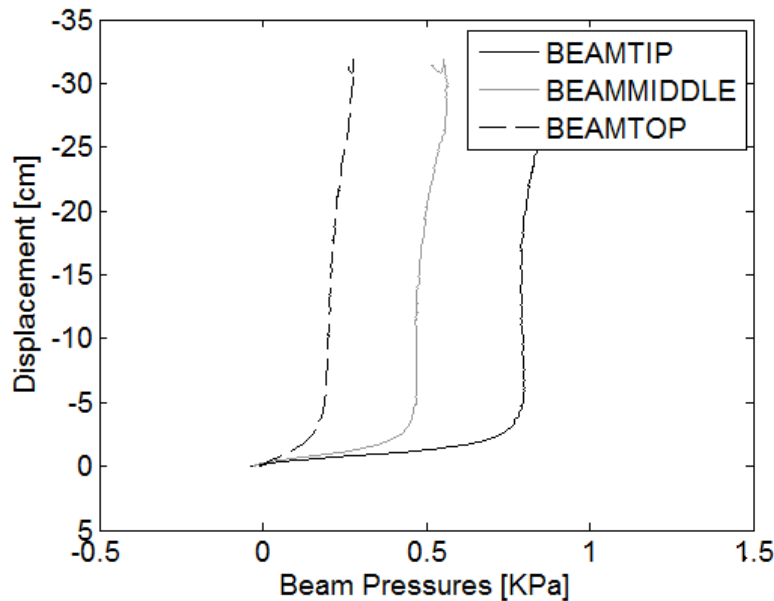


Figure 3.15: Excess pore pressures created at the boundary during uninstillation.

3.1.6 k_p and k_f Coefficients

After the collection of all data from the installation, uninstillation, and soil resistance before and after the installation, the k_p and k_f coefficients can be calculated. k_p is the coefficient related with the tip resistance of the bucket and k_f is the one related with the skirt friction. The explanation of how they are calculated and other details of these two coefficients can be found in Appendix B and in Sgourakis et al. [2016]. In order to calculate these coefficients, the soil resistance obtained from CPT tests is the most crucial one. The following table shows the names and the details of CPT tests performed.

Name	Time Location	Used for
CPT1	Before installation	Tip resistance
CPT2	Before installation	Tip resistance
CPT3	Before installation	Tip resistance
CPT4	Before installation	Tip resistance
CPT1i	After installation	Tip resistance and inside skirt friction
CPT4i	After installation	Tip resistance and inside skirt friction
CPT2o	After installation	Tip resistance and outside skirt friction
CPT3o	After installation	Tip resistance and outside skirt friction

Table 3.6: CPT tests performed.

First, the k_f coefficient is calculated from the uninstillation data, since for this process only the skirt friction of the bucket is involved. Thus, the tip resistance is equal to 0. In order to calculate the internal skirt friction of the bucket, CPT1i and CPT4i are used. For the external skirt friction CPT2o and CPT3o are used. In Figure 3.16, results for k_f are

depicted over the depth. The first value, when the bucket is fully installed, is 8.97×10^{-04} and the mean value is 7.51×10^{-04} .

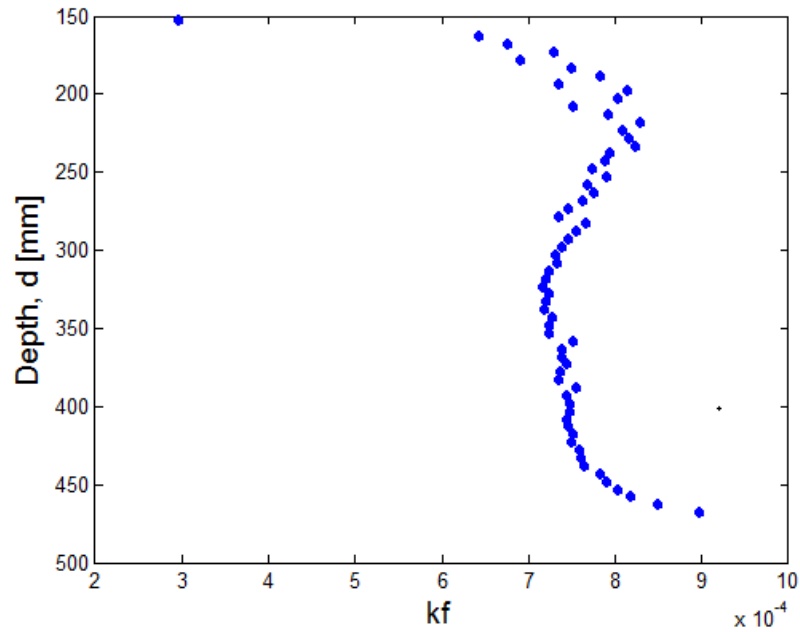


Figure 3.16: k_f coefficient.

After k_f calculations, k_p coefficient can be calculated using the CPT tests before installation, along with the installation load. In Figure 3.17, results for k_p are illustrated over the depth. First value, when the bucket is fully installed, is 0.2242 and the mean value is 0.5493.

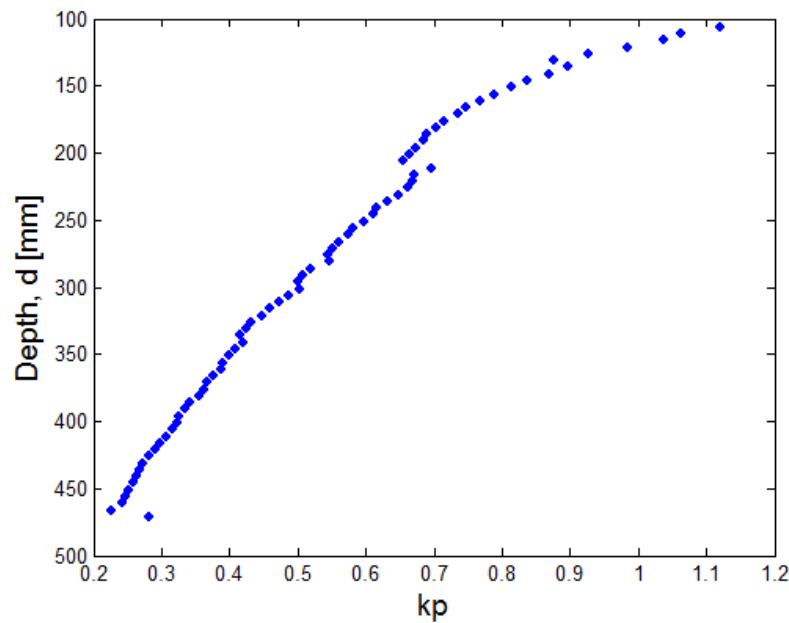


Figure 3.17: k_p coefficient.

3.2 Test N_o 5

The main difference between test type B and type A is that during the installation, only suction and the self-weight of the bucket is used and uninstallation was done with 201 kg of dead-weight over the bucket.

3.2.1 Cone Penetration Test before Installation of the Bucket

Soil properties are calculated in the same way for all the different procedures. Result for the 4 CPTs performed before installation are shown in Figure 3.18.

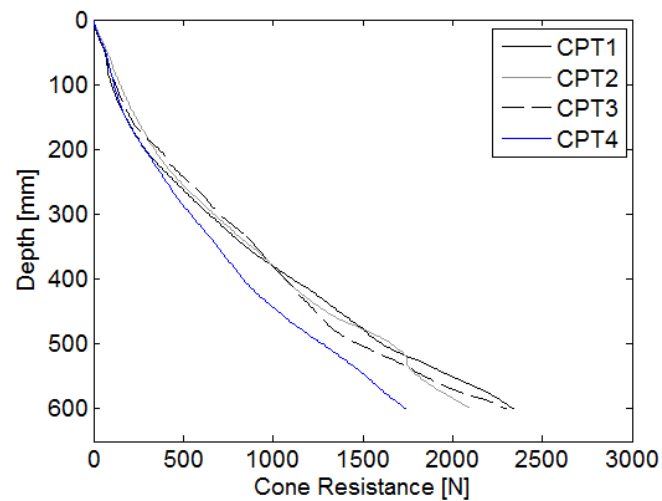


Figure 3.18: Cone resistance before installation of the bucket.

Furthermore, the relative density of the soil over the depth is illustrated in Figure 3.19.

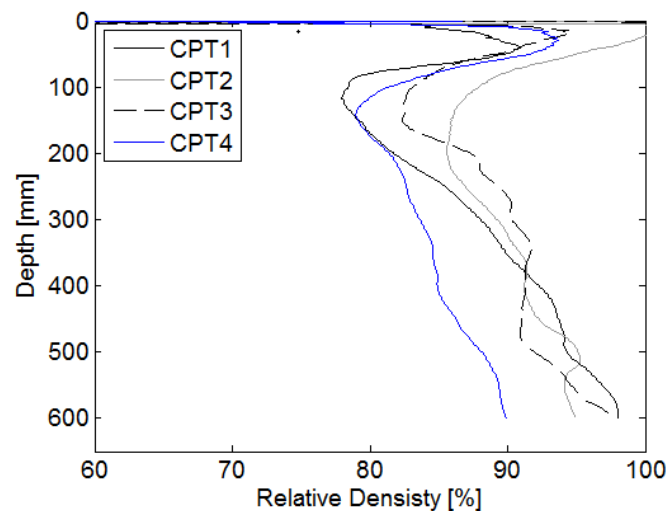


Figure 3.19: Relative density of the soil before installation of the bucket.

3.2.2 Installation of the Bucket

In this test there are 2 steps during the installation procedure instead of the 3 that were explained in the previous section. First is installation due to self-weight in order to ensure a seal component between the skirt of the bucket and the surrounding soil [Koterás et al. 2016]. After the displacement is steady, suction starts to act jointly with the self-weight of the bucket, until it is fully installed.

In the following table the location and the name for each pressure transducer placed on top of the bucket is explained.

Name	Location
PP1	Outside of the skirt, 335 mm over the tip
PP2	Outside of the skirt, 170 mm over the tip
PP3	On the tip
PP5	Inside of the skirt, 335 mm over the tip
PP6	Inside of the skirt, 170 mm over the tip
PP7	Under the lid, inside

Table 3.7: Description of pressure transducers.

In Figure 3.20 the corrected excess pore pressures that were generated during installation are shown.

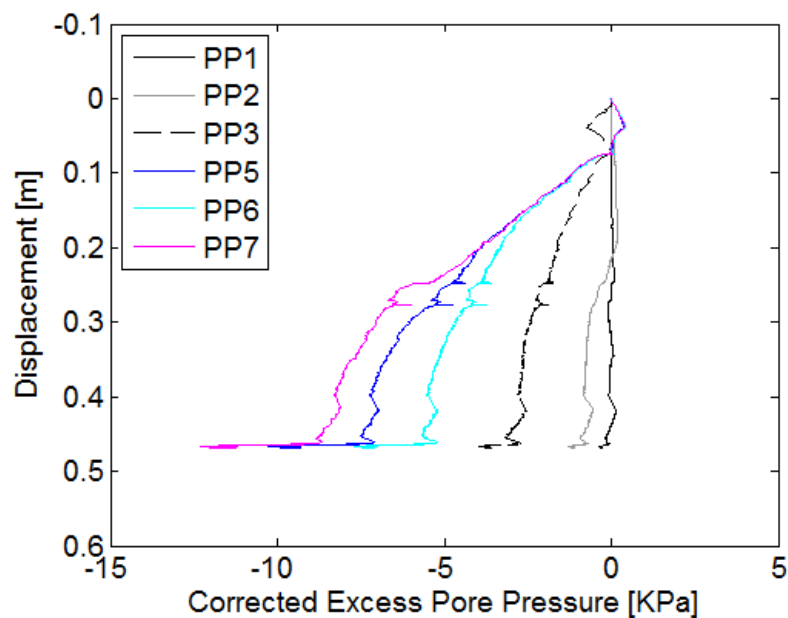
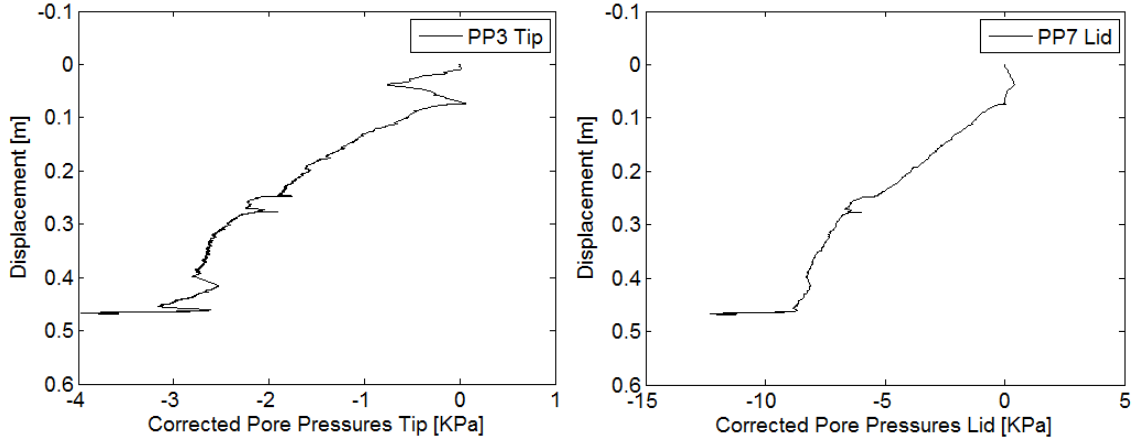


Figure 3.20: Corrected excess pore pressures.

In Figure 3.21 the corrected excess pore pressures at the tip and under the lid of the bucket are shown, respectively.



(a) Cor. excess pore pressure at the tip.

(b) Cor. excess pore pressure under the lid.

Figure 3.21: Corrected excess pore pressures at the tip and under the lid of the bucket.

In the following table different steps during installation and the displacement range for each can be seen.

Step Number	Description	Displacement Range
1	Loading only with self-weight of the bucket	0 mm-82.0 mm
2	Loading with self-weight of the bucket and suction	82.0 mm-468.6 mm

Table 3.8: Steps of the installation procedure.

Additionally, the next table shows the applied suction for 5 different displacement steps.

Step Number	Suction	Displacement
1	1.206 kPa	100 mm
2	3.936 kPa	200 mm
3	7.044 kPa	300 mm
4	7.663 kPa	400 mm
5	11.670 kPa	468.6 mm

Table 3.9: Applied suction for every 100 mm of installation.

It can be concluded that the maximum suction that is applied is around 12 kPa. The installation procedure for this test lasted almost 6 hours and full installation was reached when 95 % of the skirt length was inside the soil.

3.2.3 Boundary contributions from the tank

Regarding the affectation of the boundaries of the yellow tank, in Figure 3.22 the excess of pore pressure created at the boundary during the installation can be seen .

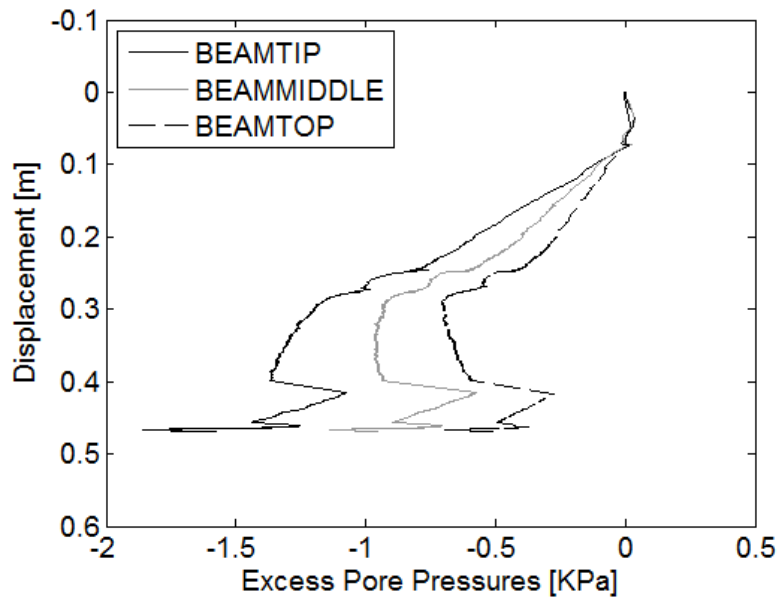


Figure 3.22: Excess of pore pressure created at the boundary during the installation.

Interpreting the measurements obtained from the beam, it can be concluded that the boundaries of the tank, do not affect the results from the installation, because the disturbances measured, found to be insignificant.

3.2.4 Cone Penetration Test after Installation of the Bucket

Figure 3.23 illustrates the soil resistance after installation.

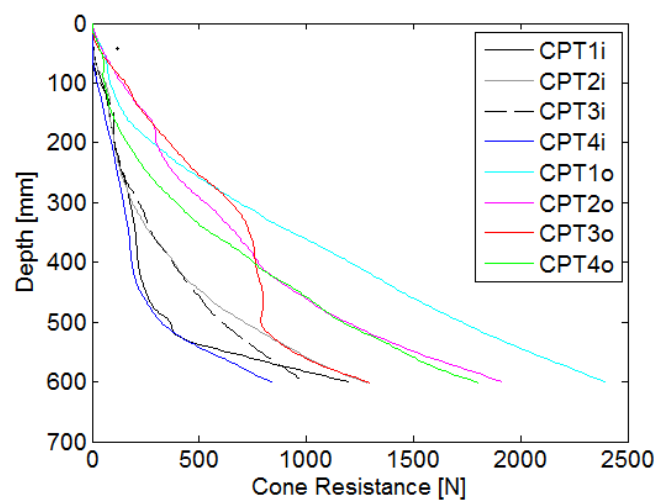


Figure 3.23: Cone resistance after installation of the bucket.

The relative density of the soil is shown over the depth in Figure 3.24.

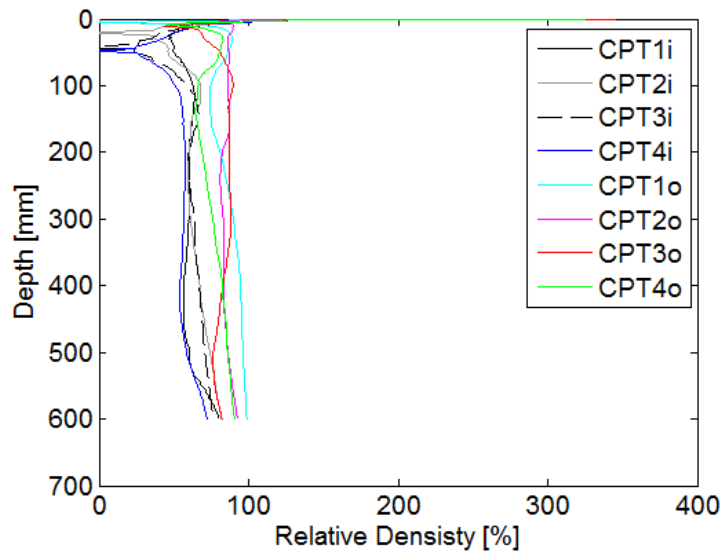


Figure 3.24: Relative density of the soil after installation of the bucket.

From the CPT results, the same conclusions as in the previous type of experiment can be extracted. The sand inside the bucket skirt has lost most of its resistance due to the seepage flow, created by the suction application. However, the soil outside the bucket skirt has barely changed its properties.

3.2.5 Uninstallation of the Bucket

The main difference of this uninstallation procedure with respect to the previous one is the 201 kg of dead-weight that was placed on top the bucket. The uninstallation lasted for almost 15 minutes. Uninstallation finished after 32 cm of displacement, so around 65 % of the bucket outside the soil. The hydraulic piston was used as an assisting tool during the whole procedure. In Figure 3.25 the corrected excess pore pressures that were generated during the uninstallation from all pressure transducers are depicted.

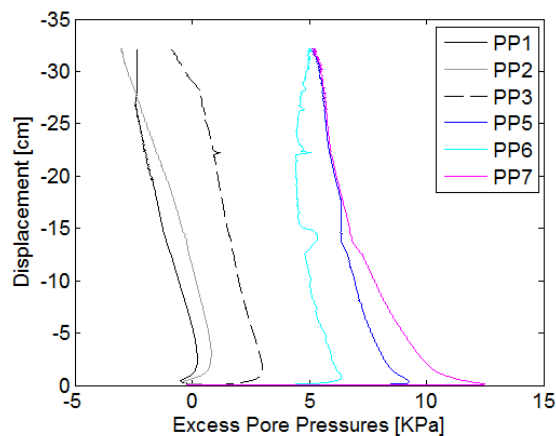


Figure 3.25: Corrected excess pore pressures from uninstallation.

In Figure 3.26 the corrected excess pore pressure at the tip and under the lid are shown, respectively.

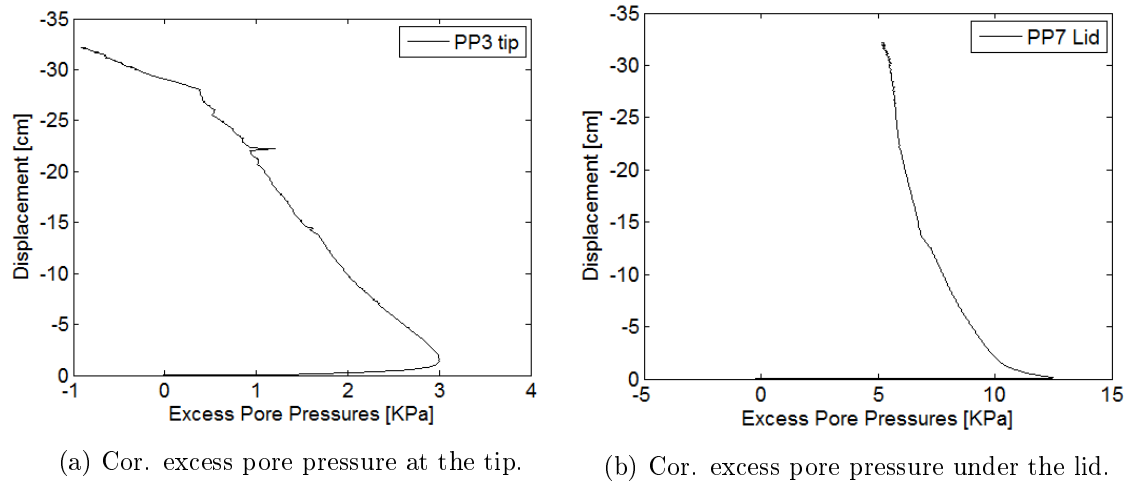


Figure 3.26: Corrected excess pore pressures at the tip and under the lid of the bucket.

From the results, it can be seen that 12.50 kPa are needed for the uninstillation to start. That is 4.28 kPa more than in the previous test and is due to the dead-weight placed on top of the bucket. Regarding the boundary contributions of the yellow tank, Figure 3.27 shows the excess of pore pressure at the boundary during uninstillation. As for the installation, the boundaries do not affect the results for the uninstillation.

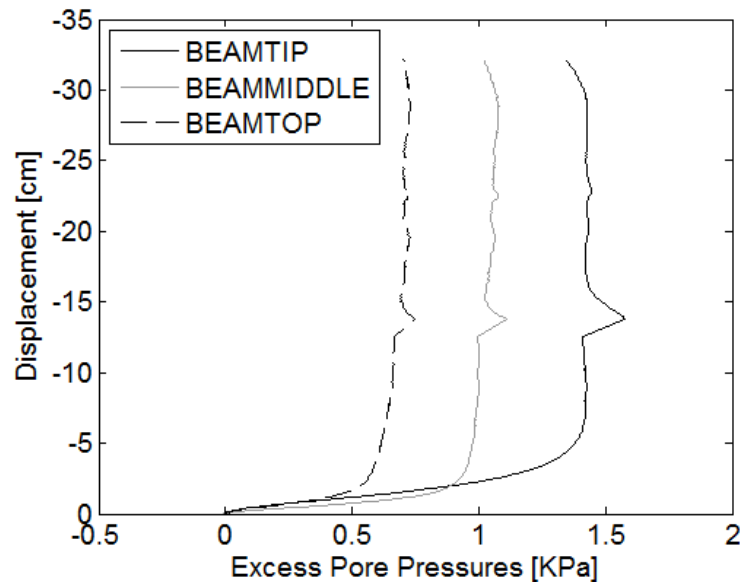


Figure 3.27: Excess of pore pressure created at the boundary during the uninstillation.

3.2.6 k_p and k_f Coefficients

k_p and k_f coefficients can be calculated again for this test. It is the same procedure than the one used with the previous test and it can be found in Appendix B and in Sgourakis

et al. [2016]. The same CPT tests were used for the calculations and the explanation can be found in Table 3.6.

By the same means that used in the previous test, the k_f coefficient is calculated from the uninstillation data, since for this process only the skirt friction of the bucket is involved. Thus, the tip resistance is equal to 0. In order to calculate the internal skirt friction of the bucket, CPT1i and CPT4i are used. For the external skirt friction CPT2o and CPT3o are used. In Figure 3.28, results for k_f are illustrated over the depth. The first value, when the bucket is fully installed is 9.32×10^{-04} and the mean value is 6.31×10^{-04} .

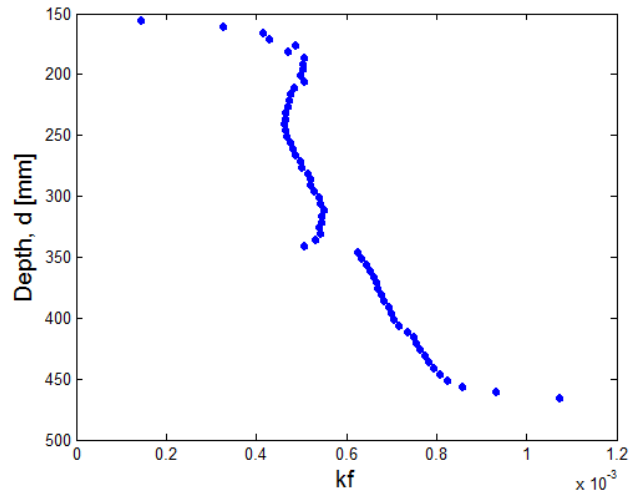


Figure 3.28: k_f coefficient.

After k_f calculations, k_p coefficient can be calculated using the CPT tests before installation, along with the installation load. In Figure 3.29, results for k_p are illustrated over the depth. First value, when the bucket is fully installed, is 0.2113 and the mean value is 0.4227.

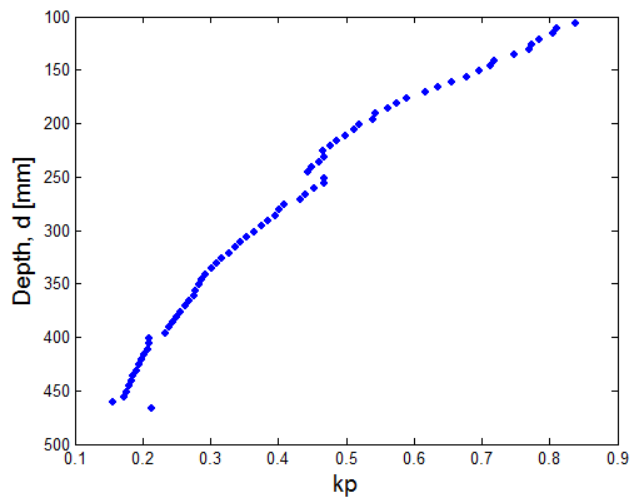


Figure 3.29: k_p coefficient.

3.3 Test N_o 8

The main difference between this test and the previous ones, is that the bucket was installed only by force, instead of suction. For this test, uninstillation was performed with 302 kg of dead-weight on top of the bucket.

3.3.1 Cone Penetration Test before Installation of the Bucket

Soil properties are calculated in the same way as in the previous tests. Result of 4 CPT tests are shown in Figure 3.30.

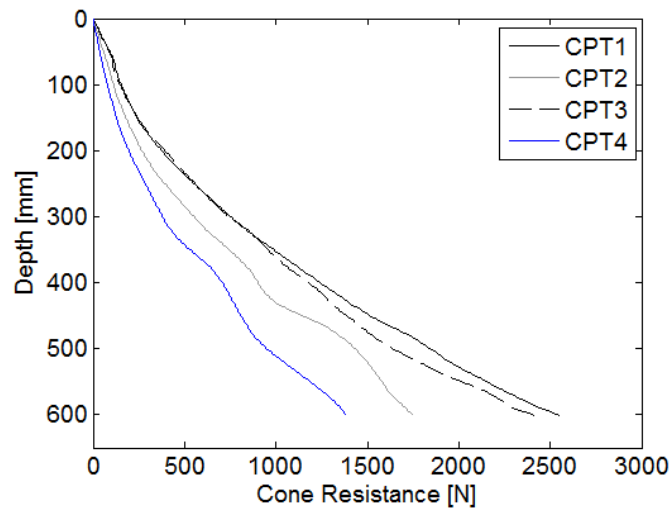


Figure 3.30: Cone resistance before installation of the bucket.

Furthermore, the relative density of the soil over the depth is shown in Figure 3.31.

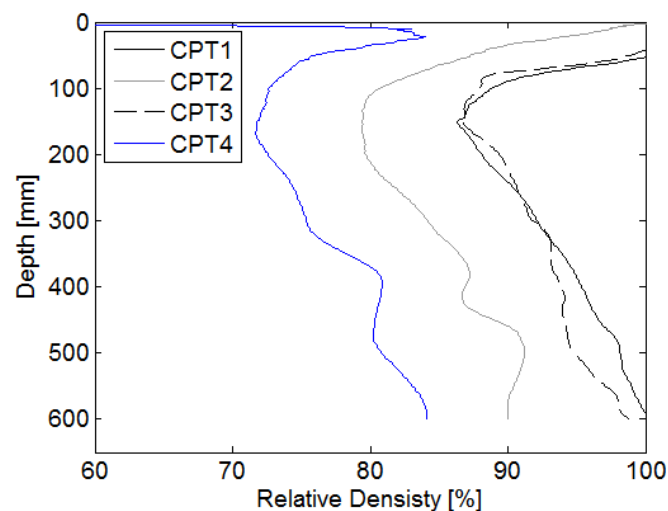


Figure 3.31: Relative density of the soil before installation of the bucket.

3.3.2 Installation of the Bucket

In this test there is only penetration by force with help of a hydraulic piston. The penetration ratio was set to be at 0.14mm/s. The experiment stopped after the displacement transducer, placed on top of the bucket was showing a constant value. The experiment lasted almost an hour and the generation of excess pore pressures are expected to be low. In table 3.7 the location and name for each pressure transducer that is placed on top of the bucket is presented. In Figure 3.32 the force applied during the installation is shown.

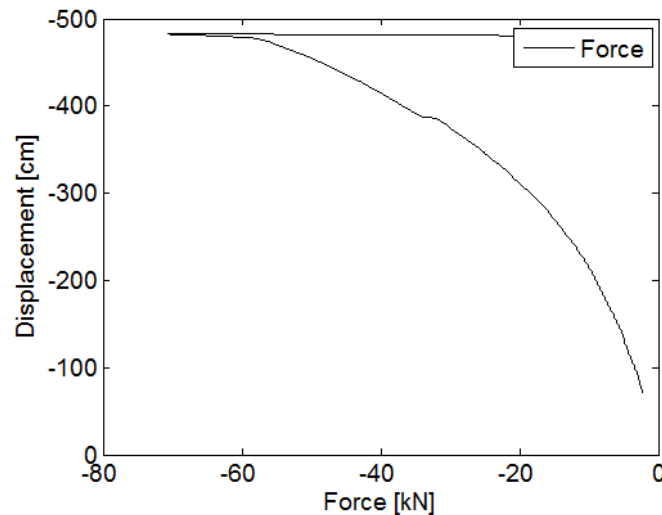


Figure 3.32: Force applied during the installation.

Figure 3.33 shows the corrected excess pore pressures that were generated during installation. In this case, since suction was not applied, the generation of excess pore pressures expected to be low, as mentioned before.

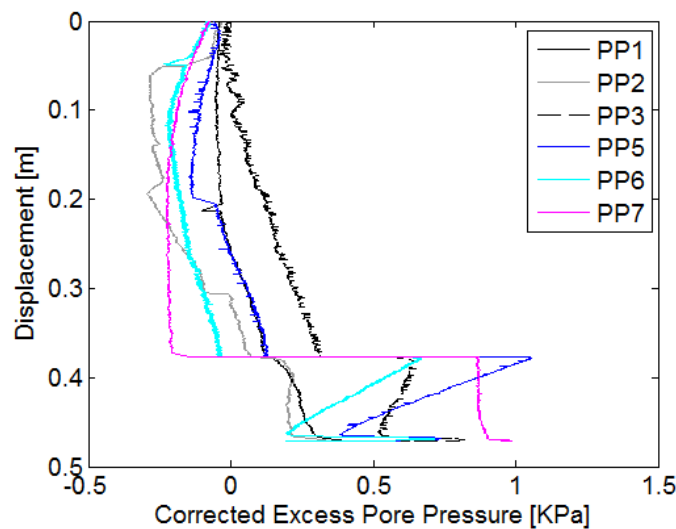


Figure 3.33: Corrected excess pore pressures.

From the 2 previous figures, it can be seen that when the displacement got approximately 38 cm, the force increased dramatically in order to continue with the installation due to soil resistance. Excess pore pressures were generated due to the sudden increase of load.

Another main difference between the previous tests is the time used for the installation. This test takes around 15 % of the time that used for the other type of tests (1 hour instead of the 6 hours used in the other test), thus it is much faster. Another good characteristic of the force installation is that the soil is not affected that much after the installation and will preserve the properties as it is explained later in this section. Figure 3.34 illustrates the corrected excess pore pressure at the tip and under the lid of the bucket, respectively.

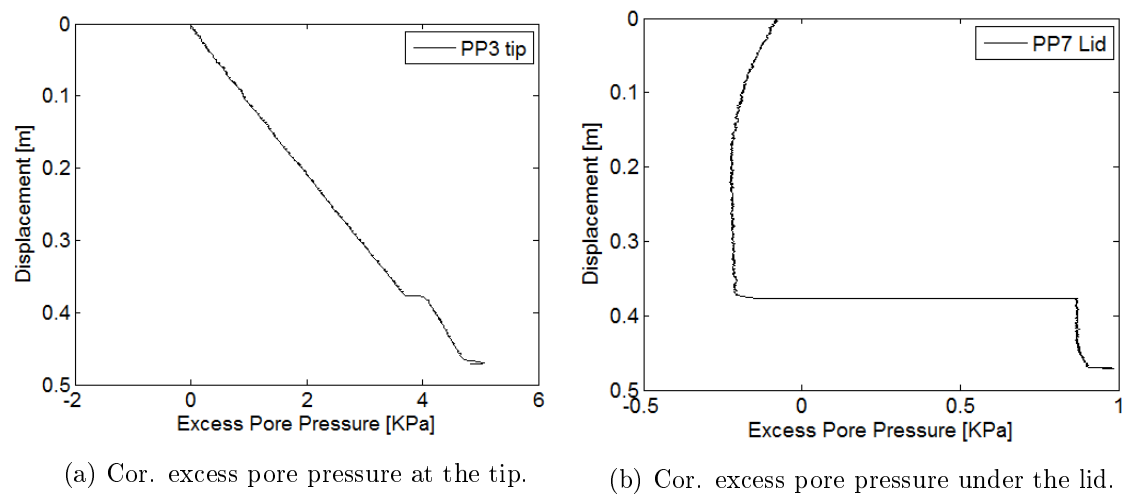


Figure 3.34: Corrected excess pore pressures at the tip and under the lid of the bucket.

In the following table the different steps during the installation and the displacement range when each step occurred can be seen.

Step Number	Description	Displacement Range
1	Loading only with self-weight of the bucket	0 mm-70.3 mm
2	Loading with self-weight of the bucket and force	70.3 mm-482.5 mm

Table 3.10: Steps during force installation of the bucket.

Additionally, the applied force for every 100 mm is shown in table 3.11.

Step Number	Force	Displacement
1	3.420 kPa	100 mm
2	9.000 kPa	200 mm
3	18.510 kPa	300 mm
4	36.900 kPa	400 mm
5	68.950 kPa	482.5 mm

Table 3.11: Steps during the installation of the bucket.

It can be seen that the maximum force that is applied is around 69 kPa. The installation of this test lasted almost 1 hour and the total installation was reached when 96.4 % of the skirt length was inside the soil.

3.3.3 Boundary contributions from the tank

Regarding the contributions of the boundaries of the yellow tank during installation, Figure 3.35 illustrates the excess pore pressures created at the boundary during installation.

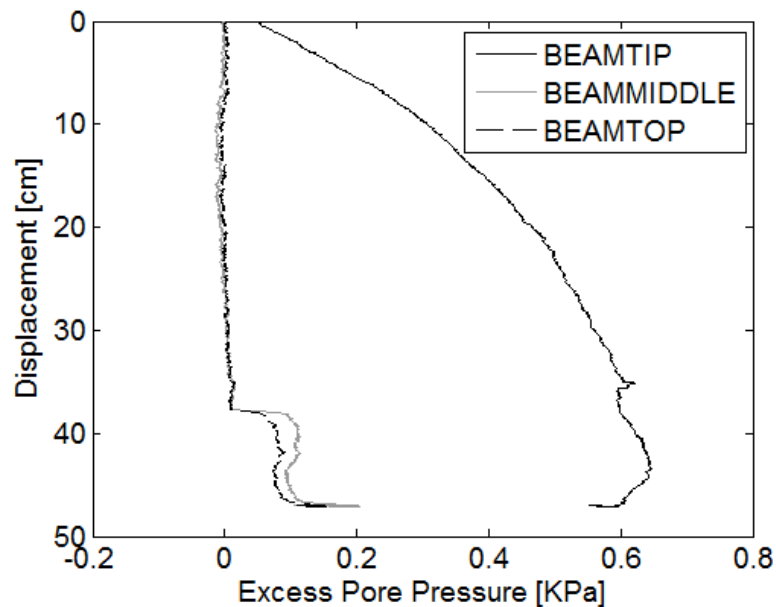


Figure 3.35: Excess of pore pressure created at the boundary during the installation.

Interpreting the measurements obtained from the beam, it can be concluded that the boundaries of the tank, do not affect the results from the installation, because the disturbances measured, found to be insignificant.

3.3.4 Cone Penetration Test after Installation of the Bucket

In Figure 3.36 the cone resistance after installation is shown. Furthermore, relative density of the soil over the depth is shown in Figure 3.37.

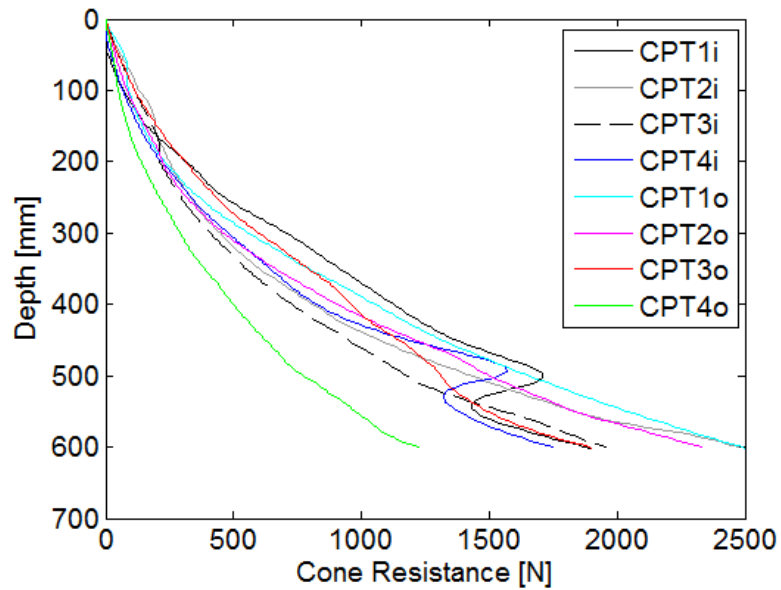


Figure 3.36: Cone resistance after installation of the bucket.

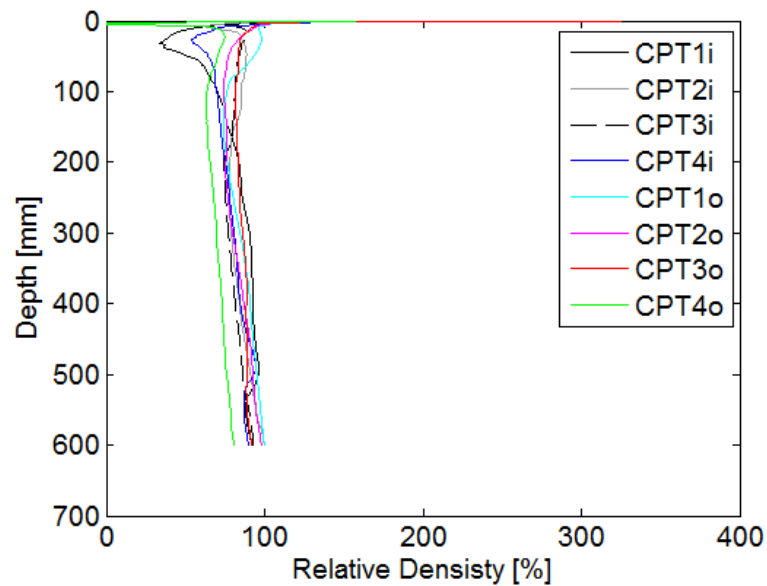


Figure 3.37: Relative density of the soil after installation of the bucket.

From CPT results, it can be seen that soil properties have not change dramatically . That is because suction was not applied during installation.

3.3.5 Uninstallation of the Bucket

The main difference of this uninstillation with respect to the previous tests is the dead-weight, that was placed on top of the bucket. In this case it was 302 kg. The uninstillation lasted around 15 minutes, the same as in the other tests. Uninstillation finished after 30.930 cm of displacement were reached, so around 62 % of the bucket outside the soil. The hydraulic piston was used as an assisting tool during the whole procedure.

In Figure 3.38 the corrected excess pore pressures that were generated during the uninstillation from all the pressure transducers are depicted.

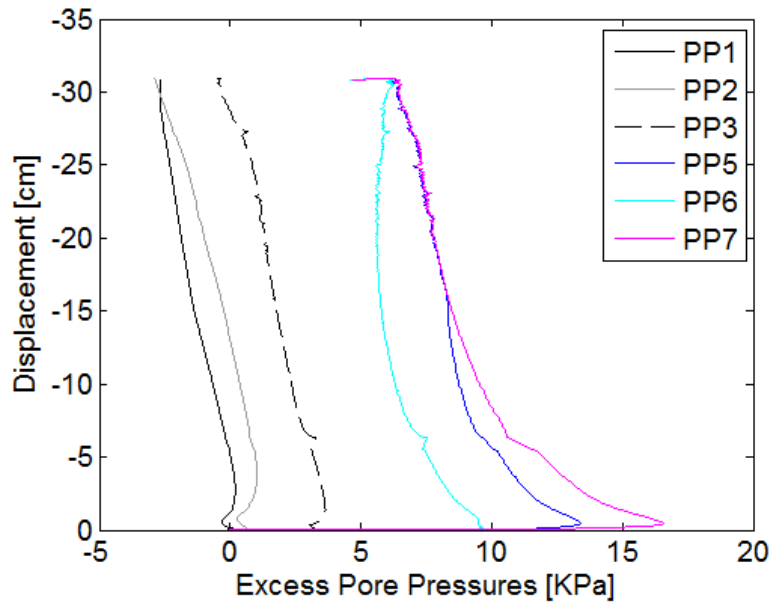
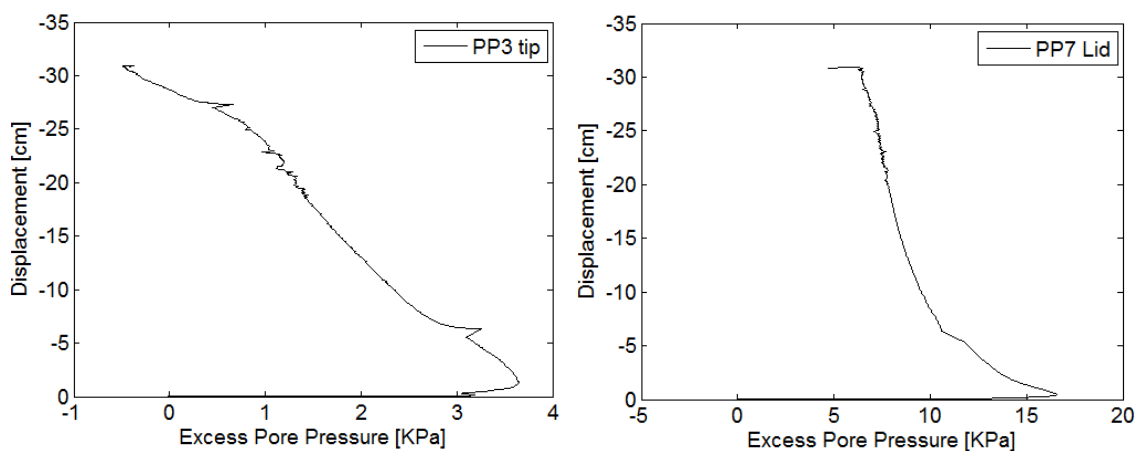


Figure 3.38: Corrected excess pore pressures.

In Figure 3.39 the corrected excess pore pressure at the tip and under the lid of the bucket are shown, respectively.



(a) Cor. excess pore pressure at the tip.

(b) Cor. excess pore pressure under the lid.

Figure 3.39: Corrected excess pore pressures at the tip and under the lid of the bucket.

From the results, it can be seen that 12.50 kPa are needed for the uninstillation to get started. That is 4.28 kPa more than in the first test and is due to the dead-weight placed over the bucket.

Regarding the boundary contributions of the yellow tank, in Figure 3.40 the excess pore pressure created at the boundary during uninstillation can be seen. As for the installation, the boundaries do not affect the results for the uninstillation.

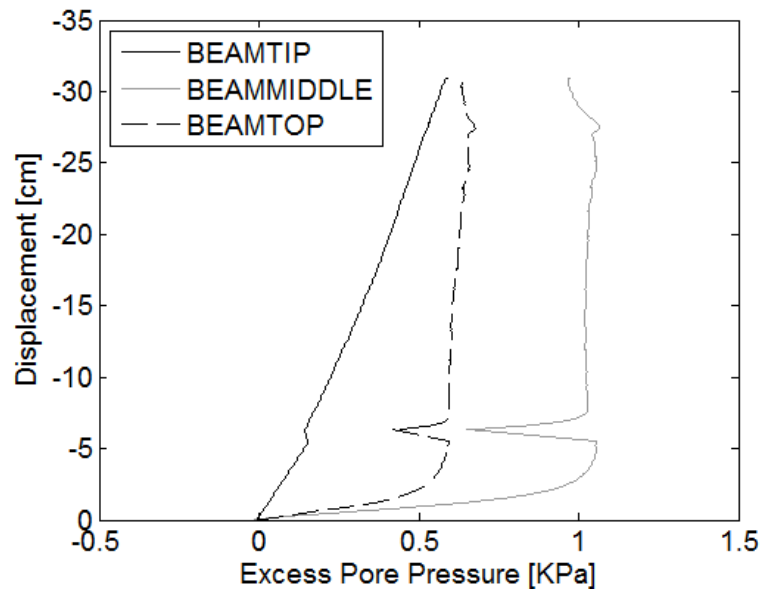
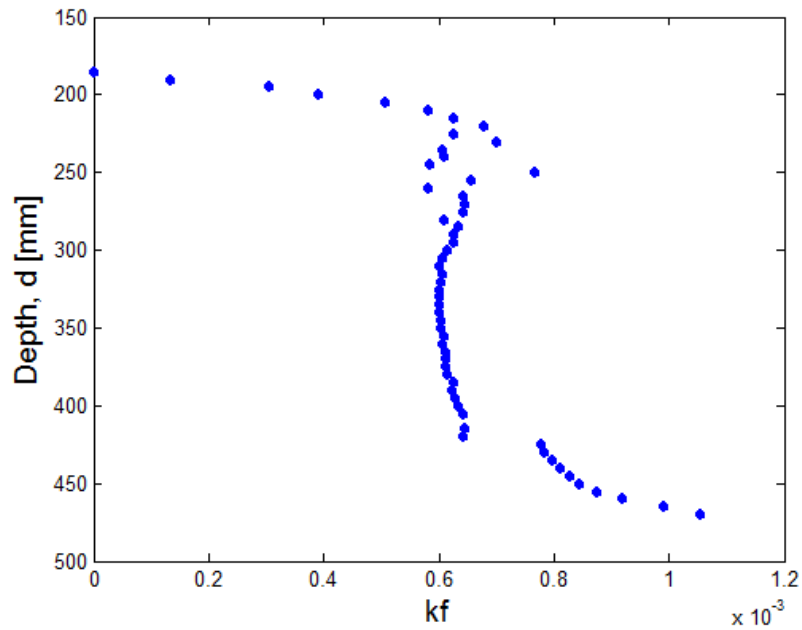


Figure 3.40: Excess of pore pressure created at the boundary during the uninstillation.

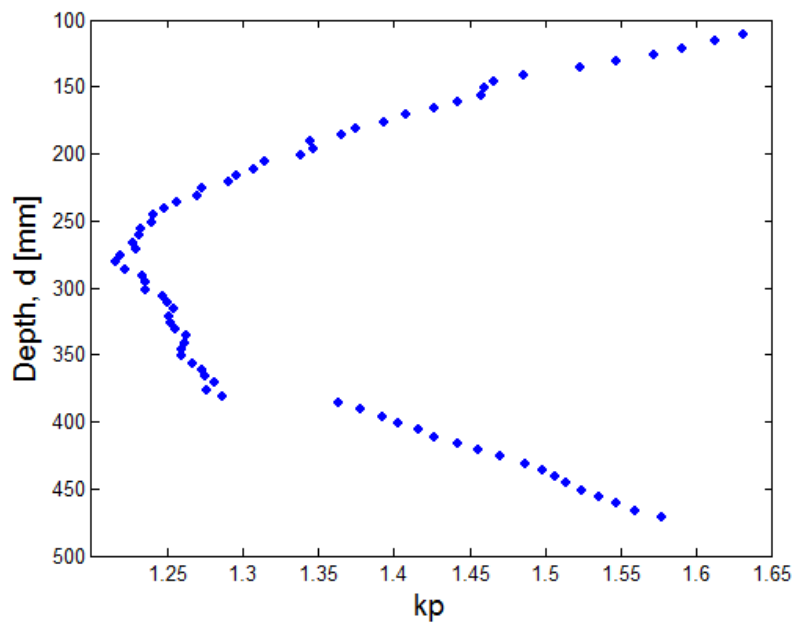
3.3.6 k_p and k_f Coefficients

k_p and k_f coefficients can be calculated again for this test. It is the same procedure than the one used with the previous test and it can be found in Appendix B and in Sgourakis et al. [2016]. The same CPT tests were used for the calculations and the explanation can be found in Table 3.6.

By the same means that used in the previous test, the k_f coefficient is calculated from the uninstillation data, since for this process only the skirt friction of the bucket is involved. Thus, the tip resistance is equal to 0. In order to calculate the internal skirt friction of the bucket, CPT1i and CPT4i are used. For the external skirt friction CPT2o and CPT3o are used. In Figure 3.41, results for k_f are illustrated over the depth. The first value, when the bucket is fully installed is 9.90×10^{-04} and the mean value is 6.30×10^{-04} .

Figure 3.41: k_f coefficient.

After k_f calculations, k_p coefficient can be calculated using the CPT tests before installation, along with the installation load. In Figure 3.42, results for k_p are illustrated over the depth. First value, when the bucket is fully installed, is 1.570 and the mean value is 1.210.

Figure 3.42: k_p coefficient.

NUMERICAL ANALYSIS 4

A numerical analysis has been carried out, in order to compare the results from the experimental work done in Aalborg University Laboratory. Suction installation and induced water pressure uninstillation tests, with different weights over the bucket were modeled. The Finite Element Program used for the calculation is PLAXIS 2D. An installation and uninstillation model (test 4 for both cases) are presented in this chapter. Rest of the experiments can be found in Appendix C. Tables 4.1 and 4.2 clarifies which installation and uninstillation tests, respectively, have been performed numerically and the location in the report of the results for each one.

Test Number	Characteristics	Numerical Model	Location in the Report
1	Suction+Force	Yes	Appendix C
2	Suction+Force	Yes	Appendix C
3	Suction+Force	Yes	Appendix C
4	Pure Suction	Yes	Chapter 4
5	Pure Suction	Yes	Appendix C
6	Pure Force	No	-
7	Pure Force	No	-
8	Pure Force	No	-
9	Pure Suction	Yes	Appendix C
10	Pure Force	No	-

Table 4.1: Installation tests.

Test Number	Characteristics	Numerical Model	Location in the Report
1	Uninstallation without weight	No	-
2	Uninstallation without weight	No	-
3	Uninstallation without weight	No	-
4	Uninstallation without weight	Yes	Chapter 4
5	Uninstallation with 201 kg	Yes	Appendix C
6	Uninstallation with 402 kg	Yes	Appendix C
7	Uninstallation with 402 kg	No	-
8	Uninstallation with 302 kg	Yes	Appendix C
9	Uninstallation with 302 kg	No	-
10	Uninstallation with 201 kg	No	-

Table 4.2: Uninstallation tests.

4.1 Dimensions of the Bucket Foundation and Model Properties

The dimensions of the bucket are the same as the ones tested in the laboratory, which means that the diameter, D was 1 m and the skirt length, h was 0.5 m. The penetration length investigated in the installation test was between 0.1 m and 0.5 m, with an interval of 0.1 m, simulating the real length of the bucket. For the uninstallation test the investigated penetration length was between 0.5 m, and 0.2 m, with an interval of 0.1 m, due to the fact that uninstallation finished always before the skirt of the bucket was fully outside the soil. The bucket foundation was simulated as an axisymmetric model. Half of the bucket was modeled due to symmetry. The bucket was modeled as an impermeable surface, where groundwater flow can not pass through. The surface does not have any parameter as no loading conditions on the structure of the bucket are involved, so no material is assigned to the bucket. The penetration length is normalized with the diameter of the bucket and the penetration ratio is obtained. Bucket and sandbox dimensions are shown in Figure 4.1. The generated mesh, along with the boundary conditions is presented in Figure 4.2.

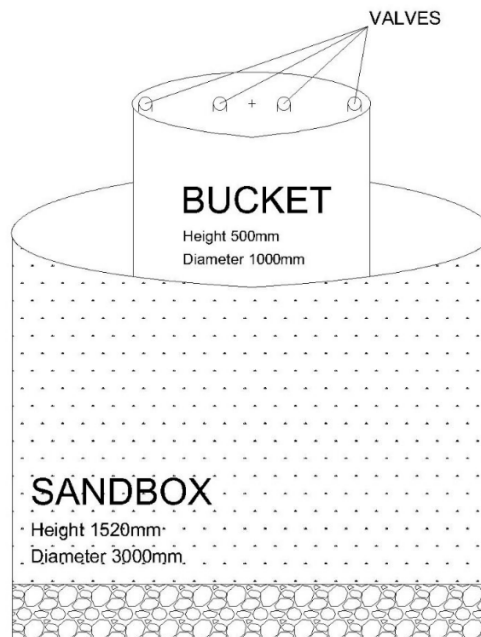


Figure 4.1: Dimensions of bucket and tank.

4.2 Calculation Model and Soil Parameters

The soil modeled as homogeneous, permeable with unit weight of 20 kN/m^3 . The model matches the characteristics of the sand, that was used in the laboratory. Calculations to check the seepage flow around the bucket in permeable soil, are performed for each penetration ratio. Steady-state groundwater flow was chosen and the groundwater head for the domain is set at 20 m above seabed. The calculation proceeds until a full-developed seepage state is achieved. Since, the groundwater head was set at 20 m above the seabed, the soil is saturated and permeability coefficient, k , is the only relevant parameter. USDA series system was chosen for the data set in flow parameters and Van Genuchten model is assigned. Since it is fully saturated flow, Van Genuchten model describes the flow with Darcy's law. The value of the permeability coefficient was set at 7.128 m/day (default value).

4.3 Boundary Conditions

The model boundaries were chosen in order to assure no influence on the results. The outer boundary and the bottom boundary were set to be 8 m, which is 8 times the diameter length. Chosen boundary does not affect pore pressure results in any of the simulations. Boundary limits are illustrated in Figure 4.2.

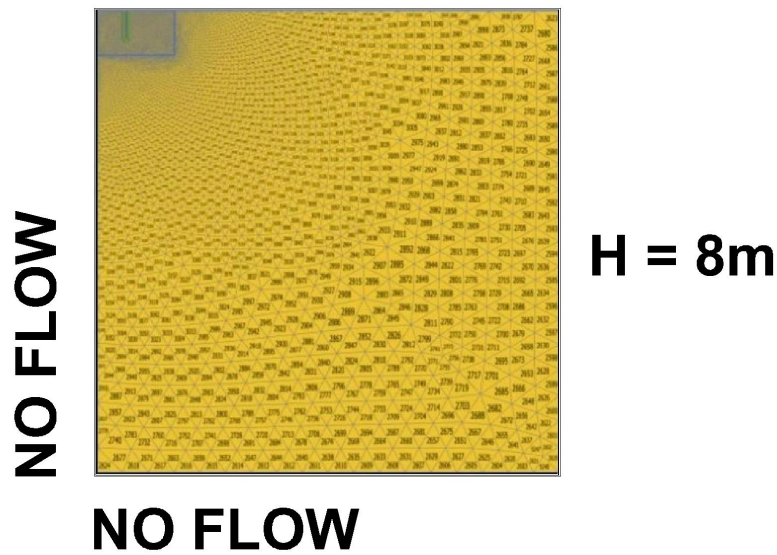


Figure 4.2: Boundary limits.

Additionally, the groundwater flow boundary conditions for the entire model were assigned. The left and bottom boundaries were closed for the flow. However, the free surface and the outer boundary have been prescribed pore pressure, coming from the established water level. Finally, in order to simulate suction a different head was set inside the bucket. As mentioned before the groundwater head was set at 20 *m*.

4.4 Convergence Analysis and Mesh

A domain size convergence analysis is performed for the case of installation with a penetration ratio 0.1. The upwards exit velocity of the groundwater flow at the free surface inside the bucket close to the skirt is investigated in relation with the number of elements used in the mesh. Results of convergence analysis are shown in table 4.3 and Figure 4.3.

Elements	Nodes	Exit Velocity
247	2120	7.258 m/day
436	3662	7.190 m/day
1003	8280	7.122 m/day
1727	14156	7.125 m/day
3519	28512	7.126 m/day
5126	41454	7.127 m/day
9014	72690	7.120 m/day

Table 4.3: Data for the convergence analysis.

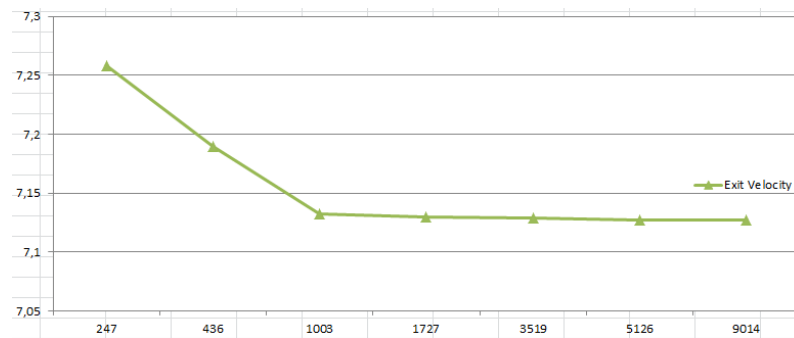


Figure 4.3: Convergence Analysis.

The mesh with 5126 elements is chosen. The mesh around the bucket was refined in order to get more accurate results, as it is the main interest of this study. As a result, the pore pressure can be extracted with more accuracy along the bucket wall. For the rest of the cases with different penetration ratios, along with the uninstalation cases, the meshes were chosen to be around the same number of elements. Thus it can be assumed that the convergence analysis is valid for all the cases. The chosen mesh is shown in Figure 4.4. The refined mesh around the bucket, which area is 0.78 m width and 0.78 m length, is shown in Figure 4.5.

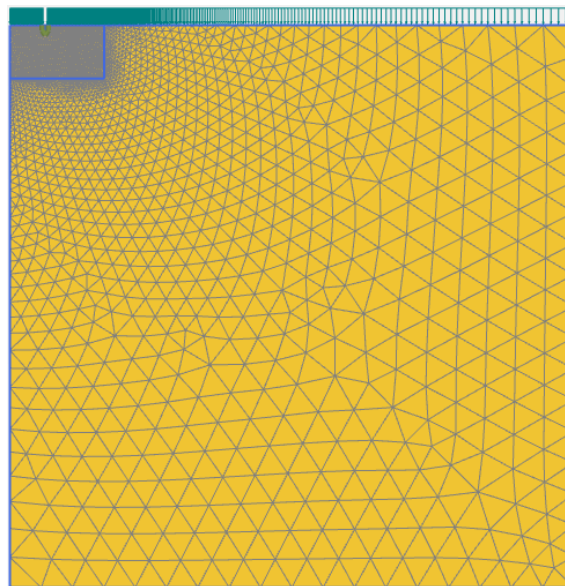


Figure 4.4: Mesh for penetration ratio 0.1.

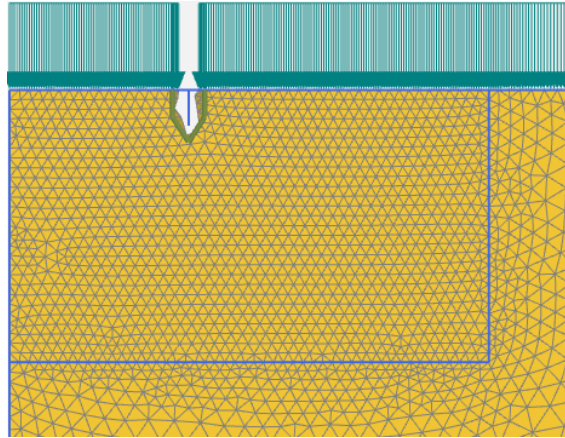


Figure 4.5: Refined mesh around the bucket for penetration ratio 0.1.

4.5 Calculation Phases-Steps of the Installation

In order to calculate the results, 2 phases for each penetration ratio were assigned. The phases were:

- **Initial phase:** Only soil volume was activated and the pore pressure in the soil is calculated based on the phreatic level. "Groundwater flow" calculation was only chosen.
- **Suction phase:** The surface that simulates the bucket skirt and interfaces were now activated. "Steady state groundwater flow" calculation type was chosen, in order to be time independent model. The interfaces on the surface were set to be impermeable. The behavior of the free surface inside the bucket was set as "Head" and an appropriate value of head is defined.

The changes in pore pressures due to applied head difference are calculated based on hydraulic conditions. Pore pressures from nodes on the interfaces are used for seepage flow analysis around the bucket skirt. The phases were the same for all the penetration ratios. In the following section, the results from installation and uninstallation test N_o 4 are presented, respectively.

4.6 Results

4.6.1 "Pure Suction" Installation, Test N_o 4

The installation model was separated in 5 discrete steps depending on the penetration ratio from 0.1 to 0.5, with an interval of 0.1. In order to simulate the applied suction, the hydraulic head at the free surface, inside the bucket was set lower than the groundwater level of the model. Therefore, the head difference is the applied suction and it increases with increasing penetration ratio. The conversion that must be done is 1 kPa equals to 0.1 m of head difference. This head difference, forces the downward movement of the

bucket. The following table shows the suction applied and its corresponding hydraulic head for each step of the installation.

Step	Penetration Ratio	Suction	Hydraulic Head
1	0.1	0.894 kPa	19.91 m
2	0.2	3.396 kPa	19.66 m
3	0.3	6.013 kPa	19.40 m
4	0.4	7.975 kPa	19.20 m
5	0.5	8.066 kPa	19.19 m

Table 4.4: Suction and hydraulic head used in each step of the installation.

The groundwater head for applied suction for penetration ratio of 0.1 is illustrated in Figure 4.6, while the groundwater head for applied suction, when the bucket is completed installed is shown in Figure 4.7. The development of the groundwater head during the installation of the bucket can be clearly seen. At the beginning of the test, the surrounding soil is more affected than in the end of the installation.

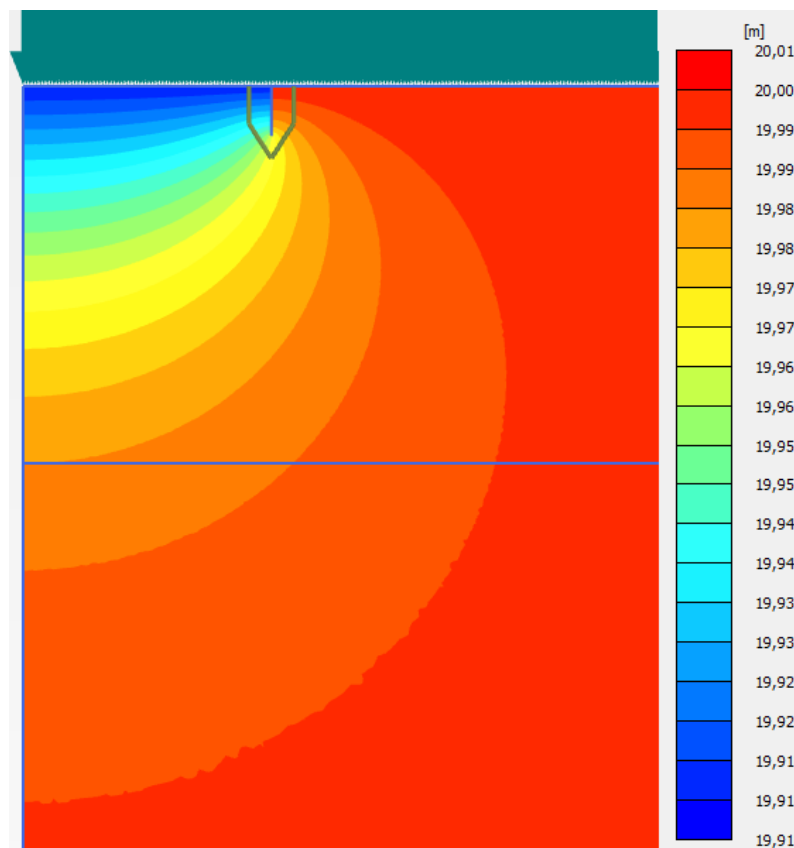


Figure 4.6: Groundwater head for applied suction for penetration ratio 0.1.

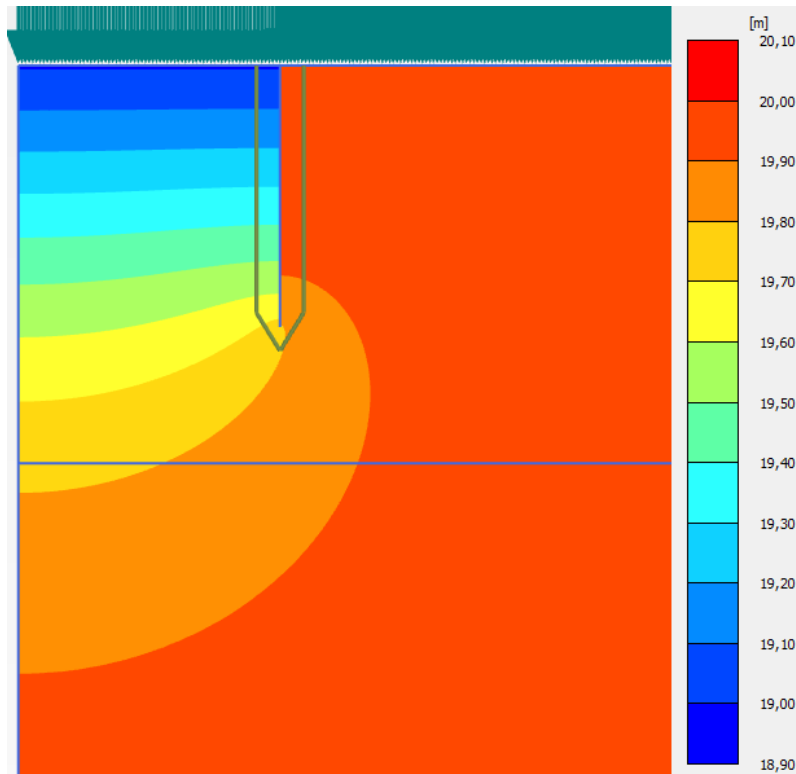


Figure 4.7: Groundwater head for applied suction for penetration ratio 0.5.

One of the first parameters that must be calculated is the critical suction that can be applied. The application of suction reduces the soil resistance at the tip of the bucket for an easier installation procedure. However, if the applied suction is over the critical value, at the free surface inside the bucket, soil penetration resistance is reduced to zero at the tip and piping occurs. If piping phenomena occurs, the installation of the bucket can not move forward and only water with sand would be pumped out.

All references to "exit", mean the free surface inside the bucket where suction is applied. The location where the "exit" parameters were obtained, is depicted with a red circle in Figure 4.8.

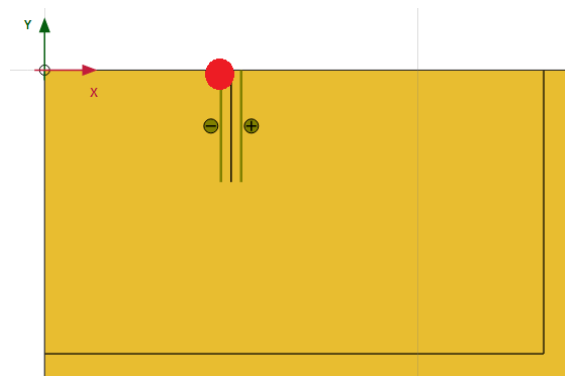


Figure 4.8: Location of "Exit".

The method used to calculate the critical suction is the one proposed by Senders and Randolph [2009]. Firstly, it is needed to calculate the value of the gradient at the exit with eq. 4.1. The value of the exit velocity is taken as close as possible of the bucket skirt.

$$i_{exit} = \frac{v_{exit}}{k} \quad (4.1)$$

Where,

i_{exit} Gradient at the free surface inside the bucket
 v_{exit} upwards exit velocity of the groundwater flow
 k Permeability coefficient

After calculating the exit gradient with the exit velocity, the seepage length at the exit can be calculated with the following equation:

$$s_{exit} = \frac{suction}{i_{exit}\gamma'} \quad (4.2)$$

Where,

s_{exit} Seepage length at the exit
 $suction$ Applied suction
 γ' Effective unit soil weight

Finally, the critical suction can be calculated with the following equation:

$$p_{crit} = s_{exit}\gamma' \quad (4.3)$$

The following table shows the values of these variables for each penetration ratio for test N_o 4:

Step	Penetration Ratio	Suction	v_{exit}	i_{exit}	s_{exit}	$p_{critical}$
1	0.1	0.894 kPa	2.790 m/day	0.391 –	0.228 m	2.285 kPa
2	0.2	3.396 kPa	6.162 m/day	0.865 –	0.393 m	3.928 kPa
3	0.3	6.013 kPa	8.096 m/day	1.136 –	0.529 m	5.294 kPa
4	0.4	7.975 kPa	8.683 m/day	1.218 –	0.655 m	6.547 kPa
5	0.5	8.066 kPa	9.462 m/day	1.327 –	0.823 m	8.234 kPa

Table 4.5: Variables values for test 4, for each penetration ratio.

It can be clearly seen that in the experiment, after penetration ratio of 0.2, the applied suction was over the theoretical critical suction. However, it is inconclusive if piping occurred, due to the fact that the bucket was fully installed. The numerical model is a simulation in order to have an overview of the real tests.

Finally, pore pressure factor, α , was calculated as a ratio of the excess pore pressure measured at the tip of bucket skirt to the applied suction and was found for all penetration ratios. The pore pressure factor was calculated with the following equation as:

$$\alpha = \frac{\Delta u_{tip}}{suction} \quad (4.4)$$

In the following table are shown the values of α for test N_o 4:

Step	Penetration Ratio	Suction	Δu_{tip}	α
1	0.1	0.894 kPa	0.353 kPa	0.394 –
2	0.2	3.396 kPa	1.123 kPa	0.330 –
3	0.3	6.013 kPa	1.707 kPa	0.284 –
4	0.4	7.975 kPa	1.980 kPa	0.248 –
5	0.5	8.066 kPa	2.263 kPa	0.207 –

Table 4.6: Values of the variables, for test N_o 4.

Numerical analysis performed by Housby and Byrne [2005] found a relatively good fit for the α factor, shown in equation 4.5.

$$\alpha = 0.45 - 0.36 \left[1 - \exp\left(\frac{h}{0.48D}\right) \right] \quad (4.5)$$

In figure 4.9 the pore pressure factor, α , is presented. The values from Plaxis are compared with the values extracted from the experiment in order to investigate deviations from Housby and Byrne [2005] solution and equation 4.5. It is obvious that α follows a decreasing path for increasing penetration ratio.

It can be clearly seen that numerical values from $h/D \geq 0.2$ are almost a perfect fit with the solution proposed by Housby and Byrne [2005]. However, the experiments show an abnormal path of α as expected, because only specific values of pore pressures were taken for the numerical analysis. That means that there is not a clear image of the what the values were the exact moment before and after the chosen value. That is something that can lead to inaccuracies.

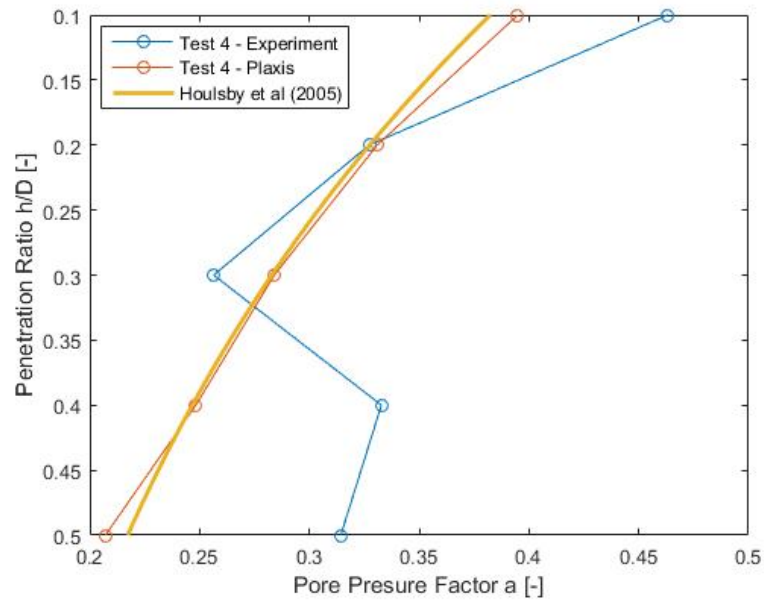


Figure 4.9: Pore pressure factor from experiments and Plaxis, along with Houlsby and Byrne [2005] solution from equation 4.5.

The development groundwater flow is shown in the next two figures. The groundwater flow for penetration ratio 0.1 is shown in Figure 4.10 and for penetration ratio of 0.5 in Figure 4.11.

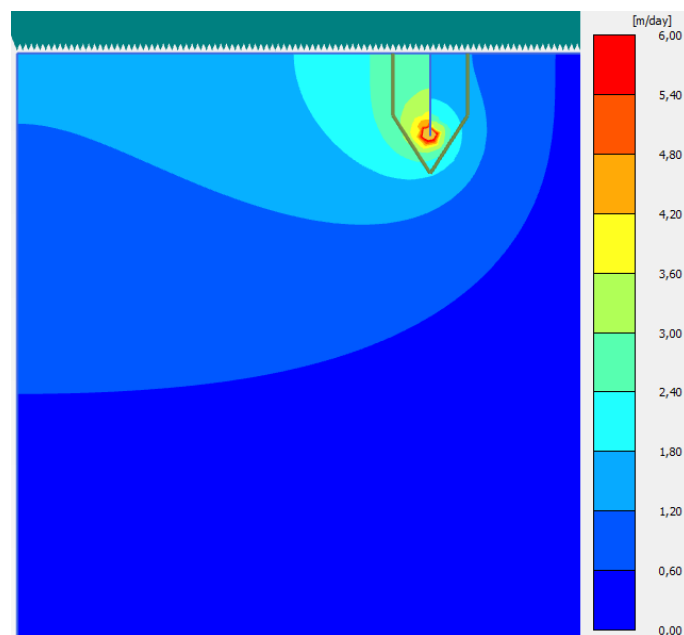


Figure 4.10: Groundwater flow for penetration ratio 0.1.

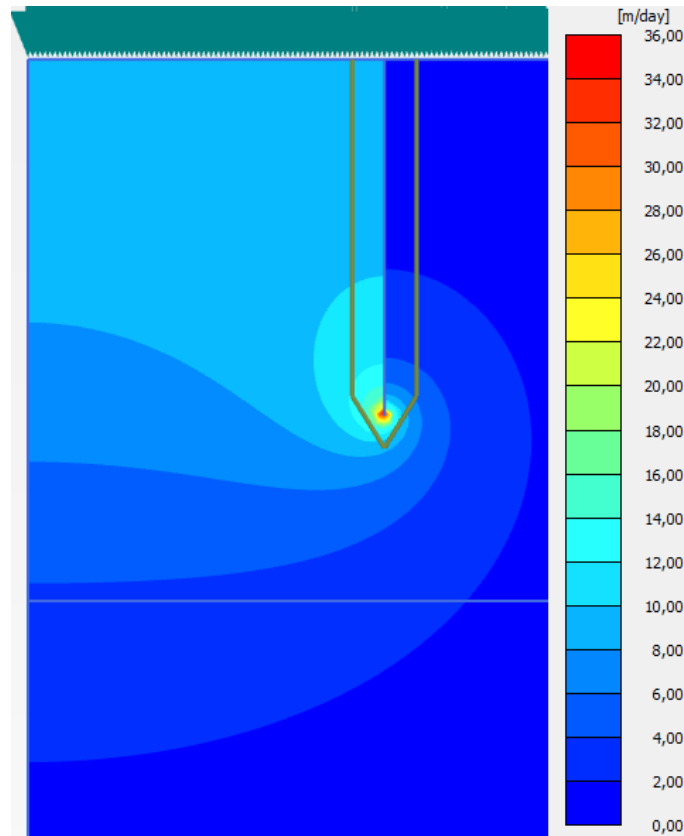


Figure 4.11: Groundwater flow for penetration ratio 0.5.

More suction applied leads to higher groundwater flow. Between the first step of the installation and last one, groundwater flow is 6 times larger. Finally, the seepage flow analysis is presented. Data from the different numerical models was obtained for the sake of calculating the seepage length. Seepage length is compared to the ones calculated with the data obtained from the experiments.

Senders and Randolph [2009] main formula to calculate the seepage in the different locations is as follows:

$$s = \frac{\textit{suction}}{\gamma_w i} \quad (4.6)$$

Where,

s	Seepage length
γ_w	Unit weight of the water
$\textit{suction}$	Applied suction
i	Hydraulic gradient

In order to calculate different seepage lengths at different locations, the hydraulic gradients are calculated from the following equations. The gradient first appears at the tip of the

bucket and then follows an upward path [Koterias et al. 2016]. Thus, the gradient at the tip of the bucket skirt, average inside, and average outside the wall of the foundation is calculated using the equations 4.7, 4.8 and 4.9, respectively.

$$i_{tip} = \frac{\Delta U_{in} - \Delta U_{out}}{2h_{zone}\gamma_w} \quad (4.7)$$

$$i_{avg,in} = \frac{suction - \Delta U_{tip}}{h\gamma_w} \quad (4.8)$$

$$i_{avg,out} = \frac{\Delta U_{top,out} - \Delta U_{tip}}{h\gamma_w} \quad (4.9)$$

Where,

i_{tip}	Hydraulic gradient around the tip
$i_{avg,in}$	Hydraulic gradient internal bucket wall
$i_{avg,out}$	Hydraulic gradient external bucket wall
ΔU_{tip}	Excess pore pressure at the tip
ΔU_{in}	Excess pore pressure inside the bucket next to the tip
ΔU_{out}	Excess pore pressure outside the bucket next to the tip
$\Delta U_{top,out}$	Excess pore pressure outside the bucket outside the bucket at the soil bed
$suction$	Applied suction
h_{zone}	Distance between the tip and locations where values ΔU_{out} and ΔU_{in} are obtained

It is crucial mentioning that numerical analysis in this section is based on calculations performed by Koterias et al. [2016], introducing a method based on DNV approach, called AAU CPT-based method, in which the effects of the seepage flow are included on the reduction of penetration resistance during installation.

Based on numerical calculations performed in finite element software Plaxis 2D and SEEP by Senders and Randolph [2009], a solution for the normalized seepage length was proposed, shown in equation 4.10. The results found to have an excellent fit with centrifuge models for installation of a suction bucket.

$$\left(\frac{s}{h}\right)_{exit} = \pi - \arctan \left[5 \left(\frac{h}{D}\right)^{0.85} \right] \left(2 - \frac{2}{2\pi} \right) \quad (4.10)$$

A study performed by Ibsen and Thilsted [2010], using finite element software FLAC 3D, proposed a similar solution for normalized seepage length, as shown in equation 4.11. The solution is based on results from installation of a suction bucket in Frederikshavn port.

$$\left(\frac{s}{h}\right)_{ref} = 2.86 - \arctan \left[4.1 \left(\frac{h}{D}\right)^{0.8} \right] \left(2 - \frac{2}{2\pi}\right) \quad (4.11)$$

Figure 4.12 presents results from the numerical calculations for the normalized seepage length for the exit, using the exit hydraulic gradient with respect to the fitted solutions from equations 4.10 and 4.11. The exit seepage length for the experiment was not possible to be calculate, since the exit velocity was not measured. Results for seepage length calculated from the average hydraulic gradient outside are presented in figure 4.13.

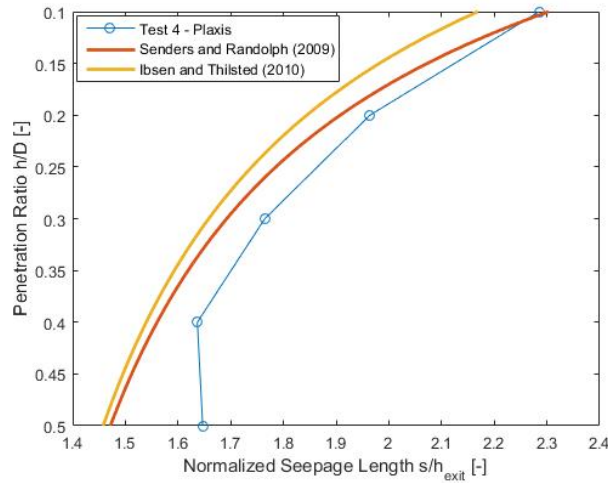


Figure 4.12: Normalized seepage length results for the exit hydraulic gradient, compared to the solutions from Ibsen and Thilsted [2010], equation 4.11 and from Senders and Randolph [2009], equation 4.10.

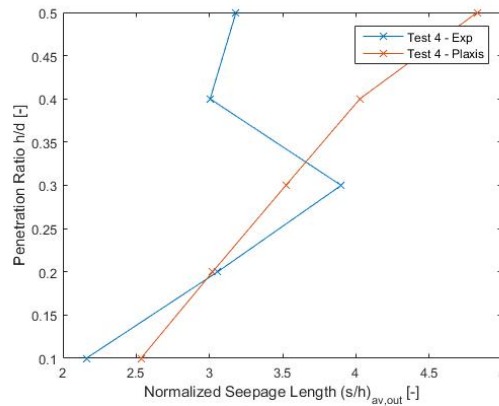


Figure 4.13: Normalized seepage length results using the average outside hydraulic gradient.

Results for seepage length calculated from the average hydraulic gradient inside are presented in figure 4.14.

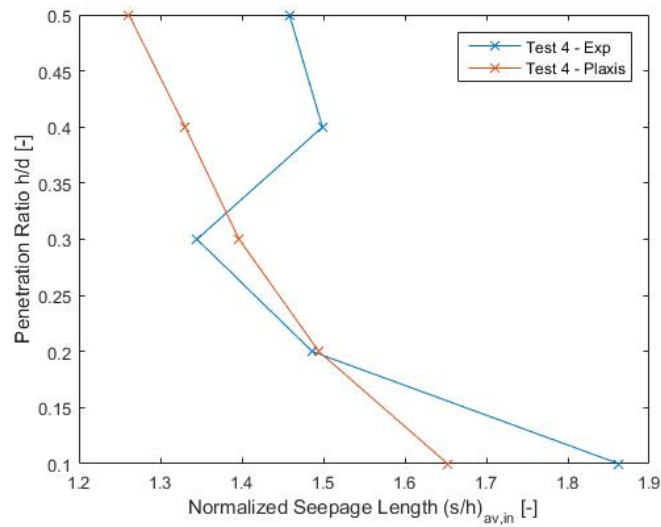


Figure 4.14: Normalized seepage length results using the average inside hydraulic gradient.

Results for seepage length calculated from the tip hydraulic gradient are presented in figure 4.15.

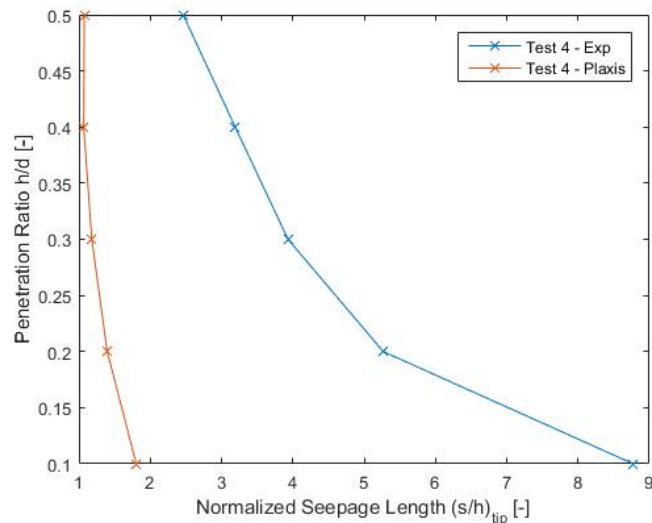


Figure 4.15: Normalized seepage length results using the tip hydraulic gradient.

The experimental values for the tip are quite higher in comparison to the ones from the Plaxis simulations. Additionally, seepage length shows a steady pattern of developing for the numerical calculation, while in the laboratory tests it increases at higher penetration ratios, for both $(s/h)_{av,in}$ and $(s/h)_{tip}$.

Comparing the seepage length at the tip to the average inside one, it can be concluded that

seepage is much higher at the tip than inside the bucket, which means that the reduction of penetration resistance at the tip is larger than inside the bucket wall, due to higher values of hydraulic gradient at the tip.

Normalized critical suction pressure is calculated based on the results of normalized seepage length at the exit, multiplying them with the penetration ratio h/D . That is the factor controlling piping failure, as mentioned in previous sections, which can cause the stop of the installation of the bucket. Based on numerical calculations performed in finite element software Plaxis and SEEP by Senders and Randolph [2009], by multiplying the equation of the normalized seepage length, shown in equation 4.10, with the penetration ratio h/D a solution for the normalized critical suction was found (equation 4.12).

$$\frac{p_{crit}}{\gamma' D} = \left(\frac{s}{h}\right)_{exit} \left(\frac{h}{D}\right) \quad (4.12)$$

From the study performed by Ibsen and Thilsted [2010], a similar solution for the critical suction, as shown in equation 4.13.

$$\frac{p_{crit}}{\gamma' D} = \left(\frac{s}{h}\right)_{ref} \left(\frac{h}{D}\right) \quad (4.13)$$

In the following figure, results by Feld [2001], Houlsby and Byrne [2005], Senders and Randolph [2009] and Ibsen and Thilsted [2010] are presented and compared with the numerical model.

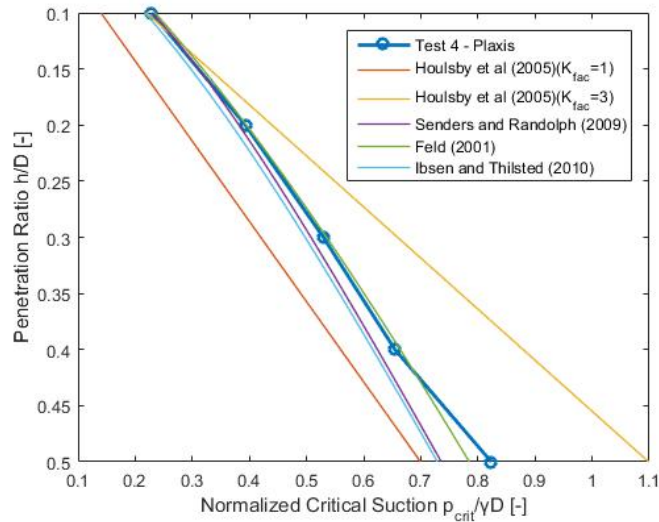


Figure 4.16: Normalized critical pressures calculated in Plaxis, in comparison to solution proposed by Feld [2001], Houlsby and Byrne [2005], Senders and Randolph [2009], and Ibsen and Thilsted [2010].

The analysis shows that the best correlation of normalized critical suction pressures is with the study conducted by Feld [2001] and Senders and Randolph [2009].

4.6.2 Uninstallation without Weight, Test N_o 4

For uninstallation tests, the investigated penetration length is between 0.5 m, when the bucket was fully installed, until 0.2 m, with an interval of 0.1 m. In order to simulate the applied pressure, the hydraulic head at the free surface inside the bucket was set higher than the groundwater level of the model. Therefore, the head difference is the applied pressure and it decreases with decreasing penetration depth. The conversion that must be done is 1 kPa equal to 0.1 m of head difference. This head difference forces a downward flow, causing upward movement of the bucket. The following table shows the pressure applied and its corresponding hydraulic head for each step of the uninstallation. The groundwater head for applied pressure for penetration ratio 0.5 is shown in Figure 4.17.

Step	Penetration Ratio	Pressure	Hydraulic Head
1	0.5	8.313 kPa	19.128 m
2	0.4	4.258 kPa	19.574 m
3	0.3	3.341 kPa	19.665 m
4	0.2	2.675 kPa	19.733 m

Table 4.7: Pressure and hydraulic head used in each step of the uninstallation.

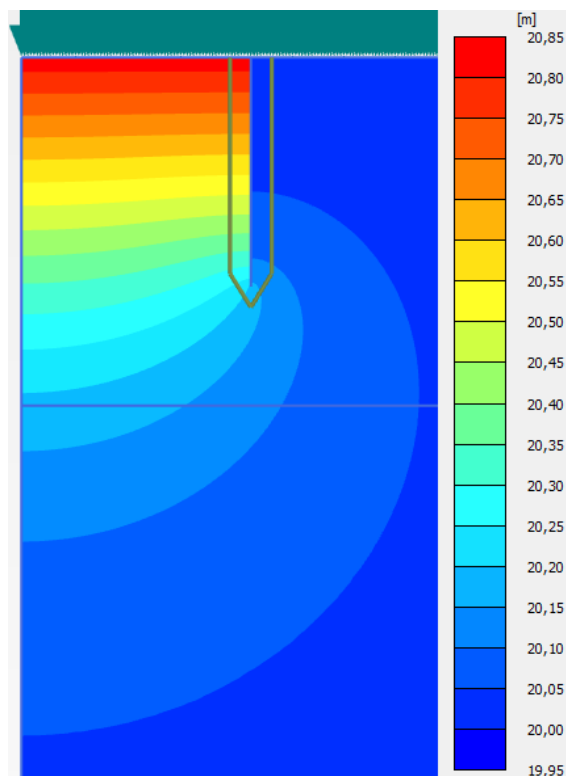


Figure 4.17: Groundwater head for applied pressure for penetration ratio 0.5.

The groundwater head for applied pressure for penetration ratio 0.2 is shown in Figure 4.18.

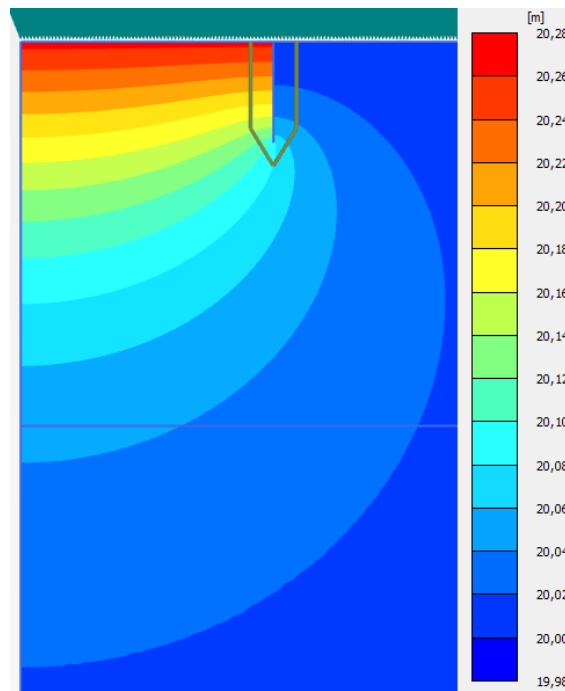


Figure 4.18: Groundwater head for applied pressure for penetration ratio 0.2.

One of the first parameters that must be calculated is the critical pressure that can be applied. If critical pressure is higher than the applied one, then uninstillation will stop. The location of the "exit" parameters obtained are illustrated with a red circle in Figure 4.19.

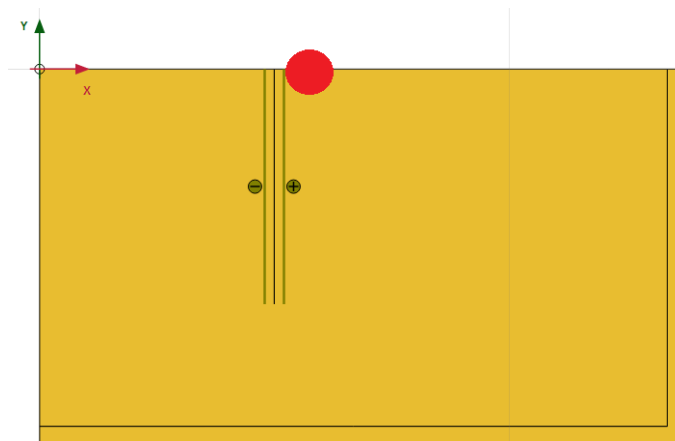


Figure 4.19: Location of "exit" for uninstillation.

The method used to calculate the critical pressure is the same as the one used for the installation by Senders and Randolph [2009]. The only difference is that the exit velocity is taken outside of the bucket skirt. The following table shows the values of the variables

for each penetration length in test number 4:

Step	Penetration Ratio	Pressure	v_{exit}	i_{exit}	s_{exit}	$p_{critical}$
1	0.5	8.313 kPa	1.011 m/day	0.142 –	5.861 m	58.611 kPa
2	0.4	4.258 kPa	0.807 m/day	0.113 –	3.761 m	37.609 kPa
3	0.3	3.341 kPa	1.037 m/day	0.145 –	2.296 m	22.965 kPa
4	0.2	2.675 kPa	1.575 m/day	0.221 –	1.211 m	12.106 kPa

Table 4.8: Values of the variables for each penetration ratio for test N_o 4.

The development of groundwater flow is shown in the following 2 figures. The groundwater flow for penetration ratio of 0.5 is shown in Figure 4.20 and for penetration ratio 0.2 in Figure 4.21.

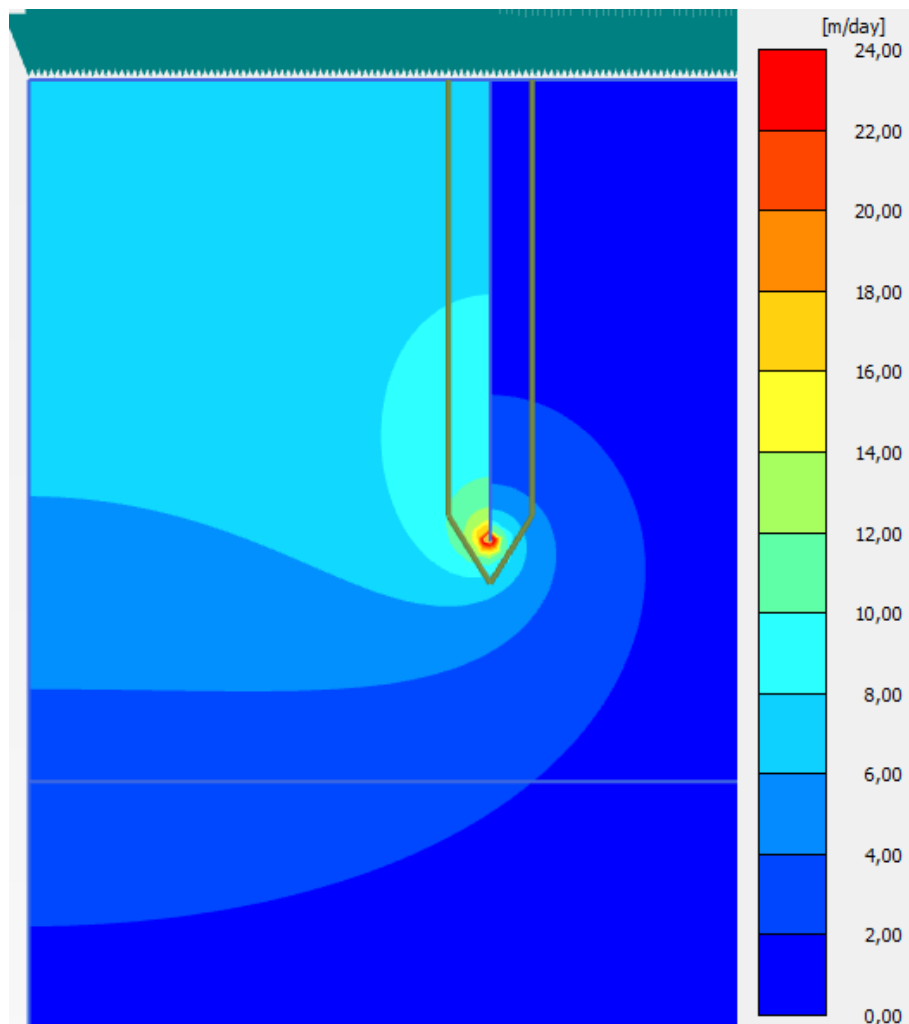


Figure 4.20: Groundwater flow for penetration ratio of 0.5.

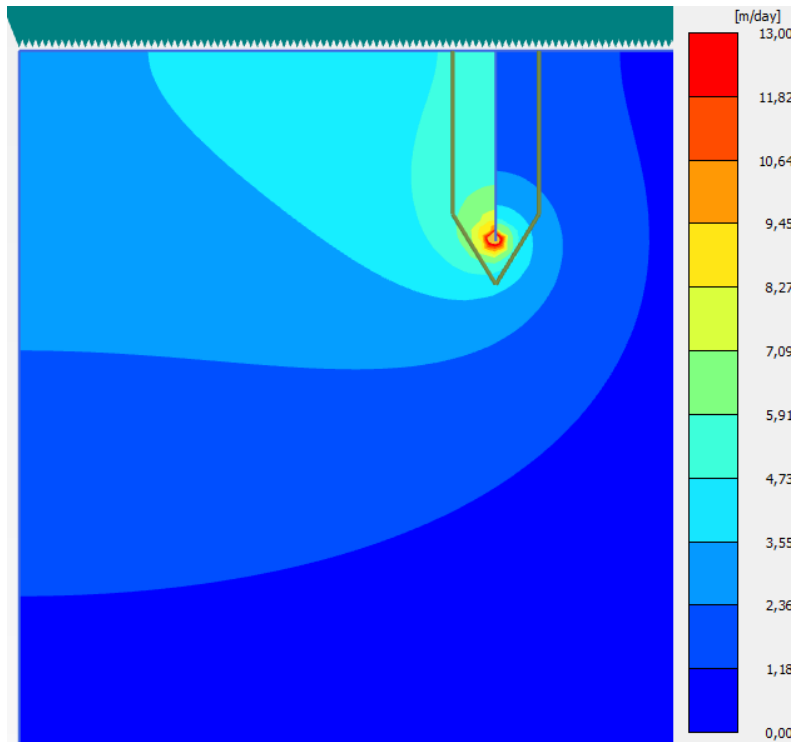


Figure 4.21: Groundwater flow for penetration ratio of 0.2.

More suction applied leads to lower groundwater flow. Between the first step of the installation and last one, groundwater flow is 2 times smaller.

Figure 4.22 illustrates the application of pressure over time for all the experiments that simulated with Plaxis 2D. The observed peaks are called break points, due to the fact that after the pressure at that point, the bucket starts moving upwards. After that point, the pressure is decreased until it reaches a certain value, responsible for the full uninstallation of the bucket.

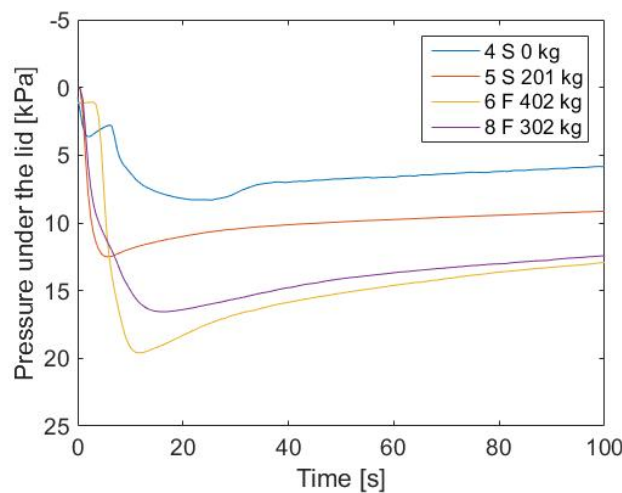


Figure 4.22: Pressure applied over time for all the tests simulated in Plaxis 2D.

Furthermore, Figure 4.23 shows the pore pressure factor obtained from the uninstillation procedure for Plaxis, compared to Houlsby and Byrne [2005] solution. It is obvious that α follows an increasing path over the uninstillation depth, as expected. Moreover, results from the numerical analysis are an almost perfect fit compared to the theoretical solution, thus the method and chosen model are considered to be valid.

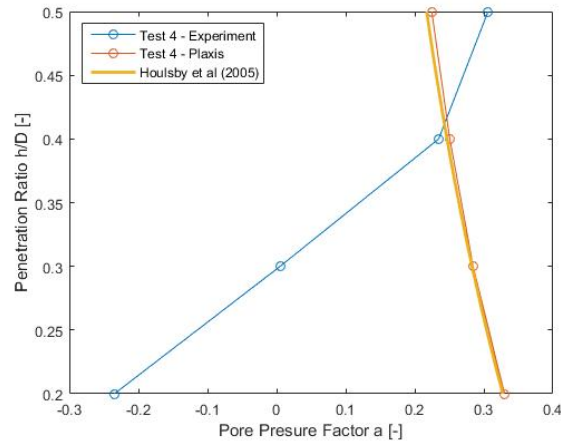


Figure 4.23: Pore pressure factor results from uninstillation in Plaxis and results from the experiment, along with Houlsby and Byrne [2005] solution.

Figures 4.24 and 4.25 illustrate the normalized seepage length during uninstillation for the average hydraulic gradient inside and at the tip, respectively. The development of the seepage length for the uninstillation follows the same pattern as in the installation procedure. Again the values at the tip seem to be higher for the tip than inside the skirt of the bucket. As mentioned before, the differences between the numerical values compared to the experimental ones are due to the fact that Plaxis after each step of calculation let the seepage dissipate in comparison to the real experiments, where that is not the case. As a conclusion, decreasing values of seepage length over the depth are observed for the laboratory uninstillation, while the numerical values show a steady path.

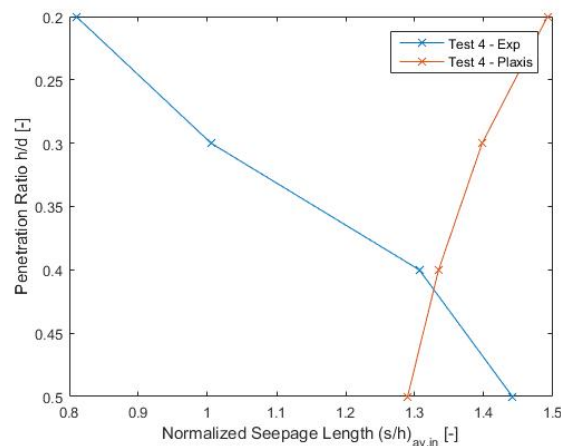


Figure 4.24: Normalized seepage length, using the average inside hydraulic gradient.

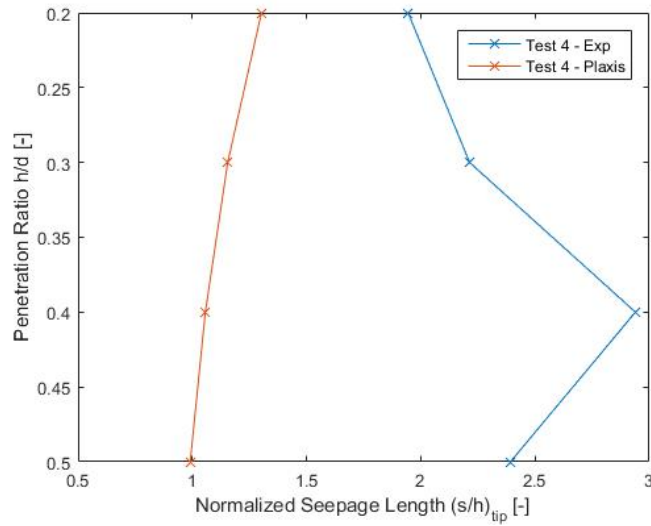


Figure 4.25: Normalized seepage length, using the average tip hydraulic gradient.

Finally, as far as the pressure applied for the uninstillation is concerned, Figure 4.26 depicts that it never exceeded the theoretical critical pressure from the numerical simulations. That means that no piping channels were created during uninstillation and that there were not any signs of severe soil damage until the water flowed out of the bucket skirt.

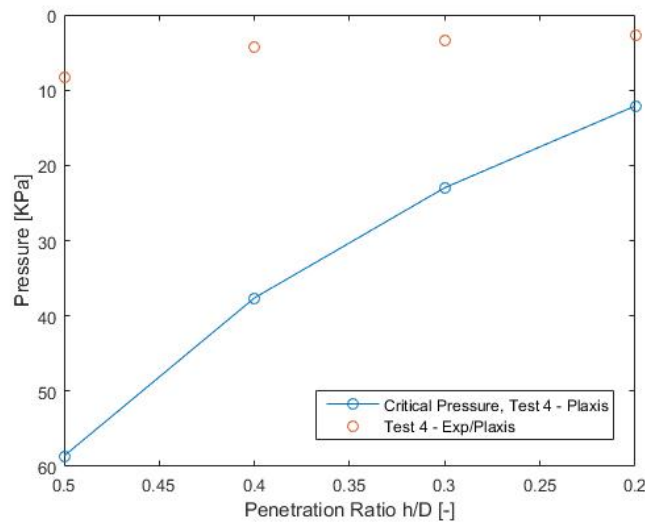


Figure 4.26: Critical suction from numerical simulation compared to the real pressure applied for uninstillation test N_o 4.

**ARTICLE I: SEEPAGE
ANALYSIS FOR SUCTION
INSTALLATION AND
UNINSTALLATION OF BUCKET
FOUNDATIONS IN SAND**

5

Seepage analysis for suction installation and uninstallation of bucket foundations in sand

T. Gitsas¹, H. M. Pandiella¹, G. N. Sgourakis¹, L. B. Ibsen¹, A. Koterass¹

Abstract

Suction bucket foundations have been used for many years in offshore industry, to support oil and gas platforms. Recently they are considered an attractive and cost effective way of supporting offshore wind turbines. Its effectiveness derives from the fact that suction, which is applied under the lid of the bucket, make installation an easier and more quiet process. When suction is applied, the downward force, due to pressure differential under the lid, increases gradually. However, in sandy soils (high coefficient of permeability) a flow between the voids of the soil is created, called seepage flow. Moreover, suction increases the excess pore pressure of the soil, leading to a decrease of the penetration resistance, making the installation of the foundation easier. The scope of this paper is to analyze and investigate the characteristics of the seepage around the bucket during the installation and uninstallation procedure of the bucket foundation. In order to achieve that, a number of medium scale experimental tests have been conducted in the laboratory facilities of Aalborg University, along with numerical simulations, resembling the experimental ones. Seepage flow around the bucket, during installation and uninstallation, is examined. The laboratory tests, as well as the numerical analysis of the flow consider homogeneous sand soil profile. Furthermore, critical pressure is calculated during seepage analysis, regarding its importance for maintaining the hydraulic seal between the skirt of the bucket and the surrounding soil. If the hydraulic seal breaks, localized piping channels are created, which may cause the bucket not to be fully installed. Results of normalized seepage length at the tip, inside and at the exit of the bucket skirt are presented and compared with solutions from other studies. The analysis confirms that the soil resistance at the tip is reduced the most during installation.

Keywords

Installation procedure — Uninstallation procedure — Critical suction — Bucket foundation — Offshore foundations — Seepage length.

¹ Department of Civil Engineering, Aalborg University, Denmark

1. Introduction

Due to expansion of the renewable energy industry, the need of creating wind farms in more challenging offshore sites has grown. These sites concern both different soil conditions and water depths (Koterass et al., 2016). Furthermore, offshore locations can allow bigger capacity wind turbines, maximizing the potential of each wind farm, without raising any objections for aesthetic reasons (Byrne and Houlsby, 2003). One of the biggest problems confronting the renewable energy industry is the installation of wind turbines in sea water, which is a much more complicated procedure than onshore. A proper and feasible installation can lead to higher levels of energy production along with lower costs and smaller impact on the environment (Lian et al., 2014).

In recent years, skirted foundations and anchors have become a more attractive solution for various types of offshore structures (Andersen et al., 2008). Specifically, the suction bucket is considered one of the most feasible solutions for wind turbine foundations. Its feasibility arises from the fact that the installation process can be a quicker, quieter and more cost effective solution compared to the

monopiles, the foundation most widely used in offshore wind turbine industry (Tjelta, 2015). Additionally, a wind turbine has a higher horizontal load and applied moment compared to the vertical one, thus the suction bucket provides a proper way of transferring these environmental loads to the seabed (Byrne et al., 2001).

Although suction bucket seemingly have a lot of advantages, the installation procedure, especially in sand and layered soils, is very challenging. Installation can be divided in two parts, the self-weight penetration and the suction installation. Self-weight penetration ensures a seal component at the edge of the bucket with the surrounding soil, in order for the suction component, under the lid of the bucket, to be performed adequately (Houlsby and Byrne, 2005). Generally, in clay the suction used is small. However, in sandy soils the penetration resistance is high, thus an under-pressure is applied within the skirt compartment to produce an increased driving force in addition to the self-weight. Suction will also, form hydraulic gradients in the sand at the tip, inside and outside the bucket skirt, which will reduce the penetration resistance of the soil (see fig. 1). Nevertheless, it is very important to mention that

exceedance of the critical hydraulic gradient may cause piping channels along the skirt, where loosening or failure of the soil is most probable to happen. The design must predict the required suction applied that will not exceed its critical value (Andersen et al. (2008), Ibsen and Thilsted (2010)).

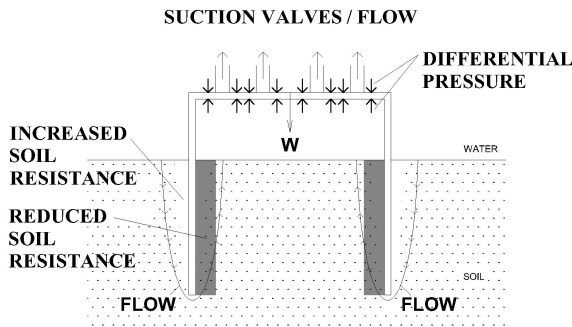


Figure 1. Seepage flow for suction installation.

This paper addresses an analysis of the seepage flow, produced by the suction under the lid of the bucket. The analysis is based on 5 suction installation and 4 induced water pressure uninstallation tests of a scaled bucket, conducted in the laboratory facilities of Aalborg University. The height of the model was 0.5 m and the diameter 1 m. Pore pressures were measured at the skirt tip and skirt wall around the bucket, as illustrated in Figure 2, by pressure transducers. The measured pressures were analyzed in order to give a good representation of the seepage length around the bucket, during installation and uninstallation. The critical pressure for each test is also calculated, along with the pore pressure factor, α , which relates the applied suction with the excess pore pressure at the tip of the bucket, Δu_{tip} . Those tests were resembled in the finite element software PLAXIS 2D, using the real suction applied during installation and the real induced water pressure during the uninstallation of the bucket in the laboratory. Results are being compared and deviations are discussed concerning a pattern of how the seepage flow affects the installation or the uninstallation of the bucket. In section 2 existing theories on the suction installation are presented. In sections 3 and 4 a brief procedure of the laboratory and numerical tests is displayed, respectively. The calculation methodology can be found in section 5, while in sections 6, 7 and 8 all the results are discussed and concluded respectively.

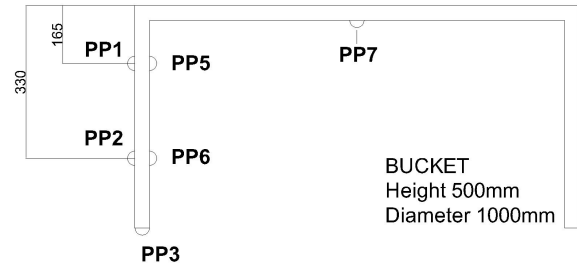


Figure 2. Pressure transducers at the skirt, the skirt tip and under the lid of the bucket on the laboratory model.

2. State of the art for seepage flow and installation procedure of the suction bucket foundation

Installation standards of bucket foundations are usually based on theories regarding pile foundations. It can be assumed that the bucket works as an open ended pile. The most common one was proposed by American Petroleum Institute (2000) concerning open ended pile foundations. Soil resistance is assumed to be the sum of the external shaft friction, the end bearing on the pile wall annulus and the total internal shaft friction or the end bearing of the plug. Additionally, the unit end bearing is dependent on the dimensionless bearing capacity factor, N_q and on the effective overburden pressure, p_o .

Det Norske Veritas Institution, also called DNV, presented a study in 1992 about penetration resistance of skirts. DNV suggests that penetration resistance of the steel skirts is the sum of friction resistance, inside, outside and at the tip of the bucket skirt, where calculations should be based on the results of in-situ testing supported by laboratory tests. For the field tests CPT data was used, since it gives a continuous record of the cone penetration resistance over the depth.

DNV method for calculating the penetration resistance based on results from CPT tests, is presented in the following eq. as:

$$R = A_{tip} k_p q_c(z) + \pi D_l k_f \int_0^z q_c(l) dz + \pi D_o k_f \int_0^z q_c(l) dz \quad (1)$$

Where,

A_{tip}	Area of the tip of the bucket
z	Penetration depth
k_p	Empirical coefficient related to the tip resistance
k_f	Empirical coefficient related to the skirt friction
q_c	Cone resistance
D_I	Inner diameter of the bucket
D_O	Outer diameter of the bucket

From both the above mentioned theories several uncertainties remain, regarding the conversion from one type of penetration resistance to another. As an example, the excess pore pressures along with the seepage flow effects are not being investigated regarding the reduction of penetration resistance. Houlsby and Byrne (2005) proposed a method based on numerical calculations, assuming that the distribution of pore pressure on the inside and outside the skirt of the bucket varies linearly with depth. Pore pressure factor, α , was calculated relating the excess pore pressure at the tip of the bucket skirt, Δu_{tip} , with the applied suction, p as:

$$\alpha = \frac{\Delta u_{tip}}{p} \quad (2)$$

Theoretically, a value of 0.5 is expected for $h/D = 0$ and a value of 0 when h/D is very large, for uniform permeability soil situation. Numerical analysis performed by Houlsby and Byrne (2005) found a relatively good fit for the results, shown in eq. 3.

$$\alpha_1 = 0.45 - 0.36 \left[1 - \exp\left(-\frac{h}{0.48D}\right) \right] \quad (3)$$

Furthermore, rewriting Houlsby and Byrne (2005) calculations in terms of critical suction, which if exceeded can cause piping of the soil, the following eq. is proposed:

$$\frac{p_{crit}}{\gamma' D} = \frac{h}{D} \left(1 + \frac{\alpha_1 k_{fac}}{1 - \alpha_1} \right) \quad (4)$$

Where, k_{fac} is the ratio k_i/k_o (k_i and k_o is the permeability inside and outside of the bucket respectively and $k_i \geq k_o$) that represent the soil permeability during suction, when the soil inside the bucket loosens, causing a higher permeability coefficient.

A simpler approach based on an assumed linear decrease in internal friction and end bearing, as the suction pressure increases from zero up to the critical value causing internal piping, was proposed by Senders and Randolph (2009). According to their research, the critical hydraulic gradient occurs at the tip of the bucket. However, due to sand constrained by other materials at that point, it was observed that the hydraulic gradient that controls when piping will occur is the exit gradient adjacent to the skirt of the

bucket. That gradient was used to estimate the reduction in penetration resistance and presented in the following eq. as:

$$i = \frac{p}{\gamma_w s} \quad (5)$$

Where, s denoted as the seepage length, γ_w as the unit weight of the water and p as the applied suction.

The critical hydraulic gradient for piping to occur, is given by eq. 6.

$$i_{crit} = \frac{\gamma'}{\gamma_w} \quad (6)$$

Therefore, the critical pressure against piping is defined as:

$$p_{crit} = s \gamma_w i_{crit} = s \gamma' \quad (7)$$

Where, γ' is the effective soil unit weight.

Based on numerical calculations performed in finite element software Plaxis and SEEP by Senders and Randolph (2009), a solution for the normalized seepage length was proposed, shown in eq. 8. The results found to have an excellent fit with centrifuge models for installation of a suction bucket. Moreover, by multiplying the eq. with the penetration ratio h/D a solution for the normalized critical suction was found (eq. 9).

$$\left(\frac{s}{h}\right)_{exit} = \pi - \arctan \left[5 \left(\frac{h}{D}\right)^{0.85} \right] \left(2 - \frac{2}{2\pi} \right) \quad (8)$$

$$\frac{p_{crit}}{\gamma' D} = \left(\frac{s}{h}\right)_{exit} \left(\frac{h}{D}\right) \quad (9)$$

A study performed by Ibsen and Thilsted (2010), using finite element software FLAC 3D, proposed a similar solution for normalized seepage length and critical suction, as shown in equations 10 and 11, for homogeneous sand soil profiles. The solution is based on results from installation of a suction bucket in Frederikshavn port.

$$\left(\frac{s}{h}\right)_{ref} = 2.86 - \arctan \left[4.1 \left(\frac{h}{D}\right)^{0.8} \right] \left(2 - \frac{2}{2\pi} \right) \quad (10)$$

$$\frac{p_{crit}}{\gamma' D} = \left(\frac{s}{h}\right)_{ref} \left(\frac{h}{D}\right) \quad (11)$$

Finally, Feld (2001) performed finite element analysis in SEEP and proposed a solution for the normalized critical suction as following:

$$\frac{p_{crit}}{\gamma' D} = 1.32 \left(\frac{h}{D} \right)^{0.75} \quad (12)$$

This article addresses results of seepage flow in homogeneous sand around the bucket, trying to investigate a correlation between the medium scaled laboratory tests and the above mentioned numerical theories. Furthermore, investigation of correlations between the critical pressures for each depth of penetration with known theories is performed.

3. Materials, equipment and procedure of the laboratory tests

In the laboratory facilities of Aalborg University suction installation and induced water pressure uninstallation tests were performed between the period of January and May 2016. The dimensions of the bucket foundation model were 1 m in diameter, D , 0.5 m in skirt height, h and 3 mm in skirt thickness, t , which corresponds to prototype foundation model with ratio of $h/D = 0.5$ (see figure 3). The material that the bucket was made of is steel and its self weight was calculated at 201 Kg or 2.01 KN. Pressure transducers were placed on the skirt of the bucket and under the lid, as shown in Figure 2, measuring excess pore pressures during installation and uninstallation. The tests were performed in a large container (sandbox) filled with gravel for the first 0.3 m and with Aalborg University No.1 sand for the next 1.2 m. Container's diameter and height were 3 and 1.52 m, respectively. A hydraulic piston used as an assisting driving tool during the whole procedure.

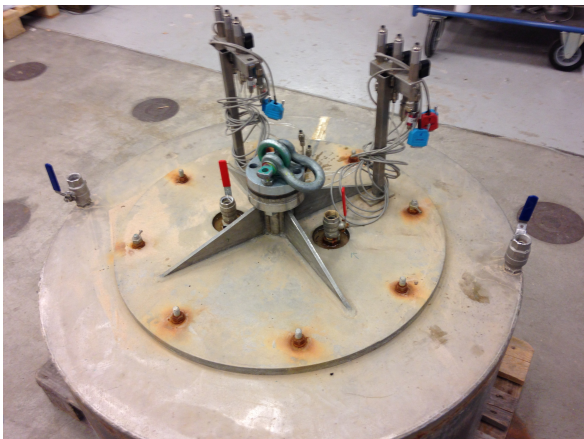


Figure 3. Foundation model used in the laboratory.

Before each experiment the soil was saturated and compacted with the use of a vibrator. The purpose of this procedure for each experiment, was to have a planned density

of the sand, regarding the fact that the soil was disturbed in the end of each test. In order to ensure good compaction of the soil, 4 CPT's were performed before each test and values of cone resistance, q_c and relative density, D_r , were acquired (see figure 4). Table 1 illustrates all suction installation and induced water pressure uninstallation tests, with their corresponding water level. Keeping the water level steady at all times during testing, assist us to correct the pore pressures with the hydrostatic one.

Test Number	Characteristics	Water Level [cm]
1 Inst.	Suction+Force	8
2 Inst.	Suction+Force	8
3 Inst.	Suction+Force	13
4 Inst.	Pure Suction	11
5 Inst.	Pure Suction	11
9 Inst.	Pure Suction	10
4 Uninst.	Uninstallation without weight	11
5 Uninst.	Uninstallation with 201K g	11
6 Uninst.	Uninstallation with 402K g	10
8 Uninst.	Uninstallation with 302K g	8

Table 1. Description of installation and uninstallation tests.

In order to achieve suction installation, four valves were placed on top of the bucket and connected with small hoses that could pump out the water. Those hoses were connected to a vacuum, which controlled the application of underpressure inside the bucket. Installation started after self-weight penetration for the sake of ensuring a seal component at the edge of the bucket with the surrounding soil (Koterass et al., 2016). In the tests denoted as "Pure Suction" in table 1, the application of suction started right after the self-weight penetration. However, in the tests denoted as "Suction + Force", additionally to the self-weight penetration, 2.01 KN more were applied before suction begun. That happened in order to resemble double the self-weight of the bucket and investigate any major differences in the 2 procedures (see Gitsas et al. (2016)). Installation finished half an hour after the displacement transducer stopped giving any signal on the computer, in order to ensure that the installation was fully completed.

As far as the uninstallation procedure is concerned, it was performed using one of the buckets valves for applying water pressure, while the other three remained closed at all times. Pressure transducer, PP7, measured the applied pressure at all times. The values obtained from the other pressure transducers were used in order to make calculations for the seepage analysis. Uninstallation finished when

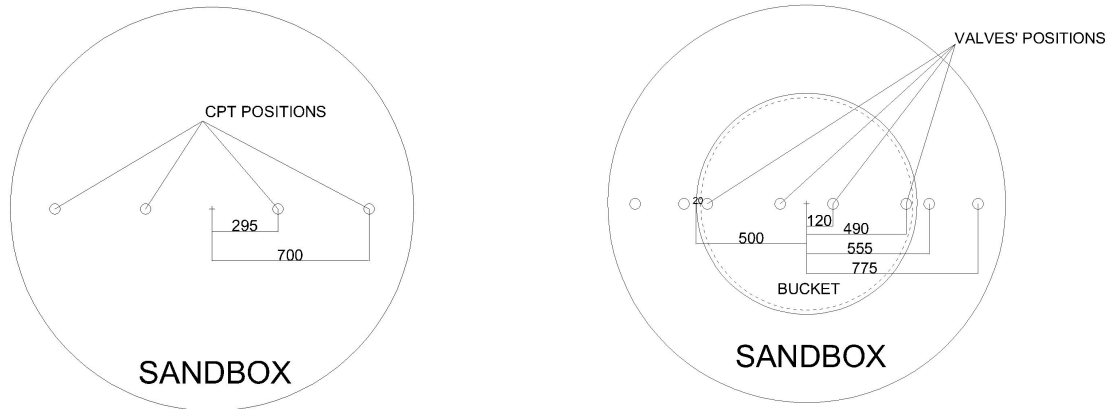


Figure 4. CPT's performed before and after installation [mm].

water flowed out of the foundation skirt.

Finally, in order to investigate any pressure changes on the boundaries, a beam with three pressure transducers was placed at the edge of the sandbox. The length of the beam was 1 m and the transducers were placed at the tip, over 0.25 m and 0.5 m of the tip, respectively. The transducers recorded data during both installation and uninstallation. Results revealed that the boundaries were slightly affected by the application of suction. A more detailed explanation for the procedure, along with all the data acquired from the tests in table 1, can be found in Gitsas et al. (2016).

4. Modeling procedure and assumptions in PLAXIS 2D

Regarding the seepage analysis, finite element software PLAXIS 2D was used. The bucket's circular geometry allows to create an axisymmetric model of diameter 0.5 m. On the one hand, installation procedure was separated in discrete steps of penetration ratio, $0.1 \leq h/D \leq 0.5$ (5 steps). On the other hand, uninstallation's discrete phases were only 4 ($0.5 \leq h/D \leq 0.2$), because laboratory tests showed that water flowed under the skirt of the bucket before it was fully uninstalled (around 0.35m of upward movement before it breaks out, see Gitsas et al. (2016)). Both cases were made with respect to the medium scale tests. Figure 5 shows the geometry of the bucket used for the analysis. Additionally, equilibrium between the driving forces and the soil penetration resistance is assumed (Koterass et al., 2016).

The model representing the wall of the bucket, was created from simple impermeable interfaces. As explained in the previous section, the boundaries set in the laboratory (around 2 m away from where the installation took place) did not show any significant changes in excess pore pressures. For this reason, the boundaries in PLAXIS were

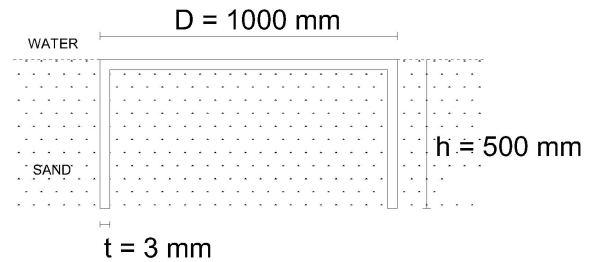


Figure 5. Simple model of the bucket penetrating in homogeneous sand, used for numerical calculations.

selected to be 16 times the diameter of the bucket for both the outer and the bottom boundary (Figure 6). For the sake of resembling the suction installation and the water induced pressure uninstillation, groundwater flow boundary conditions need to be applied. The free surface boundaries and the outer boundary were set at a prescribed hydraulic head value (20 m above seabed). For the installation and the uninstillation a smaller and higher value of pressure head is assigned, respectively, inside the bucket. In both cases, seepage was created around the bucket skirt. For "Suction + Force" tests, the following eq. was used to transform force into pressure.

$$P = \frac{F}{A} \tag{13}$$

Where, F is the applied force and A is the area under the lid of the bucket.

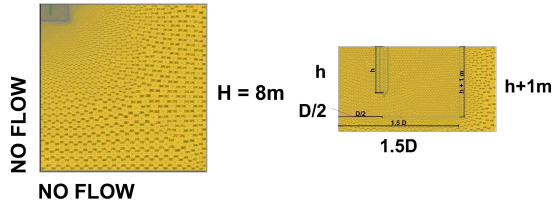


Figure 6. PLAXIS mesh and boundary conditions representation.

The soil is homogeneous, permeable with a unit weight of 20 kN/m^3 , resembling Aalborg University's sand $N_o 1$, used in the laboratory. The soil is saturated and permeability coefficient, k , is the only relevant parameter. USDA classification system is chosen on the flow parameters tab and Van Genuchten model is assigned. Since it is fully saturated Van Genuchten model describes flow with Darcy's law. The permeability coefficient used for the sand is the default value set in USDA series system with the value of 7.128 m/day .

The idea behind the numerical analysis is to investigate how seepage flow is developing in real experiments and then compared to the numerical results. It is of great importance mentioning that in the experiments denoted as "Suction + Force", for the installation procedure suction was applied after the bucket was installed for at least 0.15 m . This means that seepage was not developed before the second discrete phase and it may cause irregularities between the numerical and experimental calculations.

5. Methodology for calculation

The suction and induced water pressure values obtained during the installation and uninstillation of the bucket respectively, are used for the simulations in PLAXIS 2D. The measurements of the pressure transducers inside and outside the skirt of the bucket can give a very good representation of the seepage flow. The excess pore pressures acquired from the laboratory test are of great importance. Firstly, results for the pore pressure factor at the tip of the bucket skirt will be presented for both numerical and experimental analysis. Secondly, normalized seepage length will be compared for both cases. In order to calculate the seepage length, from eq. 5, the hydraulic gradient, controlling the piping failure have to be calculated. The gradient first appears at the tip of the bucket and then follows an upward path (Koterass et al., 2016). Thus, the gradient at the tip of the bucket skirt, average inside and outside the wall of the foundation is calculated using the equations 14, 15 and 16 respectively.

$$i_{tip} = \frac{\Delta U_{in} - \Delta U_{out}}{2h_{zone}\gamma_w} \quad (14)$$

$$i_{avg,in} = \frac{p - \Delta U_{tip}}{h\gamma_w} \quad (15)$$

$$i_{avg,out} = \frac{\Delta U_{top,out} - \Delta U_{tip}}{h\gamma_w} \quad (16)$$

Where, ΔU_{tip} is the excess pore pressure at the skirt tip, ΔU_{in} is the excess pore pressure inside the bucket, very close above the tip, ΔU_{out} is the excess pore pressure outside the bucket wall, very close above the tip, $\Delta U_{top,out}$ is the excess pore pressure outside the bucket at $z = 0$, always taken as 0, p is the applied suction for each penetration ratio and h_{zone} is the distance between the tip of the skirt from where the values ΔU_{out} and ΔU_{in} were obtained.

From the aforementioned eq. the critical suction pressure can be obtained from eq. 7. Furthermore, from Darcy's law the gradient at the exit is calculated from the following eq. as:

$$i_{exit} = \frac{v_{exit}}{k} \quad (17)$$

Where, v_{exit} is the exit velocity of the water inside the bucket and k the permeability of the soil.

It is crucial mentioning that in the experimental part this value could not be calculated, because there was not a clear image of how or when the water had started flowing out from the foundation. Calculations for the exit gradient are only given in PLAXIS 2D. The numerical analysis in this paper is based on the calculations performed by Koterass et al. (2016), introducing a method based on DNV approach, called AAU CPT-based method, in which the effects of the seepage flow are included on the reduction of penetration resistance during installation.

6. Results from installation and discussion

In Figure 7 the pore pressure factor, α , is presented for homogeneous sand soil profile. The values from the experiments and Plaxis simulations are averaged in order to investigate deviations from Houlsby and Byrne (2005) solution from eq. 3. It is obvious that α follows a decreasing path for increasing penetration ratio. It can be clearly seen that numerical values from $h/D \geq 0.2$ are almost a perfect fit with the solution proposed by Houlsby and Byrne (2005). However, the experiments show an abnormal path of α as expected, because the values of pore pressures that were used for the calculations, do not have a continuation. The meaning is that from the thousand values of data, there were only selected 5 representing each discrete step. Thus, in order to eliminate any inaccuracies more discrete steps have to be taken from the experiments.

Furthermore, the values for $h/D = 0.1$ are relatively high and out of the figure, because in the 3 tests denoted

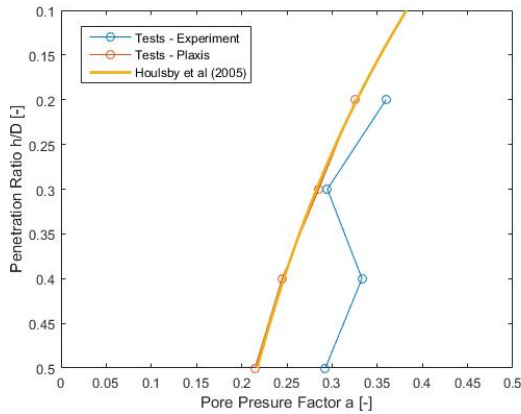


Figure 7. Pore pressure factor results from experiments and Plaxis, along with Houlsby and Byrne (2005) solution from eq. 3.

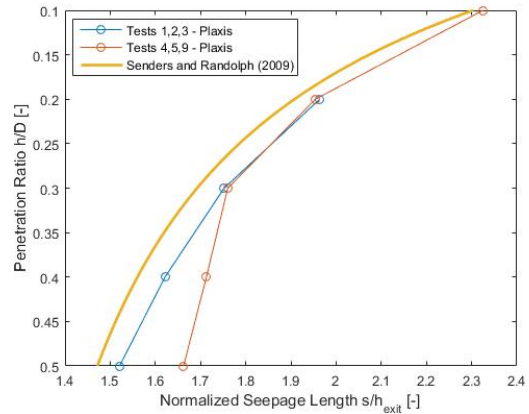


Figure 9. Normalized seepage length results for the exit hydraulic gradient, compared to the solutions from Senders and Randolph (2009), eq. 8.

as "Force + Suction", suction started being applied after the bucket penetration with force ended, which was measured to be around 0.15 m. Hence, from eq. 2, if suction is 0 the pore pressure factor tends to infinity. The results for the first 0.1 m for the experiments and Plaxis were taken out of the Figure 7.

Figures 8 and 9 present results from the numerical calculations for the normalized seepage length, using the exit hydraulic gradient with respect to the fitted solutions from eq. 10 and 8.

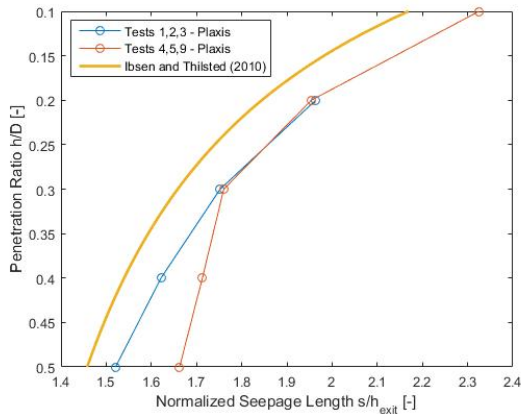


Figure 8. Normalized seepage length results for the exit hydraulic gradient, compared to the solutions from Ibsen and Thilsted (2010), eq. 10.

The smallest values are observed at the tip of the bucket skirt, which means that seepage starts to develop and expand from that point on. Senders and Randolph (2009) solution shows a better correlation with the results from this study. However, as mentioned before, for tests 1, 2 and 3, suction applied after 0.15 m of penetration, thus seepage length has not crated before that value is reached. For the tests denoted as "Pure Suction", the seepage length

demonstrates a higher value at the tip than on the other tests. This is due to the fact that critical hydraulic gradient, controlling the piping failure, was quite large around the tip. If critical pressure for the exit seepage length is exceeded then piping channels are expected to be created.

Results for seepage length calculated from the average hydraulic gradient inside and at the tip of the bucket, are presented in Figure 10. As expected, for the three first tests the seepage length is almost zero before the application of the suction. Moreover, the experimental values for the tip are quite higher in comparison to the ones from the Plaxis simulations. That is why, the software let the seepage dissipate after each step for a long time, while in real experiments the seepage length will only increases at higher penetration ratios, for both $(s/h)_{av,in}$ and $(s/h)_{tip}$.

Comparing the seepage length at the tip to the average inside one, it can be concluded that seepage is much higher at the tip than inside the bucket, which means that the reduction of penetration resistance at the tip is larger than inside the bucket wall, due to higher values of hydraulic gradient at the tip.

Normalized critical suction pressure is calculated based on the results of normalized seepage length at the exit, multiplying them with the penetration ratio h/D . That is the factor controlling piping failure, as mentioned in previous sections, which can cause an incomplete installation of the bucket. In the following Figures, (11, 12, 13 and 14) results by Feld (2001), Houlsby and Byrne (2005), Senders and Randolph (2009) and Ibsen and Thilsted (2010) are presented and compared with our study.

The analysis shows that the best correlation of normalized critical suction pressures is with the study conducted by Feld (2001) and Senders and Randolph (2009). This proves that the analysis made in this article is valid. It can be concluded that the pressures increase over each step, for all cases, which means that the soil resistance expect to be decreased.

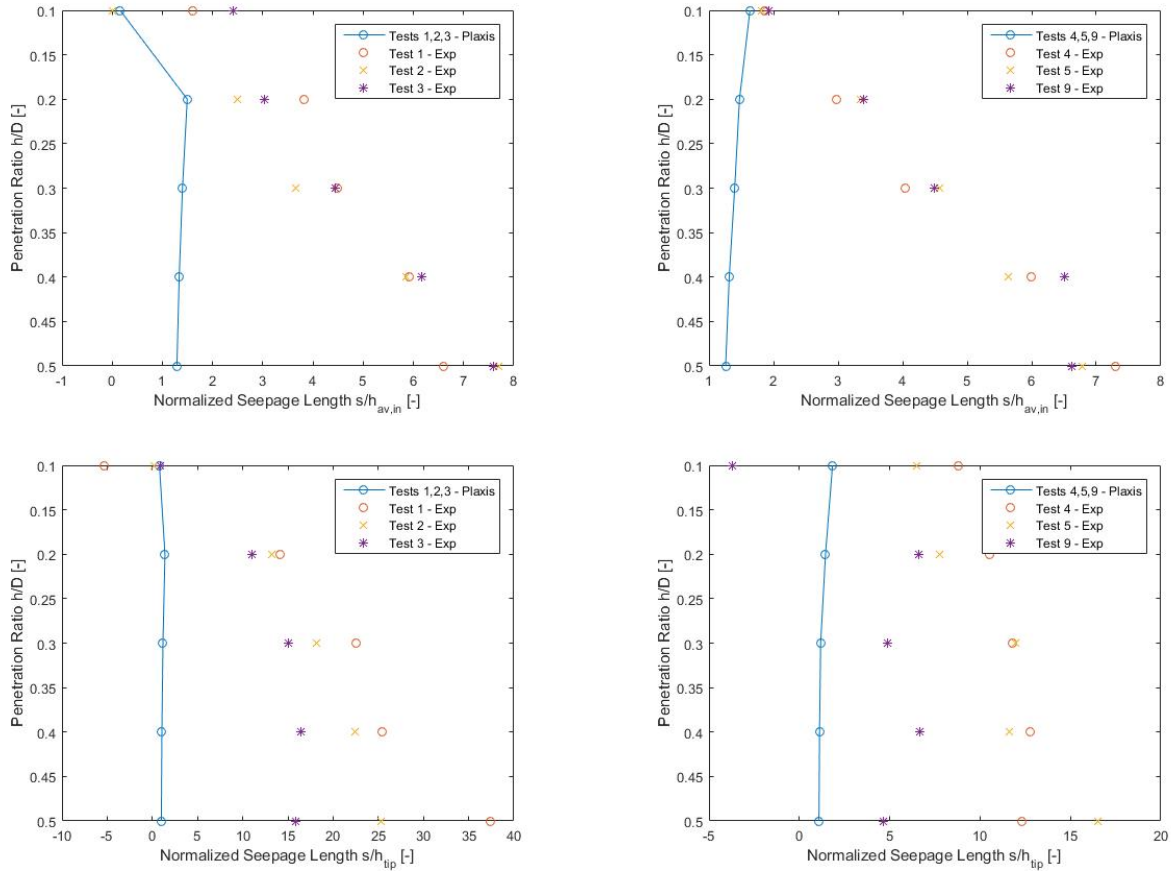


Figure 10. Normalized seepage length, using the average inside and tip hydraulic gradient for all medium scaled laboratory tests in comparison to the Plaxis simulations.

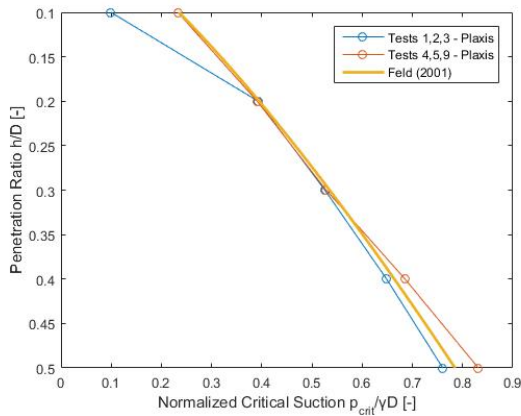


Figure 11. Normalized critical pressures calculated in Plaxis, in comparison to solution proposed by Feld (2001), eq. 12.

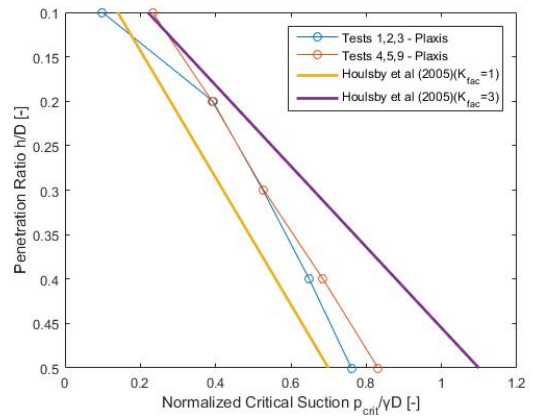


Figure 12. Normalized critical pressures calculated in Plaxis, in comparison to solution proposed by Houlby and Byrne (2005), eq. 4.

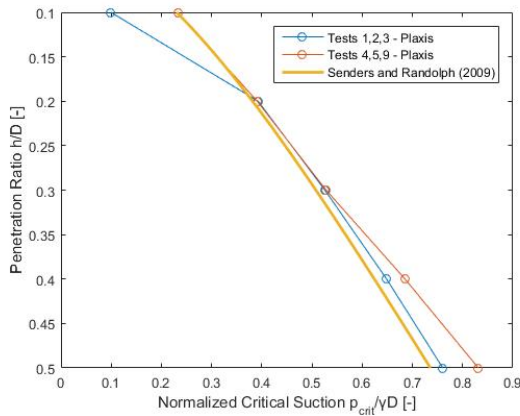


Figure 13. Normalized critical pressures calculated in Plaxis, in comparison to solution proposed by Senders and Randolph (2009), eq. 9.

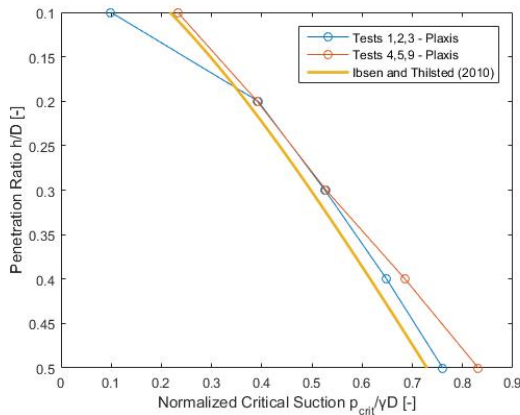


Figure 14. Normalized critical pressures calculated in Plaxis, in comparison to solution proposed by Ibsen and Thilsted (2010), eq. 11.

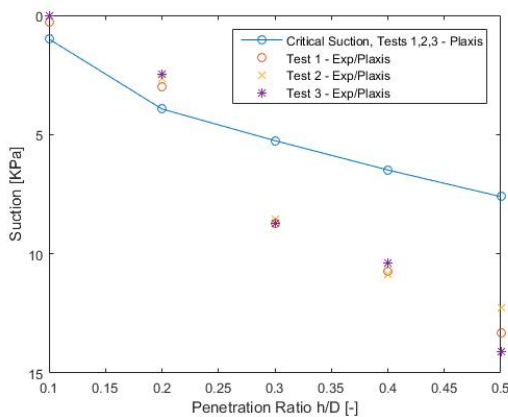


Figure 15. Critical suction from numerical simulation compared to the real suction applied for tests 1, 2 and 3, over the penetration ratio.

Finally, Figures 15 and 16 illustrate the critical suction measured from the numerical simulations along with the real suction applied at each step from the experiments. It can be clearly seen that in both cases, from penetration ratio higher than 0.3, the theoretical critical suction was exceeded. However, due to the fact that no piping observed during the installation (see Figure 17), it can be concluded that the critical value of suction was higher than the theoretical one, calculated in Plaxis. An average value of suction application, at the last step, for all the experiments was measured to be around 12 KPa, while the corresponding critical one was around 7 KPa.

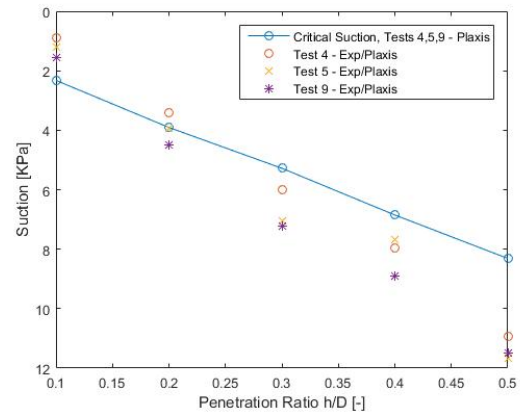


Figure 16. Critical suction from numerical simulation compared to the real suction applied for tests 4, 5 and 9, over the penetration ratio.



Figure 17. Suction installation of the bucket in the laboratory facilities of Aalborg University.

7. Results from uninstallation and discussion

Figure 18 illustrates the application of pressure over time for the corresponding experiments. The obvious peak that it is observed, is called break point, due to the fact that after the pressure at that point, the bucket starts moving upwards. In other words, is the critical pressure point for the beginning of the bucket's uninstallation. After that

point, the pressure is decreased until it reaches a certain value, responsible for the full uninstallation of the bucket. Those values seem to deviate according to the additional weight placed on top of the bucket.

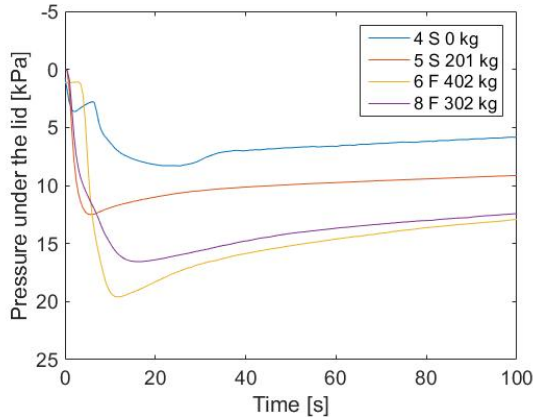


Figure 18. Uninstallation pressure for the experiments over time.

Furthermore, Figure 19 shows the pore pressure factor obtained from the uninstallation procedure for Plaxis, compared to Houlsby and Byrne (2005) solution. It is obvious that α follows an increasing path over the uninstallation depth, as expected. Moreover, results from the numerical analysis are an almost perfect fit compared to the theoretical solution, thus the method and the chosen model considered to be valid.

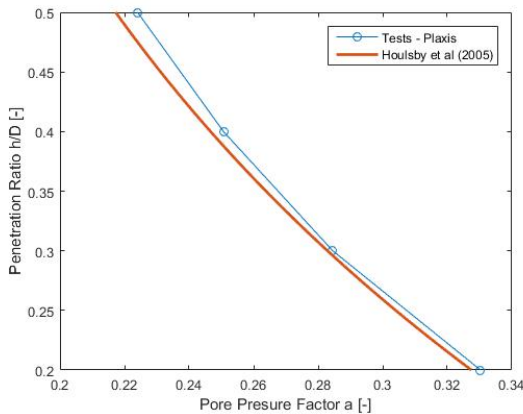


Figure 19. Pore pressure factor results from uninstallation in Plaxis, along with Houlsby and Byrne (2005) solution from eq. 3.

Figures 20 and 21 illustrate the normalized seepage length during uninstallation for the average hydraulic gradient inside and at the tip, respectively. The development of the seepage length for the uninstallation follows the same pattern as in the installation procedure. Again the values at the tip seem to be higher for the tip than inside the skirt of the bucket. As mentioned before, the differences between

the numerical values compared to the experimental ones are due to the fact that Plaxis after each step of calculation let the seepage fully developed in comparison to the real experiments, where that is not the case. As a conclusion, decreasing values of seepage length over the depth are observed for the laboratory uninstallation, while the numerical values show a steady path.

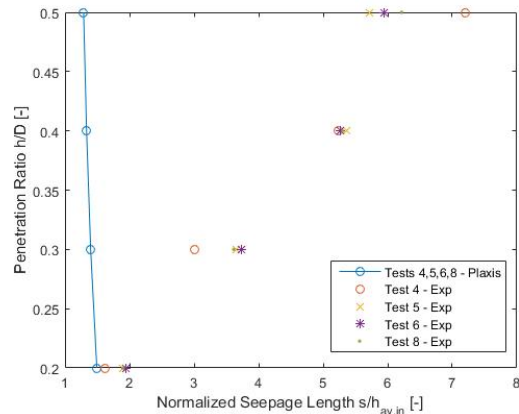


Figure 20. Normalized seepage length, using the average inside hydraulic gradient for all medium scaled laboratory tests in comparison to the Plaxis simulations.

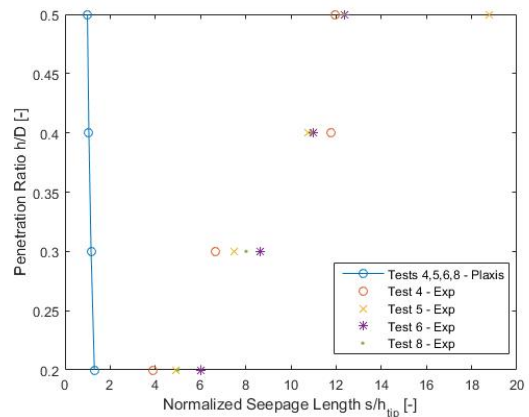


Figure 21. Normalized seepage length, using the average tip hydraulic gradient for all medium scaled laboratory tests in comparison to the Plaxis simulations.

Finally, as far as the pressure applied for the uninstallation is concerned, Figure 22 depicts that it never exceeded the theoretical critical pressure from the numerical simulations. That means that no piping channels were created during uninstallation and that there were not any signs of severe soil damage until the water flowed out of the bucket skirt.

8. Conclusions

This paper addresses an analysis of seepage length and critical pressure for a medium scale bucket foundation model,

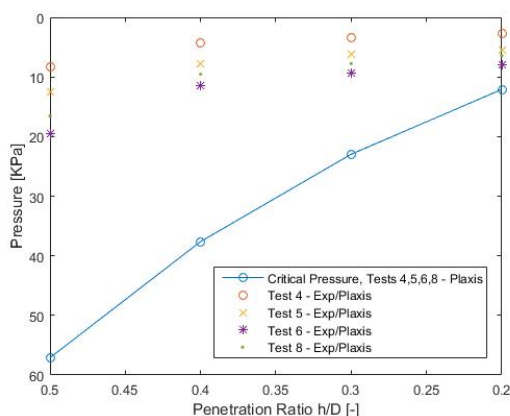


Figure 22. Critical pressure from numerical simulation compared to the real pressure applied for uninstillation tests 4, 5, 6 and 8, over the penetration ratio.

due to suction applied under the lid. Results are presented for both suction installation and induced water pressure uninstillation procedure, conducted in the facilities of Aalborg University. Data obtained from these tests is resembled in the finite element software PLAXIS 2D, in discrete steps of penetration ratio for homogeneous sand soil profile, and a comparison between known theories, experiments and numerical simulations is performed.

Calculations for the pore pressure factor, α , the normalized seepage length at the exit, the average inside and at the tip of the bucket skirt, along with critical suction pressure are presented throughout this article. Concluding on results, it was proved that the values of the hydraulic gradient at the tip are much higher compared to the ones inside and at the exit of the bucket skirt. As a result, the soil resistance at the tip is the one that shows larger reduction, as expected. Furthermore, no piping channels were created during the installation, even though the theoretical critical suction pressure was exceeded by the applied suction in the laboratory. That can be due to the fact that Plaxis independent steps do not take into account the applied suction from previous steps. Finally, during the uninstillation the values of theoretical critical pressure were not exceeded at all different weight simulations, until the bucket was almost out of the soil. All results show a high correlation with solutions from other studies for homogeneous sand, confirming the validity of this research.

Results from the experiments can be analyzed in more discrete steps for a better conclusion on how reality deviates from numerical simulations. Further analysis on how the soil parameters are affected, due to suction or a comparison with full scale models should be conducted. In this way a complete design method for installation and uninstillation of suction buckets in sandy soil profiles, could be proposed. Finally, it is of crucial importance to mention that there are not any known theories proposing a critical pressure path for the uninstillation procedure. Thus, this research

is considered a step forward on this direction.

References

- American Petroleum Institute (2000). Recommended practice for planning, designing and constructing fixed offshore platforms—working stress design.
- Andersen, K. H., Jostad, H. P., and Dyvik, R. (2008). Penetration resistance of offshore skirted foundations and anchors in dense sand. *JOURNAL OF GEOTECHNICAL AND GEOENVIRONMENTAL ENGINEERING*, pages 106–116.
- Byrne, B., Villalobos, F., Houlsby, G. T., and Martin, C. M. (2001). Laboratory testing of shallow skirted foundations in sand.
- Byrne, B. W. and Houlsby, G. T. (2003). Foundations for offshore wind turbines. *The Royal Society*, page 2909–2930.
- Feld, T. (2001). Suction bucket, a new innovative foundation concept applied to offshore wind turbines. *Aalborg University*.
- Gitsas, T., Pandiella, M. H., and Sgourakis, G. N. (2016). Installation of suction bucket foundations in sand.
- Houlsby, G. T. and Byrne, B. W. (2005). Calculation procedures for installation of suction caissons. *Oxford University*.
- Ibsen, L. B. and Thilsted, C. L. (2010). Numerical study of piping limits for suction installation of offshore skirted foundations and anchors in layered sand. *Frontiers in Offshore Geotechnics II*.
- Koteras, A. K., Ibsen, L. B., and Clausen, J. (2016). Seepage study for suction installation of bucket foundation in different soil combinations. *Aalborg University*.
- Lian, J., Chen, F., and Wang, H. (2014). Laboratory tests on soil-skirt interaction and penetration resistance of suction caissons during installation in sand. *Ocean Engineering*, pages 1–13.
- Senders, M. and Randolph, M. F. (2009). Cpt-based method for the installation of suction caissons in sand. *JOURNAL OF GEOTECHNICAL AND GEOENVIRONMENTAL ENGINEERING*, 135:14–25.
- Tjelta, T. I. (2015). The suction foundation technology. *International Symposium on Frontiers in Offshore Geotechnics III (ISFOG)*, pages 85–93.

**ARTICLE II: CALCULATION
OF EMPIRICAL COEFFICIENTS
ASSOCIATED WITH TIP
RESISTANCE AND SKIRT
FRICTION OF A BUCKET
FOUNDATION**

6

Calculation of empirical coefficients associated with tip resistance and skirt friction of a bucket foundation

G. N. Sgourakis¹, T. Gitsas¹, H. M. Pandiella¹, L. B. Ibsen¹, A. Koterakos¹

Abstract

Nowadays, growth of the renewable energy industry has led to larger demand for energy farms both onshore and offshore. As a result, new, more innovative and cost effective ways for wind turbine foundations have to be investigated. Onshore foundations have a rather simple design method, while offshore the design is much more challenging. A feasible and cost effective way of offshore foundation has proven to be the suction bucket or suction caisson, in comparison to the most common mono-pile, a foundation supporting almost 95% of the existing wind turbines. Although many studies have been conducted for the installation of the suction bucket in sand, only few investigate the interaction between the sand and the caisson. The purpose of this article is to investigate and propose values for the coefficients that relate bucket's wall friction and tip resistance to the sand during installation, based on medium-scale installation tests of a scaled model of bucket foundation in the laboratory facilities of Aalborg University. Those are denoted as k_p and k_f empirical coefficients, associated with the tip resistance and skirt friction of the bucket respectively. Experiments included bucket's installation by force, followed by a monotonic pullout load application performed by Vaitkunaite et al. (2015) and a force installation followed by a water pressure induced uninstillation performed by Gitsas et al. (2016). Each experiment was preceded with cone penetration tests (*CPT's*) in order to investigate soil conditions, such as cone resistance, q_c over the depth. Moreover, penetration resistance is calculated based on an empirical model in which k_p and k_f coefficients are of great importance. A model like that calculates penetration resistance as a function of cone resistance, directly obtained from *CPT* tests. Results for the empirical coefficients, from the two different experimental methods are being analyzed and compared to the values obtained from other studies.

Keywords

Empirical coefficients — Installation procedure — Medium-scale tests — Bucket foundation — Offshore foundations

¹ Department of Civil Engineering, Aalborg University, Denmark

1. Introduction

Bucket foundations have been used to support offshore oil and gas platforms for many decades. However, in recent years suction buckets are being used in wind-offshore industry, due to multiple advantages concerning economic feasibility and environmental-friendly installation principles. Compared to an oil platform, a wind turbine has lower weight, thus is subjected to larger wind, wave, and current loads. In the North Sea, the horizontal load from waves is significantly larger than the one from the wind. However, because the latter acts at a much higher point, it provides more overturning moment than wave loading (Houlsby et al., 2005). Thus, horizontal loads and overturning moment are substantial compared to the vertical load (Byrne and Houlsby, 2003). It is necessary to determine an appropriate foundation configuration that will allow these loads to be transferred safely to the surrounding soil, but an optimal foundation design for wind turbines is not a straight forward solution (Byrne et al., 2001).

In order to increase the moment fixity jacket and tripod foundations supported with three or four suction buckets are usually considered by the engineers. Those solutions can resist large compressive loads, but tensile capacity is

rather smaller (Lian et al., 2014). If a significant tension can be allowed at the upwind side of the structure, then the spacing of the foundation and therefore the overall size of the structure, can be greatly reduced (Kelly et al., 2004). Hence, it is important while designing the best foundation solution with respect to cost effectiveness, to design also for proper resistance to tensile loading. Furthermore, one of the challenges regarding bucket foundations, is how to effectively reduce installation costs, while keeping the required stability and bearing capacity of the soil. Penetration resistance during installation for clay soil profiles is way smaller compared to sandy soils, resulting to higher installation costs. Reduction of penetration resistance has achieved by the use of suction technology. Suction is the under-pressure applied inside the skirt of the bucket to produce an increased driving force in addition to the self-weight. Penetration resistance will be reduced due to gradients formed in the sand at the tip, inside and outside of the bucket skirt. Moreover, a suction bucket can be removed easily by reattaching the installation pumps and pump water into the cavity, where overpressure will create a force that pulls the bucket out of the soil (Byrne and Houlsby, 2003).

Although many studies have proposed design methods for suction buckets installation in sand, only few are focusing on the interaction between the sand and the skirt of the bucket during penetration. This can be achieved by analyzing the penetration resistance. Calculations of penetration resistance can be divided into two categories. The first one is based on bearing capacity or effective stresses theory, most commonly used. This research focuses on the second category based on an empirical model, in which penetration resistance is a function of cone resistance, q_c directly taken from the CPT tests (Det Norske Veritas, 1992). Using experimental data for the installation and uninstallation of a medium-scale bucket foundation model, penetration resistance is calculated and the empirical coefficients k_p and k_f which are associated with the tip resistance and the skirt friction of the bucket respectively, are obtained. Results of the coefficients for two different test procedures are presented and evaluated.

The arrangement of this paper is as follows. In Section 2 different studies from empirical calculations are presented. In Section 3 a brief review of the equipment, material and the procedure used in the laboratory is given. The methodology for the empirical coefficients calculations can be found in Section 4, while the results and the conclusions are presented in Sections 5 and 6 respectively.

2. State of the art for the empirical coefficients

Installation standards of bucket foundations are usually based on theories regarding pile foundations. It can be assumed that the bucket works as an open ended pile. The most common one was proposed by American Petroleum Institute (2000) concerning open ended pile foundations. Soil resistance is assumed to be the sum of the external shaft friction, the end bearing on the pile wall annulus and the total internal shaft friction or the end bearing of the plug. Additionally, the unit end bearing is dependent on the dimensionless bearing capacity factor, N_q and on the effective overburden pressure, p_o .

Det Norske Veritas Institution, also called DNV, in 1992 presented a study about penetration resistance of bucket skirts. DNV suggests that penetration resistance of the steel skirts is the sum of friction resistance, inside, outside and at the tip of the bucket skirt, where calculations should be based on the results of in-situ testing supported by laboratory tests. For the field tests CPT data was used, since it gives a continuous record of the cone penetration resistance over the depth.

DNV method for calculating the penetration resistance based on results from CPT tests, is presented in the following equation as:

$$R = R_f + R_{tip} \quad (1)$$

Where,

$$R_f = \pi D_I k_f \int_0^z q_c(l) dz + \pi D_O k_f \int_0^z q_c(l) dz \quad (2)$$

$$R_{tip} = A_{tip} k_p q_c(z) \quad (3)$$

Where,

A_{tip}	Area of the tip of the bucket
z	Penetration depth
k_p	Empirical coefficient related to the tip resistance
k_f	Empirical coefficient related to the skirt friction
q_c	Cone resistance
D_I	Inner diameter of the bucket
D_O	Outer diameter of the bucket

Det Norske Veritas (1992) proposes reference values for k_p and k_f coefficients for North Sea sand and they are presented in table 1.

Empirical coefficients	k_p	k_f
Lowest expected	0.3	0.001
Highest expected	0.6	0.003

Table 1. Recommended values from DNV for empirical coefficients k_p and k_f .

A method proposed by Lehane et al. (2005) based on the API (2000) standard called UWA-05 design method, was developed for open and closed ended driven piles in sand. Alternatively to DNV, the UWA-05 method suggests that k_f is a function of the internal and external diameter ratio of the pile. UWA-05 design method is developed for open and closed ended driven piles in sand. The empirical coefficient k_f is calculated with the following equation as:

$$k_f = C \left[1 - \left(\frac{D_I}{D_O} \right)^2 \right]^{0.3} \tan \delta \quad (4)$$

Where,

C	Constant, assumed 0.021 in Lehane et al. (2005)
δ	Interface friction angle
D_I	Inner diameter of the bucket
D_O	Outer diameter of the bucket

In another study performed by Andersen et al. (2008), results about skirt friction and tip resistance coefficients are presented for prototype models, along with small scale laboratory tests. Calculations in this study, are based on the DNV standard. It has to be mentioned that in our study only tests that the bucket was installed with additional weight

and not by underpressure application will be considered. Therefore, the prototype models installed by force in Andersen et al. (2008) study, were denoted as Draupner E and Sleipner T. Different values of k_f were assumed in order to calculate k_p . As far as the laboratory tests are concerned, the bucket tested had a diameter, D of 0.557 m, skirt thickness, t of 8 mm, and 0.32 m skirt height, h . Tests run in a tank with a diameter of 1.6 m. The value for k_f was set to 0.0053 in order to have the best fit with the measured penetration resistance. In table 2 an overview of Andersen et al. (2008) results for k_p and k_f are presented.

Case	k_p	k_f
Draupner E	0.01–0.08	0–0.0015
Sleipner T	0.05–0.13	0–0.0015
PEN 1-3	1.03–1.19	0.0053

Table 2. Values from Andersen et al. (2008) for empirical coefficients k_p and k_f , for different cases.

Senders and Randolph (2009) conducted jacked tests (without suction), at a penetration ratio of 0.1 mm/s. Using the UWA-05 method (equation 4), proposed by Lehane et al. (2005), they found a k_f value of 0.0015 for an interface friction angle of 22 degrees (constant C was assumed to be 0.012). The k_p value was assumed to be 0.2 due to the fact that sand used was very dense.

Furthermore, Lian et al. (2014) carried out small-scaled tests, without suction to get unreduced penetration resistance under no pore water flow. The penetration resistance was calculated by the CPT-based method using averaged values of q_c . Results show that the best correlation to their calculations are obtained with the values proposed by DNV (1992) (see table 1).

The method followed in this article is based on the DNV (1992) approach for calculating the empirical coefficients. An investigations of how the coefficients vary due to differences in cone resistance will be presented. This article does not analyze tests, where suction was applied during the installation of the bucket.

3. Materials, Equipment, and Procedure of the Laboratory Tests

In the laboratory facilities of Aalborg University two different experimental studies have been performed by Vaitkunaite et al. (2015) and Gitsas et al. (2016). The medium scaled model of bucket foundation used in both studies, had the same dimensions and self-weight. The dimensions were 1 m in diameter, D , 0.5 m in skirt height, h and 3 mm in skirt thickness, t , which corresponds to prototype foundation model with ratio of $h/D = 0.5$ (see Figure 1). The material that the bucket was made of is steel and its self weight was calculated at 201 Kg or 2.01 KN. Tests were performed in a large container (sandbox) filled with gravel for the first 0.3 m and with Aalborg University No.1

sand for the next 1.2 m. Container's diameter and height were 3 and 1.52 m respectively. A hydraulic piston used as an assisting tool during the whole procedure.

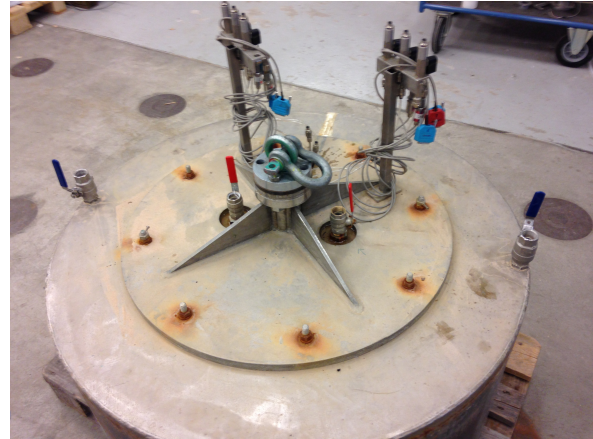


Figure 1. Foundation model used in the experiments performed by Gitsas et al. (2016).

In Figure 2, the test set-up plan from Vaitkunaite et al. (2015) is illustrated. 4 CPT's were carried out in order to investigate soil conditions before installation. 7 installation test procedures (denoted as *st04*, *st05*, *st06*, *st08*, *st09*, *st11*, *st12*) were performed in dense sand, followed by the application of monotonic tensile load. The values of q_c for each test were averaged and presented in Figure 3

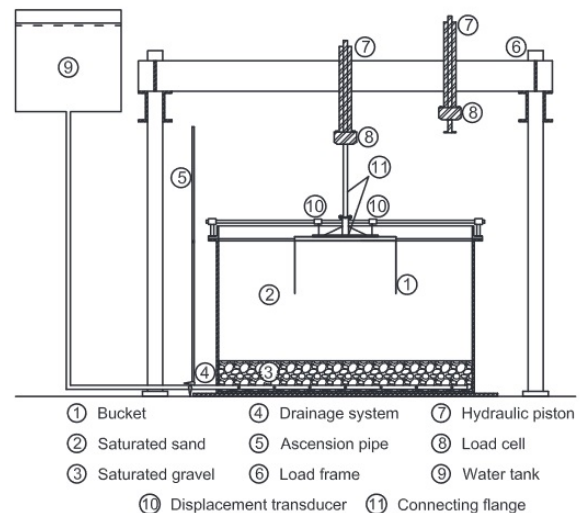


Figure 2. Test set-up plan, Vaitkunaite et al. (2015).

During the installation of the bucket foundation, axial, compressional load was applied and penetration displacement was measured. For this procedure the soil resistance against penetration is a sum of friction on the bucket skirt and tip resistance (Vaitkunaite et al., 2015). Installation started with positioning the bucket right on the soil surface level, while zeroing the signal of the load cell. The penetration rate was set at 0.2 mm/s. Installation ended when

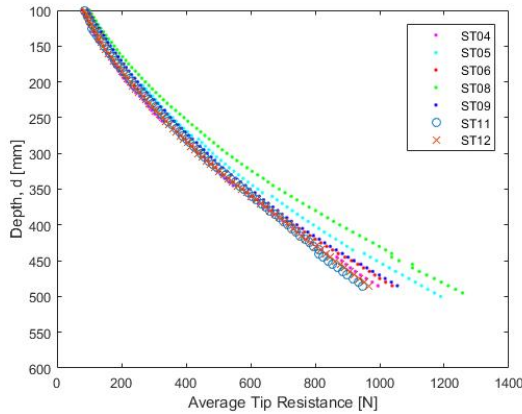


Figure 3. Average cone resistance q_c for every test from Vaitkunaite et al. (2015).

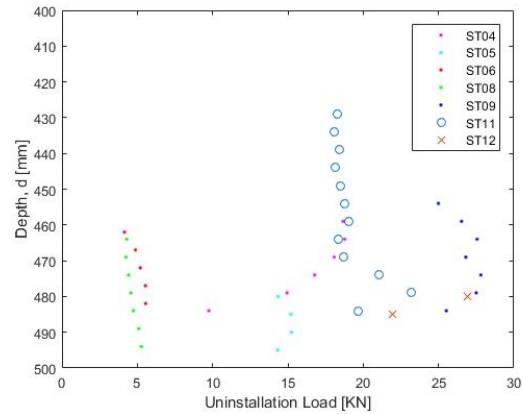


Figure 5. Tensile loading over the depth for every test from Vaitkunaite et al. (2015).

50 kN force was reached. After that compressive pre-load started of additional 20 kN. This force applied to ensure that the bucket is fully installed (Vaitkunaite et al., 2015). In Figure 4 the installation load increasing over the depth for all 7 tests is depicted.

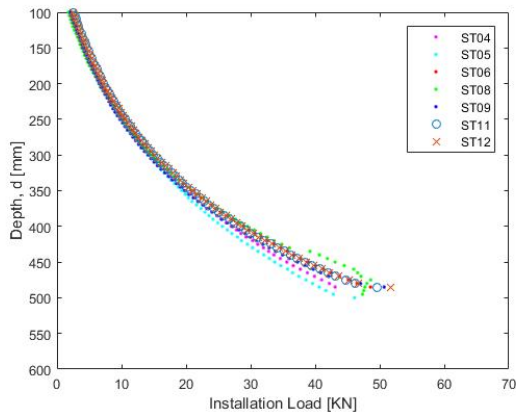


Figure 4. Installation load over the depth for every test obtained from Vaitkunaite et al. (2015).

After installing the bucket, tensile pullout tests were carried out. During the pullout of the bucket by the tensile load application, the penetration resistance of the soil comes only from friction at the skirt. Thus, the tip resistance is assumed to be zero. This difference between the installation and pullout procedure, where the tip resistance does not have any influence, is of great importance for calibrating the empirical coefficients. The load cell was positioned right above the bucket model and has a capacity of 250kN, (Vaitkunaite et al., 2015). In Figure 5 the tensile load over the depth for each test from Vaitkunaite et al. (2015), is presented.

Regarding the tests conducted by Gitsas et al. (2016), they consisted of a force installation procedure (almost the same procedure followed by Vaitkunaite et al. (2015))

followed by a water pressure induced uninstillation. The test names and characteristics are presented in table 3.

Test Number	Characteristics
6 Inst.	Force
7 Inst.	Force
8 Inst.	Force
10 Inst.	Force
6 Uninst.	Uninstillation with 402 Kg
7 Uninst.	Uninstillation with 402 Kg
8 Uninst.	Uninstillation with 302 Kg
10 Uninst.	Uninstillation with 201 Kg

Table 3. Description of installation and uninstillation tests performed by Gitsas et al. (2016).

Before each test, 4 CPT tests were performed in order to obtain cone resistance values. Furthermore, after installation and before uninstillation 8 more CPT tests were conducted (4 inside through the valves, and 4 outside the bucket’s skirt on the surrounding soil). Figure 6 presents the places in the sandbox where CPT’s were conducted. Additionally, Figure 7 present the average values of cone resistance obtained from the CPT tests before installation.

The installation procedure followed by Gitsas et al. (2016) was performed in the same manner as the one followed by Vaitkunaite et al. (2015). The difference is that the penetration rate was set at 1 mm/s instead of 2 and that no pre-load was applied. Installation finished after the displacement transducer stopped giving any signal on the computer, meaning that no further installation could be achieved. Figure 8 depicts the load applied for full installation of the bucket.

As far as the uninstillation procedure is concerned, it

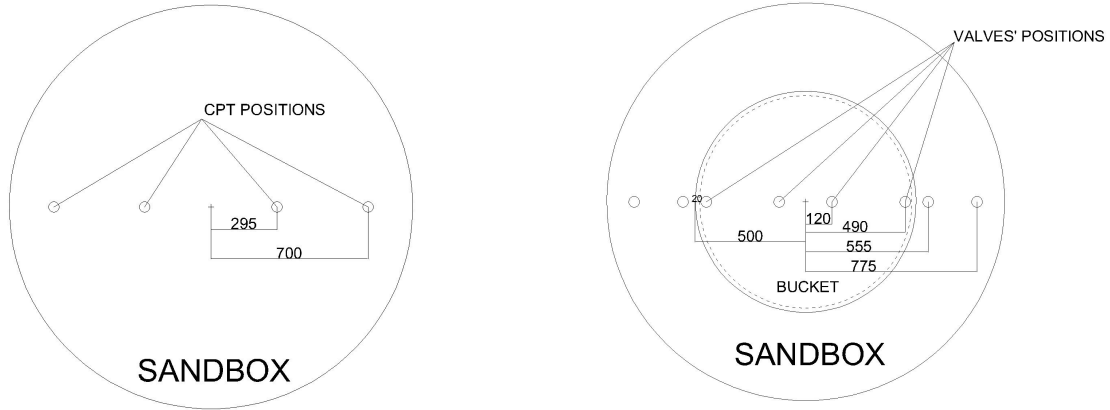


Figure 6. CPT's performed before and after installation by Gitsas et al. (2016) [mm].

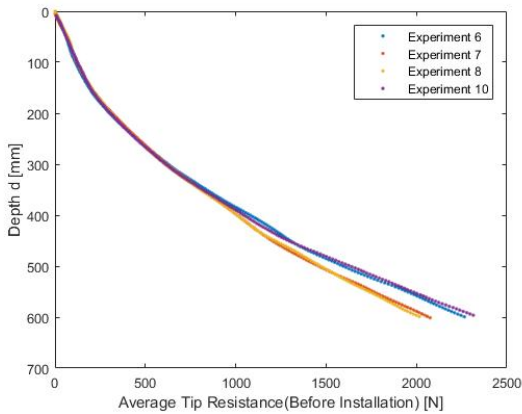


Figure 7. Average tip resistance over the depth for all the tests performed by Gitsas et al. (2016), before the installation of the bucket.

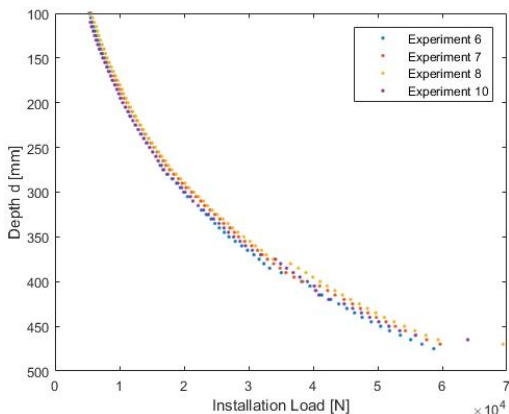


Figure 8. Installation load over the depth for all the tests performed by Gitsas et al. (2016).

was performed by using one of the buckets valves for water pressure application, while the other three remained closed at all times. Pressure transducer placed under the lid of the bucket, measured the pressure during the whole procedure. By the use of equation 5, the applied pressure was transformed into force and Figure 9 shows the results of the uninstillation force. The procedure finished when water flowed out of the foundation skirt, which was measured to be approximately 0.35 m of height. Finally different weights of the bucket were simulated by applying additional load on top of the bucket. Differences found not to be substantial as it can be clearly seen in Figure 9.

$$F = PA \tag{5}$$

Where, P is the applied pressure and A is the area under the lid of the bucket.

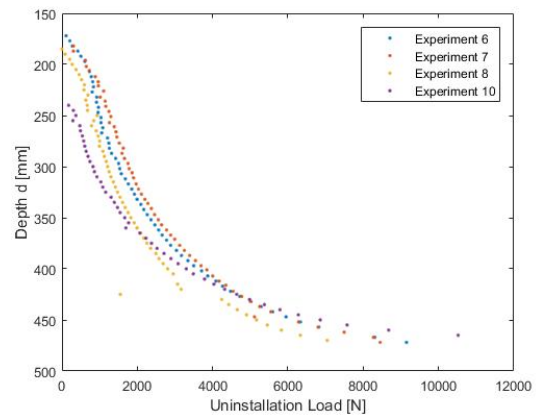


Figure 9. Uninstillation load over the depth for all the tests performed by Gitsas et al. (2016).

4. Methodology for calculating the empirical coefficients

The governing equation for penetration resistance of the bucket foundation is obtained by equilibrium between forces and soil resistance against the penetration (Andersen et al., 2008). The penetration resistance is then given by:

$$R = G' + F \quad (6)$$

Where,

- R Total penetration resistance
- G' Self-weight of the bucket adjusted for buoyancy
- F Hydraulic force applied on the bucket

In this paper the self-weight of the structure is included in the application of the force, thus it is not going to be visible in the equations for calibrating the empirical coefficients. Additionally, the total penetration resistance is a summation of two components; the tip resistance of the skirt, R_{tip} and the skirt friction, R_f .

$$R = R_{tip} + R_f \quad (7)$$

The skirt friction consists of the inner skirt friction R_{fI} and the outer skirt friction R_{fO} .

$$R_f = R_{fI} + R_{fO} \quad (8)$$

The total skirt friction is calculated with the CPT-based method from DNV (1992). As mentioned earlier, this method relates the cone resistance q_c to the side friction and tip resistance, using the empirical coefficients k_p and k_f . By integration along the inner and outer area of the skirt, the total skirt friction is obtained from equation 8 as:

$$R_f = \pi D_I k_f \int_0^z q_c(l) dz + \pi D_O k_f \int_0^z q_c(l) dz \quad (9)$$

The tip resistance of the caisson, used in equation 7, is:

$$R_{tip} = A_{tip} k_p q_c(z) \quad (10)$$

As a starting point for the calibration of the empirical coefficients the values from the tensile and uninstillation tests were used. That is due to the fact that during uninstillation the tip resistance is assumed to be zero. Hence, only the skirt friction of the bucket is responsible for the soil resistance. In this way calculation of k_f coefficient can be achieved. After analyzing results from the CPT's, averaged values of cone resistance q_c for every 5 mm depth is obtained. While in Vaitkunaite et al. (2015) tests, there

were only 4 CPT's before installation, in Gitsas et al. (2016) experiments, soil conditions were examined after the installation by performing 8 CPT tests more. The analysis of Vaitkunaite et al. (2015) results is based only on those 4 CPT tests before installation. However, for calculating the k_f from Gitsas et al. (2016) tests, the CPT's after installation are used. In Figure 6 the 2 CPT tests inside and the 2 outside, on the boundaries of the bucket, were averaged for each test and their values are presented over the depth in Figures 10 11.

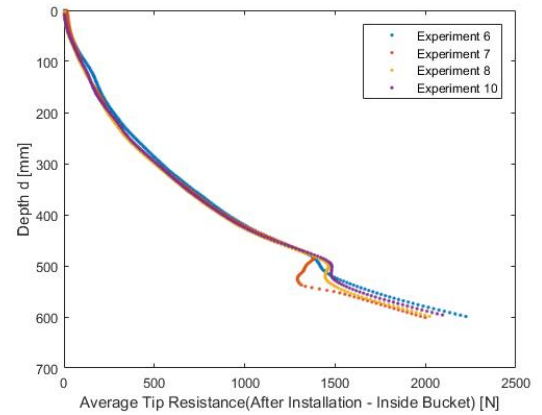


Figure 10. Average q_c over the depth for the 2 CPT's inside, on the bucket's boundaries performed by Gitsas et al. (2016).

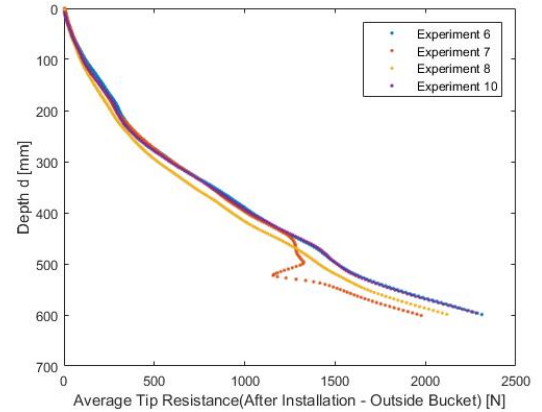


Figure 11. Average q_c over the depth for the 2 CPT's outside, on the bucket's boundaries performed by Gitsas et al. (2016)..

From the combination of equations 6, 7 and 9 the following equation is obtained:

$$F_{tensile/uninstal} = R_f, \quad (11)$$

Where, $F_{tensile/uninstal}$ is the tensile or the uninstillation load measured through the experimental tests.

Equation 11 can be rewritten based on equation 9 by isolating the empirical coefficient k_f as:

$$k_f = \frac{F_{tensile/uninstal}}{\pi(D_I + D_O) \int_0^z q_c(l) dz} \quad (12)$$

From the tensile/uninstallation procedure, values for the k_f are calculated and an averaged value is used for further analysis of the installation tests. Using the average value of k_f , a set of k_p values is obtained for each penetration depth. During installation of the bucket, soil resistance comes from the skirt friction and the skirt tip. Therefore, combining equations 6, 7, 9 and 10, leads to the following equation:

$$F_{inst} = R_f + R_{tip}, \quad (13)$$

where F_{inst} is the installation load, measured in the laboratory experiments.

From equation 13, the empirical coefficient k_p is isolated as:

$$k_p = \frac{F_{inst} - R_{fI} - R_{fO}}{A_{tip} q_c(d)} \quad (14)$$

In the next section results for k_p and k_f are presented and compared for both Vaitkunaite et al. (2015) and Gitsas et al. (2016) tests.

5. Results and Discussion

In Figures 3, 7, 10 and 11 all the average values of cone resistance for each test are presented. It is crucial mentioning that the CPT's conducted by Vaitkunaite et al. (2015) show a substantial deviation with the ones made by Gitsas et al. (2016). The average values of cone resistance for all the experiments deviate by almost 1 KN in q_c . Better compaction and vibration of the soil before each experiment leads to higher values of cone resistance. Moreover, the results of q_c before and after installation performed by Gitsas et al. (2016), do not illustrate any big deviations, due to the fact that the soil inside and outside the bucket was not highly affected by the installation procedure.

Regarding the installation load applied in both cases, Figures 4 and 8 show that the force needed for the bucket to be fully installed was measured to be around 60 KN for all the different tests. Values obtained for the first 100 mm are not included, in order to avoid inaccuracies produced by the equipments in the laboratory.

As mentioned earlier the tensile and uninstallation loads are the only ones responsible for the evaluation of k_f . Figures 5 and 9 present the tensile and uninstallation loads over the depth for each procedure. From Vaitkunaite et al. (2015) procedure, large deviations among the different

tests is observed. By performing monotonic pullout tests at different rates it is possible to examine whether there is any rate dependence in the response of the bucket (Byrne and Houlsby, 2002). Concerning Gitsas et al. (2016) procedure, uninstallation loads show a small deviation among the tests, even though different weights of the bucket were simulated.

In Figure 12 values for the empirical coefficient related to skirt friction, k_f are presented for both cases. It can be clearly seen that large deviations take place. Table 4 shows average values of tensile and uninstallation load for each experiment, in order to take a better look on the results. As it can be clearly seen, for higher values of tensile/uninstallation load, higher values of k_f are obtained. As an example, the mean value of k_f for static test *st09* is equal to 0.0045, whereas in test *st08* is equal to 0.00068, almost an order smaller. Tensile load in one case was measured to be -27 KN, while in the other case was -5.3 KN. From equation 12, the load responsible for the uninstallation is proportional to the k_f and in combination with the low values of q_c , a high value of k_f is expected. Furthermore, the same pattern is observed in the values obtained by Gitsas et al. (2016). Higher average uninstallation load leads to slightly higher k_f .

The values of the empirical coefficient associated with the tip resistance of the bucket, k_p are illustrated in Figure 13 for both procedures. In both cases k_p appears to follow the same pattern, even though the average values from table 4 are highly different. A decrease of k_p until the 3/5 of the depth is observed, followed by a slight increase when going deeper in the soil (almost never until its initial value though). However, from table 4 a clear connection between k_f and k_p can not be concluded, only that in most cases higher k_f leads to lower k_p values. Using the average value of k_p these 2 cases can be compared to other studies.

Test No.	$F_{tensile/uninstal}$ [KN]	k_f mean	k_p mean
st04	-18.8	0.00305	0.44
st05	-15.2	0.00214	0.42
st06	-5.6	0.00088	0.65
st08	-5.3	0.00064	0.55
st09	-27	0.00392	0.4
st11	-23.2	0.00362	0.43
st12	-27	0.00392	0.4
6	-3	0.00069	1.23
7	-2.7	0.00081	1.25
8	-3.3	0.00063	1.21
10	-2.5	0.00054	1.32

Table 4. Values for average tensile/uninstallation load $F_{tensile/uninstal}$, mean k_f and k_p for all cases.

DNV (1992) proposed that values of k_f should be in the range of 0.001-0.003 and k_p between 0.3-0.6 for field models. However, Andersen et al. (2008), after performing

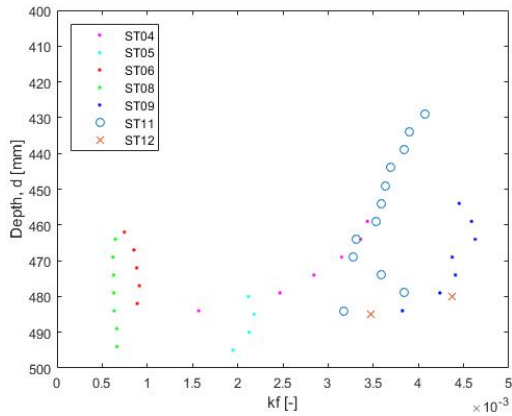


Figure 12. k_f values over the depth for the application of tensile and uninstillation load respectively.

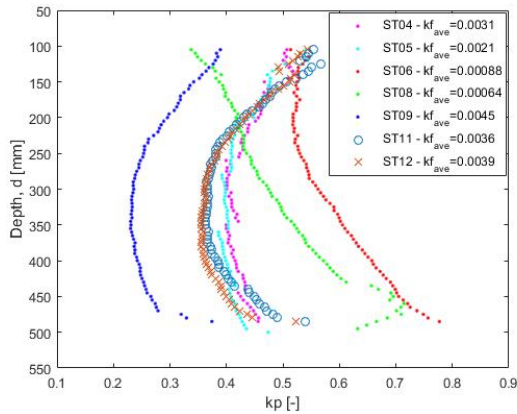
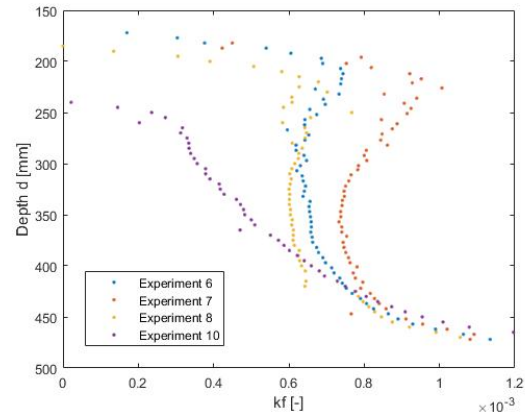


Figure 13. k_p values over the depth for the application of tensile and uninstillation load respectively.

small-scale laboratory tests along with values obtained from prototypes, came to the conclusion that a bigger range of values can be used (see table 2). In table 4 the average values of k_f and k_p over the depth are presented. It can be concluded that most of the values obtained are inside the acceptable range for the small-scale testing, as mentioned above. k_p values from Gitsas et al. (2016) show a very good correlation with respect to the ones that Andersen et al. (2008) calculated in their experiments. However, k_f deviation seems quite high. This can happen because in Andersen et al. (2008) k_f value was assigned contrary to Gitsas et al. (2016) that k_f was calculated from CPT tests performed after installation.

6. Conclusions

In the present study, an analysis based on the empirical model that connects the penetration resistance to the cone resistance, q_c , has been performed. In order to achieve that, medium-scaled laboratory tests, regarding the installation and uninstillation procedure of a bucket foundation in dense sand, were performed by Vaitkunaite et al. (2015) and Gitsas et al. (2016). The scaled foundation model

used in both studies had dimensions of 1m in diameter, D and 0.5m in skirt length, h ($h/D = 0.5$). Throughout this paper, results for cone penetration data, installation and uninstillation load have been provided, for the sake of finding a solution for the empirical coefficients k_f and k_p , based on the method provided by DNV (1992), called CPT-based method. Obtaining these coefficients can lead to a better understanding on how to calculate the penetration resistance of the soil.

Values of k_f obtained from Vaitkunaite et al. (2015) experiments, show a large deviation due to substantial differences in the application of tensile load. Higher pullout load provides higher k_f coefficients. k_p was found in the range of DNV (1992) proposed values. As far as the experiments performed by Gitsas et al. (2016) are concerned, k_p values found to be in the range of 1.21-1.32, having a very good correlation with other studies that have already calculated the k_p coefficient. Values of k_f appear to be small compared to other studies and in the range of 0.00054-0.00081.

Future work should be focused on performing experiments in layered soil profiles, where the cone resistance

changes significantly between the different type of soils. Back calculations on the existing results, due to the fact that the method followed in this article is not considered straightforward, would give a more clear look on the empirical coefficients. Furthermore, a validation of the existing results with full-scale installation tests would be an improvement on the existing theory and a more often practice of it could be implemented. The results presented here are considered to be a step forward in the development of an improved model of calculating soil penetration resistance based on CPT results.

Senders, M. and Randolph, M. F. (2009). Cpt-based method for the installation of suction caissons in sand. *JOURNAL OF GEOTECHNICAL AND GEOENVIRONMENTAL ENGINEERING*, 135:14–25.

Vaitkunaite, E., Nielsen, B. N., and Ibsen, L. B. (2015). Bucket foundation model testing under tensile axial loading. *Aalborg University*.

References

- American Petroleum Institute (2000). Recommended practice for planning, designing and constructing fixed offshore platforms—working stress design.
- Andersen, K. H., Jostad, H. P., and Dyvik, R. (2008). Penetration resistance of offshore skirted foundations and anchors in dense sand. *JOURNAL OF GEOTECHNICAL AND GEOENVIRONMENTAL ENGINEERING*, pages 106–116.
- Byrne, B., Villalobos, F., Houlsby, G. T., and Martin, C. M. (2001). Laboratory testing of shallow skirted foundations in sand.
- Byrne, B. W. and Houlsby, G. T. (2002). Experimental investigations of response of suction caissons to transient vertical loading. *JOURNAL OF GEOTECHNICAL AND GEOENVIRONMENTAL ENGINEERING*.
- Byrne, B. W. and Houlsby, G. T. (2003). Foundations for offshore wind turbines. *The Royal Society*, page 2909–2930.
- Det Norske Veritas (1992). Foundations.
- Gitsas, T., Pandiella, M. H., and Sgourakis, G. N. (2016). Installation of suction bucket foundations in sand.
- Houlsby, G. T., Ibsen, L. B., and Byrne, B. W. (2005). Suction caissons for wind turbines. *Frontiers in Offshore Geotechnics*.
- Kelly, R. B., Byrne, B. W., Houlsby, G. T., and Martin, C. M. (2004). Tensile loading of model caisson foundations for structures on sand. *Oxford University*.
- Lehane, B. M., Schneider, J. A., and Xu, X. (2005). The uwa-05 method for prediction of axial capacity of driven piles in sand.
- Lian, J., Chen, F., and Wang, H. (2014). Laboratory tests on soil-skirt interaction and penetration resistance of suction caissons during installation in sand. *Ocean Engineering*, pages 1–13.

**ARTICLE III: CALCULATION
OF β FACTORS FROM
INSTALLATION OF A
MEDIUM-SCALE MODEL OF
BUCKET FOUNDATION IN
DENSE SAND**

7

Calculation of β factors from installation of a medium-scale model of bucket foundation in dense sand

H. M. Pandiella¹, T. Gitsas¹, G. N. Sgourakis¹, L. B. Ibsen¹, A. Koterias¹

Abstract

Suction bucket foundations have been used for many years in offshore industry, to support oil and gas platforms. Nowadays, they are considered a feasible and cost effective way of supporting offshore wind turbines. Its effectiveness derives from the fact that suction, which is applied under the lid of the bucket, make installation an easier and more quiet process. When suction is applied, the downward force, due to pressure differential on the lid, increases gradually forcing the bucket into the ground. However, in sandy soils (high coefficient of permeability) a flow between the voids of the soil is created, called seepage flow, which reduces the penetration resistance making the installation an easier procedure. Moreover, decrease of penetration resistance due to suction, can be caused by the increase in the excess pore pressure of the soil during installation. Although many studies have been conducted for the installation of suction buckets in sand, only few investigate the interaction between the sand and the caisson. The scope of this paper is to investigate the coefficients that relate bucket's wall friction and tip resistance to the sand, during suction and force installation. Those are denoted as k_p and k_f empirical coefficients and their values are based on CPT tests conducted before and after installation. As mentioned before, suction installation decreases the soil penetration resistance, thus the coefficients calculated from the force penetration of the bucket, are expected to be highly different. Those differences can be described by the β factors, which are based on the suction applied during installation. Using the AAU CPT- based method proposed by Koterias et al. (2016), calculations of β factors are performed and a range of values is proposed. Tests included installation by suction or by force and induced water pressure uninstillation of a scaled model of bucket foundation in the laboratory facilities of Aalborg University. .

Keywords

Empirical Coefficients — Installation Procedure — Medium-Scale Tests — Bucket Foundation — Offshore Foundations

¹Department of Civil Engineering, Aalborg University, Denmark

1. Introduction

For offshore wind turbines the horizontal load from waves is significantly larger than the one from the wind. Additionally, because the latter acts at a much higher point, it provides more overturning moment than wave loading (Houlsby et al., 2005). Thus, horizontal loads and overturning moment are substantial compared to the vertical load (Byrne and Houlsby, 2003). It is necessary to determine an appropriate foundation configuration that will allow these loads to be transferred safely to the surrounding soil, but an optimal foundation design for wind turbines is not a straight forward solution (Byrne et al., 2001). Nowadays, skirted foundations and anchors have become a more attractive solution for various types of offshore structures (Andersen et al., 2008). Specifically, the suction bucket is considered one of the most feasible solutions for wind turbine foundations. Its feasibility arises from the fact that the installation process can be a quicker, quieter and more cost effective solution compared to the monopiles, the foundation most widely used in offshore wind turbine industry (Tjelta, 2015). However, one of the biggest problems the renewable energy industry confronts, is the installation of wind turbines in sea water, which is a much more complicated procedure

than onshore. A proper and feasible installation can lead to higher levels of energy production along with lower costs and smaller impact on the environment (Lian et al., 2014).

Suction installation can be divided in two parts, the self-weight penetration and the suction installation. Self-weight penetration ensures a seal component at the edge of the bucket with the surrounding soil, in order for the suction component, under the lid of the bucket, to be performed adequately (Houlsby and Byrne, 2005). Generally, in clay the suction used is small. However, in sandy soils the penetration resistance is high, thus an under-pressure is applied within the skirt compartment to produce an increased driving force in addition to the self-weight. Suction will also form hydraulic gradients in the sand at the tip, inside and outside the bucket skirt, which will reduce the penetration resistance of the soil (see Figure 1). Nevertheless, it is very important to mention that exceedance of the critical hydraulic gradient may cause piping channels along the skirt, where loosening or failure of the soil is most probable to happen. The design must predict the required suction applied that will not exceed its critical value (Andersen et al. (2008), Ibsen and Thilsted (2010)).

Although many studies have proposed design methods

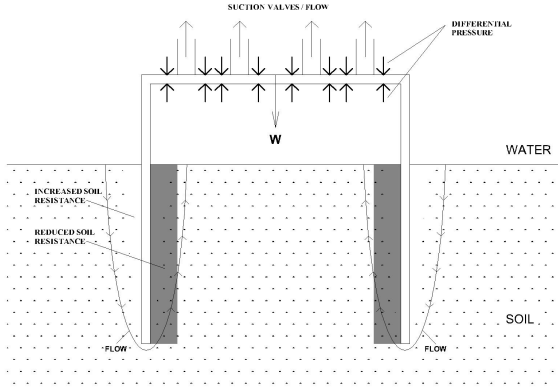


Figure 1. Seepage flow for suction installation.

for suction bucket installation in sand, only few are focusing on the interaction between the sand and the skirt of the bucket during penetration. This can be achieved by analyzing the penetration resistance. This research focuses on an empirical model, in which penetration resistance is a function of cone resistance, q_c directly taken from the CPT tests (Det Norske Veritas, 1992). The analysis is based on 6 suction and 4 force installation tests followed by induced water pressure uninstillation of a scaled bucket, conducted in the laboratory facilities of Aalborg University. The height of the model was 0.5 m and the diameter 1 m. Pore pressures were measured at the tip and skirt wall around the bucket, as illustrated in Figure 2, by pressure transducers. Penetration resistance is calculated and the empirical coefficients k_p and k_f which are associated with the tip resistance and the skirt friction of the bucket respectively, are obtained for both installation procedures. Results are being compared in order to calculate and propose values for the β factors, which are representation of the reduction of soil resistance due to suction. In section 2 existing theories on the empirical coefficients are presented. In section 3 a brief explanation on the procedure followed in the laboratory is displayed. The methodology for the calculations of the empirical coefficients can be found in section 4, while in sections 5, 6 and 7 all the results are presented, discussed and summarized respectively.

2. State of Art for the empirical coefficients

Installation standards of bucket foundations are usually based on theories regarding pile foundations. It can be assumed that the bucket works as an open ended pile. The most common one was proposed by American Petroleum Institute (2000) concerning open ended pile foundations. Soil resistance is assumed to be the sum of the external shaft friction, the end bearing on the pile wall annulus and the total internal shaft friction or the end bearing of the plug. Additionally, the unit end bearing is dependent on

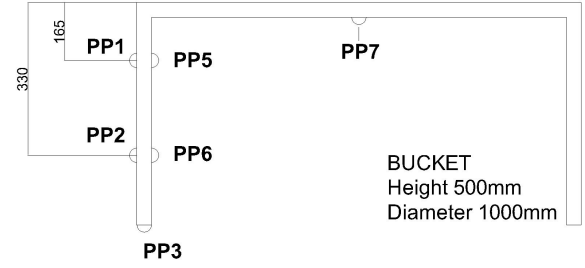


Figure 2. Pressure transducers at the skirt, the skirt tip and under the lid of the bucket on the laboratory model.

the dimensionless bearing capacity factor, N_q and on the effective overburden pressure, p_o .

Det Norske Veritas Institution, also called DNV, in 1992 presented a study about penetration resistance of bucket skirts. DNV suggests that penetration resistance of the steel skirts is the sum of friction resistance, inside, outside and at the tip of the bucket skirt, where calculations should be based on the results of in-situ testing supported by laboratory tests. For the field tests CPT data was used, since it gives a continuous record of the cone penetration resistance over the depth.

DNV method for calculating the penetration resistance based on results from CPT tests, is presented in the following equation as:

$$R = R_{fI_f} + R_{fO_f} + R_{tip_f} \quad (1)$$

Where,

$$R_{fI_f} = \pi D_I k_{fI} \int_0^z q_c(l) dz \quad (2)$$

$$R_{fO_f} = \pi D_O k_{fO} \int_0^z q_c(l) dz \quad (3)$$

$$R_{tip_f} = A_{tip} k_p q_c(z) \quad (4)$$

Where,

A_{tip}	Area of the tip of the bucket
z	Penetration depth
k_{pf}	Empirical coefficient from force procedure
k_{fI_f}	Empirical coefficient from force procedure
k_{fO_f}	Empirical coefficient from force procedure
q_c	Cone resistance
D_I	Inner diameter of the bucket
D_O	Outer diameter of the bucket

Det Norske Veritas (1992) proposes reference values for k_p and k_f coefficients for North Sea sand and they are presented in table 1.

Empirical coefficients	k_p	k_f
Lowest expected	0.3	0.001
Highest expected	0.6	0.003

Table 1. Recommended values from DNV for empirical coefficients k_p and k_f .

A method proposed by Lehane et al. (2005) called UWA-05 design method, was developed for open and closed ended driven piles in sand. This method suggests that k_f is a function of the internal and external diameter ratio of the pile. UWA-05 design method is developed for open and closed ended driven piles in sand. The empirical coefficient k_f associated with the skirt friction of the bucket is calculated with the following eq. as:

$$k_f = C \left[1 - \left(\frac{D_I}{D_O} \right)^2 \right]^{0.3} \tan \delta \quad (5)$$

Where,

C	Constant, assumed 0.021 in Lehane et al. (2005)
δ	Interface friction angle
D_I	Inner diameter of the bucket
D_O	Outer diameter of the bucket

In addition to DNV (1992) theory, a study conducted by Koteras et al. (2016) presents the AAU CPT-based method, which takes into account the penetration resistance reduction due to suction by introducing the β factors in the equations 6, 7 and 8 as:

$$R_{fI_s} = \pi \beta_{in} D_I k_{fI_f} \int_0^z q_c(l) dz \quad (6)$$

$$R_{fO_s} = \pi \beta_{out} D_O k_{fO_f} \int_0^z q_c(l) dz \quad (7)$$

$$R_{tip_s} = A_{tip} \beta_{tip} k_{pf} q_c(z) \quad (8)$$

Where,

$$\beta_{in} = \left(1 - r \frac{p}{p_{crit,avg,in}} \right) \quad (9)$$

$$\beta_{out} = \left(1 + r \frac{p}{p_{crit,avg,out}} \right) \quad (10)$$

$$\beta_{tip} = \left(1 - r \frac{p}{p_{crit,tip}} \right) \quad (11)$$

Where,

p	Applied suction
$p_{crit,avg,in}$	Critical suction average inside
$p_{crit,avg,out}$	Critical suction average outside
$p_{crit,avg,tip}$	Critical suction average at the tip
r	Restriction Factor

The subscript s , denotes the soil penetration resistance that was calculated with respect to suction installation. The subscript f denotes all the values calculated with respect to force installation.

In another study performed by Andersen et al. (2008), results about skirt friction and tip resistance coefficients are presented for prototype models, along with small scale laboratory tests. Calculations in this study, are based on the DNV standard. It has to be mentioned that the in current study, both tests that the bucket was installed with additional weight and by underpressure application under the lid will be considered. Therefore, the prototype models installed by force in Andersen et al. (2008) study, were denoted as Draupner E and Sleipner T and the ones installed by suction as Hardening A7, A8 and Prototype A. Different values of k_f were assumed in order to calculate k_p . As far as the laboratory tests are concerned, the bucket tested had a diameter, D of 0.557 m, skirt thickness, t of 8 mm, and 0.32 m skirt height, h . Tests run in a tank with a diameter of 1.6 m. The value for k_f was set to 0.0053 in order to have the best fit with the measured penetration resistance. Tests PEN 1-3 were preceded with installation by force and tests PEN 5, 9 and 12 with installation by suction. In table 2 an overview of Andersen et al. (2008) results for k_p and k_f are presented.

Case	k_p	k_f
Force		
Draupner E	0.01–0.08	0–0.0015
Sleipner T	0.05–0.13	0–0.0015
PEN 1-3	1.03–1.19	0.0053
Suction		
Hardening A7	0.37–0.45	0.001–0.0015
Hardening A8	0.55–0.60	0.001–0.0015
Prototype A	0.13–0.15	0.001–0.0015
PEN 5	1.24	0–0.0053
PEN 9	0.95	0.0053
PEN 12	0.93	0.0053

Table 2. Values from Andersen et al. (2008) for empirical coefficients k_p and k_f , for different cases.

Senders and Randolph (2009) conducted jacked tests (without suction), at a penetration ratio of 0.1 mm/s. Using the UWA-05 method (eq. 5), proposed by Lehane et al. (2005), they found a k_f value of 0.0015 for an interface friction angle of 22 degrees (constant C was assumed to be 0.012). The k_p value was assumed to be 0.2 due to the fact that sand used was very dense. For the suction installation tests that Senders and Randolph (2009) conducted, no calculations for empirical coefficients were performed.

Furthermore, Lian et al. (2014) carried out small-scaled tests, without suction to get unreduced penetration resistance under no pore water flow. The penetration resistance was calculated by the CPT-based method using averaged values of q_c . Results show that the best correlation to their calculations are obtained with the values proposed by DNV (1992) (see table 1).

The method followed in this article is based on the AAU CPT-based method proposed by Koteras et al. (2016) for calculating the empirical coefficients. An analysis of how the coefficients k_p and k_f , along with the cone resistance vary, due to differences in installation procedure is presented. Regarding those differences, calculations of the β factors will be performed by analyzing and comparing the coefficients obtained from suction to the ones obtained from force installation.

3. Materials, Equipment, and Procedure of the Laboratory Tests

In the laboratory facilities of Aalborg University suction or force installation and induced water pressure uninstillation tests were performed between the period of January and May 2016. The dimensions of the bucket foundation model were 1 m in diameter, D , 0.5 m in skirt height, h and 3 mm in skirt thickness, t , which corresponds to prototype foundation model with ratio of $h/D = 0.5$ (see Figure 3). The material that the bucket was made of is steel and its

self weight was calculated at 201 Kg or 2.01 KN. Pressure transducers were placed on the skirt of the bucket and under the lid, as shown in figure 2, measuring excess pore pressures during installation and uninstillation. The tests were performed in a large container (sandbox) filled with gravel for the first 0.3 m and with Aalborg University No.1 sand for the next 1.2 m. Container's diameter and height were 3 and 1.52 m respectively. A hydraulic piston used as an assisting driving tool during the whole procedure.

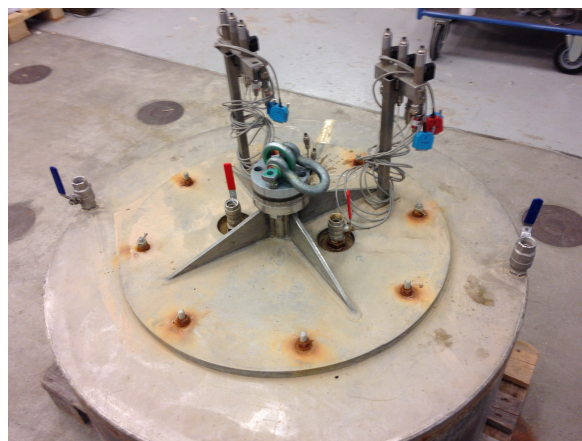


Figure 3. Foundation model used in the experiments performed by Gitsas et al. (2016).

Before each experiment the soil was saturated and compacted with the use of a vibrator. The purpose of this procedure was to have a planned density of the sand, regarding the fact that the soil was destroyed in the end of each test. In order to ensure good compaction of the soil, 4 CPT tests were performed before each test and values of cone resistance, q_c , were acquired. Furthermore, after installation and before uninstillation 8 more CPT tests were conducted (4 inside through the valves, and 4 outside the bucket's skirt on the surrounding soil). Figure 7 presents the places in the sandbox where CPT's were conducted. Table 3 illustrates all experiments performed with their corresponding water level. Keeping the water level steady at all times during testing, assist us to correct the pore pressures with the hydrostatic one.

Regarding the installation, two different procedures were followed. The first one was by applying suction under the lid of the bucket. In order to achieve that, four valves were placed on top of the bucket and connected with small hoses that could pump out the water. Those hoses were connected to a vacuum, which controlled the application of underpressure inside the bucket. Installation started after self-weight penetration for the sake of ensuring a seal component at the edge of the bucket with the surrounding soil. In the tests denoted as "Pure Suction" in table 3, the application of suction started right after the self-weight penetration. However, in the tests denoted as "Suction + Force", additionally to the self-weight penetration, 2.01 KN more were applied before suction begun. That happened in

Test Number	Characteristics	Water Level [cm]
1 Inst.	Suction+Force	8
2 Inst.	Suction+Force	8
3 Inst.	Suction+Force	13
4 Inst.	Pure Suction	11
5 Inst.	Pure Suction	11
6 Inst.	Force	10
7 Inst.	Force	7
8 Inst.	Force	8
9 Inst.	Pure Suction	10
10 Inst.	Force	10
1 Uninst.	Uninstallation without weight	8
2 Uninst.	Uninstallation without weight	8
3 Uninst.	Uninstallation without weight	13
4 Uninst.	Uninstallation without weight	11
5 Uninst.	Uninstallation with 201Kg	11
6 Uninst.	Uninstallation with 402Kg	10
7 Uninst.	Uninstallation with 402Kg	7
8 Uninst.	Uninstallation with 302Kg	8
9 Uninst.	Uninstallation with 302Kg	10
10 Uninst.	Uninstallation with 201Kg	10

Table 3. Description of installation and uninstallation tests.

order to resemble double the self-weight of the bucket and investigate any major differences in the 2 procedures (see Gitsas et al. (2016)). Installation finished half an hour after the displacement transducer stopped giving any signal on the computer, in order to ensure that the installation was fully complete. Figures 4 and 5 depict the installation load applied of the corresponding experiments.

For the force installation procedure the soil resistance against penetration is a sum of friction on the bucket skirt and tip resistance (Vaitkunaite et al., 2015). Installation started with positioning the bucket right on the soil surface level, while zeroing the signal of the load cell. The penetration rate was set at 0.1 mm/s. Installation finished after the displacement transducer stopped giving any signal on the computer, meaning that no further installation could be achieved. Figure 6 illustrates the load applied for installation of the bucket for the corresponding experiments.

As far as the uninstallation procedure is concerned, it

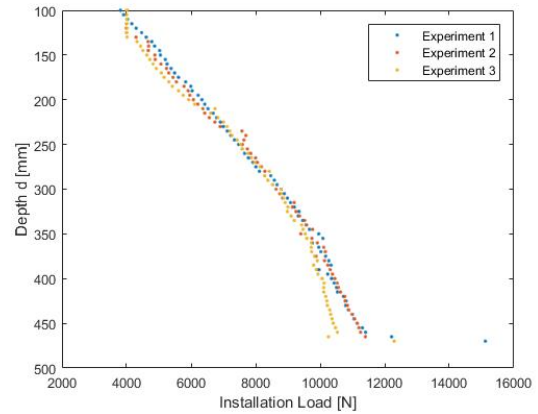


Figure 4. Installation load over the depth for tests 1, 2, 3.

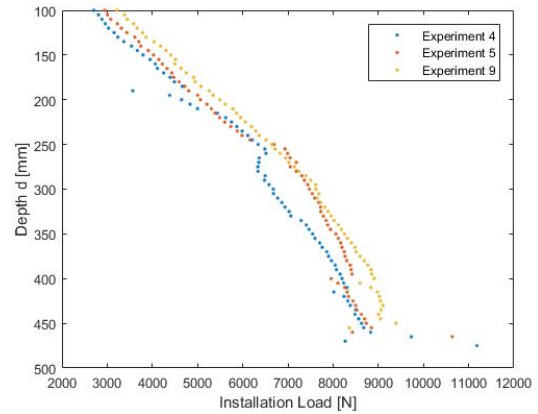


Figure 5. Installation load over the depth for tests 4, 5, 9.

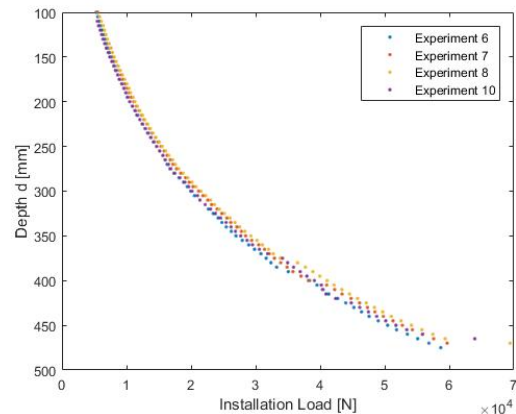


Figure 6. Installation load over the depth for tests 6, 7, 8, 10.

was performed by using one of the buckets valves for water pressure application, while the other three remained closed at all times. Pressure transducer placed under the lid of the bucket, measured the pressure during the whole procedure. By the use of eq. 12, the applied pressure was transformed

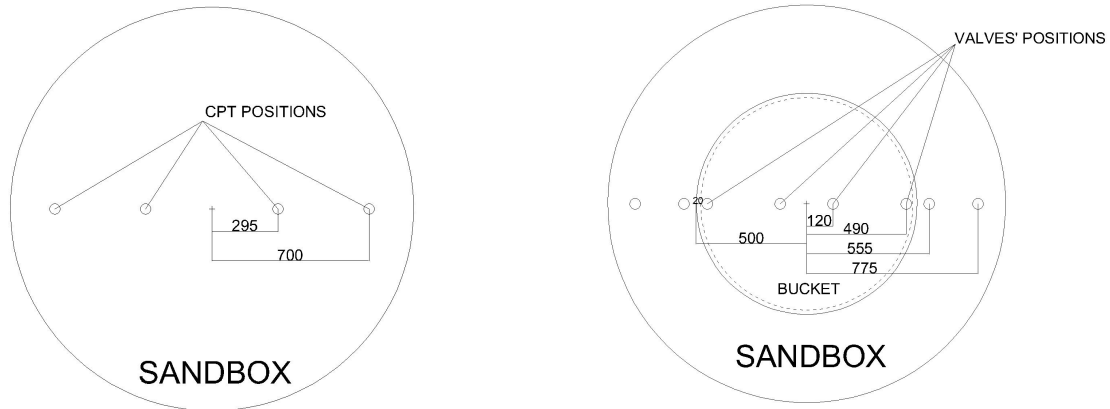


Figure 7. CPT's performed before and after installation.

into force and Figures 8, 9 and 10 show the results of the uninstallation force of the corresponding experiments. The procedure finished when water flowed out of the foundation skirt, which was measured to be approximately at 0.35 m of height. Finally different weights of the bucket were simulated by applying additional load on top of the bucket. Differences found not to be substantial as it can be clearly seen in the next figures.

$$F = PA \tag{12}$$

Where, P is the applied pressure and A is the area under the lid of the bucket.

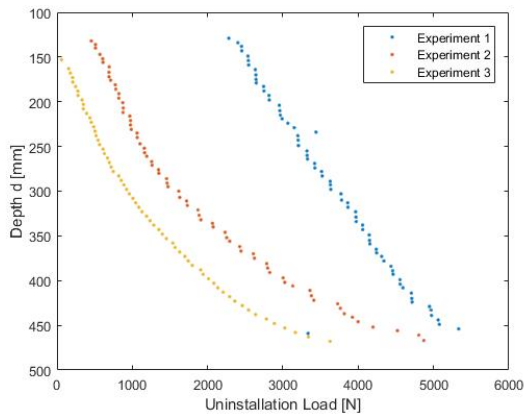


Figure 8. Uninstallation load over the depth for tests 1, 2, 3.

Finally, in order to investigate any pressure changes on the boundaries, a beam with three pressure transducers was placed at the edge of the sandbox. The length of the beam was 1 m and the transducers were placed at the tip, over 0.25 m and 0.5 m of the tip, respectively. The transducers recorded data during both installation and uninstallation.

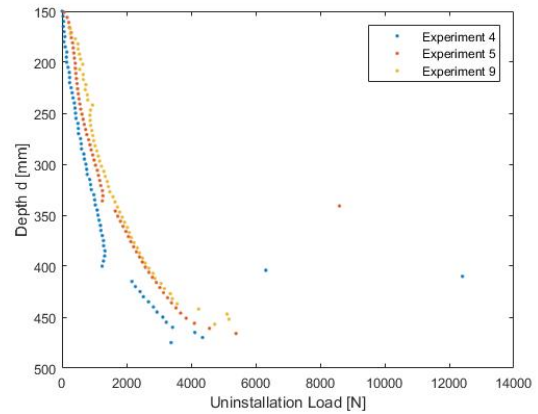


Figure 9. Uninstallation load over the depth for tests 4, 5, 9.

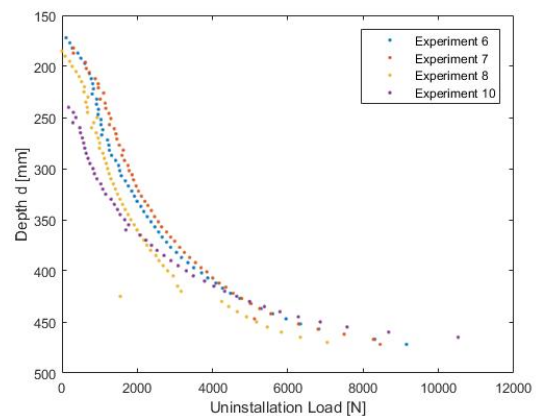


Figure 10. Uninstallation load over the depth for tests 6, 7, 8, 10.

Results revealed that the boundaries were slightly affected by the application of suction. A more detailed explanation

for the procedure, along with all the data acquired from the tests in table 3, can be found in Gitsas et al. (2016).

4. Methodology for the Calibration of Empirical Coefficients and β Factors

The governing equation for penetration resistance of the bucket foundation is obtained by equilibrium between forces and soil resistance against the penetration (Andersen et al., 2008). The penetration resistance is then given by:

$$R = G' + F \quad (13)$$

Where,

- R Total penetration resistance
- G' Self-weight of the bucket adjusted for buoyancy
- F Force or suction applied on the bucket

In this paper the self-weight of the structure is included in the application of the force, thus it is not going to be visible in the equations for calibrating the empirical coefficients. Additionally, the total penetration resistance is a summation of two components; the tip resistance of the skirt, R_{tip} and the skirt friction, R_f , according to DNV (1992).

$$R = R_{tip} + R_f \quad (14)$$

The skirt friction consists of the inner skirt friction R_{fI} and the outer skirt friction R_{fO} .

$$R_f = R_{fI} + R_{fO} \quad (15)$$

The total skirt friction is calculated with the CPT-based method from DNV (1992). As mentioned earlier, this method relates the cone resistance q_c to the side friction and tip resistance, using the empirical coefficients k_{pf} and k_{ff} . The subscript f denotes the values that came from force installation, in order to separate them from the ones that come from suction installation, in which the subscript is going to be the letter s . By integration along the inner and outer area of the skirt, the total skirt friction is obtained from eq. 15 as:

$$R_{ff} = \pi D_I k_{ff} \int_0^z q_c(l) dz + \pi D_O k_{ff} \int_0^z q_c(l) dz \quad (16)$$

The tip resistance of the caisson, used in eq. 14, is:

$$R_{tipf} = A_{tip} k_{pf} q_c(z) \quad (17)$$

As a starting point for the calibration of the empirical coefficients the values from the uninstallation tests were

used. That is due to the fact that during uninstallation the tip resistance is assumed to be zero. Hence, only the skirt friction of the bucket is responsible for the soil resistance. In this way calculation of k_f coefficient can be achieved. After analyzing results from the CPT's, averaged values of cone resistance q_c for every 5 mm depth is obtained. For the calculations of k_f only the CPT's after installation are used. In Figure 7 the 2 CPT tests inside and the 2 outside on the boundaries of the bucket, were averaged for each test and their values are presented over the depth in Figures 11 12, 13, 14, 15 and 16.

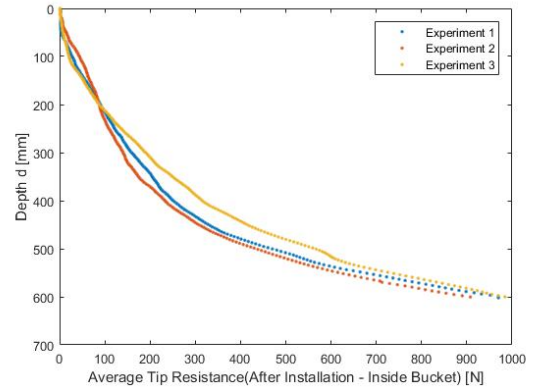


Figure 11. Average q_c over the depth for the 2 CPT's inside, on the bucket's boundaries for tests 1, 2, 3.

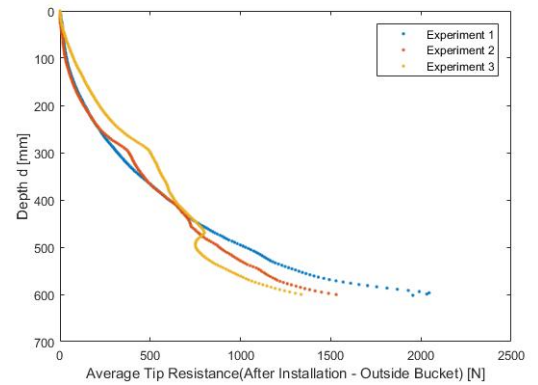


Figure 12. Average q_c over the depth for the 2 CPT's outside, on the bucket's boundaries for tests 1, 2, 3.

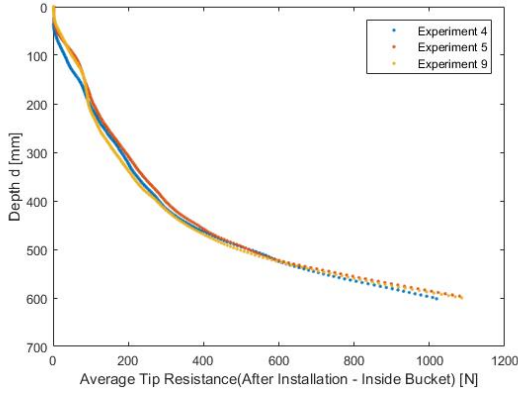


Figure 13. Average q_c over the depth for the 2 CPT's inside, on the bucket's boundaries for tests 4, 5, 9.

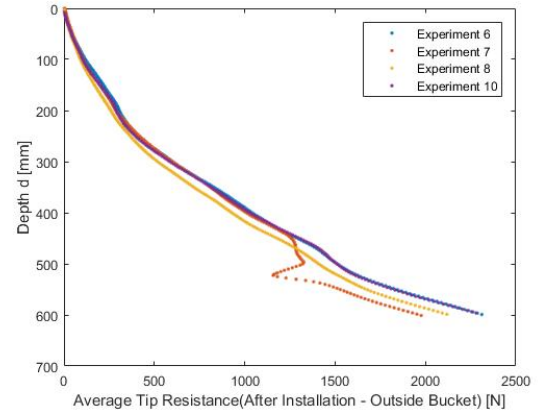


Figure 16. Average q_c over the depth for the 2 CPT's outside, on the bucket's boundaries for tests 6, 7, 8, 10.

From the combination of equations 13, 14 and 16 the following equation is obtained:

$$F_{uninstal_f} = R_{f_f}, \quad (18)$$

Where, $F_{uninstal_f}$ is the applied uninstallation load from a force installation experiment.

Equation 18 can be rewritten based on eq. 16 by isolating the empirical coefficient k_{f_f} as:

$$k_{f_f} = \frac{F_{uninstal_f}}{\pi(D_I + D_O) \int_0^z q_c(l) dz} \quad (19)$$

From the uninstallation procedure, values for the k_{f_f} are calculated and an averaged value is used for further analysis of the installation tests. Using the average value of k_{f_f} , a set of k_{p_f} values is obtained for each penetration depth. During installation of the bucket, soil resistance comes from the skirt friction and the skirt tip. Therefore, combining equations 13, 14, 16 and 17, leads to the following equation:

$$F_{inst_f} = R_f + R_{tip_f}, \quad (20)$$

where F_{inst_f} is the applied installation load from the force installation experiments.

From eq. 20, the empirical coefficient k_{p_f} is isolated as:

$$k_{p_f} = \frac{F_{inst_f} - R_{f_l} - R_{f_o}}{A_{tip} q_c(d)} \quad (21)$$

The values of q_c used for the calculations of k_{p_f} , corresponds to the CPT tests conducted before the installation of the bucket. The averaged values of q_c over the depth are illustrated in Figures 17, 18 and 19.

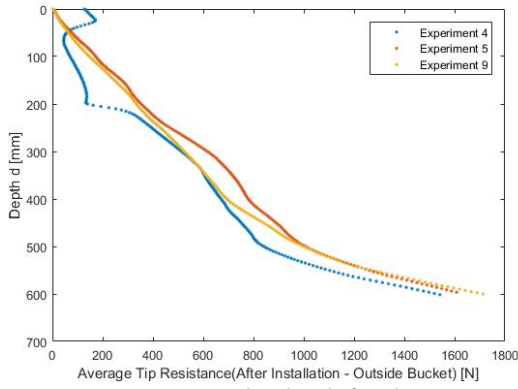


Figure 14. Average q_c over the depth for the 2 CPT's outside, on the bucket's boundaries for tests 4, 5, 9.

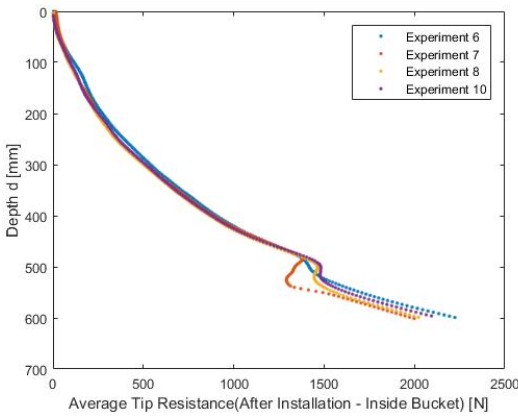


Figure 15. Average q_c over the depth for the 2 CPT's inside, on the bucket's boundaries for tests 6, 7, 8, 10.

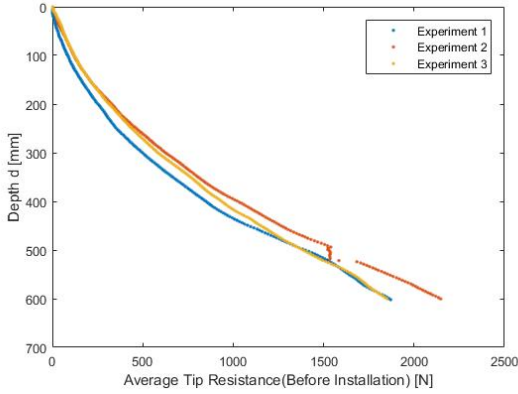


Figure 17. Average tip resistance over the depth for tests 1, 2 and 3, before the suction installation of the bucket.

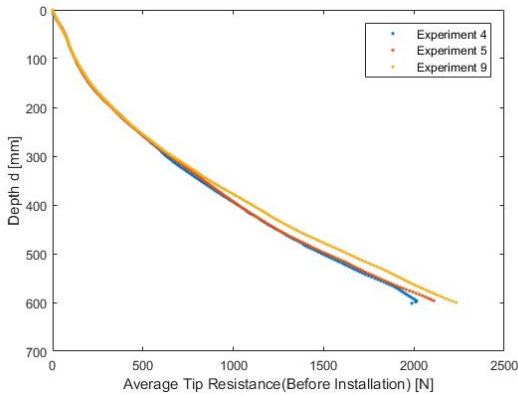


Figure 18. Average tip resistance over the depth for tests 4, 5 and 9, before the suction installation of the bucket.

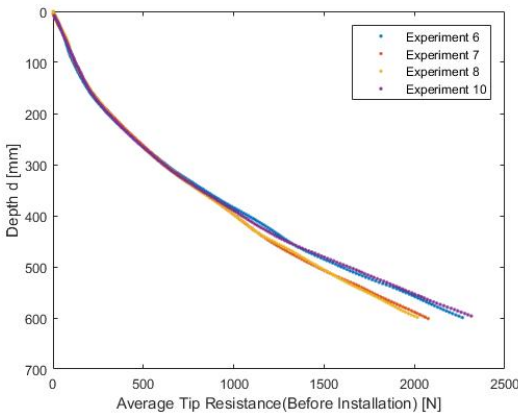


Figure 19. Average tip resistance over the depth for tests 6, 7, 8 and 10 before the force installation of the bucket.

Even though the aforementioned procedure is applied only for tests that include installation by force, in this article the same procedure will be followed in order to calculate k_{p_s} and k_{f_s} coefficients for installation by suction. In addition to that, differences between the coefficients from force

and suction installation allow to calibrate the β factors proposed by Koterias et al. (2016) from eq. 6, 7 and 8. Those equations are based on the simple model, presented in eq. 22, 23 and 24 that connects k_{f_f} to k_{f_s} and k_{p_f} to k_{p_s} .

$$k_{f_{I_s}} = \beta_{avg,in} k_{f_{I_f}} \quad (22)$$

$$k_{f_{O_s}} = \beta_{avg,out} k_{f_{O_f}} \quad (23)$$

$$k_{p_s} = \beta_{tip} k_{p_f} \quad (24)$$

For the sake of simplicity in the calculations, $\beta_{avg,out}$ and $\beta_{avg,in}$ are calculated as an average value called $\beta_{in,out}$. The same applies for k_{f_I} and k_{f_O} , which were calculated as an average k_f for inside and outside the bucket skirt. In both cases the values of q_c obtained after installation for inside and outside the bucket's skirt, were averaged and used in the calculation process. Results for the k_p , k_f and the β factors are presented in the next sections.

5. Results of k_p and k_f Coefficients

In Figures 17 and 18 the cone resistance is observed to be quite high compared to Figures 11, 12, 13 and 14, in which suction has clearly affected the soil. Especially, the CPT tests conducted inside the the bucket's skirt after installation show a substantial difference even with the ones conducted outside the skirt, in the surrounding soil. However, from Figures 15, 16 and 19 it can be concluded that the soil was not highly affected from the force installation procedure.

Regarding the installation load from Figures 4, 5 and 6 it can be clearly seen that there are substantial differences between the two procedures. When installing with suction the procedure is very slow and there has to be caution regarding the exceedance of the critical suction pressure. The maximum load applied for full suction installation was measure to be around 12 KN. However, the force installation procedure is quicker and the high resistance of the soil demands a higher installation load, which measured to be around 60 KN for fully installed bucket. Due to these differences, k_p coefficient is highly affected.

As far as the uninstillation is concerned, Figures 8, 9 and 10 show that there are not any crucial deviations on the applied load during the procedure, even though different weights of the bucket were simulated. Small differences in uninstillation load will lead to similar k_f coefficients. Table 4 presents the average values of uninstillation load, k_p and k_f coefficients for all tests performed by Gitsas et al. (2016)

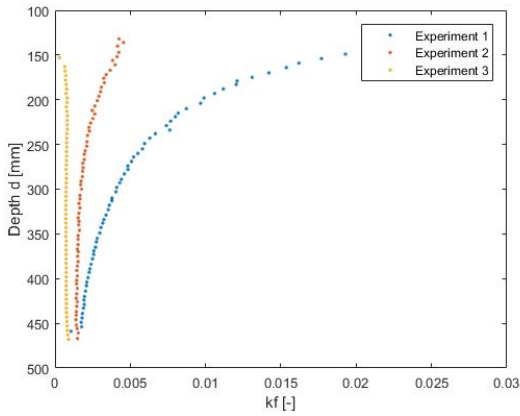


Figure 20. k_f values over the depth for tests 1, 2 and 3.

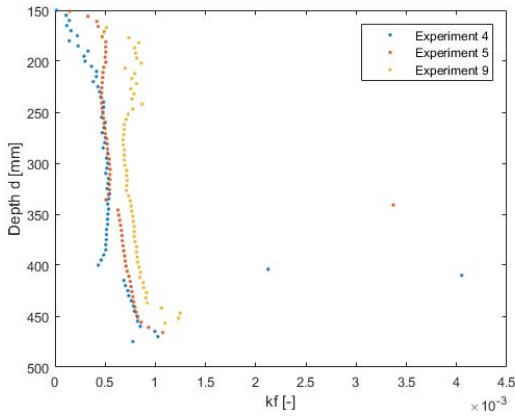


Figure 21. k_f values over the depth for tests 4, 5 and 9.

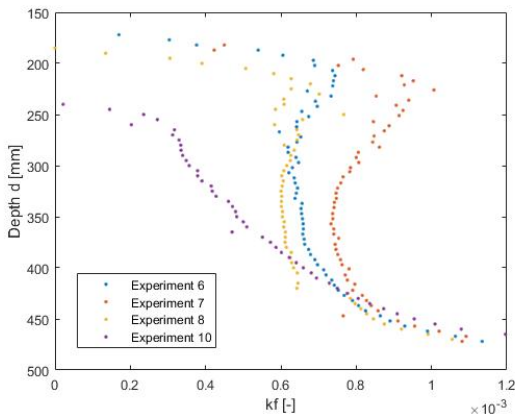


Figure 22. k_f values over the depth for tests 6, 7, 8 and 10.

Figures 20, 21 and 22 illustrate the variations of k_f coefficients over the depth for all the experiments. The average values for each test are presented in table 4, in order to take a better look on the results. As already mentioned k_f is proportional to the uninstallation load and inversely

to the cone resistance, based on eq. 19. This means that high uninstallation load with low cone resistance after the experiments will lead to a high value of k_f . That is the case in tests 1 and 2, where the k_f coefficient is relatively high compared to the values of the other tests.

In Figures 23, 24 and 25 the k_p coefficients over the depth are depicted for all cases. The averaged values of each test presented in table 4, show high deviations between the suction installation experiments compared to the force ones. Those differences come from the fact that the installation load varied substantially for the different procedures, as mentioned before. In addition to that, the cone resistance values that used for the calculations were similar, because they are the ones obtained before the installation. Furthermore, k_f values do not seem to affect the tip resistance coefficient highly due to the fact that no crucial variations were observed.

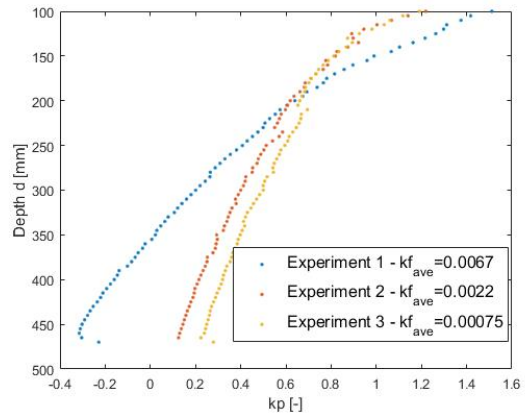


Figure 23. k_p values over the depth for tests 1, 2 and 3.

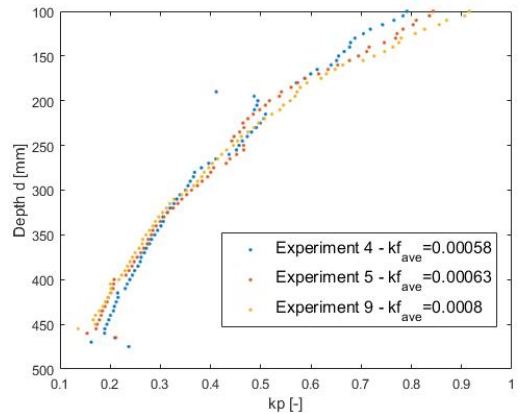


Figure 24. k_p values over the depth for tests 4, 5 and 9.

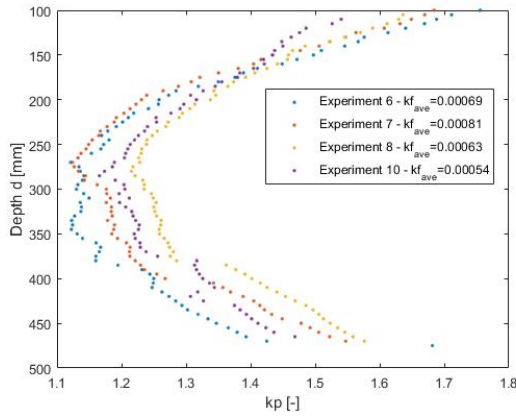


Figure 25. k_p values over the depth for tests 6, 7, 8 and 10.

Test No.	avg. $F_{uninstal}$ [KN]	avg. k_f	avg. k_p
1	-3.9	0.0067	0.3465
2	-2.2	0.0022	0.4871
3	-1.6	0.00075	0.5493
4	-1.3	0.00058	0.4089
5	-1.9	0.00063	0.4228
6	-3	0.00069	1.23
7	-2.7	0.00081	1.25
8	-3.3	0.00063	1.21
9	-2.1	0.0008	0.4363
10	-2.5	0.00054	1.32

Table 4. Average values for uninstillation load, k_f and k_p for all cases.

All results show high correlations with the proposed coefficients from DNV (1992) standard and Andersen et al. (2008) study. Thus, the analysis performed in this article is valid. However, due to experimental inaccuracies and lack of known theories about β factors, a lot of uncertainties can arise. In the next section, the values of k_f and k_p are averaged for three different cases. An average value of coefficients is obtained for tests denoted as "Suction + Force" (1, 2 and 3), "Pure Suction" (4, 5 and 9) and "Force" (6, 7, 8 and 10). The coefficients acquired for the three different cases are presented in table 5. The two suction installation coefficients are compared to the force ones and β values are obtained.

Case	avg. k_f	avg. k_p
"Suction + Force"	0.003217	0.4363
"Pure Suction"	0.00067	0.4227
"Force"	0.000667	1.25

Table 5. Averaged k_p and k_f for different installation procedures.

6. Results of β Factors

Figures 26 and 27 illustrate the $\beta_{in,out}$ factors over the depth, obtained for the two different cases. The values acquired for the case of "Pure Suction" seem quite smaller following a steady path over the depth compared to the ones for the case of "Suction + Force", which follow an increasing path. However, after a point, β values in Figure 26 exceed the value of 1, which is the highest expected for these calculations. This may have happened due to inaccuracies on the experimental results, leading to faulty calculations of k_f and k_p coefficients. As a result, β values are highly affected and exceed the maximum value.

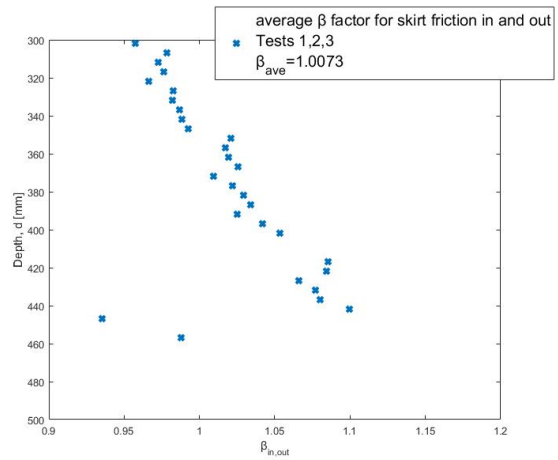


Figure 26. $\beta_{in,out}$ for "Suction + Force" installation case.

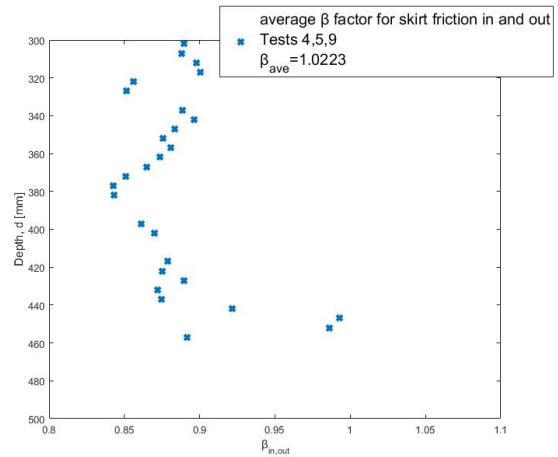


Figure 27. $\beta_{in,out}$ for "Pure Suction" installation case.

Same pattern is observed for the values obtained for the β_{tip} , as shown in Figures 28 and 29. For the first case, β_{tip} presents a decreasing path over the depth, while in the second one a more steady path is followed. However, in both cases, even though the values of the coefficient are very close to 1, the critical value is exceeded, which make the results inaccurate due to uncertainties.

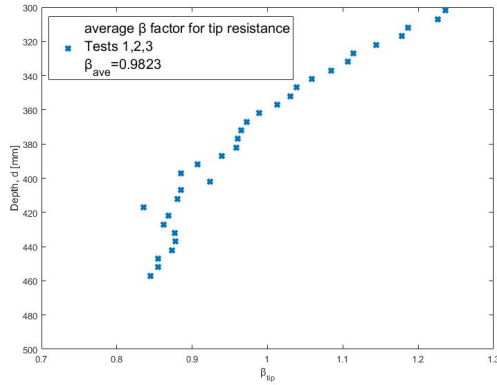


Figure 28. β_{tip} for "Suction + Force" installation case.

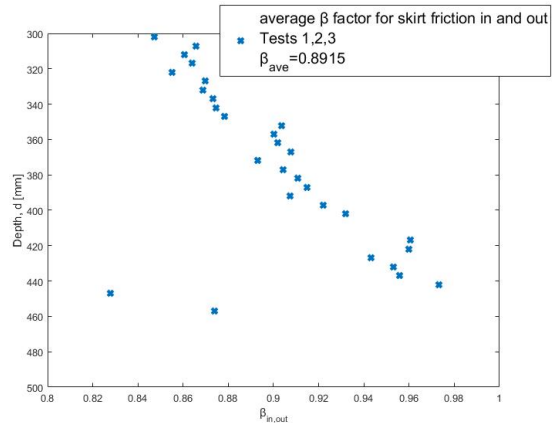


Figure 30. $\beta_{in,out}$ for new average $k_f = 0.00354$, for "Suction + Force" case.

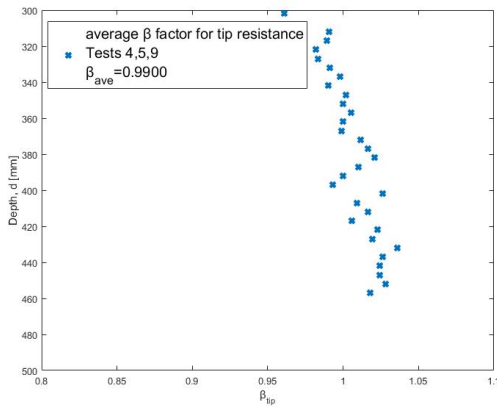


Figure 29. β_{tip} for "Pure Suction" installation case.

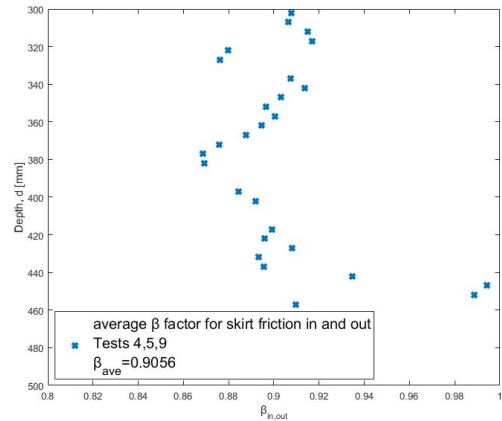


Figure 31. $\beta_{in,out}$ for new average $k_f = 0.000804$, for "Pure Suction" case.

After the beginning of uninstillation the k_f coefficient decreases due to the fact that skirt friction is lower than the real one. It is safe to assume a higher average value of k_f and propose new values of β factors. Higher value of k_f coefficient for the suction cases, will lead to a reduction on the β factors. The new values of k_f are shown in table 6. For the case of "Suction + Force" a value 10 % higher was chosen and for the case of "Pure Suction" a value 20 % higher in order to compare with the value from the "Force" case. k_p coefficients remained the same and results are presented in the next figures.

Case	new avg. k_f
"Suction + Force"	0.00354
"Pure Suction"	0.000804
"Force"	0.000667

Table 6. New k_f coefficients for the different installation procedures.

Figures 30, 31, 32 and 33 illustrate the new, optimal values obtained for the β factors associated with the friction inside and outside of the skirt and at the tip of the bucket, respectively. In all cases, the β is close to 1, which theoretically means that the applied suction was not close to the critical one and the results of β factors are not highly affected by the different procedures. However, in reality, the critical suction was measured to be very close to the applied one and reduced values of β factors were expected. The average proposed values of $\beta_{in,out}$ and β_{tip} are presented in table 7.

Case	$\beta_{in,out}$	β_{tip}
"Suction + Force"	0.8915	0.9315
"Pure Suction"	0.9056	0.9415

Table 7. Proposed values of $\beta_{in,out}$ and β_{tip} from the experiments conducted by Gitsas et al. (2016).

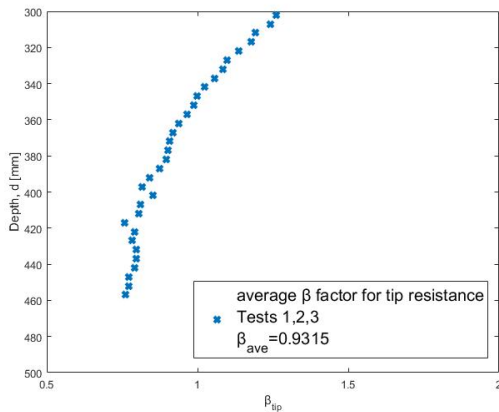


Figure 32. β_{tip} for new average $k_f = 0.00354$, for "Suction + Force" case.

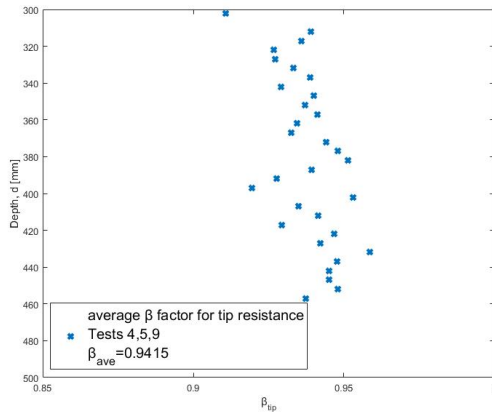


Figure 33. β_{tip} for new average $k_f = 0.000804$, for "Pure Suction" case.

7. Conclusions

In the present study, an analysis based on the empirical model that connects the penetration resistance to the cone resistance, q_c , has been performed. Furthermore, based on a study conducted by Koteras et al. (2016), soil resistance reduction factors due to suction installation, were calculated. In order to achieve that, medium-scaled laboratory tests, regarding the installation and uninstallation procedure of a bucket foundation in dense sand, were performed. Experiments included two installation methods, installation by suction and installation by force, while only one for uninstallation, induced water pressure uninstallation. The scaled foundation model used in this study had dimensions of 1m in diameter, D and 0.5m in skirt length, h ($h/D = 0.5$). Throughout this paper, results for cone penetration data, installation load, uninstallation load and for the empirical coefficients k_f and k_p have been provided, for the sake of finding values of β factors, based on the method provided by Koteras et al. (2016), called AAU CPT-

based method. Obtaining β factors can lead to a better understanding on how the resistance of the sand is affected from suction installation of a bucket foundation and the interaction between the sand and the bucket skirt during installation and uninstallation procedure.

Values of k_f obtained for all tests, show small deviations due to the fact that there were not any substantial differences in the uninstallation load. Furthermore, they seem to have high correlation with the proposed values of the DNV standard. However, k_p values tend to get higher values for the force installation procedure compared to the suction one, regarding the crucial difference in the installation load for these two procedures. The force installation load found to be 6 times higher than the one applied for the suction installation. Results of the k_p coefficient, also show high correlation with known studies.

The calculation of k_p and k_f coefficients for different procedures allowed us to calibrate values of the β factors, that are introduced in the penetration resistance equation, in order to take into consideration the reduction of soil resistance due to suction. The original values of k_f used for the result acquisition show inaccuracies with respect to the β factors. However, new, higher k_f were assumed and the values of $\beta_{in,out}$ and β_{tip} were calculated. The average values proposed for the experiments conducted by Gitsas et al. (2016) are close to 0.9. That means that the critical suction pressure is not exceeded during suction application, theoretically. The fact that there are not any known studies to confirm or validate this research make the results inconclusive, but not inaccurate. The validity of this research comes from the fact that the empirical coefficients are inside the proposed range of known studies.

Future work should be focused on performing full-scale installation tests both with the application of suction and force in order to validate the results presented in this study. Back calculations on the existing results, due to the fact that the method followed in this article is not considered straightforward, would give a more clear look on the empirical coefficients and the β factors. Furthermore, experiments in layered soil profiles, where the cone resistance changes significantly between the different type of soils, would be an improvement on the existing theory and a more often practice of it could be implemented. The results presented here are considered to be a step forward in the development of an improved model of calculating soil penetration resistance for suction installation of bucket foundations, based on CPT results.

References

- American Petroleum Institute (2000). Recommended practice for planning, designing and constructing fixed offshore platforms—working stress design.
- Andersen, K. H., Jostad, H. P., and Dyvik, R. (2008). Penetration resistance of offshore skirted foundations and

anchors in dense sand. *JOURNAL OF GEOTECHNICAL AND GEOENVIRONMENTAL ENGINEERING*, pages 106–116.

Byrne, B., Villalobos, F., Houlsby, G. T., and Martin, C. M. (2001). Laboratory testing of shallow skirted foundations in sand.

Byrne, B. W. and Houlsby, G. T. (2003). Foundations for offshore wind turbines. *The Royal Society*, page 2909–2930.

Det Norske Veritas (1992). Foundations.

Gitsas, T., Pandiella, M. H., and Sgourakis, G. N. (2016). Installation of suction bucket foundations in sand.

Houlsby, G. T. and Byrne, B. W. (2005). Calculation procedures for installation of suction caissons. *Oxford University*.

Houlsby, G. T., Ibsen, L. B., and Byrne, B. W. (2005). Suction caissons for wind turbines. *Frontiers in Offshore Geotechnics*.

Ibsen, L. B. and Thilsted, C. L. (2010). Numerical study of piping limits for suction installation of offshore skirted foundations and anchors in layered sand. *Frontiers in Offshore Geotechnics II*.

Koteras, A. K., Ibsen, L. B., and Clausen, J. (2016). Seepage study for suction installation of bucket foundation in different soil combinations. *Aalborg University*.

Lehane, B. M., Schneider, J. A., and Xu, X. (2005). The uwa-05 method for prediction of axial capacity of driven piles in sand.

Lian, J., Chen, F., and Wang, H. (2014). Laboratory tests on soil-skirt interaction and penetration resistance of suction caissons during installation in sand. *Ocean Engineering*, pages 1–13.

Senders, M. and Randolph, M. F. (2009). Cpt-based method for the installation of suction caissons in sand. *JOURNAL OF GEOTECHNICAL AND GEOENVIRONMENTAL ENGINEERING*, 135:14–25.

Tjelata, T. I. (2015). The suction foundation technology. *International Symposium on Frontiers in Offshore Geotechnics III (ISFOG)*, pages 85–93.

Vaitkunaite, E., Nielsen, B. N., and Ibsen, L. B. (2015). Bucket foundation model testing under tensile axial loading. *Aalborg University*.

CONCLUSIONS AND DISCUSSION 8

The current master thesis has been a research study regarding the suction bucket foundations, an innovative and cost effective foundation type for wind turbines. The analysis performed with respect to installation and uninstallation tests of a medium-scale bucket foundation model, in the laboratory facilities of Aalborg University. Due to the fact that research concerning installation of bucket foundations in sand is still work in process, the current research contributes to a better understanding between foundation and sand interaction, during suction installation and induced water pressure uninstallation. The thesis includes three research articles with respect to bucket foundation analysis and the results will be summarized in the following.

Suction application under the lid of the bucket during installation, creates a pressure differential that allows the foundation to be installed and also, reduces the soil resistance making the installation an easier procedure. However, a flow between the voids of the sand is created, called seepage flow. In the first article a numerical analysis for the seepage flow and the critical pressures of the suction bucket, during installation and uninstallation, have been performed. The laboratory experiments had been resembled in the finite element software Plaxis 2D. In order to achieve that the real suction measured from the experiments, applied in the software at each discrete step. Results confirmed that soil resistance at the tip is the one that shows larger reduction due to higher hydraulic gradient at that point for the installation procedure. Furthermore, even though the theoretical critical values of suction pressure were exceeded, no piping channels were observed in the laboratory. Regarding the induced water pressure uninstallation the theoretical critical pressure was not exceeded at all times. All results show high correlation with solutions from other studies for homogeneous sand making this research valid.

Except for suction installation tests, installation by force tests were performed. Although a lot of studies investigate and propose solutions for installation of bucket foundations in sandy soils, there are only a few analyzing the interaction between the bucket and the soil during installation. In order to achieve that, empirical coefficients k_p and k_f associated with tip resistance and skirt friction of the bucket respectively, have been calculated with respect to the CPT-based method proposed by DNV (1992). Coefficients were calculated from laboratory tests conducted for the current study and by Vaitkunaite et al. [2015]. Values of k_f obtained from Vaitkunaite et al. [2015] experiments, show a large deviation due to substantial differences in the application of tensile load. Higher pullout load provides higher k_f coefficients. k_p was found in the range of DNV (1992) proposed values. Concerning the experiments performed for the current study k_p values found to

be in the range of 1.21-1.32, having a very good correlation with other studies that have already calculated the k_p coefficient. Values of k_f appear to be small compared to other studies and in the range of 0.00054-0.00081.

Finally, in the last article both suction and force installation procedures are taken into account, in order to acquire and propose values for the reduction soil resistance factors, called β factors. Analysis proved to be challenging, due to the fact that these factors have never been calibrated before and exist only from a theoretical standpoint. The basic assumption was to compare the k_p and k_f coefficients, obtained for the different installation methods and based on the AAU CPT-based method proposed by Koteras et al. [2016] acquire values for the average β inside, outside and at the tip of the bucket. Results of β showed inaccuracies by using the original average values of k_f , because calculations do not taken into consideration the high importance of skirt friction in the beginning of the uninstillation. Thus, higher averaged k_f values were assumed and β factors were acquired in the range of 0.90 for inside and outside the bucket skirt and 0.93 at the tip. That means that the theoretical critical suction pressure is not exceeded during suction application. The fact that there are not any know studies to confirm or validate this research make the results inconclusive, but not inaccurate. Since this study is important for creating a model that can propose reduction factors of soil resistance during suction application, future work should be focused on performing full-scale installation tests, in order to validate the results from the present study.

BIBLIOGRAPHY

- American Petroleum Institute (API). Recommended practice for planning, designing and constructing fixed offshore platforms—working stress design., 2000.
- K. H. Andersen, H. P. Jostad, and R. Dyvik. Penetration resistance of offshore skirted foundations and anchors in dense sand. *JOURNAL OF GEOTECHNICAL AND GEOENVIRONMENTAL ENGINEERING*, pages 106–116, 2008.
- T. L. Andersen. Powerpoint presentation "wave forces on offshore structures i: Coastal, offshore, and port engineering. *Aalborg University*, 2015.
- M. Arshad and B. O’Kelly. Offshore wind-turbine structures: a review. *Trinity College Dublin*, 2015.
- E. W. E. Association. European wind energy association, 2014.
- B. W. Byrne and G. T. Houlsby. Foundations for offshore wind turbines. *The Royal Society*, page 2909–2930, 2003.
- Det Norske Veritas. Foundations., 1992.
- E. DONG. Monopile, a. URL <http://www.dongenergy.com/en>.
- E. DONG. Suction bucket jacket structure, b. URL <http://www.dongenergy.com/en>.
- E. DONG. Bucket structure sketch, c. URL <http://www.dongenergy.com/en>.
- E. Energy. E.on climate and renewables, 2015.
- T. Feld. Suction bucket, a new innovative foundation concept applied to offshore wind turbines. *Aalborg University*, 2001.
- E. Gicon. Floating structure. URL <http://www.gicon-engineering.com/home.html>.
- G. T. Houlsby and B. W. Byrne. Calculation procedures for installation of suction caissons. *Oxford University*, 2005.
- L. B. Ibsen and C. L. Thilsted. Numerical study of piping limits for suction installation of offshore skirted foundations an anchors in layered sand. *Frontiers in Offshore Geotechnics II*, 2010.
- A. K. Koteras, L. B. Ibsen, and J. Clausen. Seepage study for suction installation of bucket foundation in different soil combinations. *Aalborg University*, 2016.
- B. M. Lehane, J. A. Schneider, and X. Xu. The uwa-05 method for prediction of axial capacity of driven piles in sand. 2007.
- J. Lian, F. Chen, and H. Wang. Laboratory tests on soil-skirt interaction and penetration resistance of suction caissons during installation in sand. *Ocean Engineering*, pages 1–13, 2014.

- M. Senders and M. F. Randolph. Cpt-based method for the installation of suction caissons in sand. *JOURNAL OF GEOTECHNICAL AND GEOENVIRONMENTAL ENGINEERING*, 135:14–25, 2009.
- G. N. Sgourakis, T. Gitsas, and M. H. Pandiella. Calculation of empirical coefficients associated with tip resistance and skirt friction of a bucket foundation. *Aalborg University*, 2016.
- E. Vaitkunaite, B. N. Nielsen, and L. B. Ibsen. Bucket foundation model testing under tensile axial loading. *Aalborg University*, 2015.
- WEU. Offshore wind foundations report, 2000.

A.1 Laboratory Guide

A.1.1 Objective

In Appendix A, a detailed guide of preparing the soil, performing CPT tests along with installing and uninstalling a scaled bucket foundation model in the facilities of Aalborg University (Figure A.1) will be provided. The installation of the bucket will be described in two different ways. First, by applying suction under the lid of the bucket and second by forcing additional weight through the hydraulic piston. Also, for the uninstallation of the foundation different weights of the bucket were simulated. Moreover, data acquisition using 'Catman Professional' software is described. The tests are used in order to acquire different parameters, such as the empirical coefficients k_p and k_f , which are associated with the tip resistance and the skirt friction of the bucket, respectively. The foundation model corresponds to 1 : 10 of a prototype model used in offshore foundation, The safety instructions are given by Vaitkunaite et al. [2015].



Figure A.1: Yellow Sandbox (Kristina).

A.1.2 Safety Equipment

Equipment	Action
Safety shoes	Wear at all times
Helmet	Wear at all times
Safety belt	Wear on the sandbox while screwing or unscrewing
Earplugs	Wear when vibrating the soil
Vibration gloves	Wear when vibrating the soil
Gloves	Not mandatory but proposed for protection from the equipment
Knee protection	Not mandatory but proposed when vibrating

Table A.1: Safety equipment and proposed action.

A.1.3 Test Model

In the following Figure a detailed presentation of the dimensions of the sandbox and the scaled bucket model is depicted.

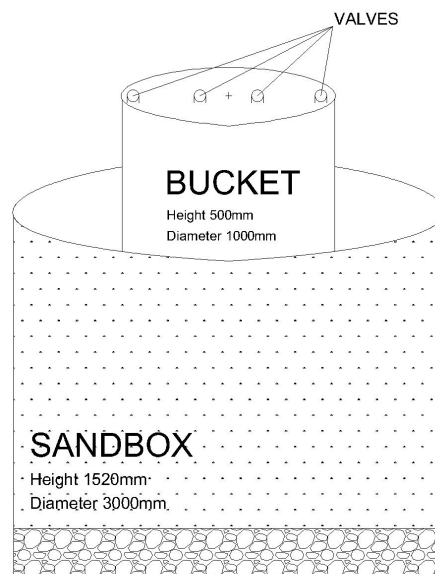


Figure A.2: Dimensions of the bucket foundation and of the sandbox.

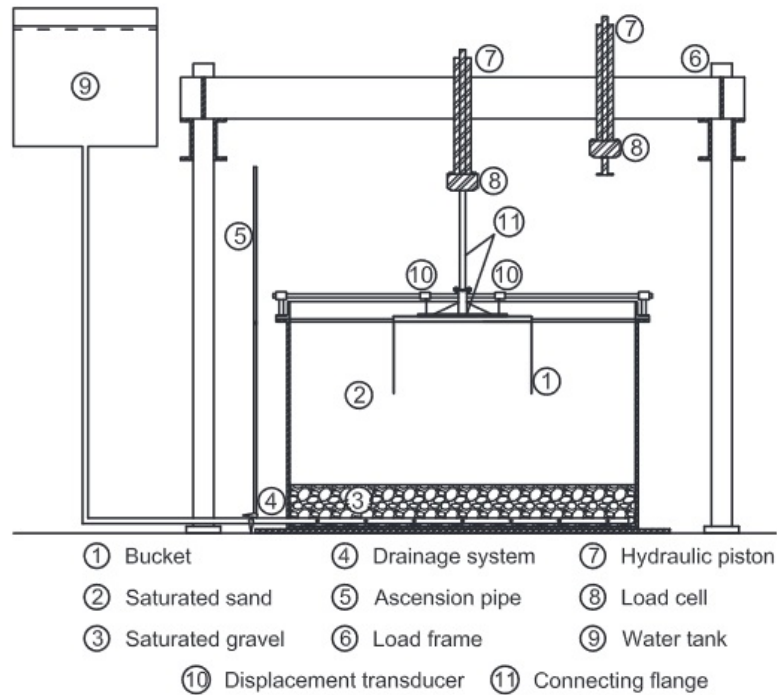


Figure A.3: Model set-up from Vaitkunaite et al. [2015].

A.1.4 Preparation and vibration of the soil

It is of great importance to have a uniform compact soil during testing the foundation. In order to achieve that a few steps have to be made.

1. After its test the soil is very loose (almost destroyed) in the position where the bucket was placed and very dense outside of this area. Also, large holes may have created due to water pressure applied during the uninstillation. In order to ensure the uniformity of the soil we let the water dry out of the sandbox opening the valve 'Out' as it can be seen in Figure A.4.

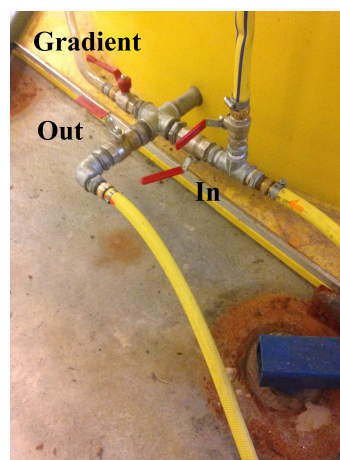


Figure A.4: Valves controlling the incoming and outcoming water supply of the yellow sandbox.

2. When the water is almost 1 *cm* above the soil surface, the valve is closed. Now, it is easier to level the soil and cover the holes by using a shovel.
3. Ensure to fill the water tank by opening the handle controlling the water. While filling the tank the 'In' valve should be closed.



(a) Water tank.



(b) Valve controlling the water tank.

Figure A.5: Water tank and its supply valve.

4. In this case the steel ring is always clamped around the sandbox. It is recommended to clean it by using the air piston after its test is performed and the water is almost dried out of the sandbox.



(a) Rings clamped around the container.



(b) Air piston.

Figure A.6: Ring

5. In order to loosen the soil a hydraulic gradient of 0.9 is applied by fully opening the 'Gradient', valve while opening the valve 'In', as shown in Figure A.4, until the water reaches the blue mark on the pipe next to the sandbox (Figure A.7). Thus, a pressure difference which ensures the next criterion is satisfied: $i = \frac{\Delta h}{H}$
 $\Rightarrow \Delta h = i \times H = 0.9 \times H$

Where, $\Delta h = 1.08m$ is the difference in the pressure head and $H = 1.20m$ is the thickness of the sand in the sandbox.



Figure A.7: Pipe controlling the gradient.

6. Make sure that the gradient is applied for at least 10 minutes or until the water level reaches 6 – 8 *cm* above the soil surface (it usually takes 30 minutes for reaching the desired level) .
7. When the desired water level is reached the valves controlling the gradient and the water coming in the container, have to be closed. Also, the 4 metallic beams are placed in position according to their numbers as it can be seen in the next Figure.



Figure A.8: 4 metallic beams, creating a frame important for the vibration procedure.

8. The wooden plates with the holes are placed on top of the beams. There are specific marks on the plates ensuring that they are sitting exactly on top of the metallic frame, without the holes being blocked by the metallic bars.

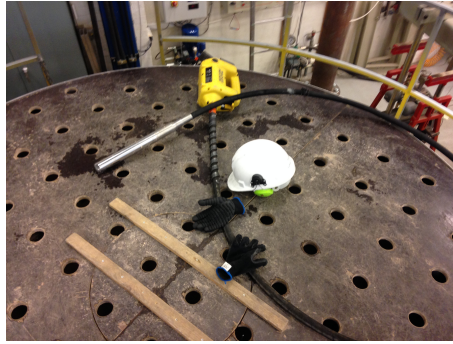


Figure A.9: Workspace for vibration.

9. Vibration can start by using the vibration gloves, the earplugs, the helmet and the vibration device. It is very important to vibrate every second hole in order to ensure a uniform compaction of the soil. In the Figure below the vibration in our case can be observed. Firstly, the 20 holes in the middle illustrated in a frame were vibrated. After that the black holes were vibrated and in the end the empty ones. Make sure that to take breaks every 30 minutes or else the vibration can cause severe dizziness and nausea.

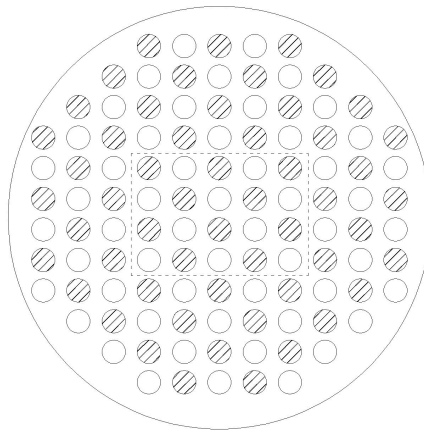


Figure A.10: Vibration plan.

10. The vibration has to be performed very carefully, otherwise results regarding the resistance of the soil can be highly affected. The same speed and angle has to be applied when putting the rod in the soil and when taking it out or else the rod can break or fail.
11. After the end of the vibration the valve 'Out' should be opened to 50% of its capacity and let the water slowly out of the container, until water level reaches approximately 1 cm.
12. Finally, using the metallic bar in which a wooden plate has been clamped on (Figure A.11), we level the surface of the sand in the middle of the sandbox.



Figure A.11: Bar used for level the soil surface.

A.1.5 CPT tests in the sandbox before and after installation.

CPT tests are performed before and after the installation of the bucket in order to have a good overview of the soil resistance around the sandbox. 4 CPT tests are conducted before the installation and 8 after the bucket is fully installed as shown in Figures A.12 and A.13.

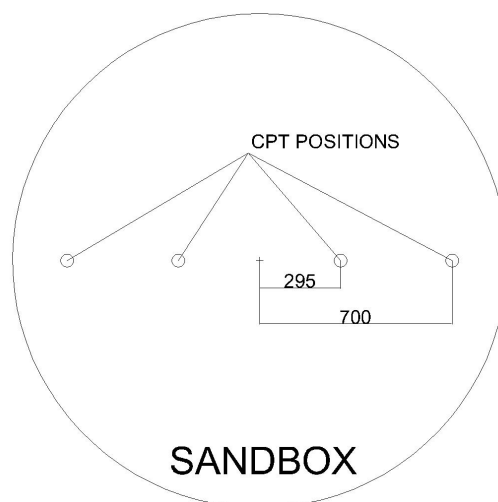


Figure A.12: CPT before installation.

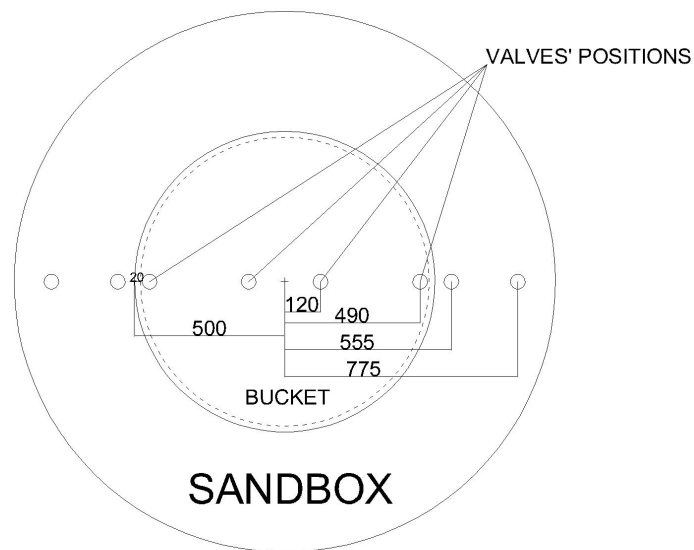


Figure A.13: CPT after installation.

The steps followed for the CPT testing are the following:

1. Prepare working space(Figure A.14).

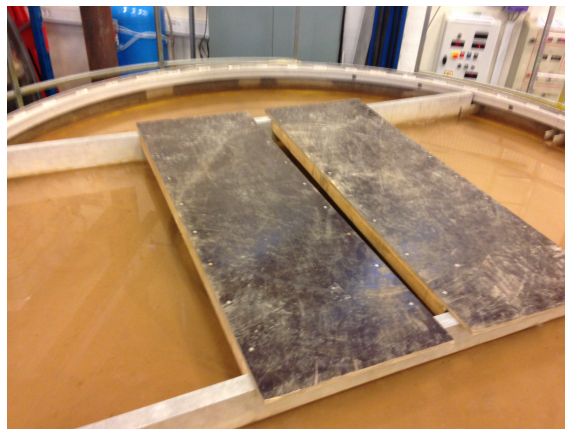


Figure A.14: Working Space for CPT tests.

2. The CPT rod should be connected in the box above the hydraulic piston in the CPT cone position as shown in Figure A.15.

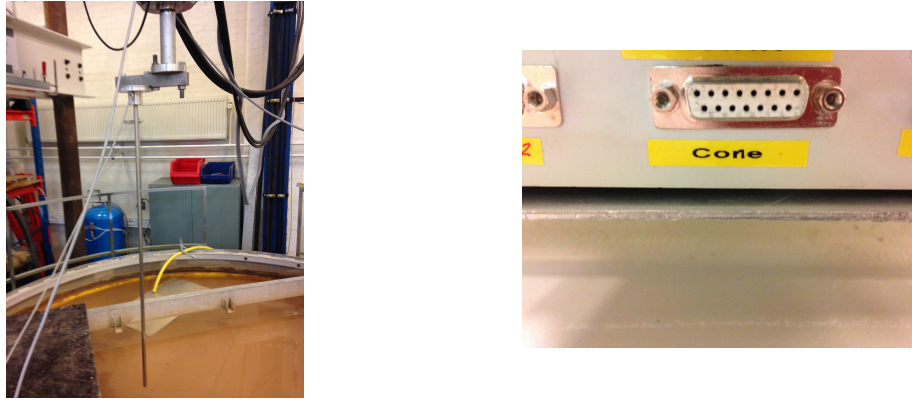


Figure A.15: CPT rod and its connection to the receiving box.

3. Move the piston to the correct position according to the CPT test that has to be performed at each time. For example 'CPT1b' position is denoted as the first position before the installation, while 'CPT1a' is denoted as the first position after the installation. Tighten the bolts on both sides.



Figure A.16: Different positions for the CPT rod.

4. The hydraulic piston is connected with a metallic head. The metallic head has to be always on the left side (when looking at the container) and by using the small bolts, the CPT rod is attached on it.



(a) CPT head.



(b) Small bolts used for connecting the head with the CPT rod.

Figure A.17: Equipment for CPT testing.

5. Make sure that the rod is always on vertical position and be very careful with the tip due to its sensitivity.
6. The hydraulic piston moves by using the yellow controller, which is connected to the control panel mounted on the wall behind the container. The CPT tests are performed with 5 mm/s speed. You can adjust the speed by using the small black handle (Figure A.18). The value on the left on the control panel is the set point we chose, while the value on the right is the actual penetration ratio(it starts when the test starts). In order for those two values to match, make sure that the pump right under the control panel is closed during the CPT testing.



Figure A.18: Control panel, yellow controller and the pump of the hydraulic piston.

7. Before using 'Catman' for data acquisition make sure that the CPT rod is placed right above the soil surface.

A.1.6 Data acquisition using Catman from CPT tests

Right after the preparation for the CPT, the software 'Catman Professional' has to be used. This software receives data from 'Spider8', in which the CPT rod is connected. It is a complicated software, so the procedure is described by uploading our own settings. In case there is a change that needs to be made ask for help from the technical stuff of the university or a professor.

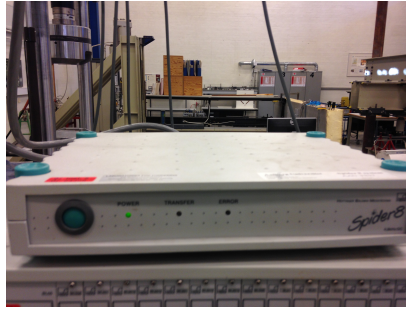


Figure A.19: Spider device.

1. Open 'Catman Professional' in the laboratory's computer.

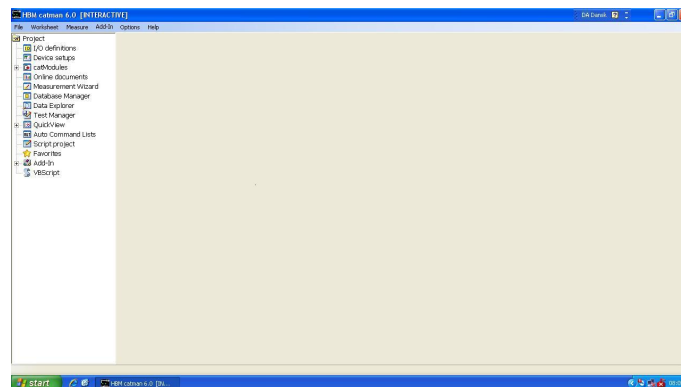


Figure A.20: Catman preface.

2. Double click on 'I/O Definitions'.
3. By clicking on the folder on top in Figure A.21, upload the correct folder (*CPTsetup_thg.IOD*)

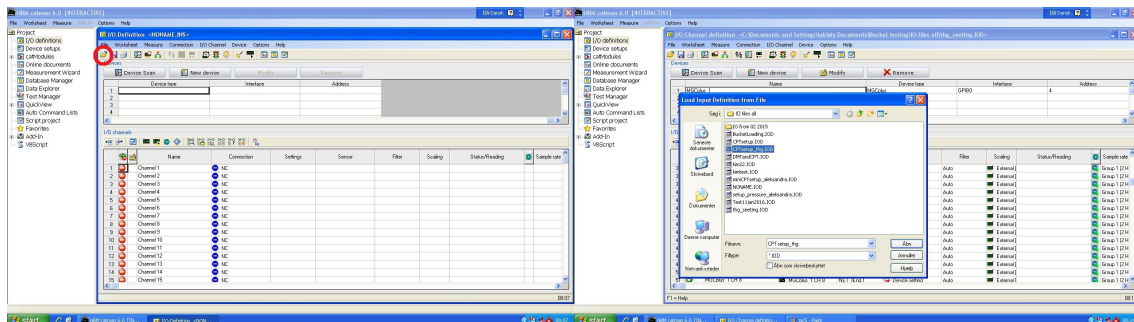


Figure A.21: Procedure for uploading the file.

4. Now a lot of channels should appear, but only *CPTcone* and *CPTdispl* are working.
5. Zero those 2 channels using the button pointed on figure A.22.



Figure A.22: CPT channels and button for zeroing the channels.

6. In order to start recording, Data Logger must be used (CatModules \Rightarrow Measuring \Rightarrow Data Logger). Do not change anything on the window and press *RUN*(Figure A.23).

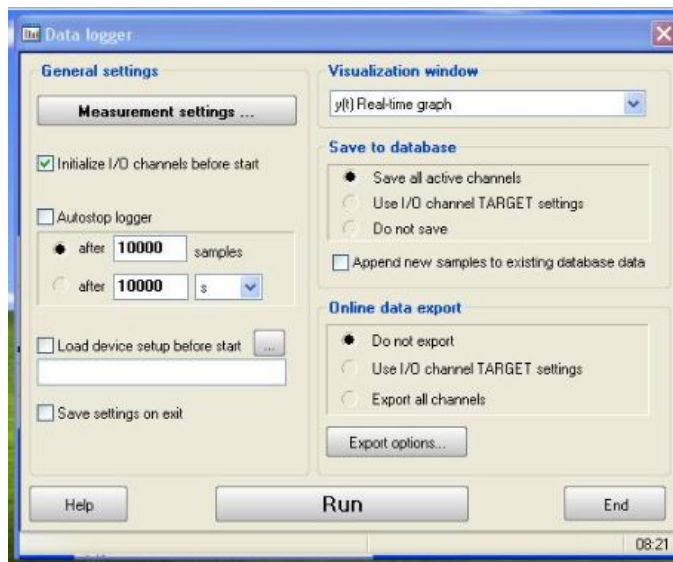


Figure A.23: Data Logger window.

7. On the right of the screen plots can be created, that illustrate at the same time the depth of the CPT and the cone resistance(Right click on the plot \Rightarrow Set up axes \Rightarrow Plots \Rightarrow Chose *CPTcone* on the Left axis and press add new data plot \Rightarrow choose *CPTdispl* on the right axis and press add new data plot \Rightarrow Apply).

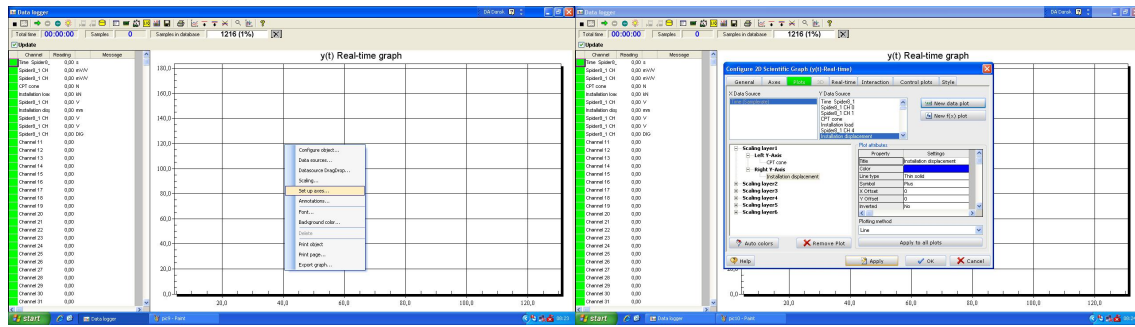


Figure A.24: Procedure for creating plots in the data logger.

8. Press the green arrow, on top of the screen, to start measuring.



Figure A.25: Start button for the test.

9. When the desired depth is achieved, first stop the test by pressing the red button on the yellow controller and then stop the measurements in 'Catman' by pressing the red button next to the green arrow.



Figure A.26: Stop button for the test.

10. In order to save the data, select the 2 channels along with the time and save them in a specific folder as ASCII + Channel information.

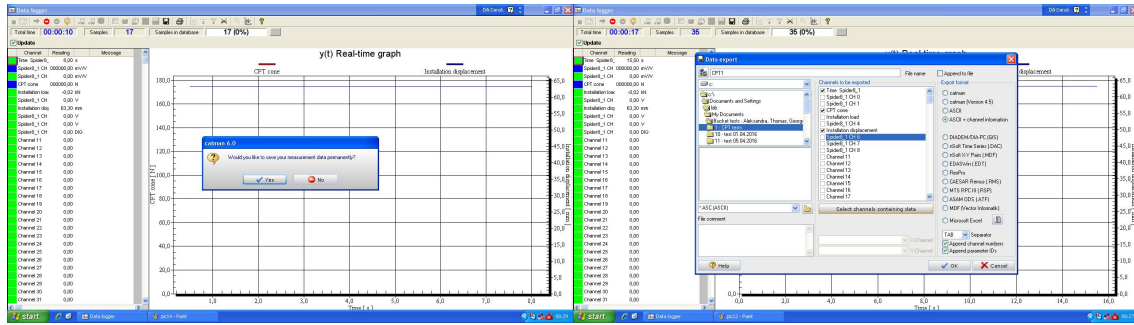


Figure A.27: Saving data procedure.

The results have to be checked after all CPT tests are finished. If they are satisfactory then move on to the next section. If the sand is too loose the soil has to be vibrated again. On the other hand, if the soil is too dense the gradient should be applied for a few minutes.

A.1.7 Installation of the beam on the boundaries of the container

In order to measure changes on the boundaries of the sandbox during the installation and uninstallation, a beam of 1 m has to be placed in the soil. The beam has 3 pressure transducers attached on it on different heights. The first one is on the tip (1 m), the second one on 0.75 m and the third on 0.5 m .

1. Clean the beam from any dry sand attached on it. Using the air piston clean the pipes connecting the pressure transducers with the beam. It is very important to unscrew the transducers before pressing air in the holes, otherwise they can be damaged.



Figure A.28: Beam for testing the boundaries.

- Put the 2 bars (number 7 and 8) above the soil and screw the piston on the edge of the of the container.



Figure A.29: Bars for preparing the workspace.

- Using the black tank, saturate the pressure transducers with a syringe.
- Move the beam right on top of the soil surface and screw it on the hydraulic piston. Connect the pressure transducers on the box placed on the right of the container.



Figure A.30: Box for connecting the pressure transducers from the beam.

- Use the yellow controller and install the beam.



Figure A.31: Installed beam on the boundaries.

There are not any measurements recorded during the installation of the beam. It is crucial to record when the bucket is being installed or uninstalled.

A.1.8 Installation of the bucket with suction

1. After performing the CPT tests and the installation of the beam, the container should be filled with water, until the water level reaches at least 10 *cm*. In order to achieve that without destroying the strength of the soil, the water is poured slowly on top of a small metallic plate by another hose connected to the water tank.



Figure A.32: Metallic plate for filling the container with water during the test.

2. Clean the bucket from dry sand attached to its surface. Using the air piston clean the pipes connecting the pressure transducers with the bucket. It is very important

to unscrew the transducers before pressing air in the holes, otherwise they can be damaged.

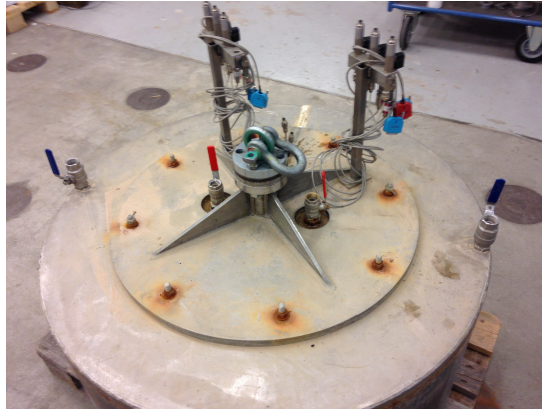


Figure A.33: Test bucket.

3. Use the crane to lift the bucket.



Figure A.34: Crane used to lift the bucket.

4. Saturate the transducers with a syringe by putting the bucket in the black tank.
5. Fix the hydraulic piston in the middle position by using the 8 black bolts(4 at each side).



Figure A.35: Black bolts used for fixing the piston in the middle position.

6. Change the head of the piston, with the one that is controlled by force.



Figure A.36: Head attached to the hydraulic piston controlled by force.

7. On the control panel change the switch in the middle from defl. → load (now the bottom part of the control panel is working).



Figure A.37: Control panel switch from displacement to force.

8. On the black box change the values of channel 41 to 0.8 and of channel 42 to 2.5.



Figure A.38: Box connected to the control panel.

9. Set the point to 0 from the control panel and open the pump, in order the real value to match with the one that is set. By setting the point to 0, it means that only the self weight of the bucket will be applied during the installation. Opening the pump ensures that the piston is working even though we are not applying any addition load.
10. Place the bucket on top of the 2 wooden plates. Connect the piston with the bucket by using 4 bolts.



Figure A.39: Connection of the bucket with the force head.

11. Connect the pressure transducers with the box on top of the piston. It is very important to connect the transducers at the same position each time, otherwise the data recordings, set in 'Catman', will be changed. In this case, PP1 is connected to the first receiver, PP2 to the second etc.

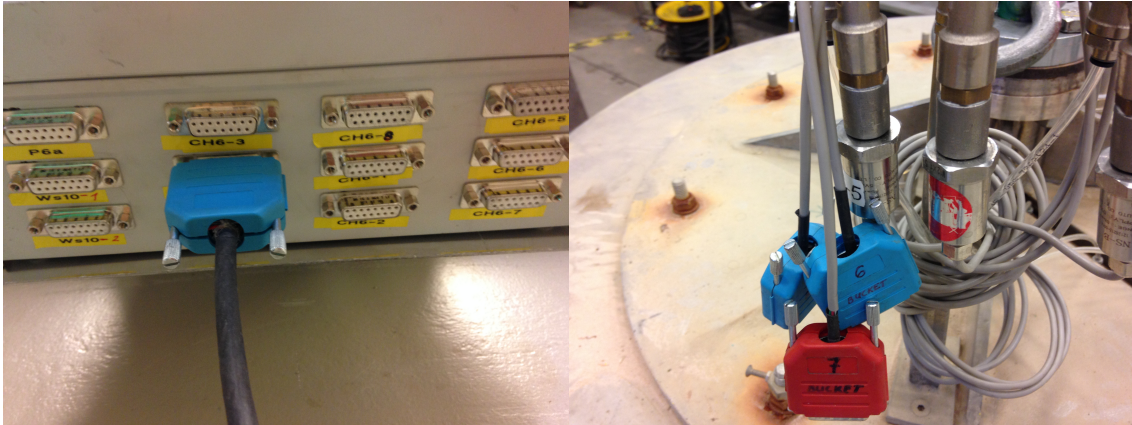


Figure A.40: Connection of the transducers to the receiving box.

12. Fix the displacement transducer on the metallic plate on top of the transducer with a clamp and connect it to the box on gate *WS10-2*. Attach the string on the bucket carefully. Make sure that the string is placed perfectly vertical with respect to the bucket.



Figure A.41: Displacement transducer.

13. Install the valves, on which the suction will be applied, on the 4 holes of the bucket. Make sure that the valves are open at all times.



Figure A.42: Suction valves.

14. Place the bucket right on top of the sand surface.
15. After zeroing all the channels in 'Catman' (see the section Data acquisition during installation), press 'down' on the yellow controller and start the test.
16. After the bucket is installed due to its self weight, connect the blue vacuum to the bucket with the 4 small hoses as it is shown in the Figure below.



Figure A.43: Connection of the pipes from the vacuum, with the valves for suction.

17. Open the pump from the handle on its left. Control the suction applied by the grey handle (for increasing the pressure, turn the handle to the right) and look on the white panel above the vacuum. The actual suction is not the one that the vacuum shows. The actual suction is measured by the pressure transducer placed on the lid of the bucket (PP7).



Figure A.44: Control system of the vacuum.

18. Make sure to perform the test slowly and never exceed the calculated critical suction. The water level should remain the same during the whole experiment. Moreover, empty the vacuum constantly, otherwise there is a great possibility of damaging it.



Figure A.45: Inside of the bucket (pressure transducer under the lid, PP7).

19. After the installation is complete, wait at least half an hour before closing the vacuum. It is very important to observe any pipping channels that will be created.

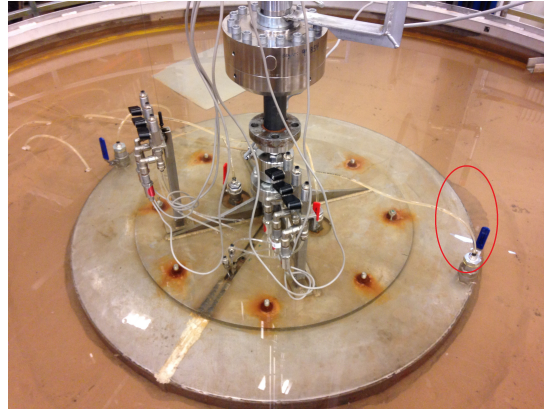


Figure A.46: Installed bucket with piping.

20. Save the results(see the section Data acquisition during installation) and disconnect the piston from the bucket. Disconnect the force head attached to the piston and place back the head used for CPT's.
21. Disconnect the 4 valves, on which the suction was applied, because CPT tests will be performed through these holes.
22. Follow the steps from the CPT testing section. Do not forget to change from Load to Defl. on the control panel.

A.1.9 Installation of the bucket with force

1. First 4 steps are the same as the previous section.
2. Use the same head attached to the piston as the one used for the CPT tests, but without the metallic bar.



Figure A.47: Head of the piston used for force installation.

3. Screw the piston on the bucket and connect the pressure and displacement transducers as explained in the previous section.
4. In the control panel the deflection is used (the upper part of the control panel is working now). Set penetration ratio at 0.13 mm/s . Make sure that the pump is closed for the value that is set to match with the actual one.
5. Make sure that the 4 holes on the bucket remain open during the whole installation.

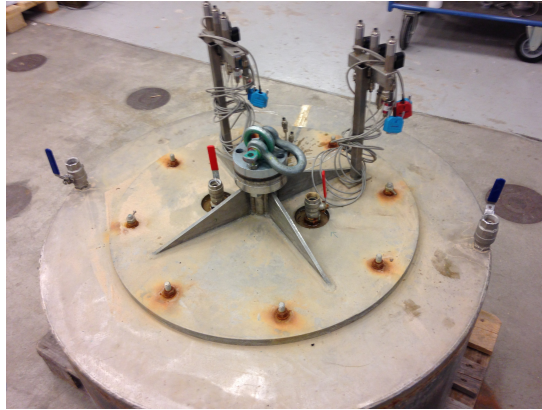


Figure A.48: Open valves on top of the bucket.

6. Place the bucket right on top of the sand surface.
7. After zeroing all the channels in 'Catman' (see the section Data acquisition during installation), press 'down' on the yellow controller and start the test.
8. After finishing the installation, same steps as in the previous section should applied before starting the CPT tests.

A.1.10 Uninstallation of the bucket

For uninstalling the bucket foundation, different weights were simulated. During the first tests, the bucket was uninstalled only applying its self weight. Later on, the tests that were performed, simulated $\times 2 (+201Kg)$, $\times 2.5(+302Kg)$ and $\times 3(+402Kg)$ the bucket's self weight.

1. Fix the hydraulic piston in the middle position by using the 8 black bolts(4 at each side).
2. Fix the head of the piston on the bucket, but leave at least 5cm space between them. This is very important, because during the uninstallation the piston is only used for stabilization of the bucket and not for pulling it out.
3. Screw the hose receiver valve in one of the two middle holes of the bucket.



Figure A.49: Connection of the bucket with the hose.

4. Connect the hose to the water and then to the valve. Pour some water inside the bucket slowly, until the air of the other 3 holes is out. Instantly close all the holes from the handles along with the water supply.
5. Put additional weight on top of the bucket (if needed).



Figure A.50: Uninstallation with weights on top of the bucket.

6. Start recording.
7. Open the water supply handle to 50% of its capacity.
8. Control the piston manually with the yellow controller at all times. It is crucial that the piston never touches the bucket, otherwise the results will be highly affected.
9. When water breaks under the bucket's skirt, stop the recordings.
10. Take away the additional weights (if needed).
11. Carefully take the bucket out of the container.
12. Uninstall the beam on the boundaries.
13. Now start again from preparing the soil.

The steps for installation with force are the same as the ones before for the laboratory's computer. For the second laptop are the following:

1. Connect the 'Spider8' USB cable to the laptop.



Figure A.53: Usb connection to the laptop.

2. Open 'CatmanEasy'.
3. Zero the channels 'InstalForce' and 'InstalDispl'.

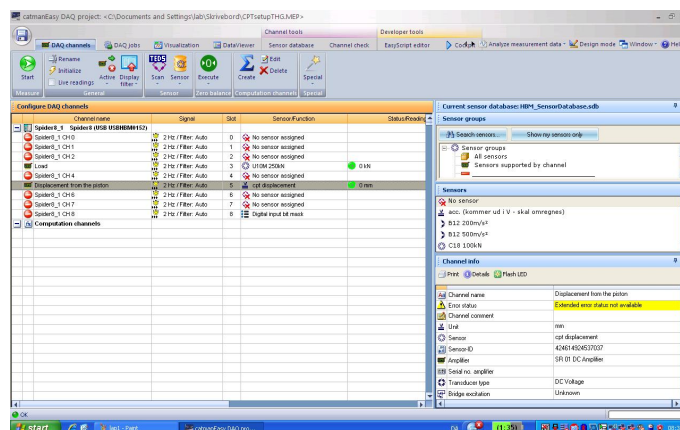


Figure A.54: Channels on 'CatmanEasy'.

4. Press 'Start' on top of the screen to start recording.
5. When the test is ended, press 'Stop' and save the results in the same manner as mentioned before.

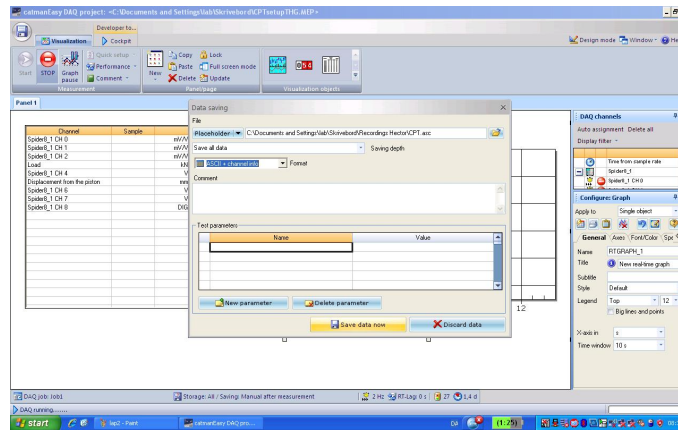


Figure A.55: Saving the results on 'CatmanEasy'.

APPENDIX: SKIRT FRICTION COEFFICIENT (k_f), TIP RESISTANCE COEFFICIENT (k_p)

B

B.1 Calculation of k_f and k_p

The procedure that used to determine the empirical coefficients related to skirt friction (k_f) and tip resistance (k_p) is an analytical method using the empirical formulas from the CPT-based method mentioned in Sgourakis et al. [2016].

The data that was necessary to accomplish the method, was gathered from two different sources. The first was the experimental work carried out by Vaitkunaite et al. [2015], where multiple bucket installation and tension (partial uninstallion) experiments were performed. Furthermore, CPT tests were performed before every installation experiment. The second source was the experimental work presented in the current paper, performed in Aalborg University Laboratory, where bucket installation and full uninstallation experiments were produced, as well as, CPT tests before and after every installation test, inside and outside of the bucket. The detailed procedure, as well as, the CPT points are mentioned in Sgourakis et al. [2016]. Thus, the data that was extracted form the prementioned sources in order to carry out the analytical method is the cone resistance, the installation and uninstallation load.

The method for each experiment begins with the calculation of the average tip resistance (q_c) over the depth, among the CPT tests (close to the skirt) after the installation of the bucket. The next step is to calculate the integral of the tip resistance over the depth from the CPT tests after the installtion of the bucket. Thus, using the uninstallation load, the skirt friction coefficient (k_f) can be determined. In the end, the average tip resistance (q_c) over the depth, among the CPT tests before the installation of the bucket, is calculated in order to determine the tip resistance coefficient (k_p) by using the installation load.

Note: The CPT tests before and after the installation procedure, inside and outside the bucket, were perfomed with respect to obtain more accurate and reallistic results of the tip resistance, needed for the calculation of k_p and k_f coefficients, respectively.

B.2 Experiments from Vaitkunaite et al. [2015]

B.2.1 Presentation of Data and Results

B.2.2 Experiment 13.02.04

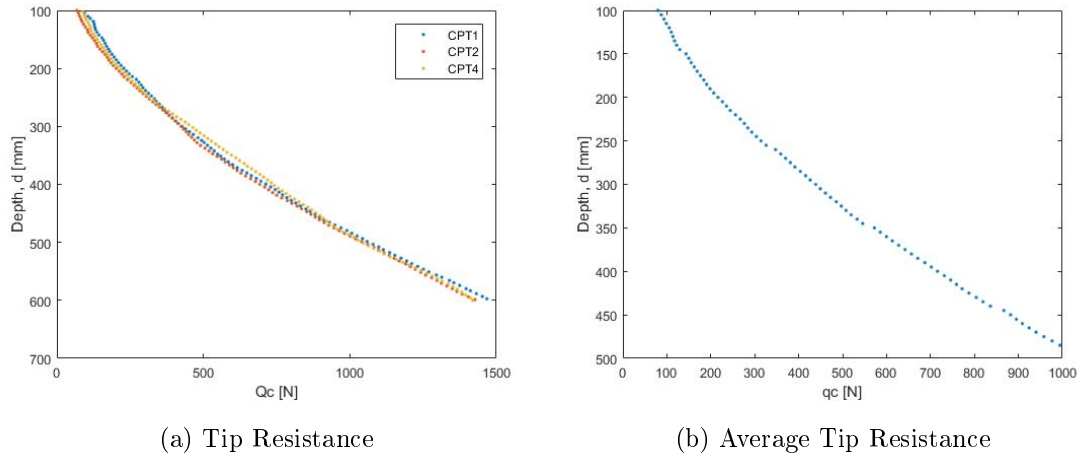


Figure B.1: CPT Data

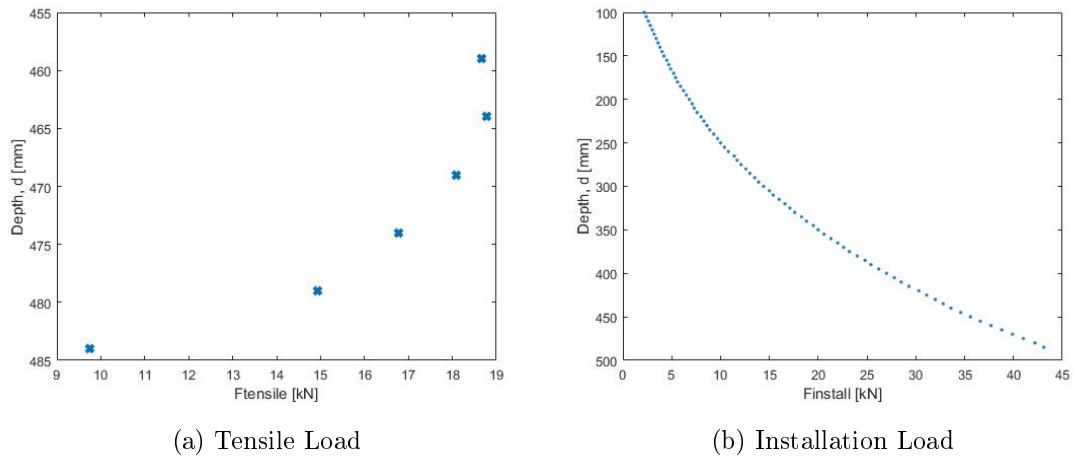
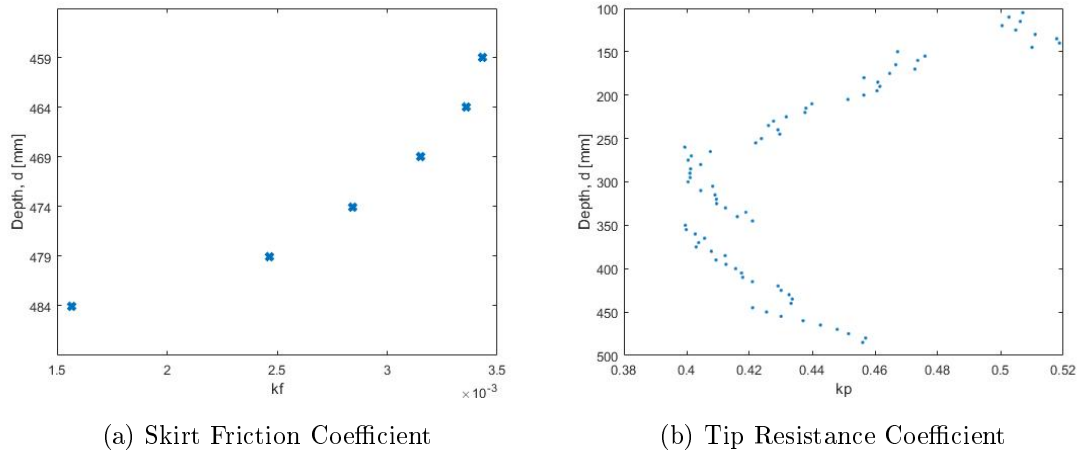


Figure B.2: Loading Data

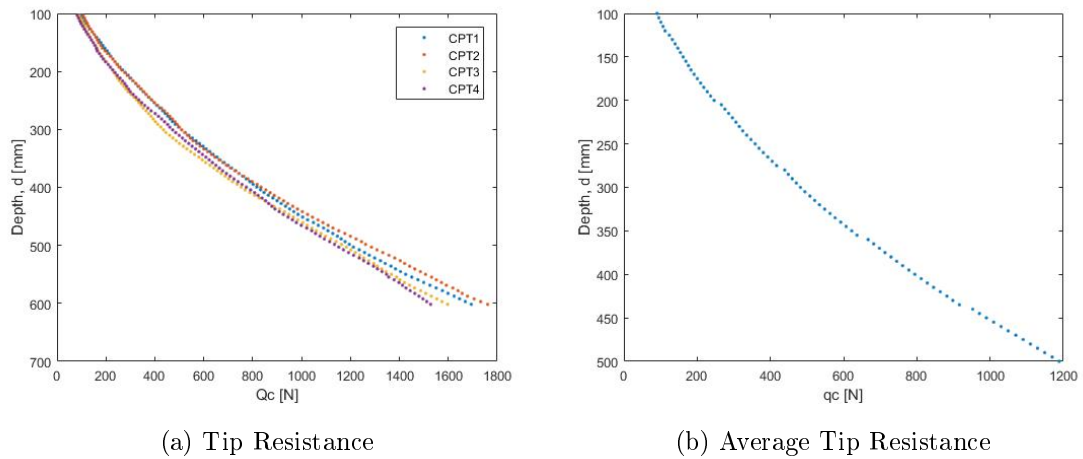


(a) Skirt Friction Coefficient

(b) Tip Resistance Coefficient

Figure B.3: Results

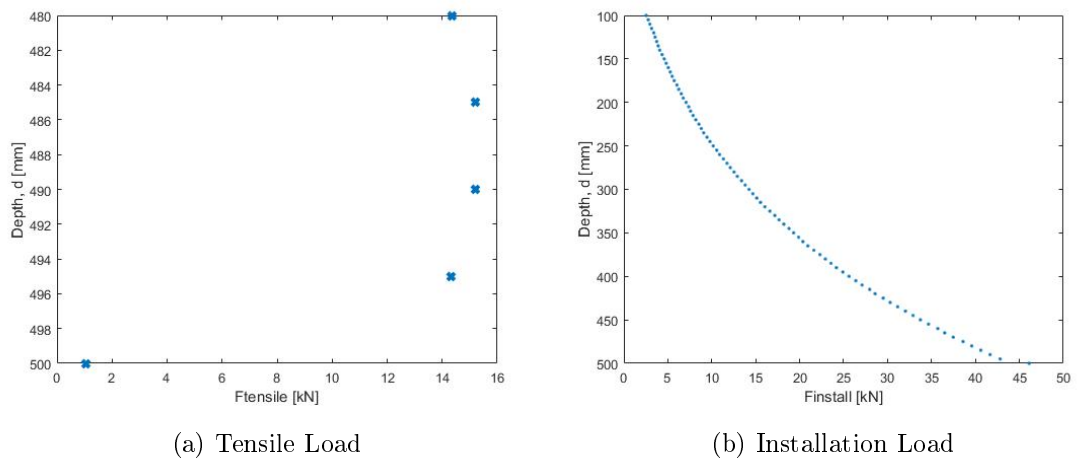
B.2.3 Experiment 13.02.05



(a) Tip Resistance

(b) Average Tip Resistance

Figure B.4: CPT Data



(a) Tensile Load

(b) Installation Load

Figure B.5: Loading Data

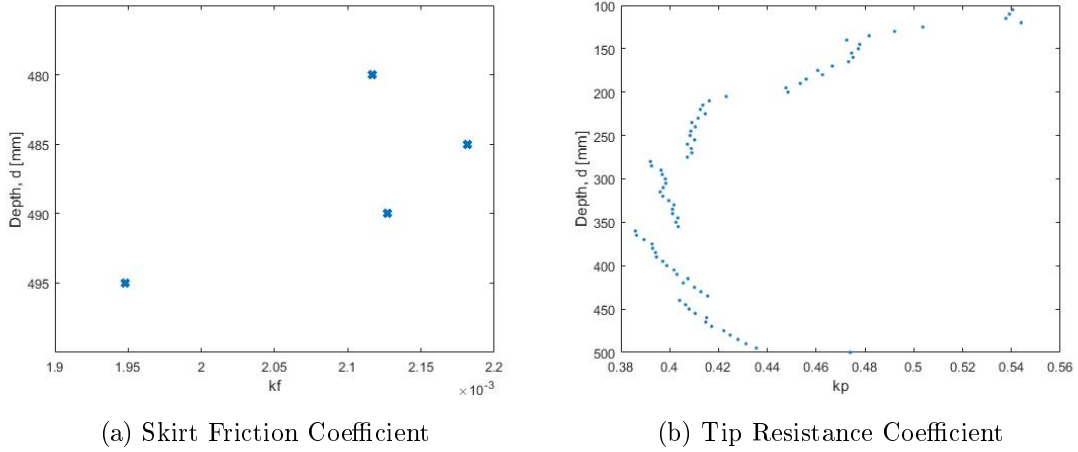


Figure B.6: Results

B.2.4 Experiment 13.02.06

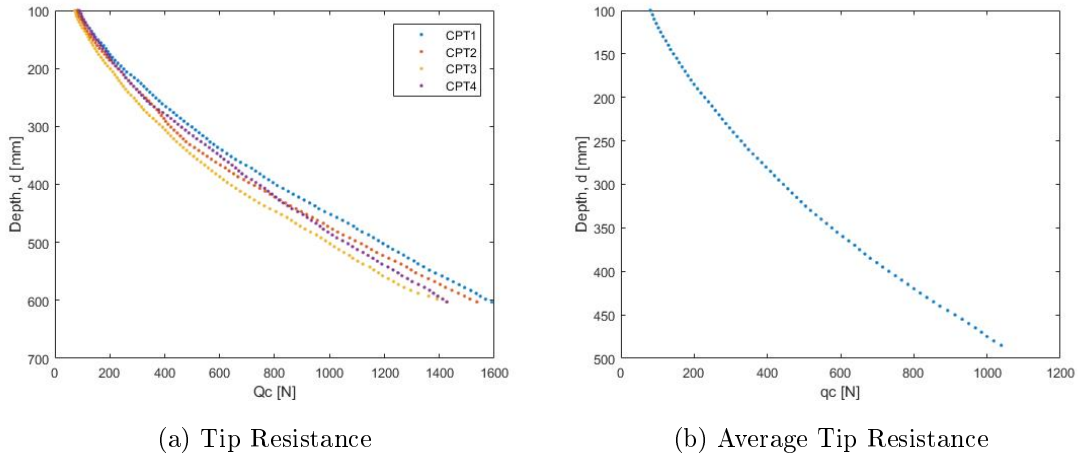


Figure B.7: CPT Data

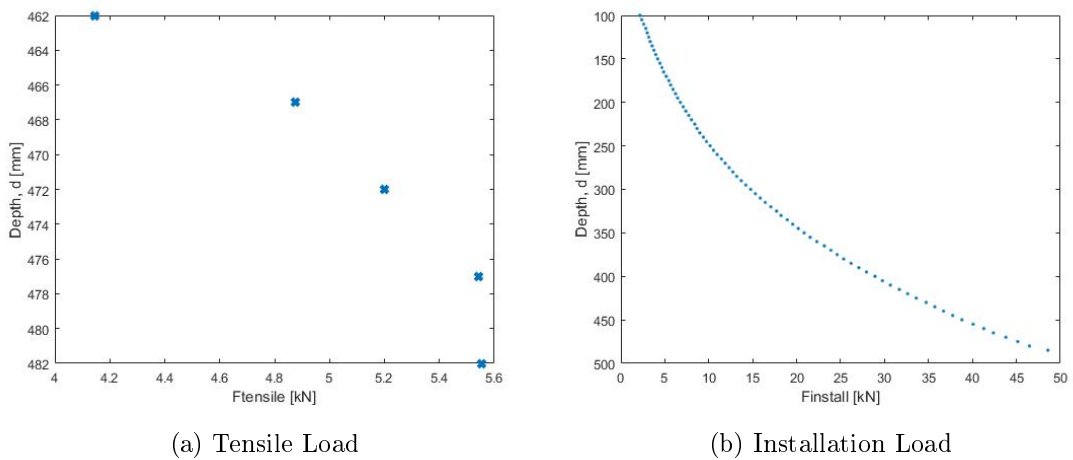
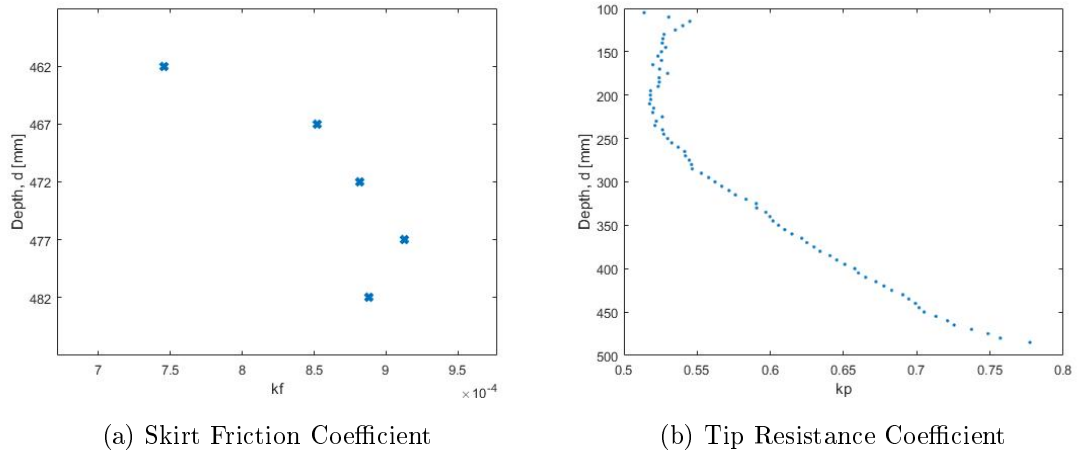


Figure B.8: Loading Data

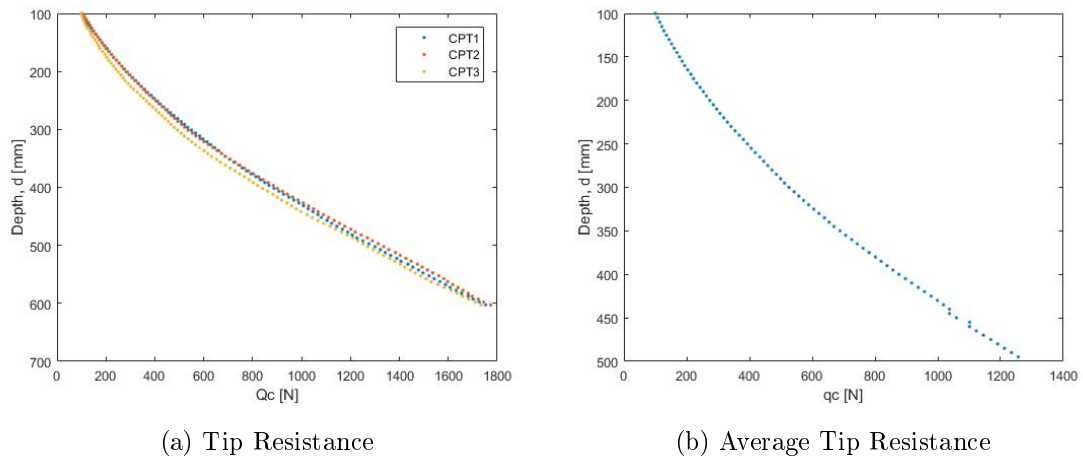


(a) Skirt Friction Coefficient

(b) Tip Resistance Coefficient

Figure B.9: Results

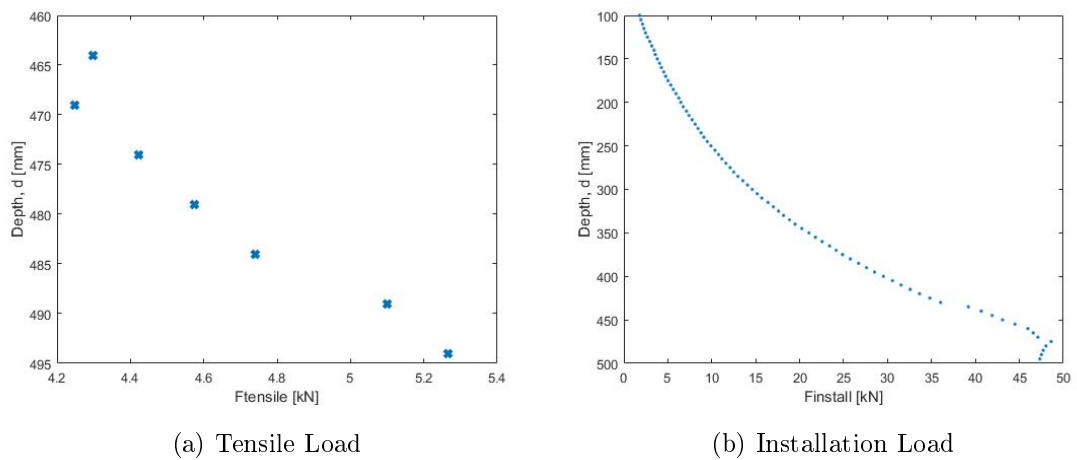
B.2.5 Experiment 13.02.08



(a) Tip Resistance

(b) Average Tip Resistance

Figure B.10: CPT Data



(a) Tensile Load

(b) Installation Load

Figure B.11: Loading Data

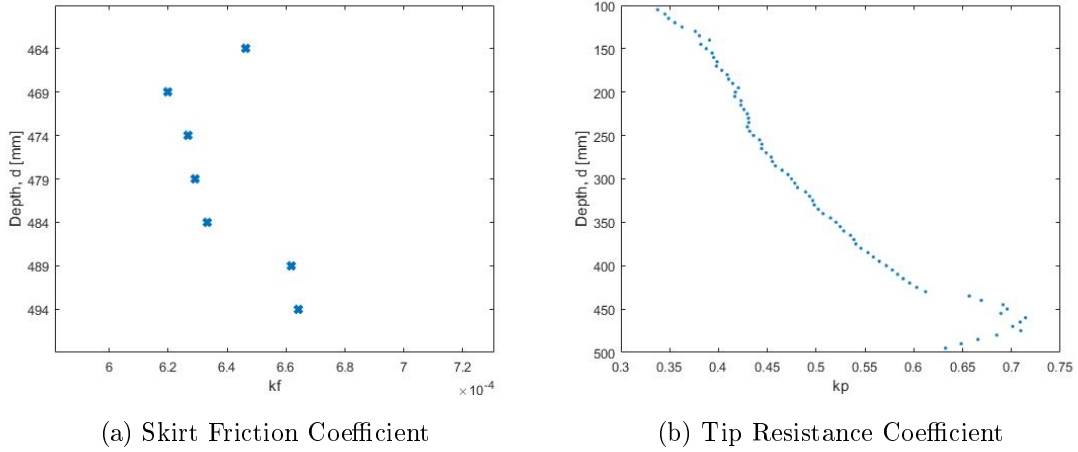


Figure B.12: Results

B.2.6 Experiment 13.02.11

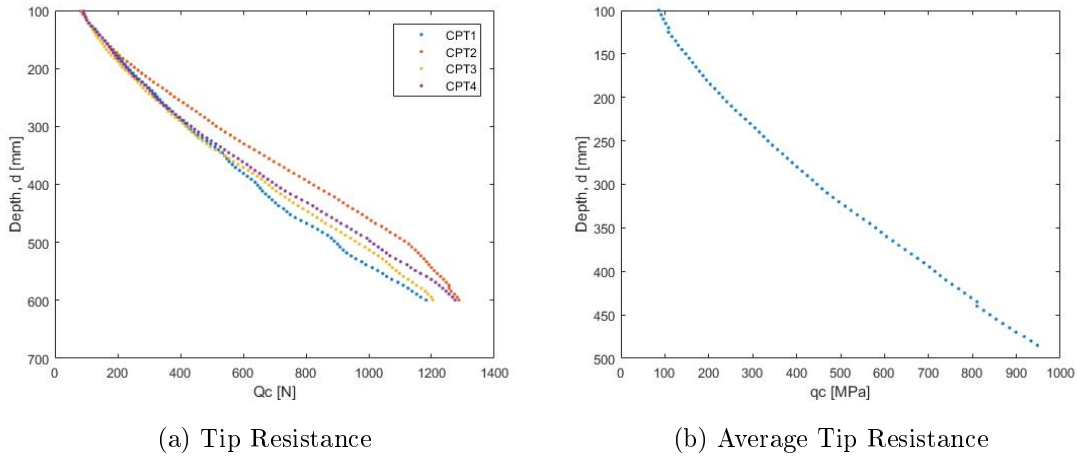


Figure B.13: CPT Data

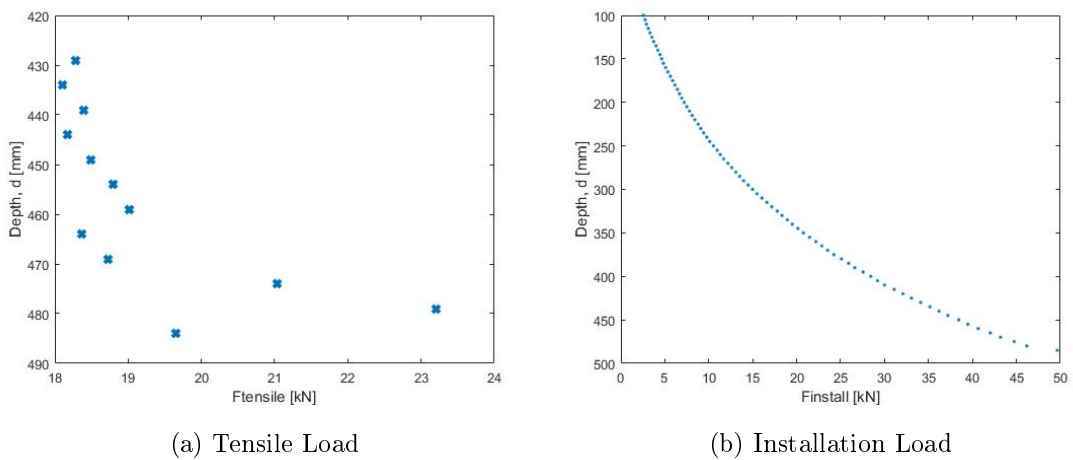
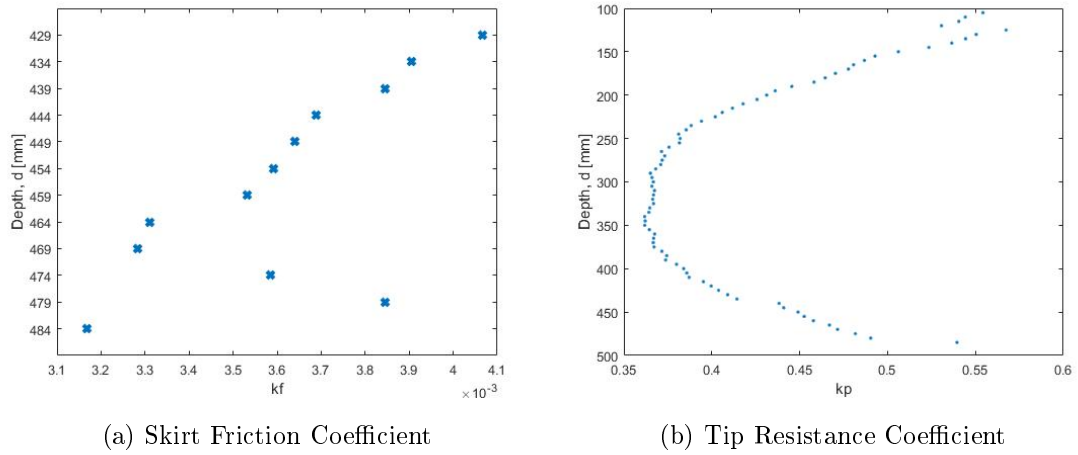


Figure B.14: Loading Data

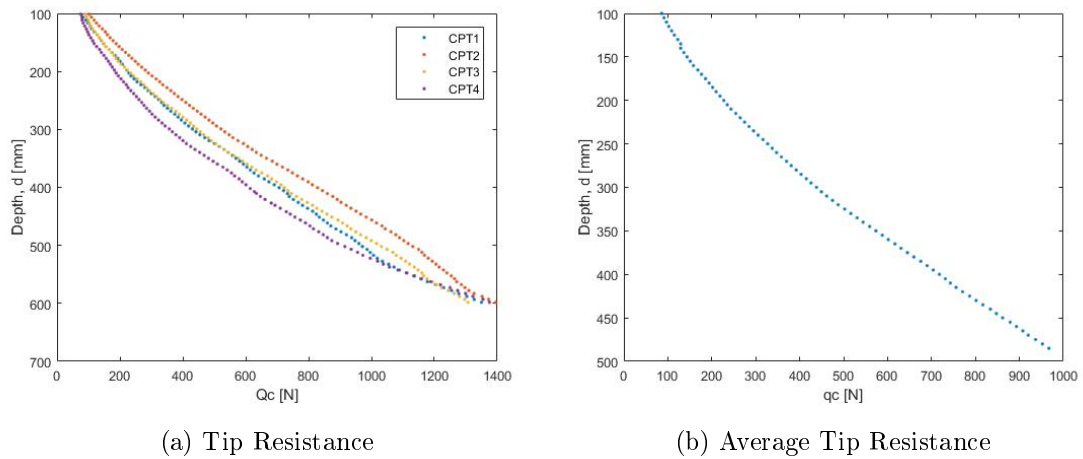


(a) Skirt Friction Coefficient

(b) Tip Resistance Coefficient

Figure B.15: Results

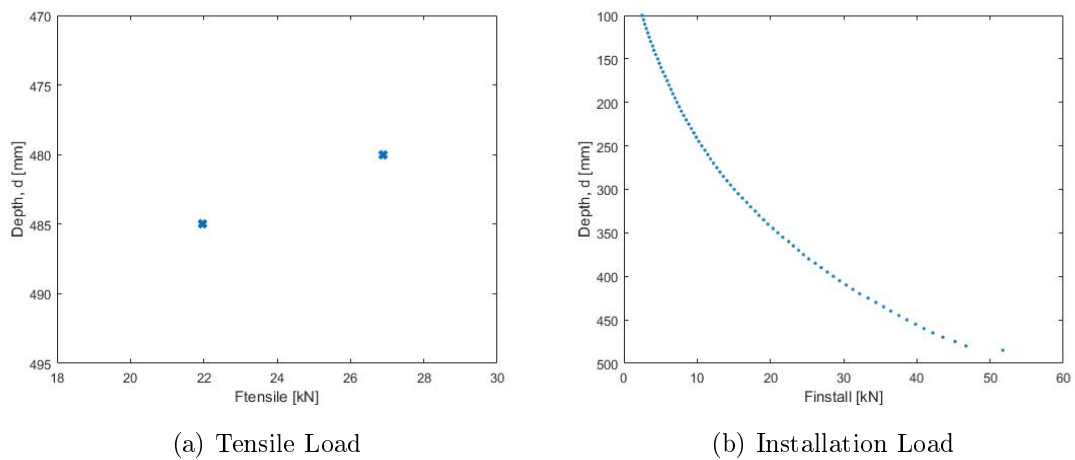
B.2.7 Experiment 13.02.12



(a) Tip Resistance

(b) Average Tip Resistance

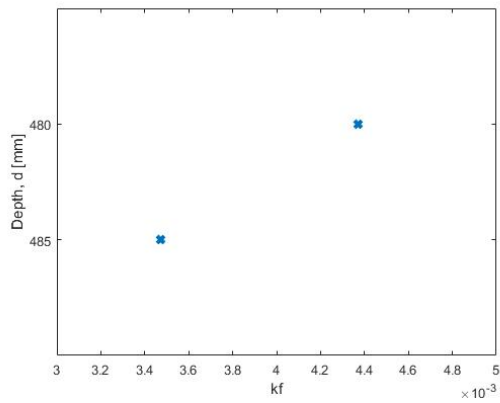
Figure B.16: CPT Data



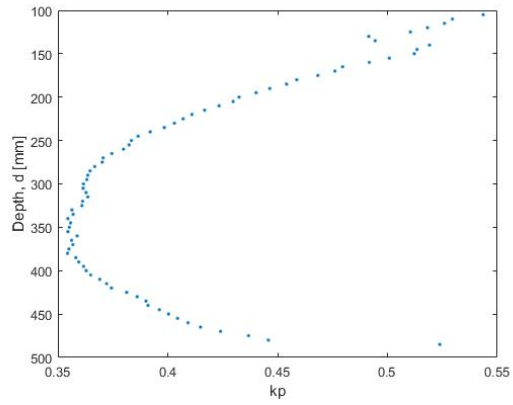
(a) Tensile Load

(b) Installation Load

Figure B.17: Loading Data



(a) Skirt Friction Coefficient



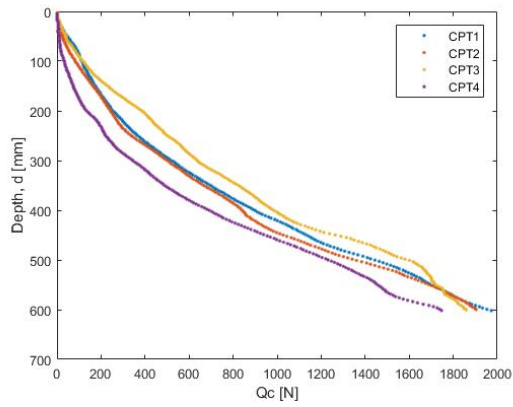
(b) Tip Resistance Coefficient

Figure B.18: Results

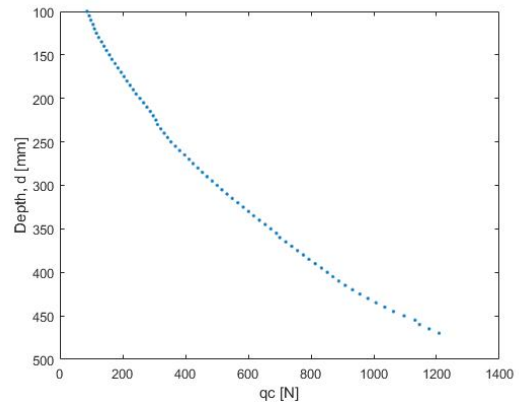
B.3 Experiments from Laboratory

B.3.1 Presentation of Data and Results

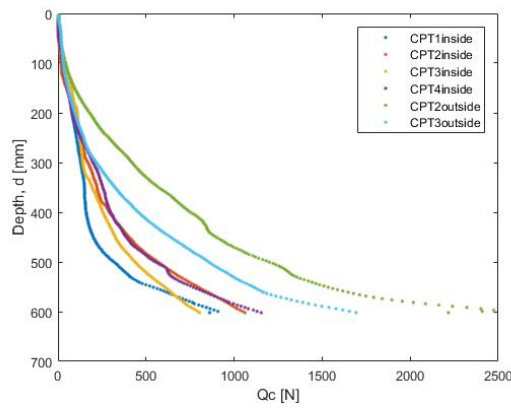
B.3.2 Experiment 10.03.2016 - Installation with Suction+2.01 kN - Uninstallation with 0 kg



(a) Tip Resistance Before Installation



(b) Average Tip Resistance Before Installation



(c) Tip Resistance After Installation

Figure B.19: CPT Data

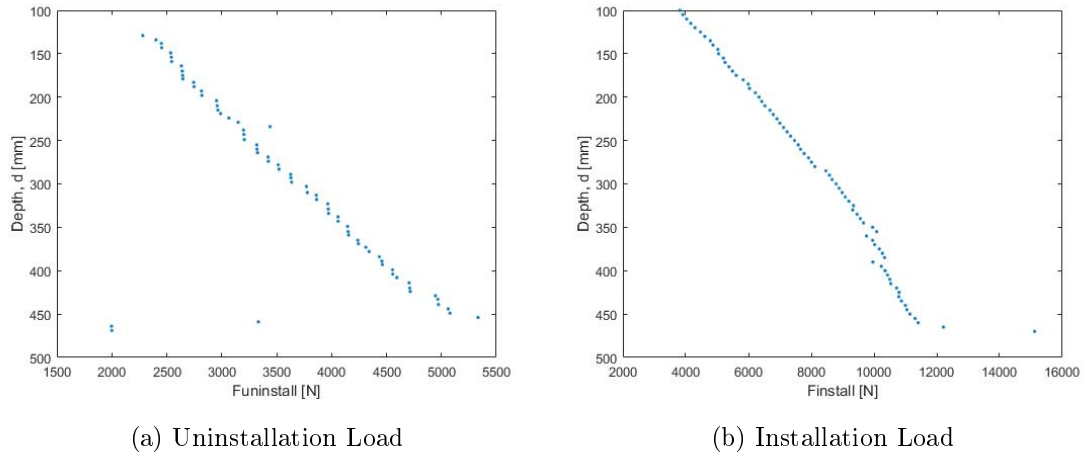


Figure B.20: Loading Data

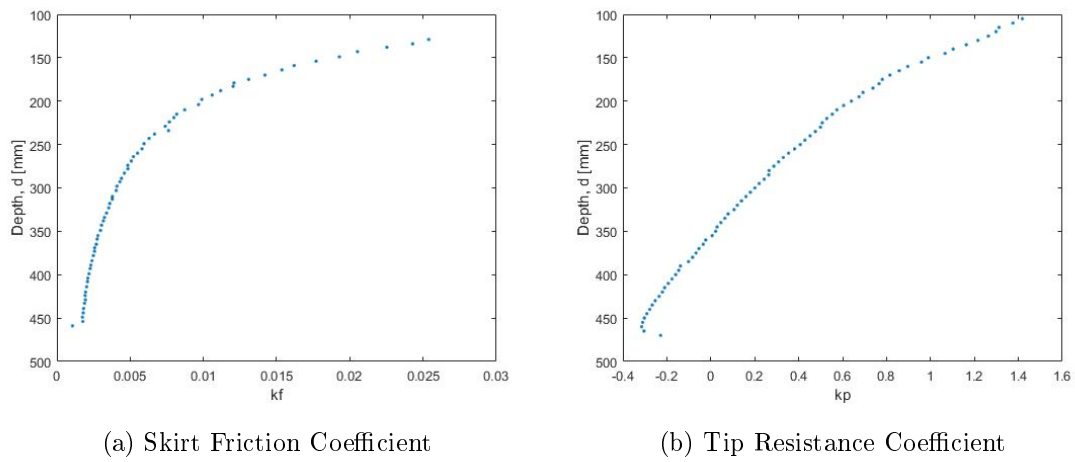
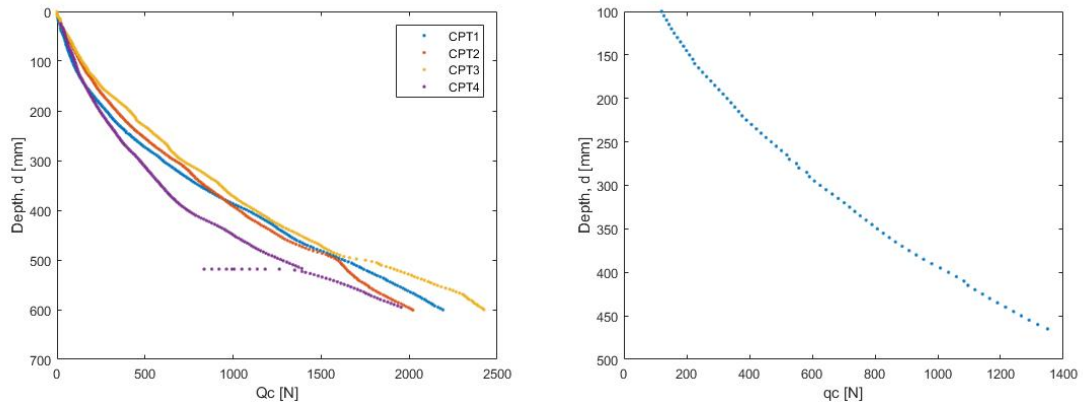
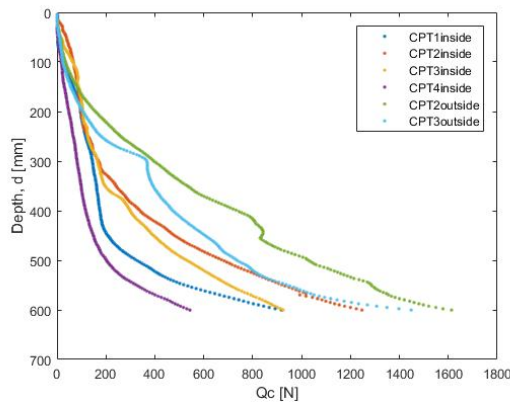


Figure B.21: Results

B.3.3 Experiment 20.03.2016 - Installation with Suction+2.01 kN - Uninstallation with 0 kg

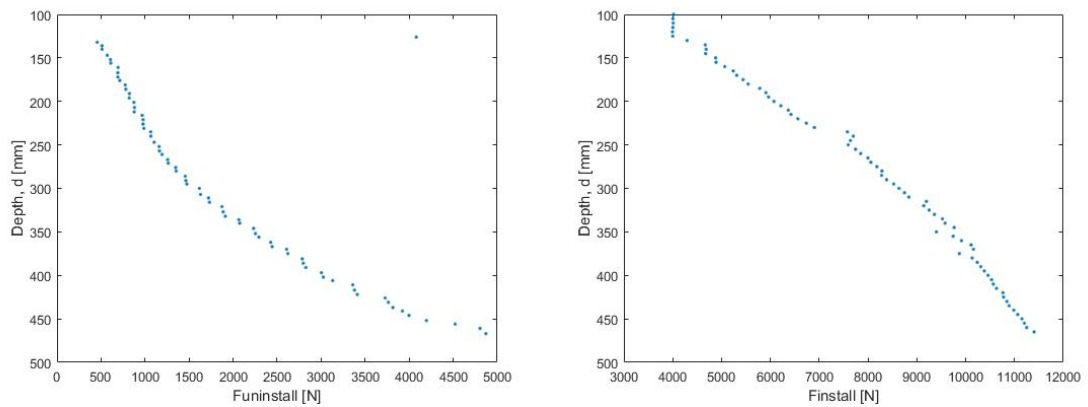


(a) Tip Resistance Before Installation (b) Average Tip Resistance Before Installation



(c) Tip Resistance After Installation

Figure B.22: CPT Data



(a) Uninstallation Load (b) Installation Load

Figure B.23: Loading Data

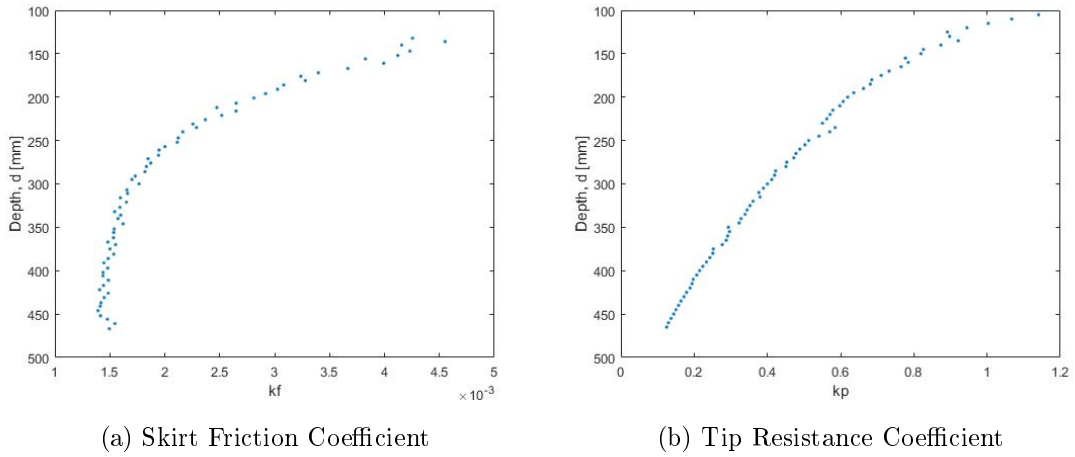
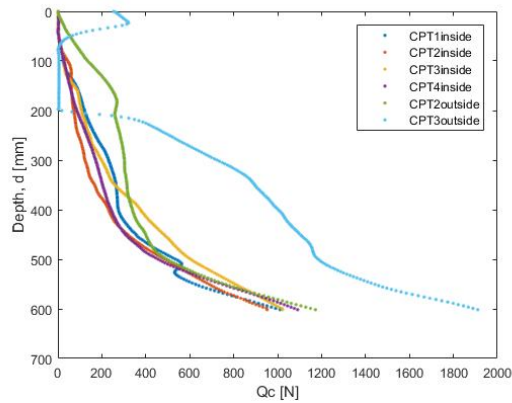
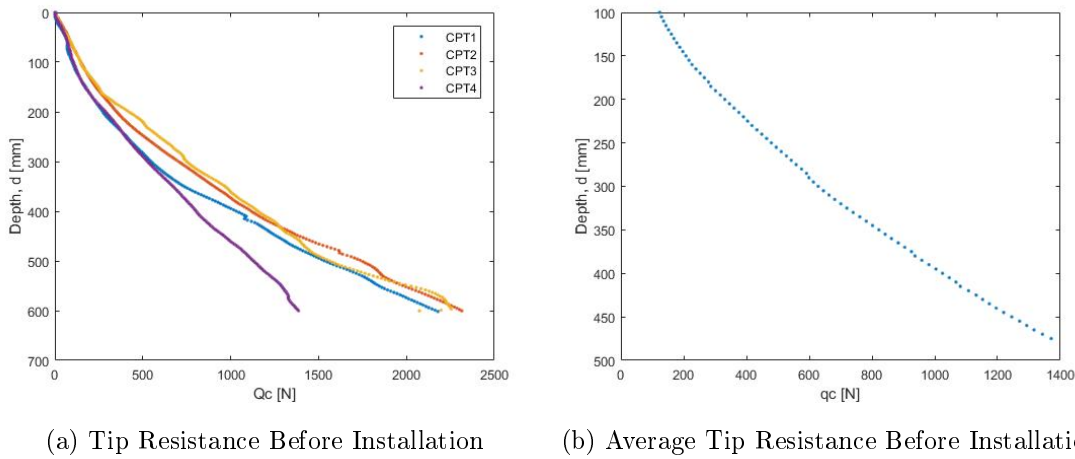


Figure B.24: Results

B.3.4 Experiment 01.04.2016 - Installation with Suction - Uninstallation with 0 kg



(c) Tip Resistance After Installation

Figure B.25: CPT Data

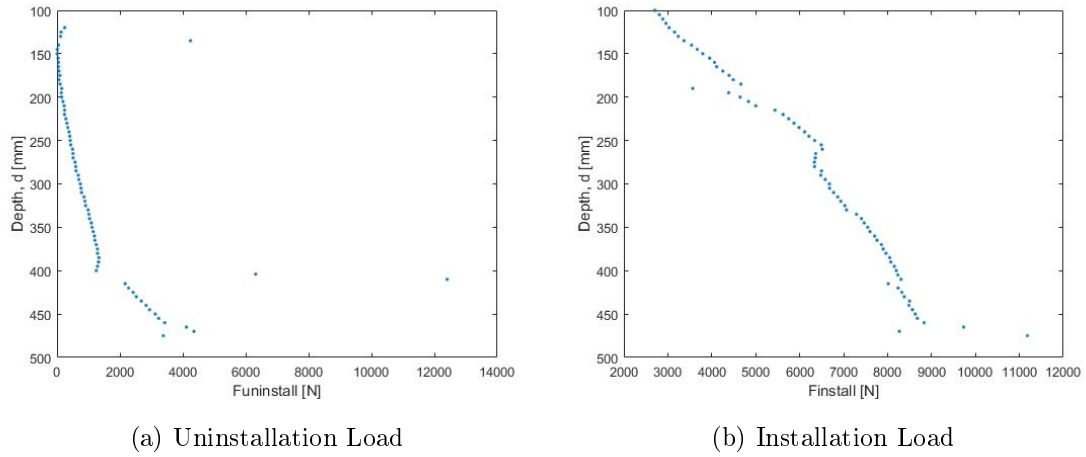


Figure B.26: Loading Data

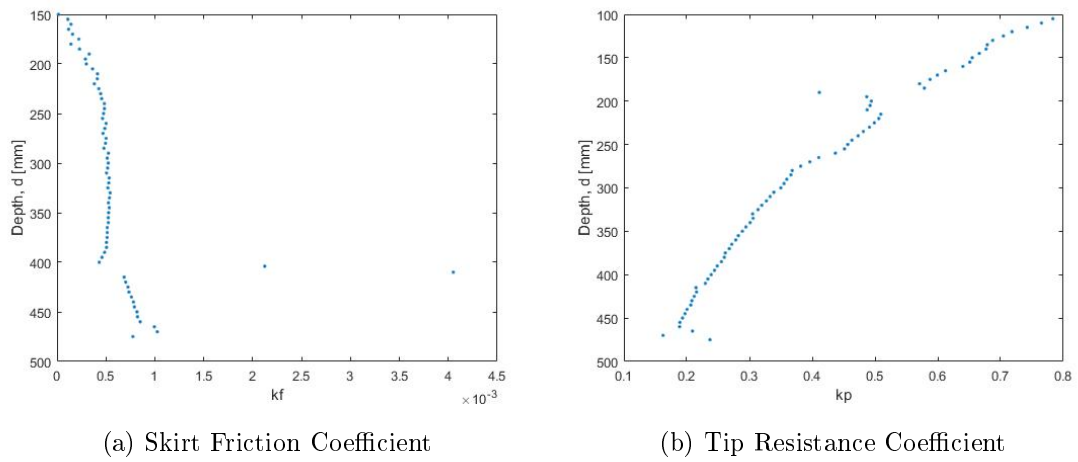
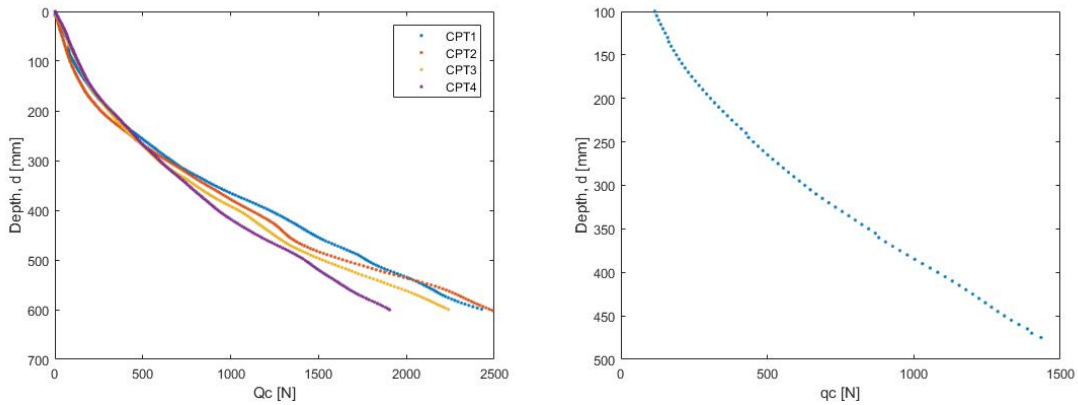
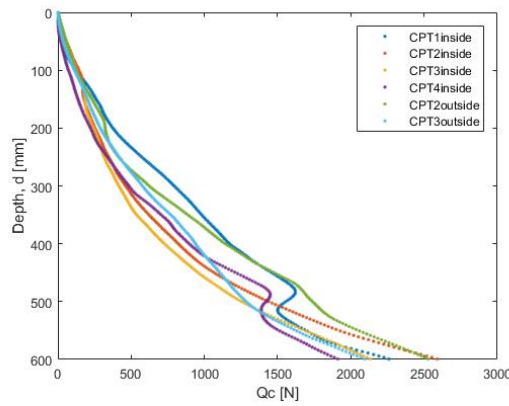


Figure B.27: Results

B.3.5 Experiment 07.04.2016 - Installation with Force - Uninstalltion with 402 kg

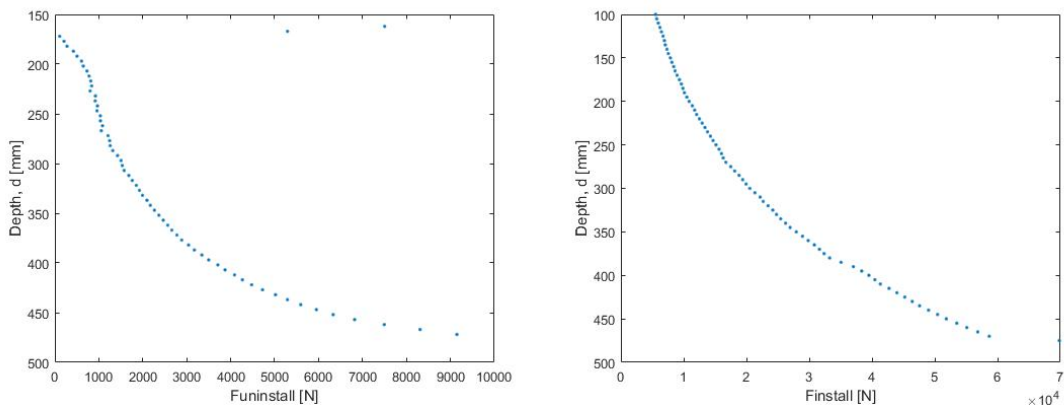


(a) Tip Resistance Before Installation (b) Average Tip Resistance Before Instalation



(c) Tip Resistance After Installation

Figure B.28: CPT Data



(a) Uninstallation Load (b) Installation Load

Figure B.29: Loading Data

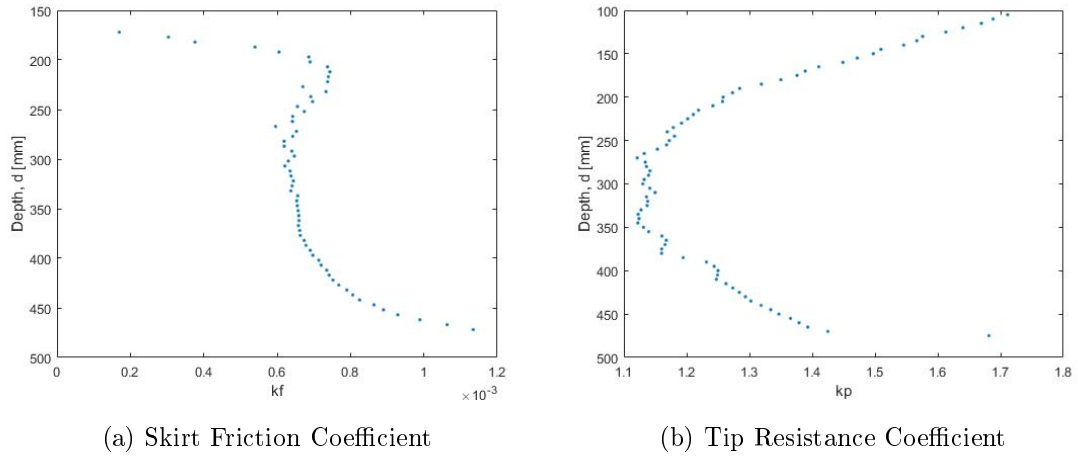
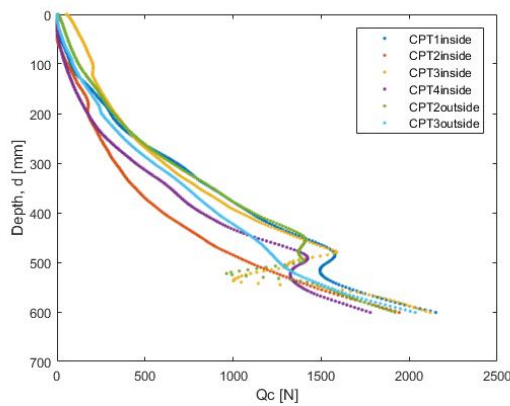
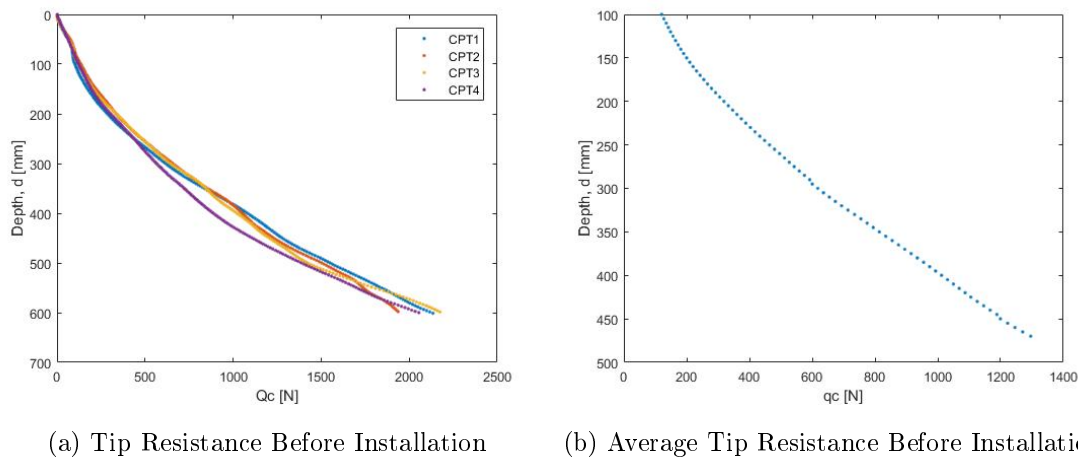


Figure B.30: Results

B.3.6 Experiment 12.04.2016 - Installation with Force - Uninstalltion with 402 kg



(c) Tip Resistance After Installation

Figure B.31: CPT Data

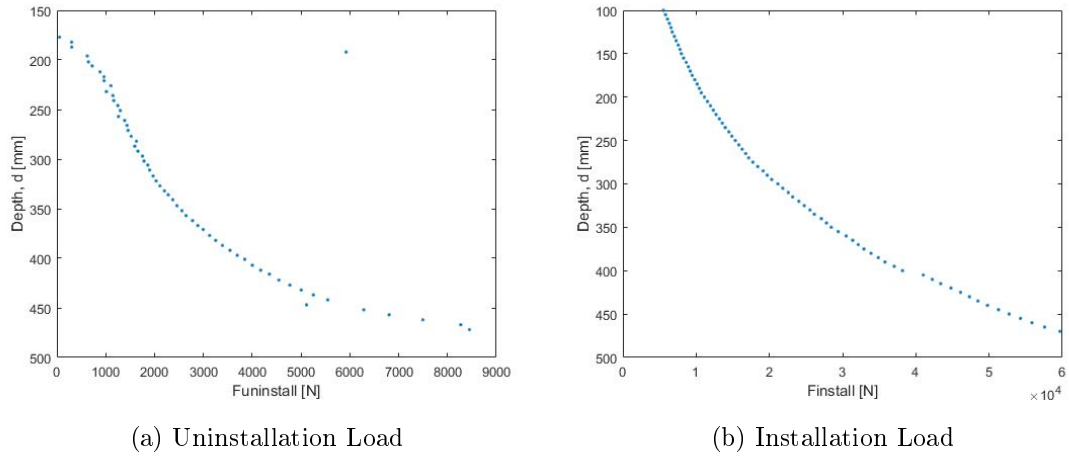


Figure B.32: Loading Data

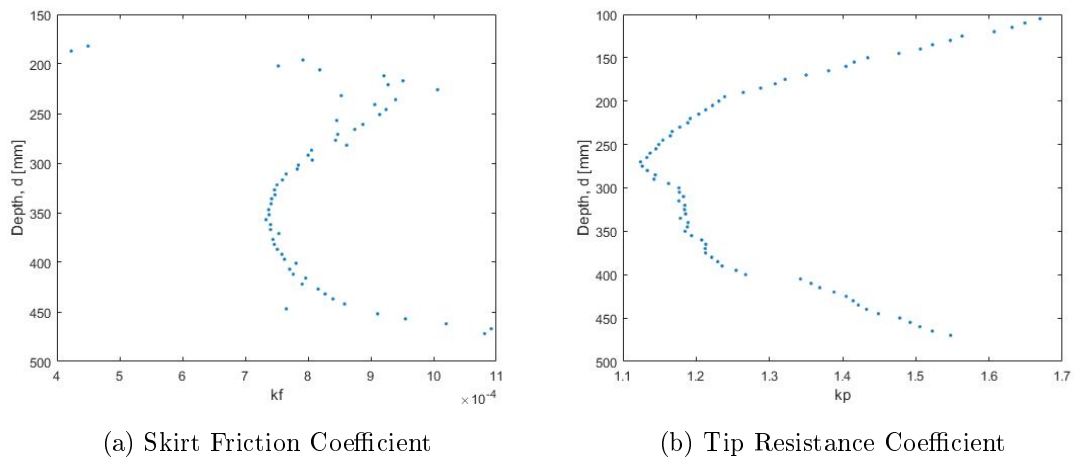
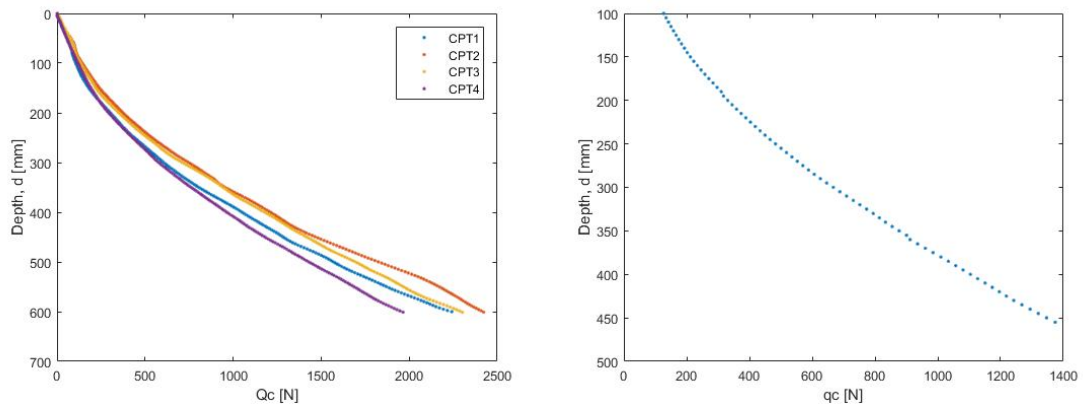
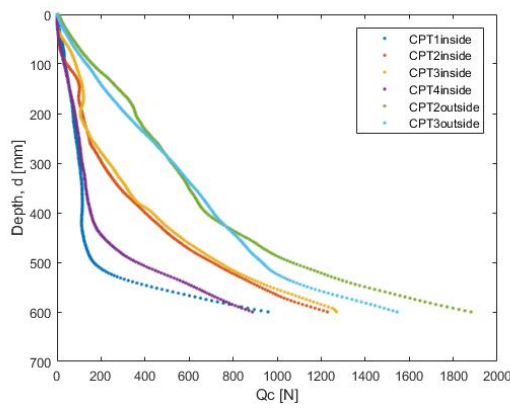


Figure B.33: Results

B.3.7 Experiment 18.04.2016 - Installation with Suction - Uninstallation with 302 kg

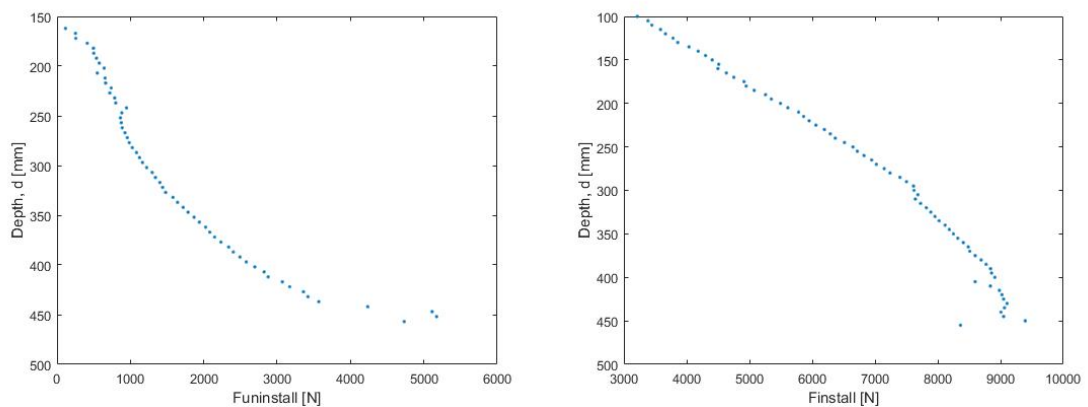


(a) Tip Resistance Before Installation (b) Average Tip Resistance Before Installation



(c) Tip Resistance After Installation

Figure B.34: CPT Data



(a) Uninstallation Load (b) Installation Load

Figure B.35: Loading Data

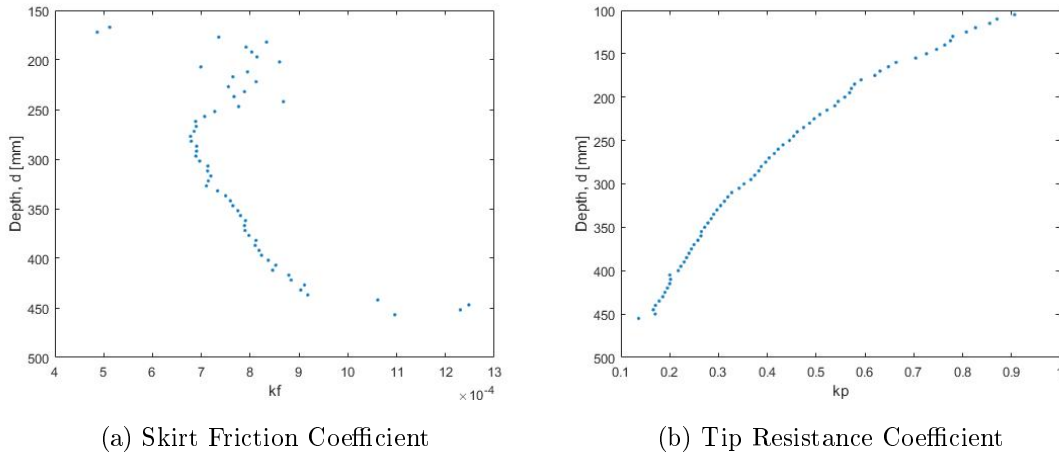
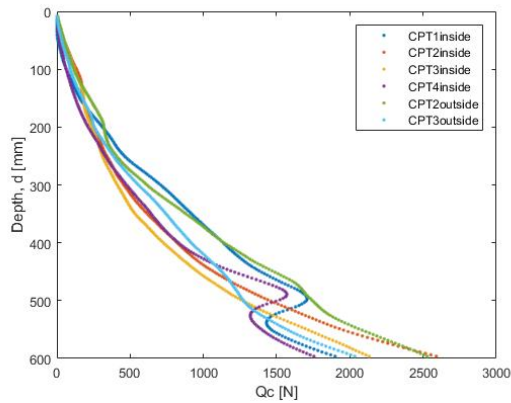
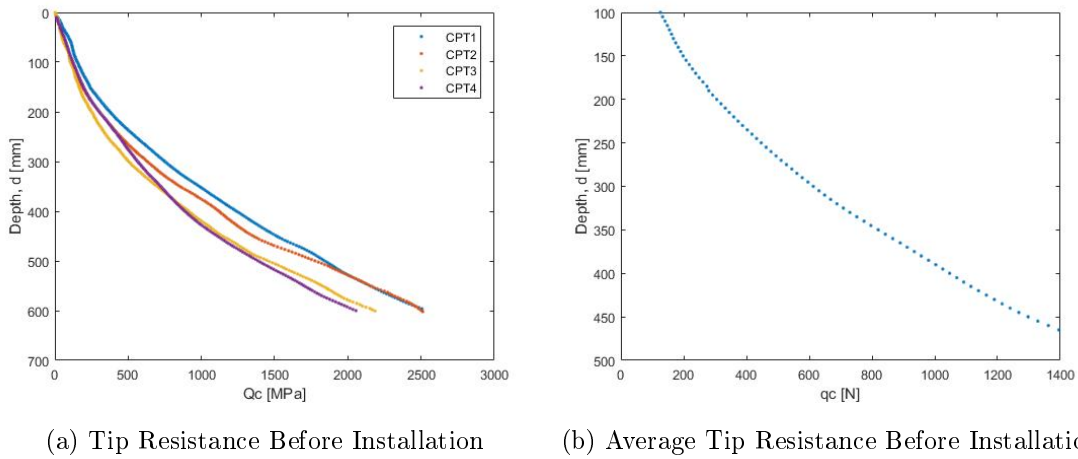


Figure B.36: Results

B.3.8 Experiment 25.04.2016 - Installation with Force - Uninstalltion with 201 kg



(c) Tip Resistance After Installation

Figure B.37: CPT Data

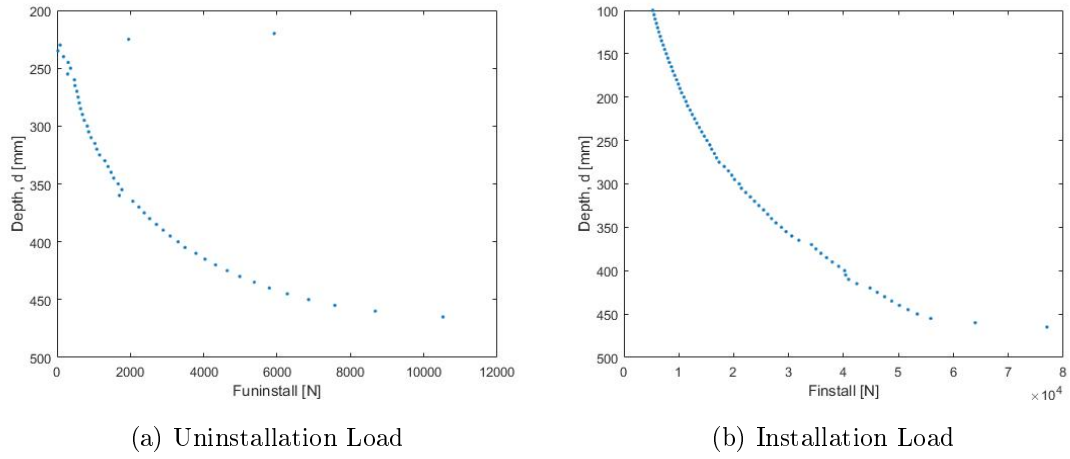


Figure B.38: Loading Data

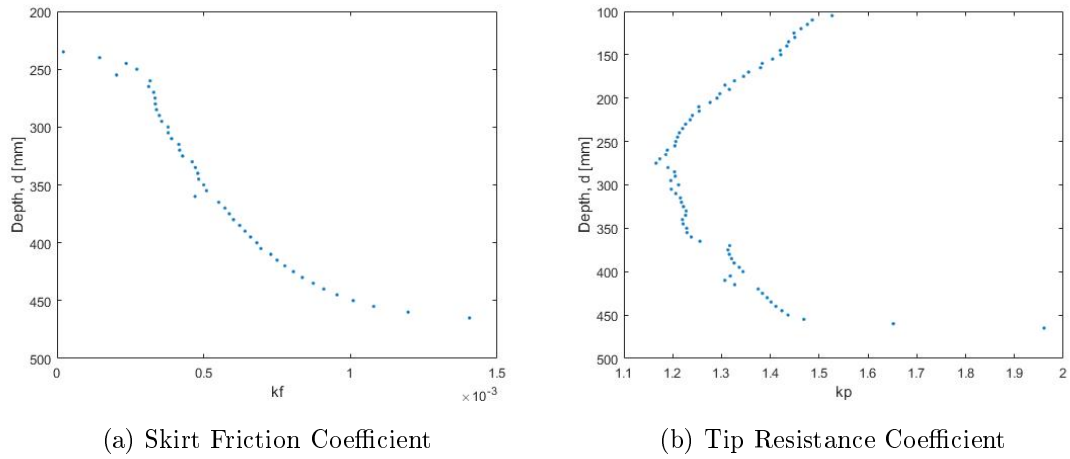


Figure B.39: Results

B.3.9 Experiment 29.03.2016 - Installation with Suction +2.01 kN - Uninstallation with 0 kg

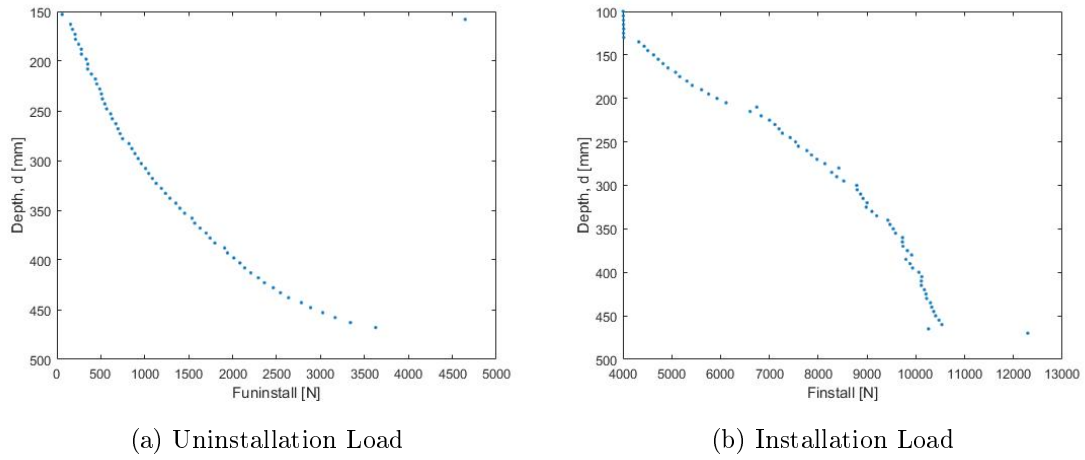


Figure B.40: Loading Data

B.3.10 Experiment 05.04.2016 - Installation with Suction - Uninstallation with 201 kg

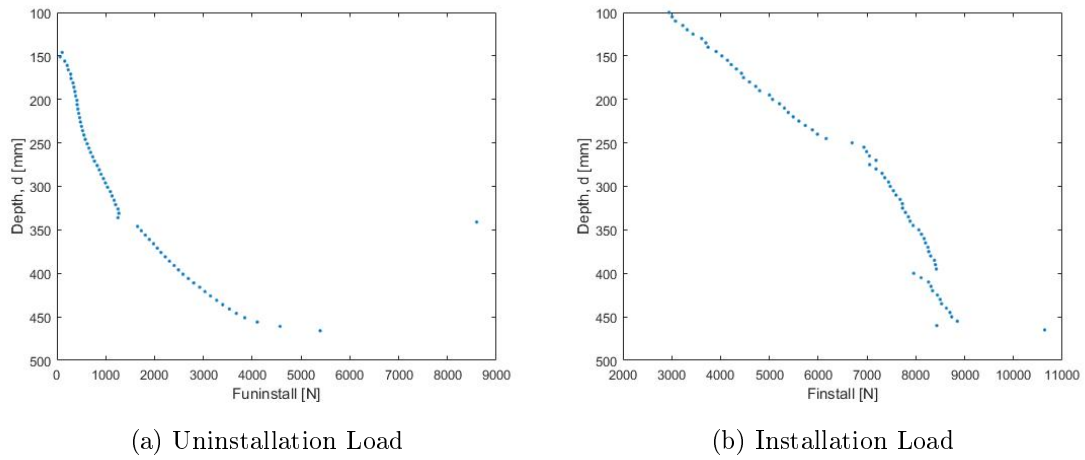


Figure B.41: Loading Data

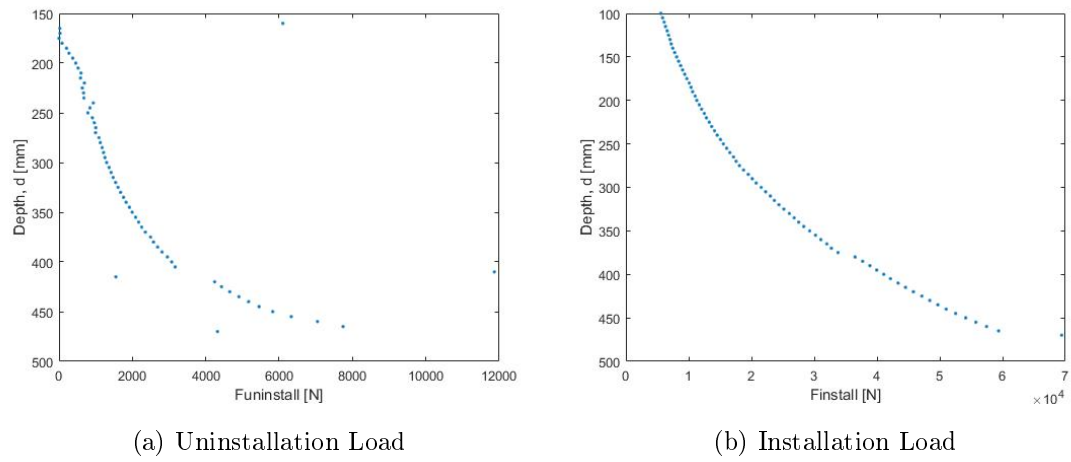
**B.3.11 Experiment 14.04.2016 - Installation with Force -
Uninstallation with 302 kg**

Figure B.42: Loading Data

APPENDIX: NUMERICAL ANALYSIS



In this Appendix the numerical results for the tests are presented. The detailed procedure is shown in chapter 4.

C.1 Installation Tests

Results from experiments 1, 2, 3, 5, and 9 are shown in this section. The detailed procedure explained in chapter 4 is based in test number 4.

C.1.1 Test Number 1-Installation "Suction+Force"

The following table shows the suction applied and its corresponding hydraulic head for each step of the installation:

Step	Penetration Length	Suction	Hydraulic Head
1	0.1 m	0.268 kPa	19.97 m
2	0.2 m	2.985 kPa	19.70 m
3	0.3 m	8.739 kPa	19.10 m
4	0.4 m	10.750 kPa	18.99 m
5	0.5 m	13.300 kPa	18.77 m

Table C.1: Suction and hydraulic head used in each step of the installation.

The groundwater head for applied suction for a penetration length of 0.1 m is shown in Figure C.1.

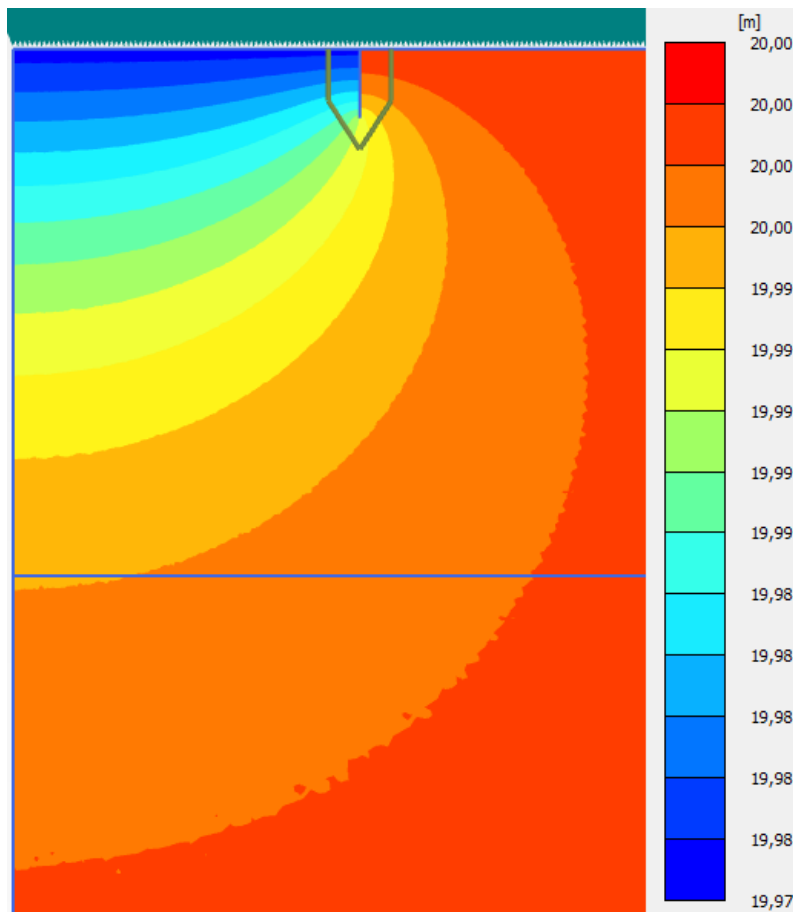


Figure C.1: Groundwater head for applied suction for a penetration length of 0.1 m.

The groundwater head for applied suction for a penetration length of 0.5 m when the bucket is completed installed is shown in Figure C.2.

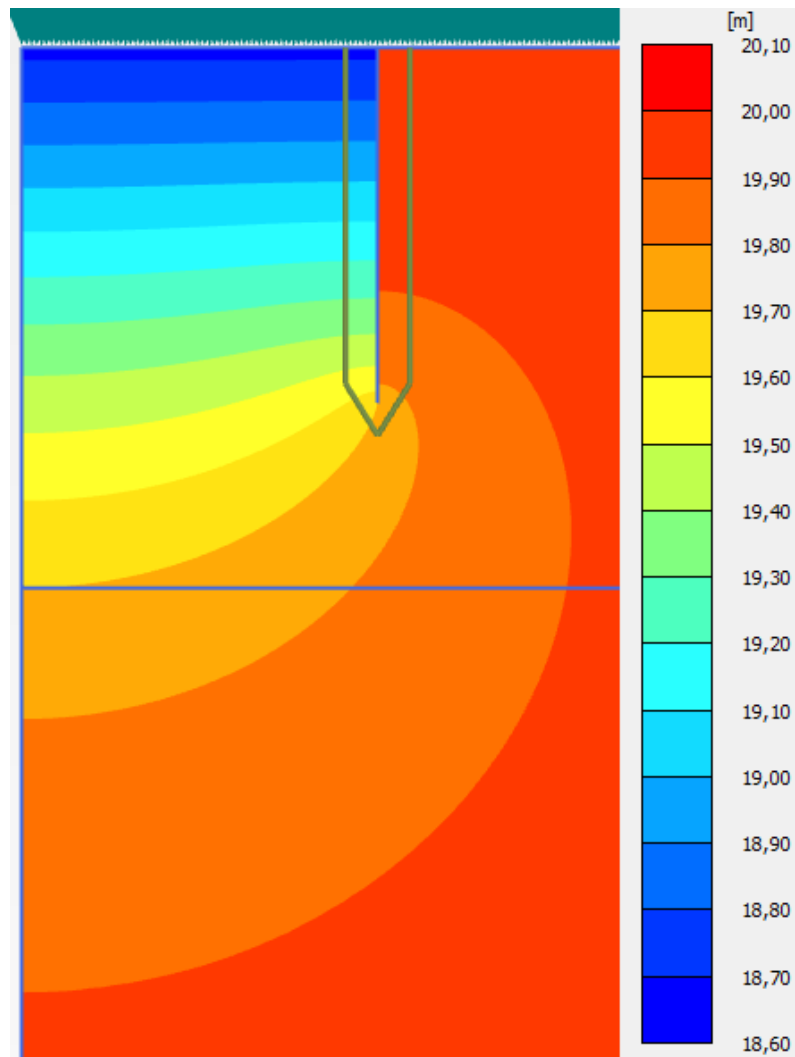


Figure C.2: Groundwater head for applied suction for a penetration length of 0.5 m.

The following table shows the values of v_{exit} , i_{exit} , s_{exit} , and $p_{critical}$:

Step	Penetration Length	v_{exit}	i_{exit}	s_{exit}	$p_{critical}$
1	0.1 m	0.775 m/day	0.108 –	0.247 m	2.473 kPa
2	0.2 m	5.437 m/day	0.762 –	0.391 m	3.913 kPa
3	0.3 m	11.793 m/day	1.654 –	0.528 m	5.282 kPa
4	0.4 m	11.815 m/day	1.657 –	0.648 m	6.485 kPa
5	0.5 m	12.460 m/day	1.748 –	0.760 m	7.608 kPa

Table C.2: Values of the variables for each penetration length.

In the following table the values of α are shown:

Step	Penetration Length	Δu_{tip}	α
1	0.1 m	0.098 kPa	0.364 –
2	0.2 m	0.991 kPa	0.332 –
3	0.3 m	2.478 kPa	0.283 –
4	0.4 m	2.694 kPa	0.250 –
5	0.5 m	2.981 kPa	0.224 –

Table C.3: Values of the variables for each penetration length.

In figure C.3 the pore pressure factor, α , is presented. The values from Plaxis are compared with the values extracted from the experiment in order to investigate deviations from Housby and Byrne [2005] solution.

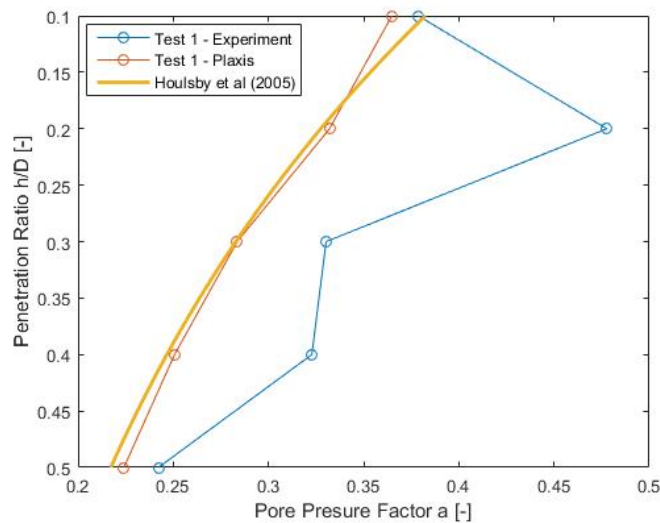


Figure C.3: Pore pressure factor results from experiments and Plaxis, along with Housby and Byrne [2005] solution.

The groundwater flow and the development of it is shown in the following 2 figures. The groundwater flow for a penetration length of 0.1 m is shown in Figure C.4 and for a penetration length of 0.5 m is shown in Figure C.5.

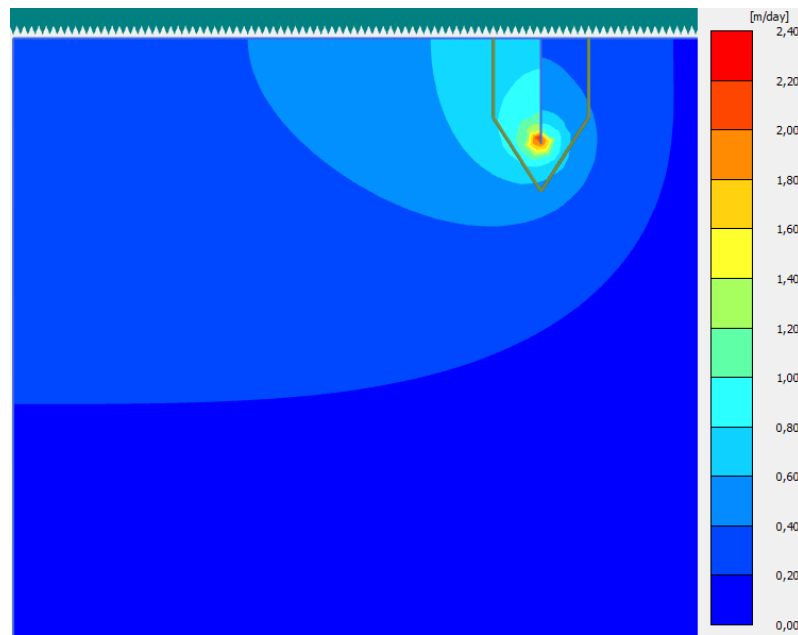


Figure C.4: Groundwater flow for a penetration length of 0.1 m.

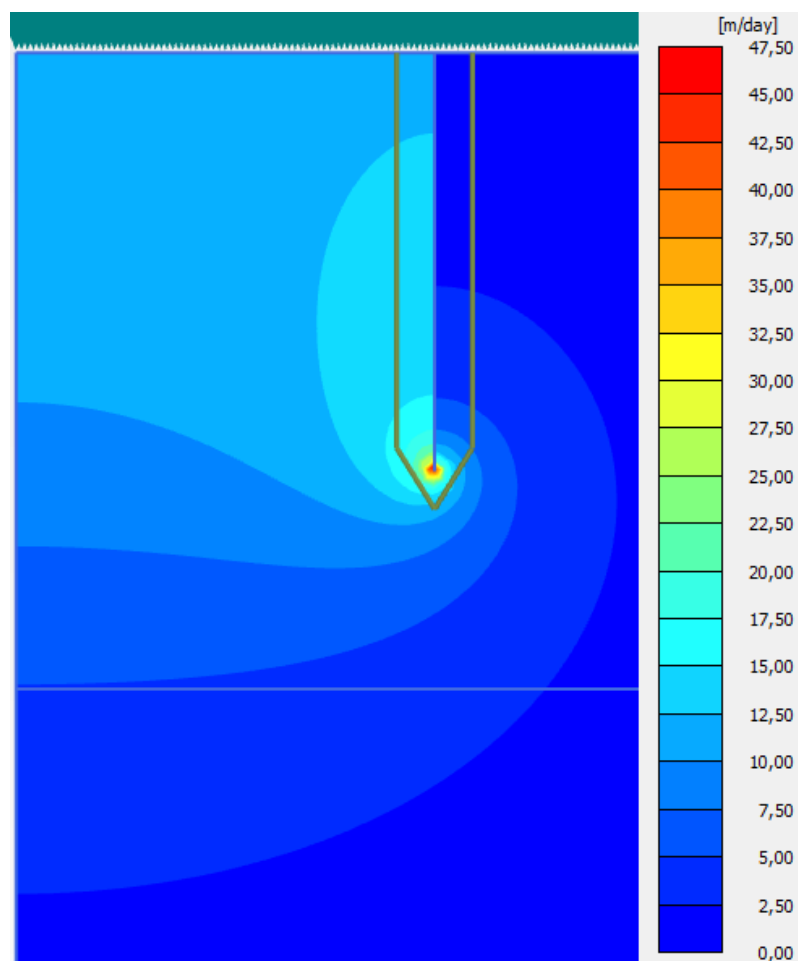


Figure C.5: Groundwater flow for a penetration length of 0.5 m.

Figure C.6 presents results from the numerical calculations for the normalized seepage length for the exit, using the exit hydraulic gradient with respect to the fitted solutions from equations 4.10 and 4.11. The seepage length exit for the experiment was not possible to calculate since the exit velocity was not measured.

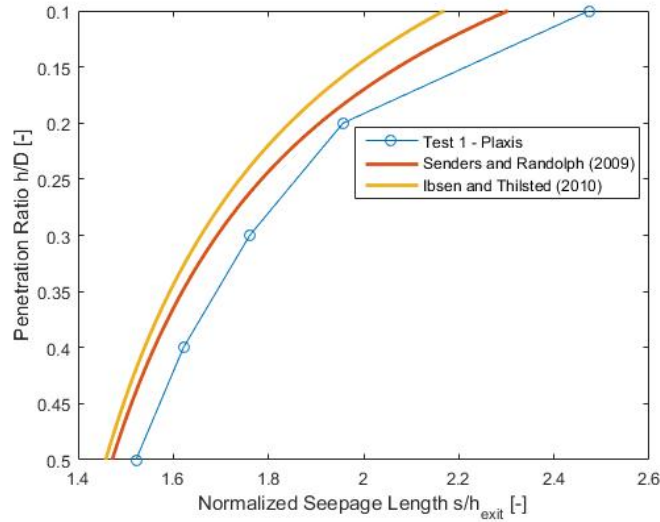


Figure C.6: Normalized seepage length results for the exit hydraulic gradient, compared to the solutions from Ibsen and Thilsted [2010], equation 4.11 and from Senders and Randolph [2009], equation 4.10.

Results for seepage length calculated from the average hydraulic gradient outside are presented in figure C.7.

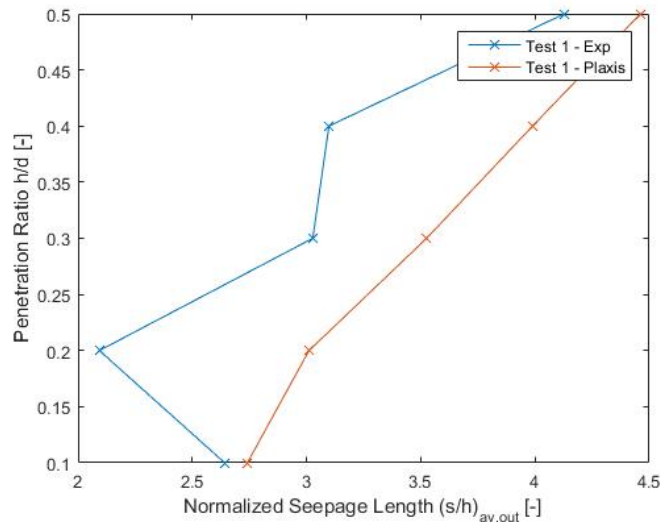


Figure C.7: Normalized seepage length results using the average outside hydraulic gradient.

Results for seepage length calculated from the average hydraulic gradient inside are presented in figure C.8.

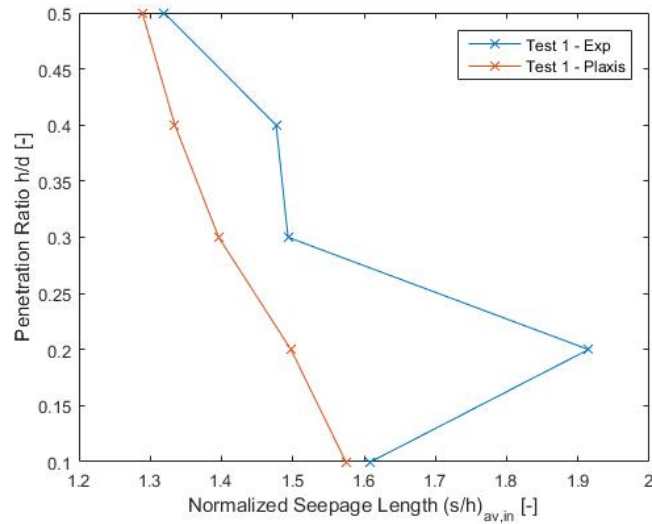


Figure C.8: Normalized seepage length results using the average inside hydraulic gradient.

Results for seepage length calculated from the tip hydraulic gradient are presented in figure C.9.

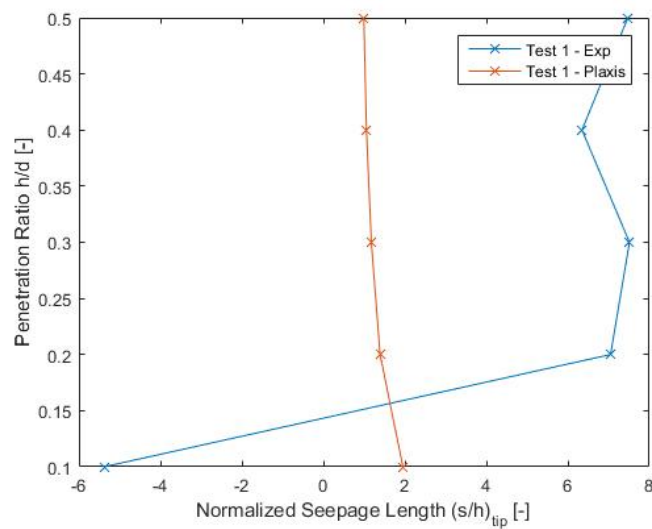


Figure C.9: Normalized seepage length results using the tip hydraulic gradient.

In the following figure, results by Feld [2001], Houlsby and Byrne [2005], Senders and Randolph [2009] and Ibsen and Thilsted [2010] are presented and compared with the numerical model for the normalized critical pressures.

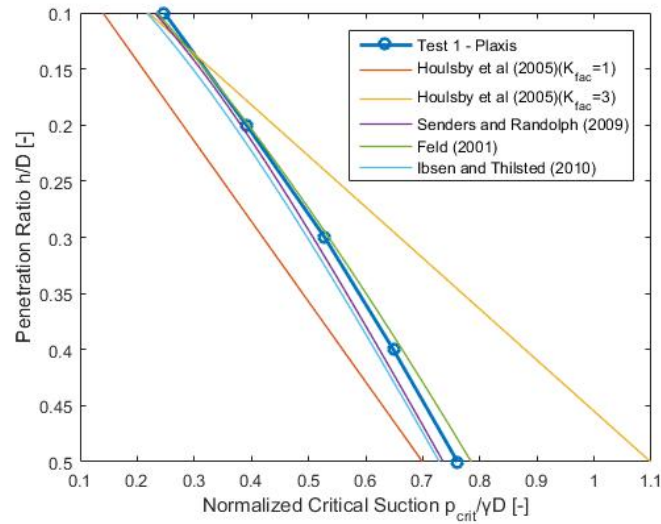


Figure C.10: Normalized critical pressures calculated in Plaxis, in comparison to solution proposed by Feld [2001], Houlsby and Byrne [2005], Senders and Randolph [2009], and Ibsen and Thilsted [2010].

C.1.2 Test Number 2-Installation "Suction+Force"

The following table shows the suction applied and its corresponding hydraulic head for each step of the installation:

Step	Penetration Length	Suction	Hydraulic Head
1	0.1 m	0.002 kPa	19.99 m
2	0.2 m	2.646 kPa	19.75 m
3	0.3 m	8.537 kPa	19.15 m
4	0.4 m	10.886 kPa	18.99 m
5	0.5 m	12.279 kPa	18.77 m

Table C.4: Suction and hydraulic head used in each step of the installation.

The groundwater head for applied suction for a penetration length of 0.1 m is shown in Figure C.11.

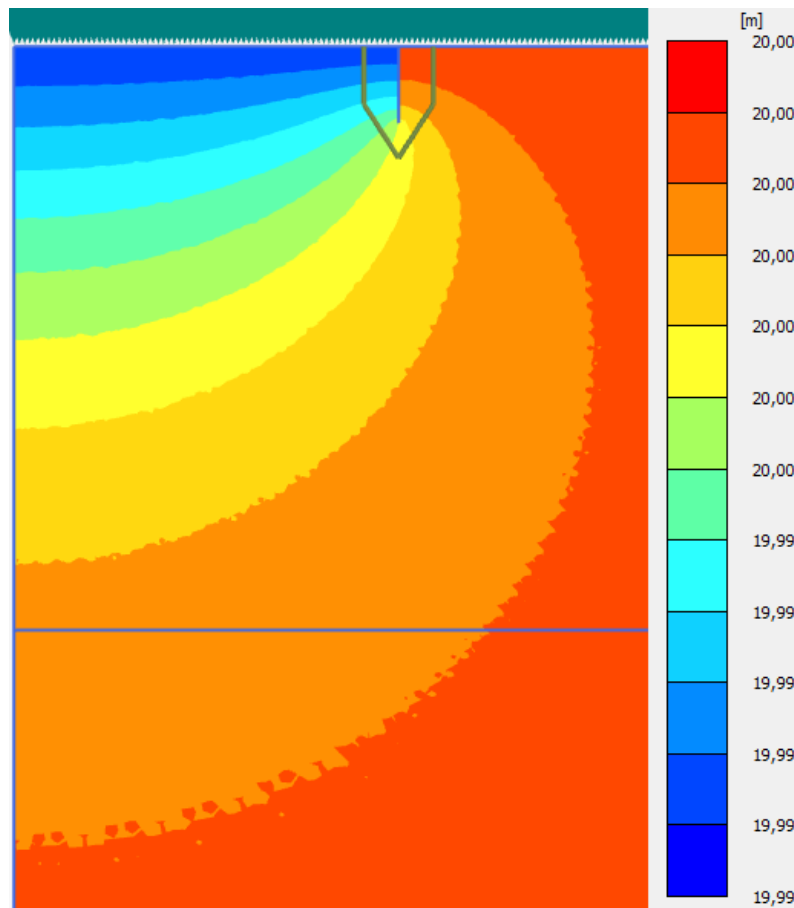


Figure C.11: Groundwater head for applied suction for a penetration length of 0.1 m.

The groundwater head for applied suction for a penetration length of 0.5 m when the bucket is completed installed is shown in Figure C.12.

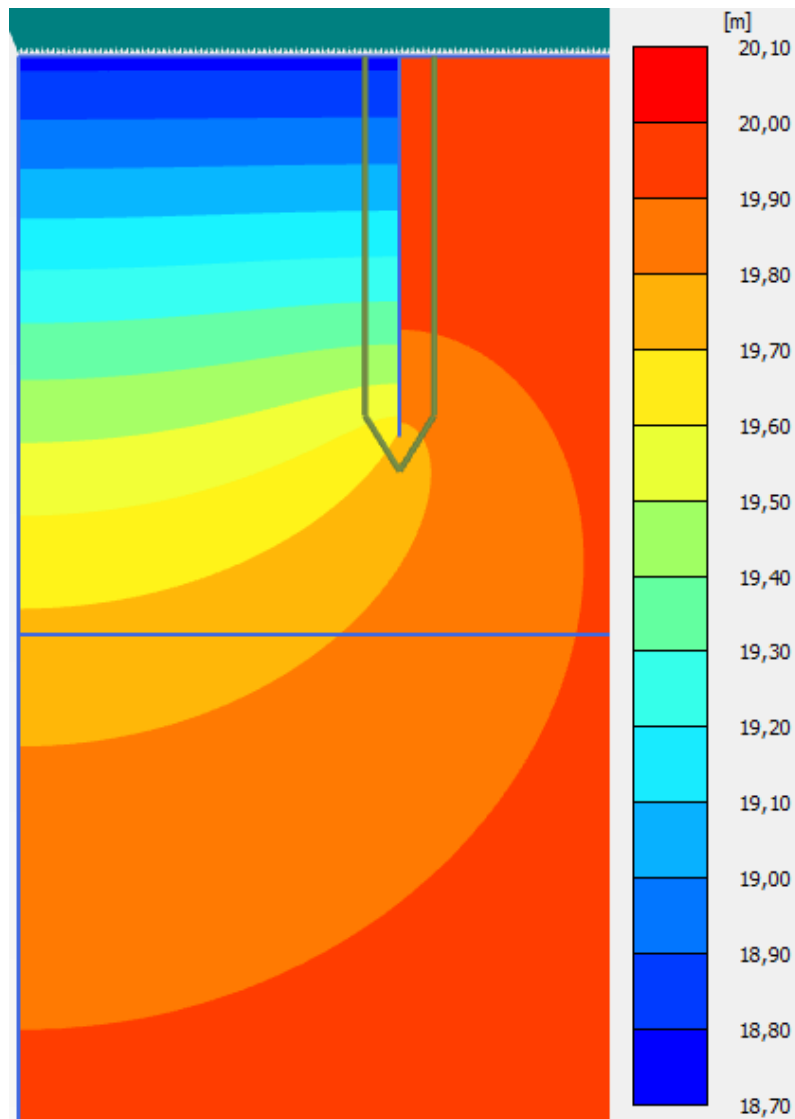


Figure C.12: Groundwater head for applied suction for a penetration length of 0.5 m.

The following table shows the values of v_{exit} , i_{exit} , s_{exit} , and $p_{critical}$:

Step	Penetration Length	v_{exit}	i_{exit}	s_{exit}	$p_{critical}$
1	0.1 m	0.310 m/day	0.043 –	0.005 m	0.052 kPa
2	0.2 m	4.712 m/day	0.661 –	0.400 m	4.002 kPa
3	0.3 m	11.604 m/day	1.627 –	0.524 m	5.244 kPa
4	0.4 m	11.964 m/day	1.678 –	0.648 m	6.485 kPa
5	0.5 m	11.523 m/day	1.616 –	0.759 m	7.595 kPa

Table C.5: Values of the variables for each penetration length.

In the following table the values of α are shown:

Step	Penetration Length	Δu_{tip}	α
1	0.1 m	0.039 kPa	17.193 –
2	0.2 m	0.859 kPa	0.324 –
3	0.3 m	2.447 kPa	0.286 –
4	0.4 m	2.728 kPa	0.250 –
5	0.5 m	2.757 kPa	0.224 –

Table C.6: Values of the variables for each penetration length.

In figure C.13 the pore pressure factor, α , is presented. The values from Plaxis are compared with the values extracted from the experiment in order to investigate deviations from Houlsby and Byrne [2005] solution.

The groundwater flow and the development of it is shown in the following 2 figures. The groundwater flow for a penetration length of 0.1 m is shown in Figure C.14 and for a penetration length of 0.5 m is shown in Figure C.15.

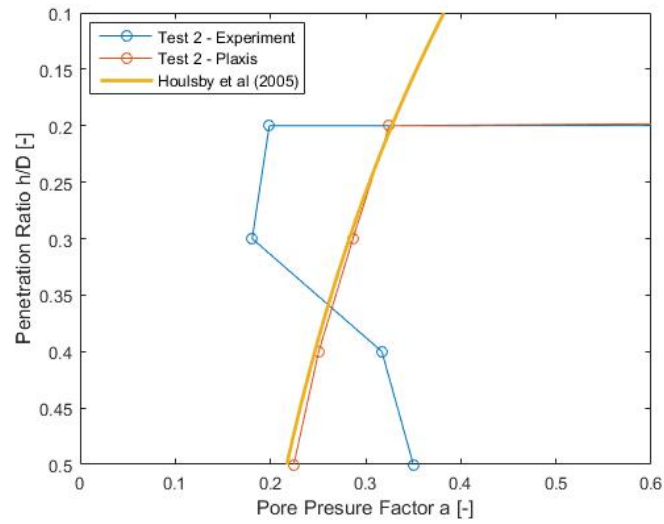


Figure C.13: Pore pressure factor results from experiments and Plaxis, along with Houlby and Byrne [2005] solution.

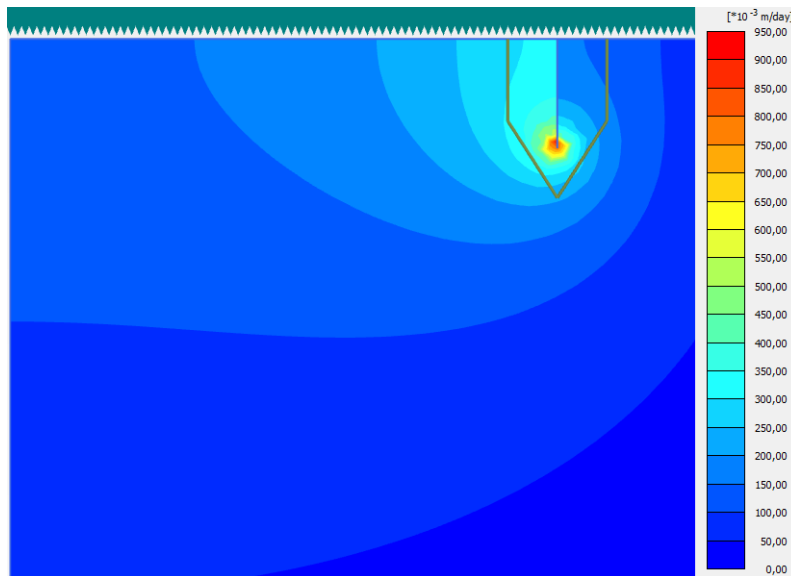


Figure C.14: Groundwater flow for a penetration length of 0.1 m.

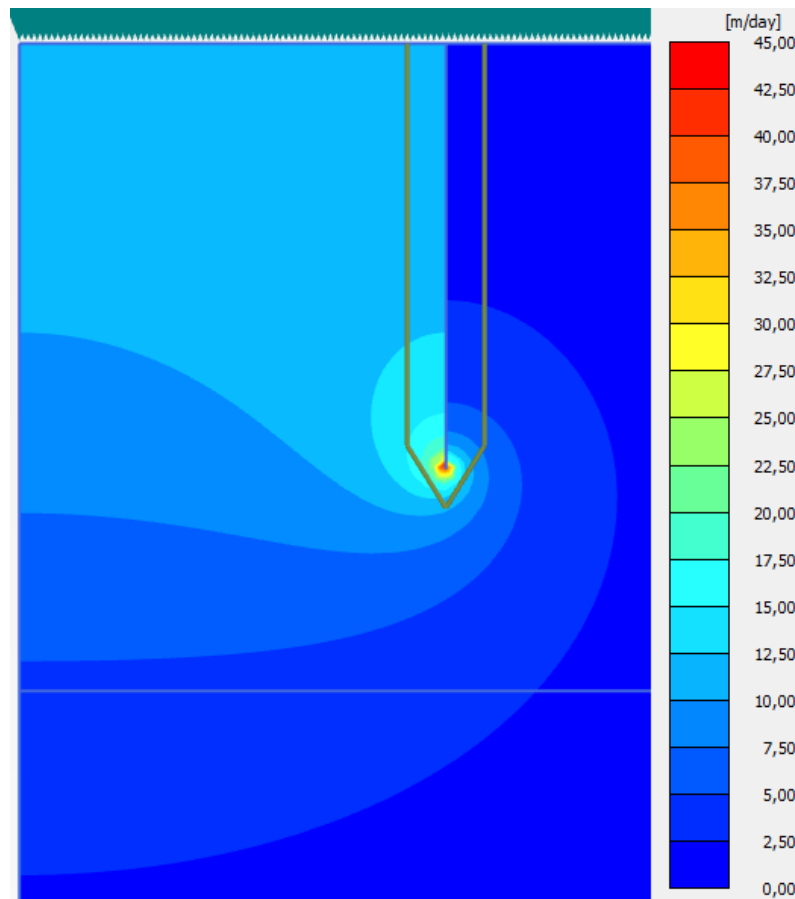


Figure C.15: Groundwater flow for a penetration length of 0.5 m.

Figure C.16 presents results from the numerical calculations for the normalized seepage length for the exit, using the exit hydraulic gradient with respect to the fitted solutions from equations 4.10 and 4.11. The seepage length exit for the experiment was not possible to calculate since the exit velocity was not measured.

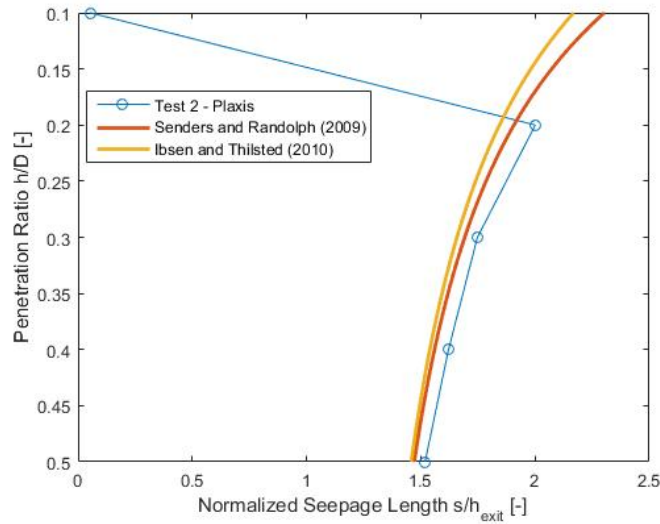


Figure C.16: Normalized seepage length results for the exit hydraulic gradient, compared to the solutions from Ibsen and Thilsted [2010], equation 4.11 and from Senders and Randolph [2009], equation 4.10.

Results for seepage length calculated from the average hydraulic gradient outside are presented in figure C.17.

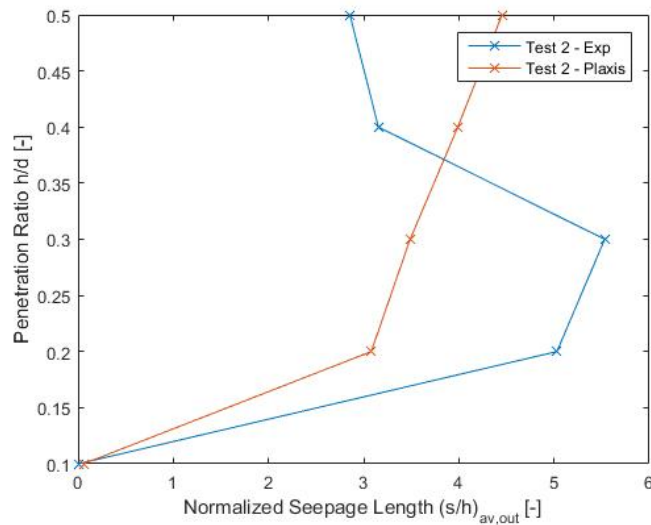


Figure C.17: Normalized seepage length results using the average outside hydraulic gradient.

Results for seepage length calculated from the average hydraulic gradient inside are presented in figure C.18.

Results for seepage length calculated from the tip hydraulic gradient are presented in figure C.19.

In the following figure, results by Feld [2001], Houlsby and Byrne [2005], Senders and

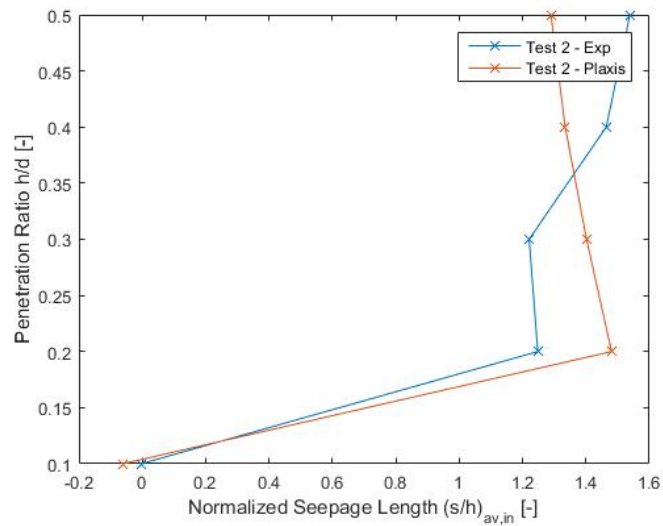


Figure C.18: Normalized seepage length results using the average inside hydraulic gradient.

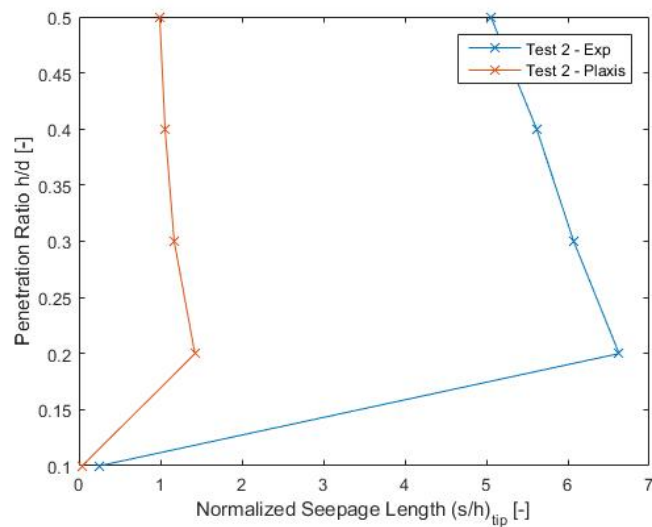


Figure C.19: Normalized seepage length results using the tip hydraulic gradient.

Randolph [2009] and Ibsen and Thilsted [2010] are presented and compared with the numerical model for the normalized critical pressures.

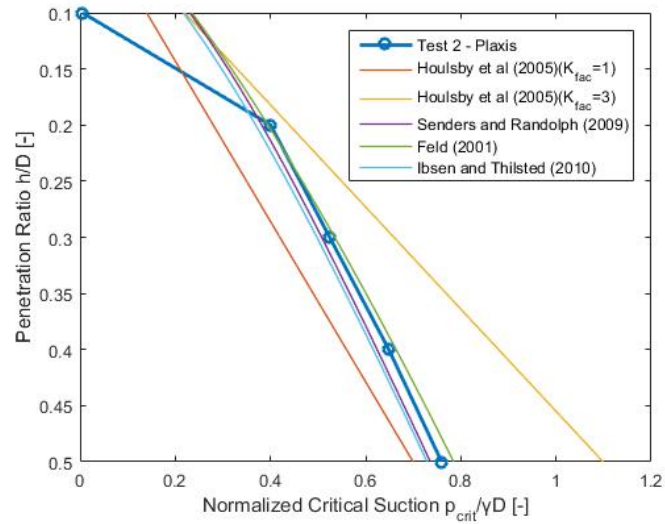


Figure C.20: Normalized critical pressures calculated in Plaxis, in comparison to solution proposed by Feld [2001], Houlsby and Byrne [2005], Senders and Randolph [2009], and Ibsen and Thilsted [2010].

C.1.3 Test Number 3-Installation "Suction+Force"

The following table shows the suction applied and its corresponding hydraulic head for each step of the installation:

Step	Penetration Length	Suction	Hydraulic Head
1	0.1 m	0.019 kPa	19.99 m
2	0.2 m	2.458 kPa	19.75 m
3	0.3 m	8.735 kPa	19.13 m
4	0.4 m	10.379 kPa	18.97 m
5	0.5 m	14.100 kPa	18.59 m

Table C.7: Suction and hydraulic head used in each step of the installation.

The groundwater head for applied suction for a penetration length of 0.1 m is shown in Figure C.21.

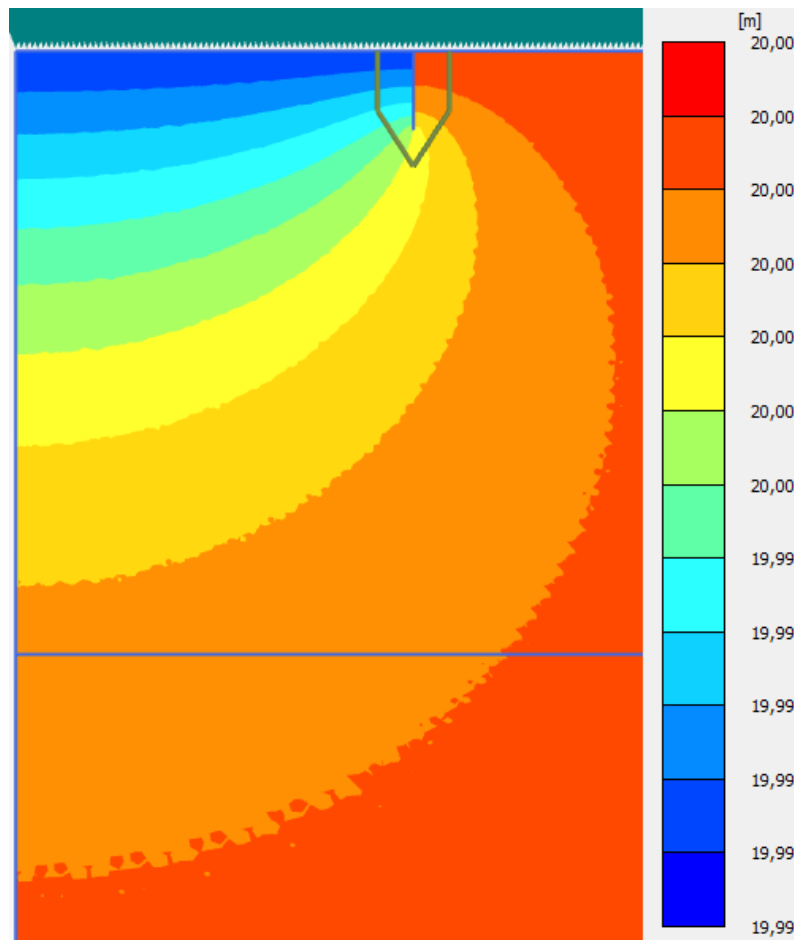


Figure C.21: Groundwater head for applied suction for a penetration length of 0.1 m.

The groundwater head for applied suction for a penetration length of 0.5 m when the bucket is completed installed is shown in Figure C.22.

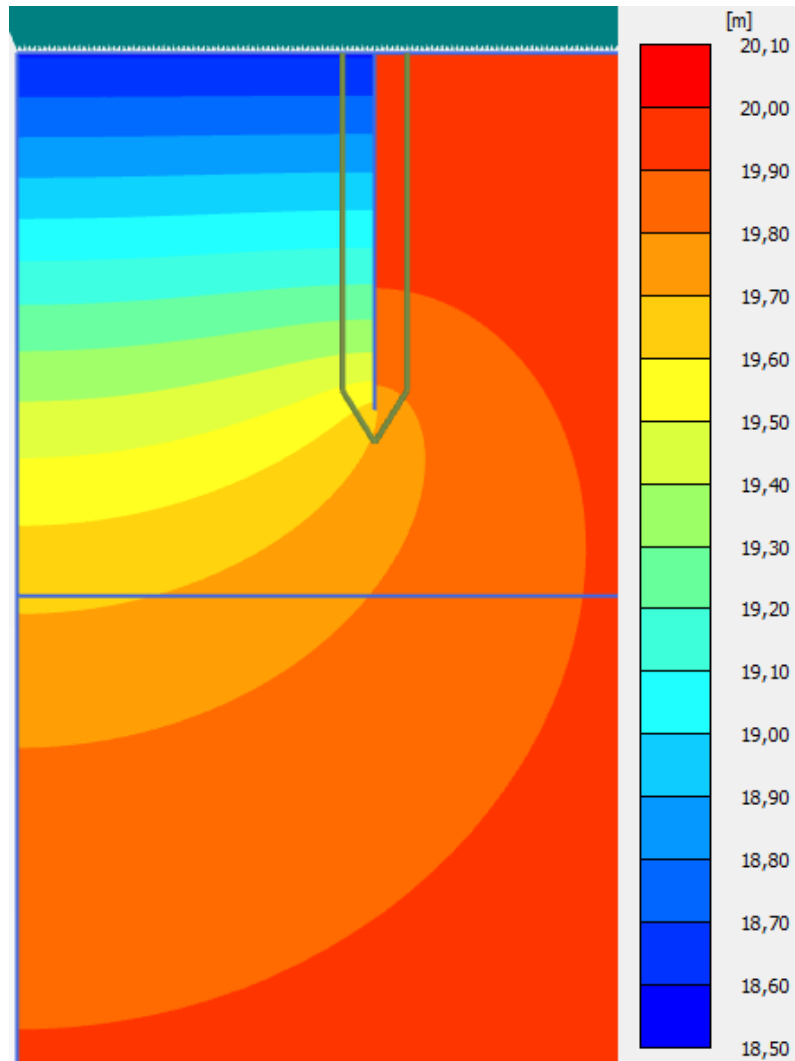


Figure C.22: Groundwater head for applied suction for a penetration length of 0.5 m.

The following table shows the values of v_{exit} , i_{exit} , s_{exit} , and $p_{critical}$:

Step	Penetration Length	v_{exit}	i_{exit}	s_{exit}	$p_{critical}$
1	0.1 m	0.310 m/day	0.043 –	0.459 m	0.459 kPa
2	0.2 m	4.531 m/day	0.635 –	1.933 m	3.866 kPa
3	0.3 m	11.874 m/day	1.665 –	1.747 m	5.243 kPa
4	0.4 m	11.407 m/day	1.600 –	1.621 m	6.485 kPa
5	0.5 m	13.209 m/day	1.853 –	1.521 m	7.608 kPa

Table C.8: Values of the variables for each penetration length.

In the following table the values of α are shown:

Step	Penetration Length	Δu_{tip}	α
1	0.1 m	0.039 kPa	1.962 –
2	0.2 m	0.826 kPa	0.336 –
3	0.3 m	2.504 kPa	0.286 –
4	0.4 m	2.601 kPa	0.250 –
5	0.5 m	3.160 kPa	0.224 –

Table C.9: Values of the variables for each penetration length.

In figure C.23 the pore pressure factor, α , is presented. The values from Plaxis are compared with the values extracted from the experiment in order to investigate deviations from Housby and Byrne [2005] solution.

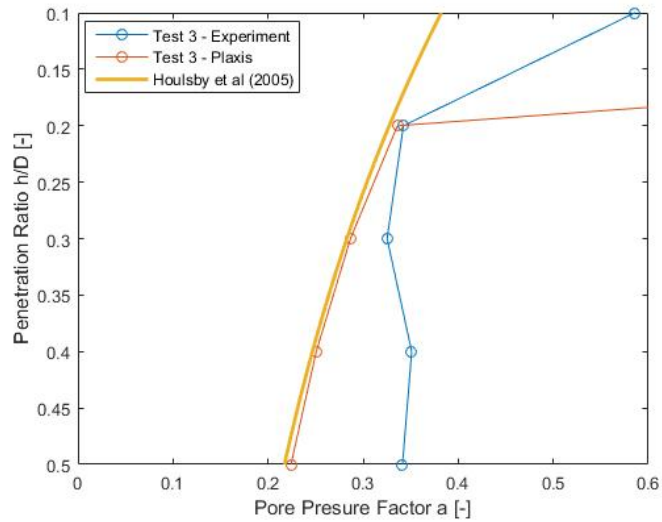


Figure C.23: Pore pressure factor results from experiments and Plaxis, along with Housby and Byrne [2005] solution.

The groundwater flow and the development of it is shown in the following 2 figures. The groundwater flow for a penetration length of 0.1 m is shown in Figure C.24 and for a penetration length of 0.5 m is shown in Figure C.25.

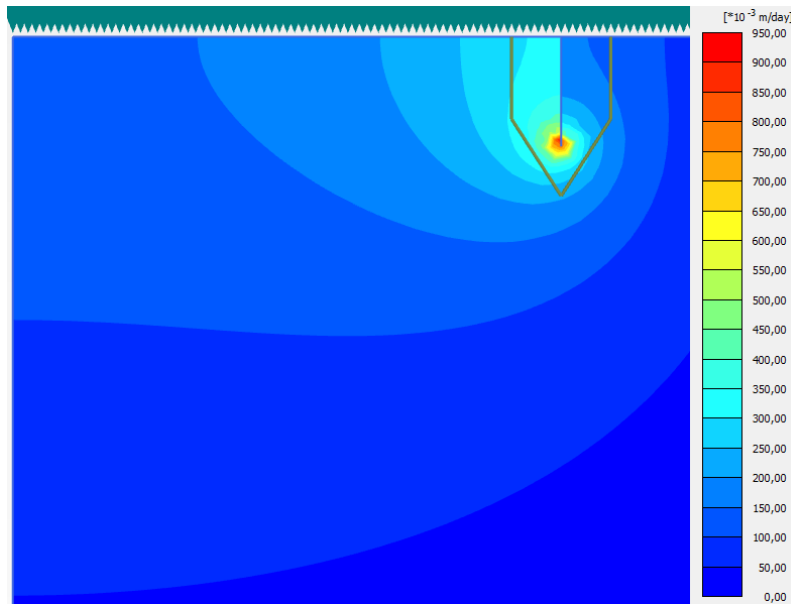


Figure C.24: Groundwater flow for a penetration length of 0.1 m.

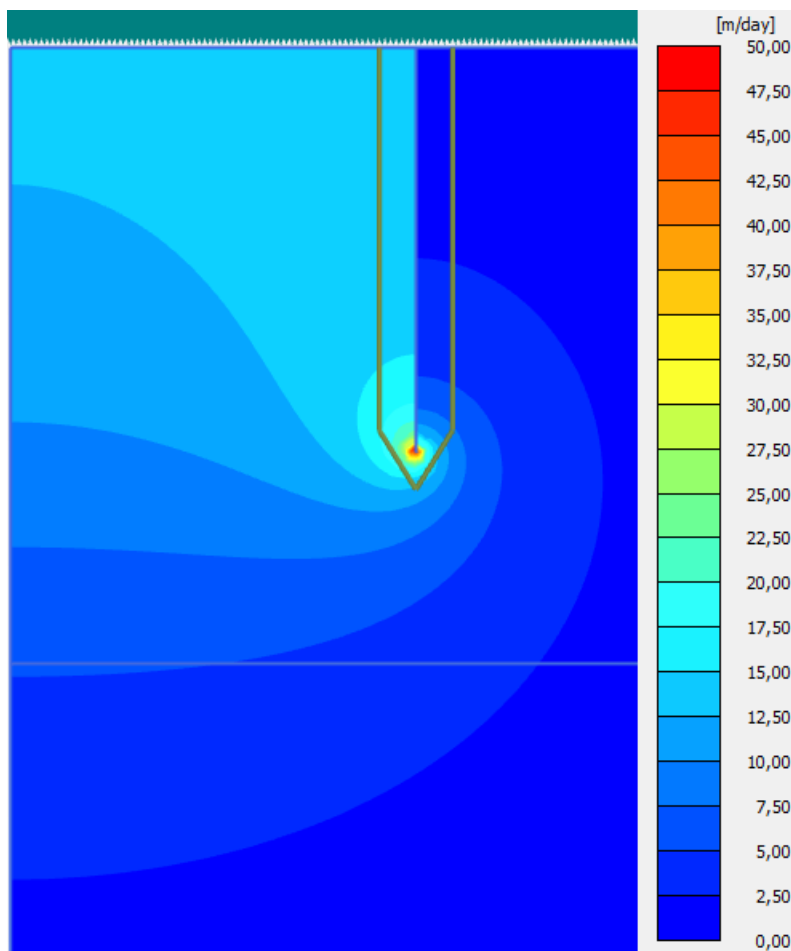


Figure C.25: Groundwater flow for a penetration length of 0.5 m.

Figure C.26 presents results from the numerical calculations for the normalized seepage length for the exit, using the exit hydraulic gradient with respect to the fitted solutions from equations 4.10 and 4.11. The seepage length exit for the experiment was not possible to calculate since the exit velocity was not measured.

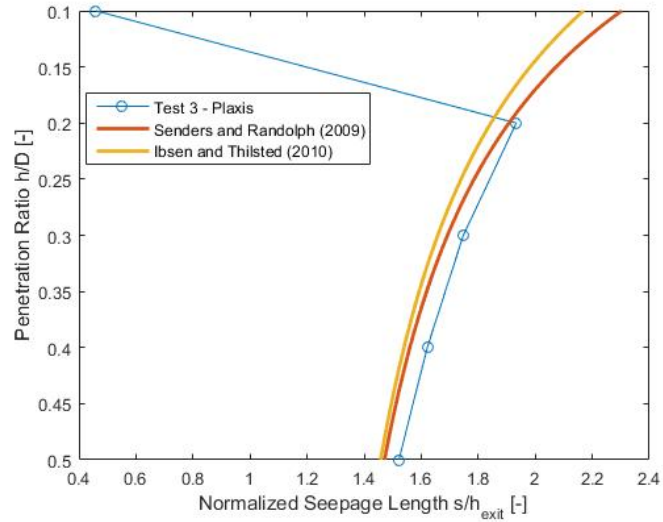


Figure C.26: Normalized seepage length results for the exit hydraulic gradient, compared to the solutions from Ibsen and Thilsted [2010], equation 4.11 and from Senders and Randolph [2009], equation 4.10.

Results for seepage length calculated from the average hydraulic gradient outside are presented in figure C.27.

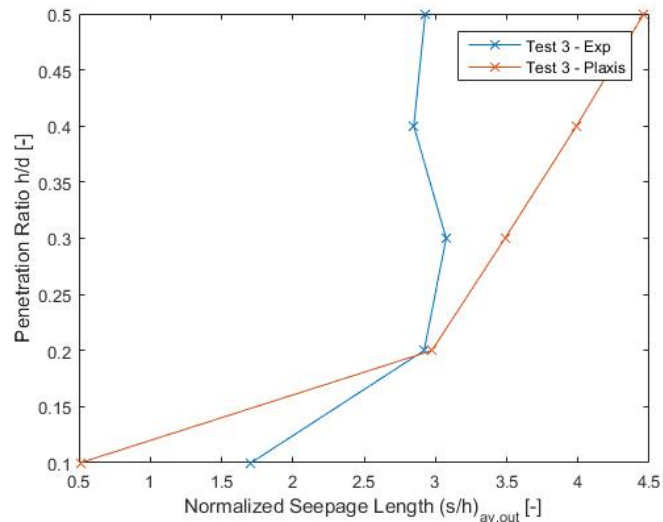


Figure C.27: Normalized seepage length results using the average outside hydraulic gradient.

Results for seepage length calculated from the average hydraulic gradient inside are presented in figure C.28.

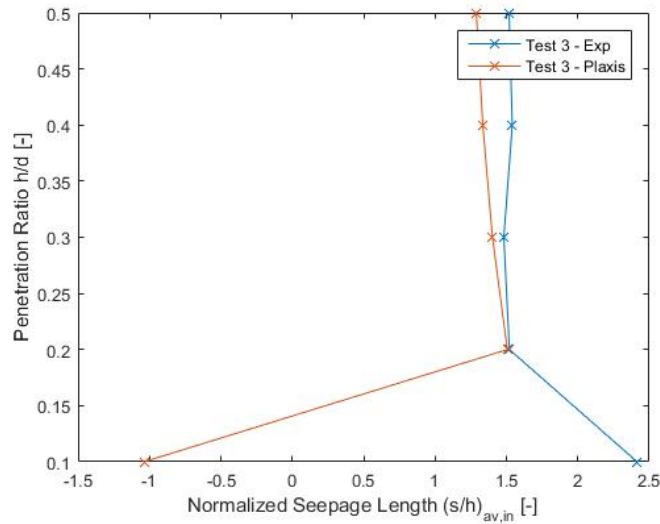


Figure C.28: Normalized seepage length results using the average inside hydraulic gradient.

Results for seepage length calculated from the tip hydraulic gradient are presented in figure C.29.

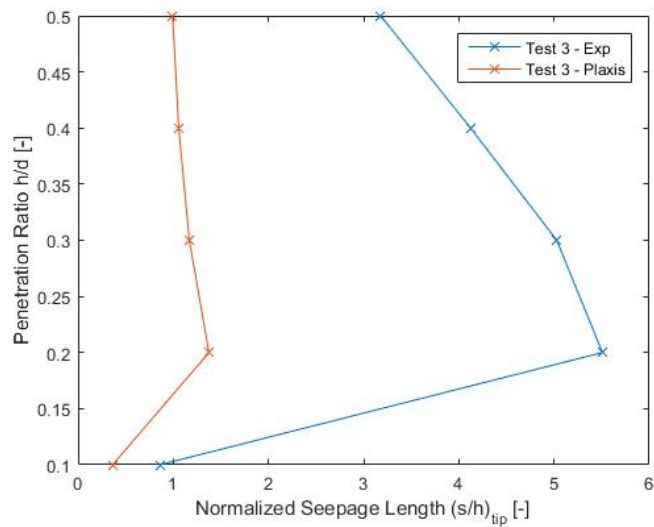


Figure C.29: Normalized seepage length results using the tip hydraulic gradient.

In the following figure, results by Feld [2001], Houlsby and Byrne [2005], Senders and Randolph [2009] and Ibsen and Thilsted [2010] are presented and compared with the numerical model for the normalized critical pressures.

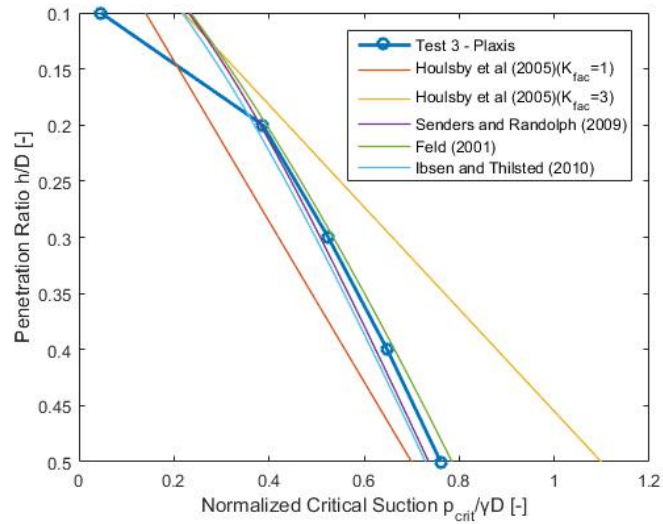


Figure C.30: Normalized critical pressures calculated in Plaxis, in comparison to solution proposed by Feld [2001], Houlsby and Byrne [2005], Senders and Randolph [2009], and Ibsen and Thilsted [2010].

C.1.4 Test Number 5-Installation "Pure Suction"

The following table shows the suction applied and its corresponding hydraulic head for each step of the installation:

Step	Penetration Length	Suction	Hydraulic Head
1	0.1 m	1.206 kPa	19.88 m
2	0.2 m	3.936 kPa	19.60 m
3	0.3 m	7.044 kPa	19.30 m
4	0.4 m	7.663 kPa	18.24 m
5	0.5 m	11.670 kPa	18.84 m

Table C.10: Suction and hydraulic head used in each step of the installation.

The groundwater head for applied suction for a penetration length of 0.1 m is shown in Figure C.31.

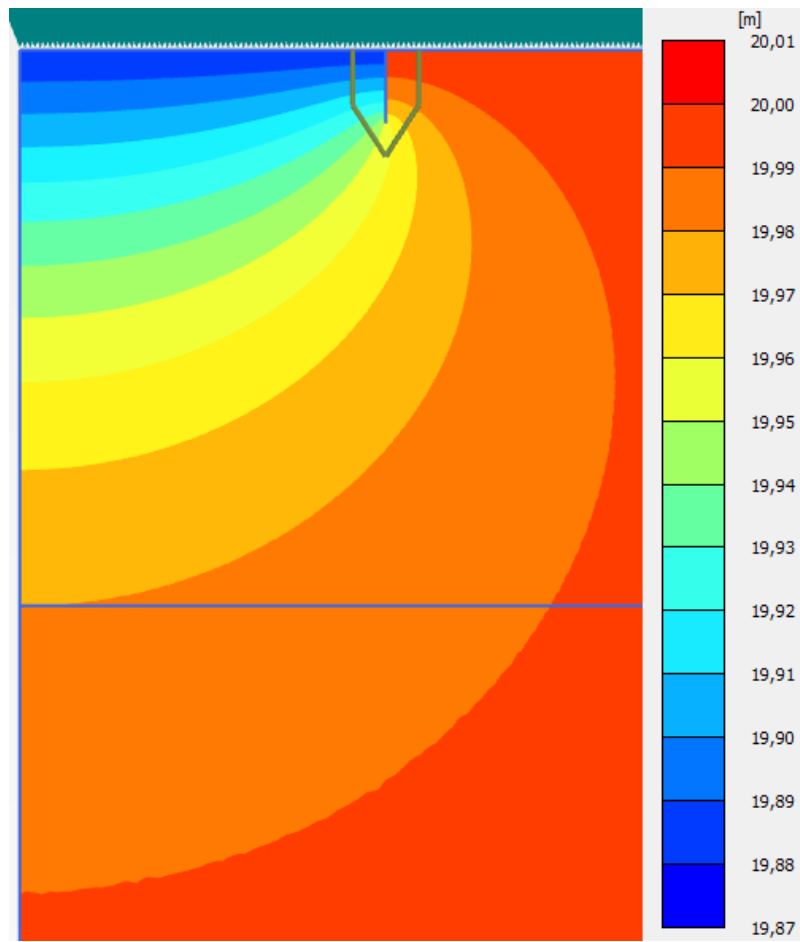


Figure C.31: Groundwater head for applied suction for a penetration length of 0.1 m.

The groundwater head for applied suction for a penetration length of 0.5 m when the bucket is completed installed is shown in Figure C.32.

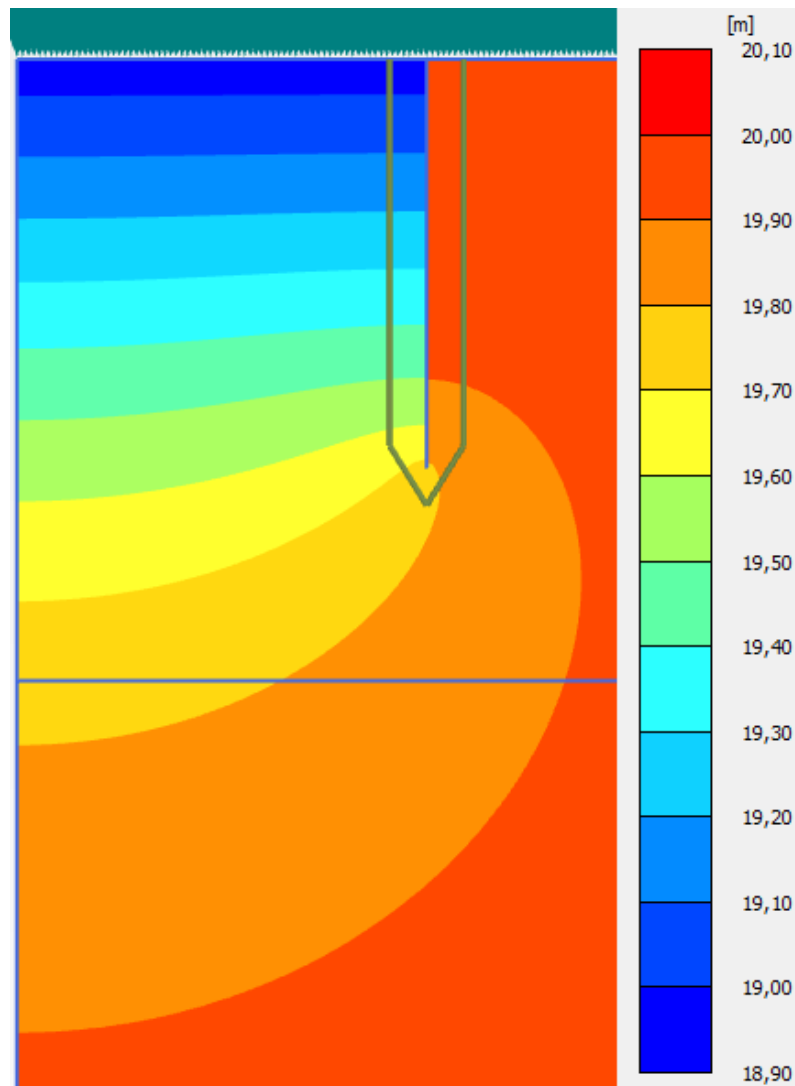


Figure C.32: Groundwater head for applied suction for a penetration length of 0.5 m.

The following table shows the values of v_{exit} , i_{exit} , s_{exit} , and $p_{critical}$:

Step	Penetration Length	v_{exit}	i_{exit}	s_{exit}	$p_{critical}$
1	0.1 m	3.720 m/day	0.521 –	2.310 m	2.310 kPa
2	0.2 m	7.249 m/day	1.017 –	1.935 m	3.870 kPa
3	0.3 m	9.445 m/day	1.325 –	1.772 m	5.316 kPa
4	0.4 m	7.254 m/day	1.017 –	1.882 m	7.529 kPa
5	0.5 m	9.930 m/day	1.393 –	1.675 m	8.377 kPa

Table C.11: Values of the variables for each penetration length.

In the following table the values of α are shown:

Step	Penetration Length	Δu_{tip}	α
1	0.1 m	0.470 kPa	0.390 –
2	0.2 m	1.321 kPa	0.335 –
3	0.3 m	1.992 kPa	0.282 –
4	0.4 m	1.654 kPa	0.215 –
5	0.5 m	2.375 kPa	0.203 –

Table C.12: Values of the variables for each penetration length.

In figure C.33 the pore pressure factor, α , is presented. The values from Plaxis are compared with the values extracted from the experiment in order to investigate deviations from Houlsby and Byrne [2005] solution.

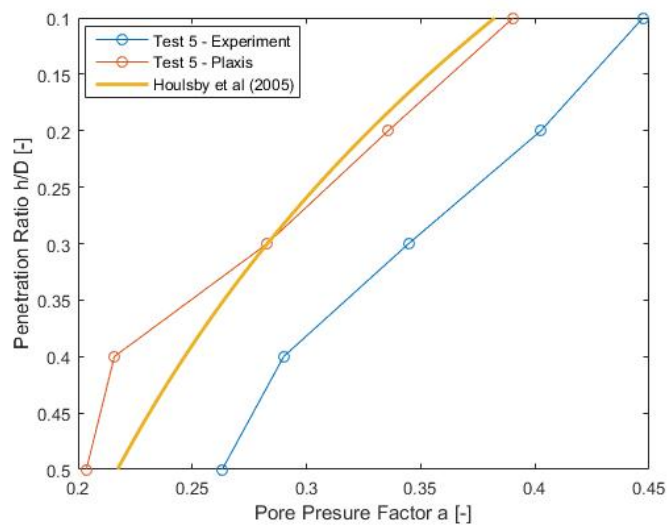


Figure C.33: Pore pressure factor results from experiments and Plaxis, along with Houlsby and Byrne [2005] solution.

The groundwater flow and the development of it is shown in the following 2 figures. The groundwater flow for a penetration length of 0.1 m is shown in Figure C.34 and for a penetration length of 0.5 m is shown in Figure C.35.

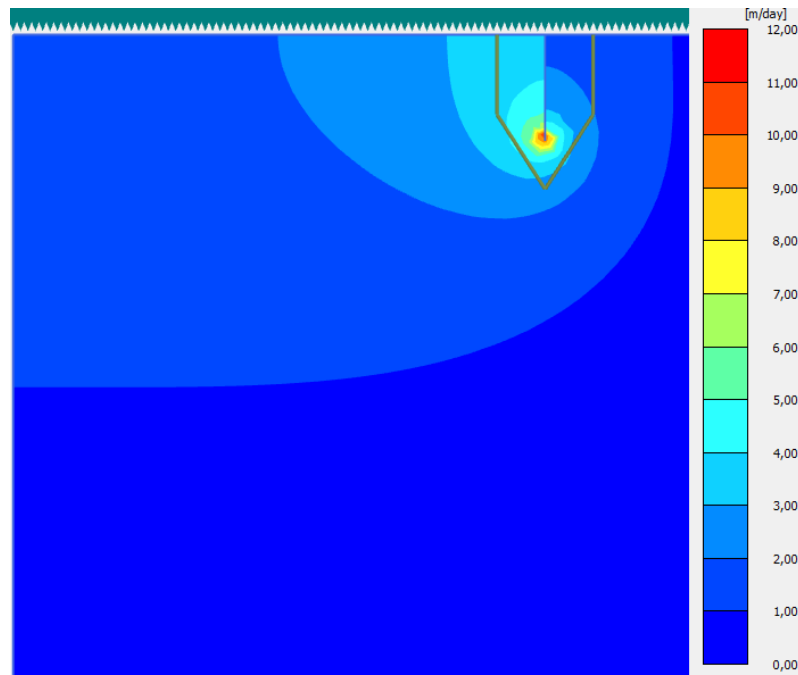


Figure C.34: Groundwater flow for a penetration length of 0.1 m.

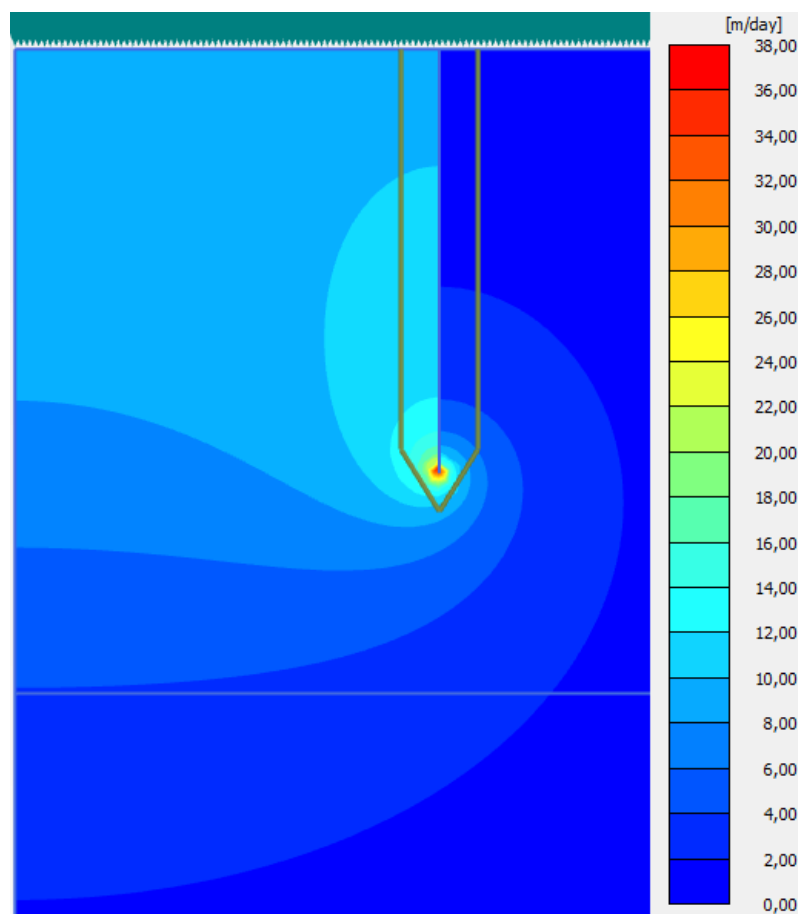


Figure C.35: Groundwater flow for a penetration length of 0.5 m.

Figure C.36 presents results from the numerical calculations for the normalized seepage length for the exit, using the exit hydraulic gradient with respect to the fitted solutions from equations 4.10 and 4.11. The seepage length exit for the experiment was not possible to calculate since the exit velocity was not measured.

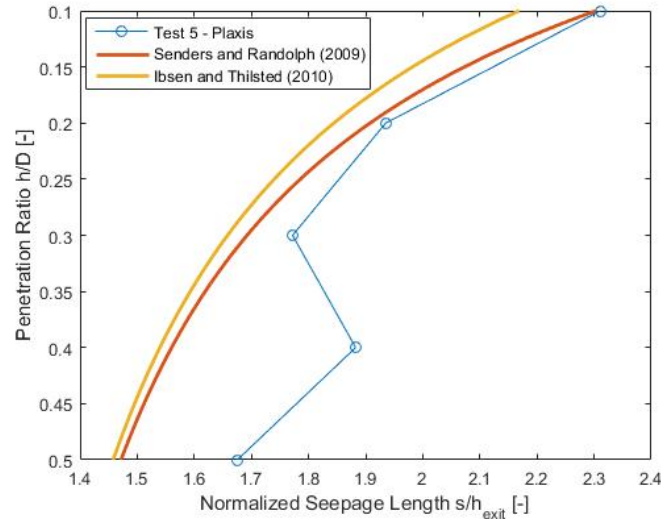


Figure C.36: Normalized seepage length results for the exit hydraulic gradient, compared to the solutions from Ibsen and Thilsted [2010], equation 4.11 and from Senders and Randolph [2009], equation 4.10.

Results for seepage length calculated from the average hydraulic gradient outside are presented in figure C.37.

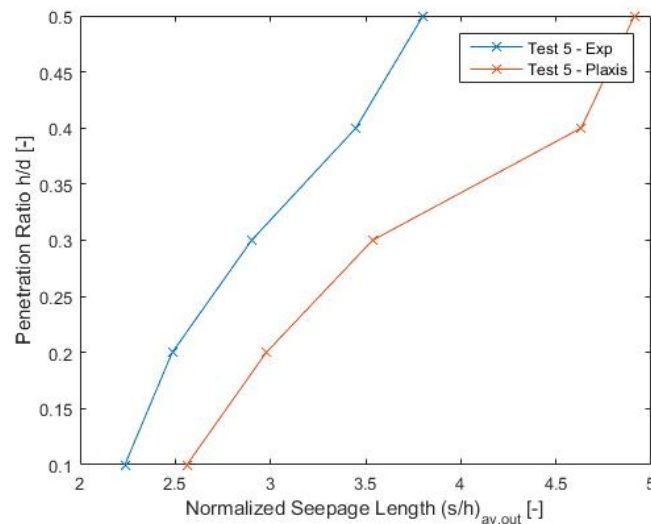


Figure C.37: Normalized seepage length results using the average outside hydraulic gradient.

Results for seepage length calculated from the average hydraulic gradient inside are presented in figure C.38.

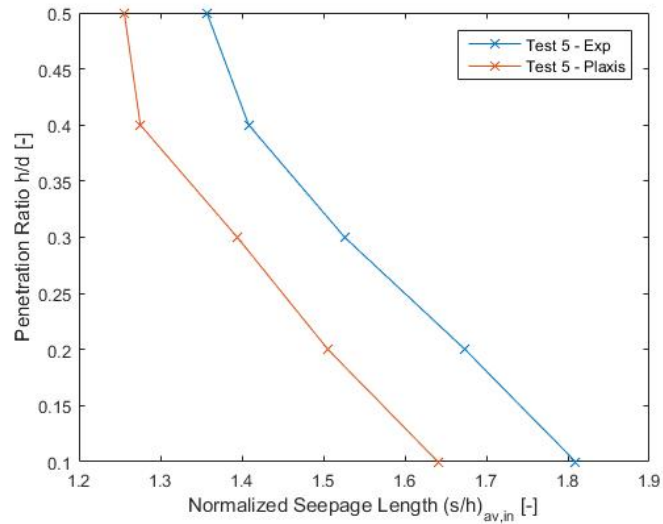


Figure C.38: Normalized seepage length results using the average inside hydraulic gradient.

Results for seepage length calculated from the tip hydraulic gradient are presented in figure C.39.

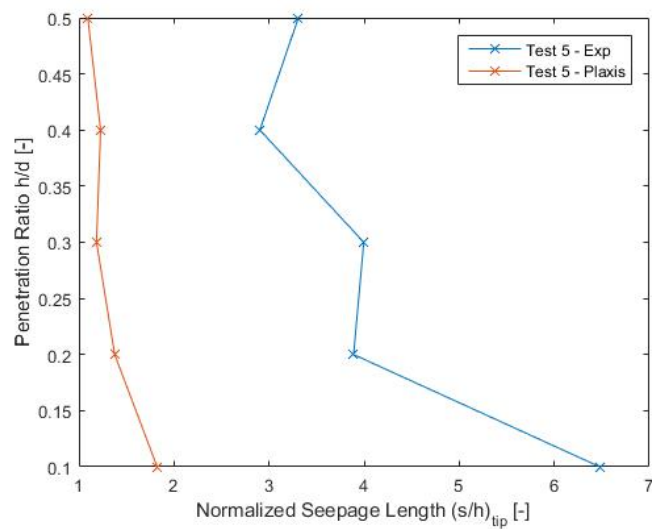


Figure C.39: Normalized seepage length results using the tip hydraulic gradient.

In the following figure, results by Feld [2001], Houlsby and Byrne [2005], Senders and Randolph [2009] and Ibsen and Thilsted [2010] are presented and compared with the numerical model for the normalized critical pressures.

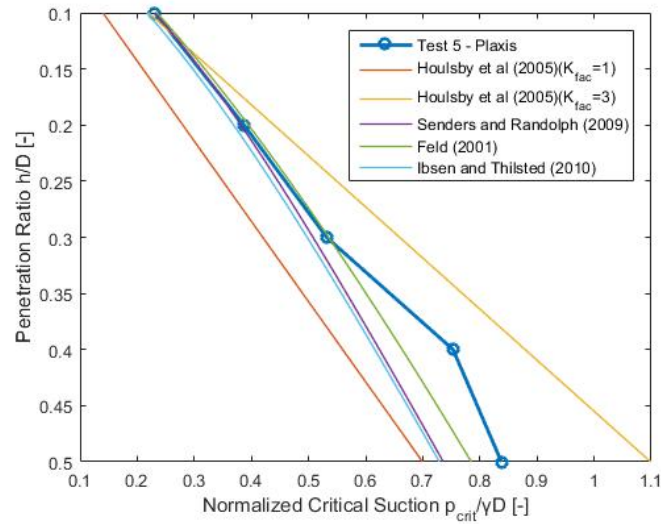


Figure C.40: Normalized critical pressures calculated in Plaxis, in comparison to solution proposed by Feld [2001], Houlsby and Byrne [2005], Senders and Randolph [2009], and Ibsen and Thilsted [2010].

C.1.5 Test Number 9-Installation "Pure Suction"

The following table shows the suction applied and its corresponding hydraulic head for each step of the installation:

Step	Penetration Length	Suction	Hydraulic Head
1	0.1 m	1.552 kPa	19.85 m
2	0.2 m	4.491 kPa	19.55 m
3	0.3 m	7.231 kPa	19.28 m
4	0.4 m	8.891 kPa	19.12 m
5	0.5 m	11.490 kPa	18.85 m

Table C.13: Suction and hydraulic head used in each step of the installation.

The groundwater head for applied suction for a penetration length of 0.1 m is shown in Figure C.41.

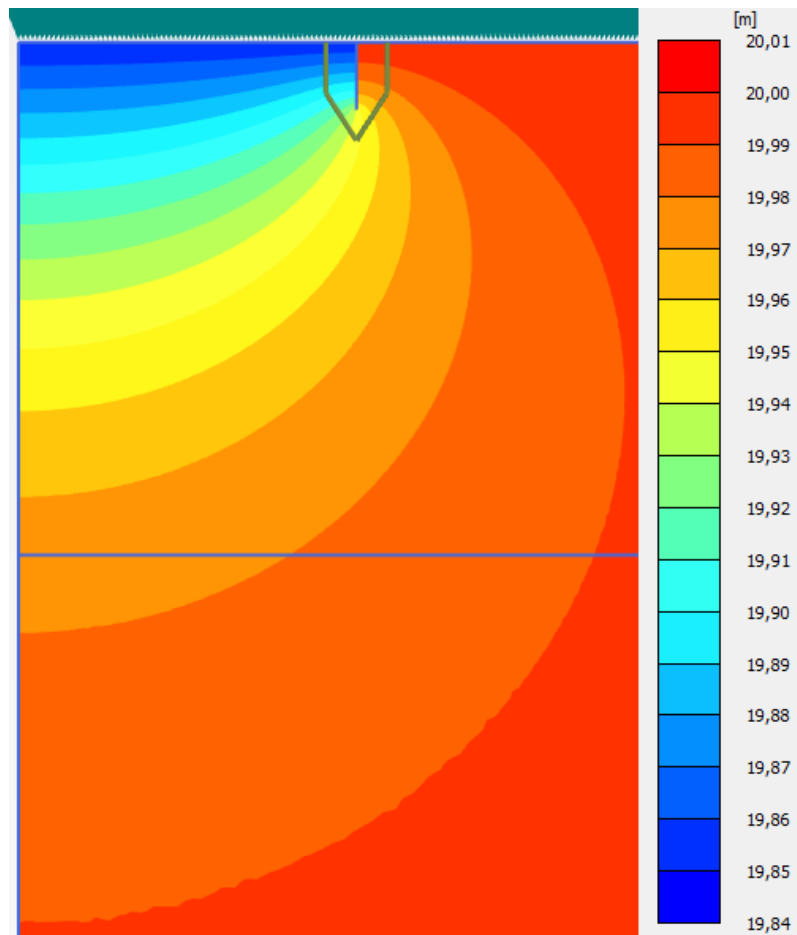


Figure C.41: Groundwater head for applied suction for a penetration length of 0.1 m.

The groundwater head for applied suction for a penetration length of 0.5 m when the bucket is completed installed is shown in Figure C.42.

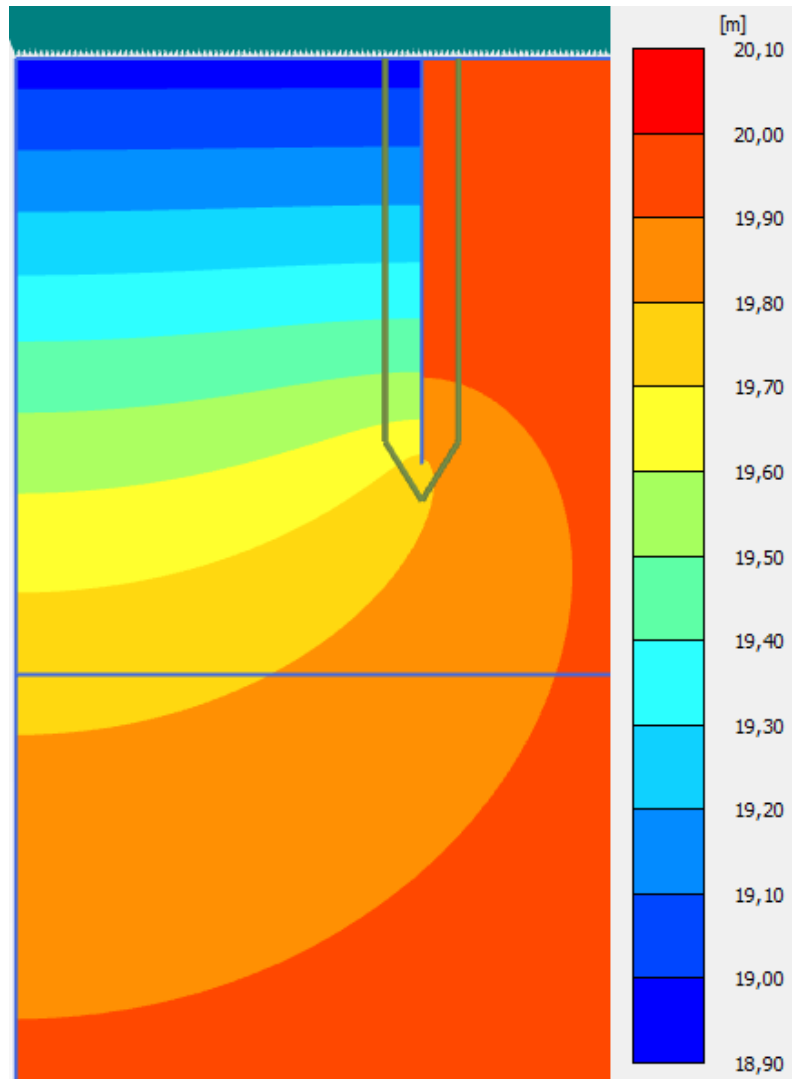


Figure C.42: Groundwater head for applied suction for a penetration length of 0.5 m.

The following table shows the values of v_{exit} , i_{exit} , s_{exit} , and $p_{critical}$:

Step	Penetration Length	v_{exit}	i_{exit}	s_{exit}	$p_{critical}$
1	0.1 m	4.650 m/day	0.652 –	2.379 m	2.379 kPa
2	0.2 m	8.155 m/day	0.762 –	1.962 m	3.925 kPa
3	0.3 m	9.850 m/day	1.381 –	1.744 m	5.232 kPa
4	0.4 m	9.782 m/day	1.372 –	1.619 m	6.478 kPa
5	0.5 m	9.837 m/day	1.380 –	1.665 m	8.325 kPa

Table C.14: Values of the variables for each penetration length.

In the following table the values of α are shown:

Step	Penetration Length	Δu_{tip}	α
1	0.1 m	0.588 kPa	0.379 –
2	0.2 m	1.321 kPa	0.294 –
3	0.3 m	2.077 kPa	0.287 –
4	0.4 m	2.231 kPa	0.250 –
5	0.5 m	2.353 kPa	0.204 –

Table C.15: Values of the variables for each penetration length.

In figure C.43 the pore pressure factor, α , is presented. The values from Plaxis are compared with the values extracted from the experiment in order to investigate deviations from Housby and Byrne [2005] solution.

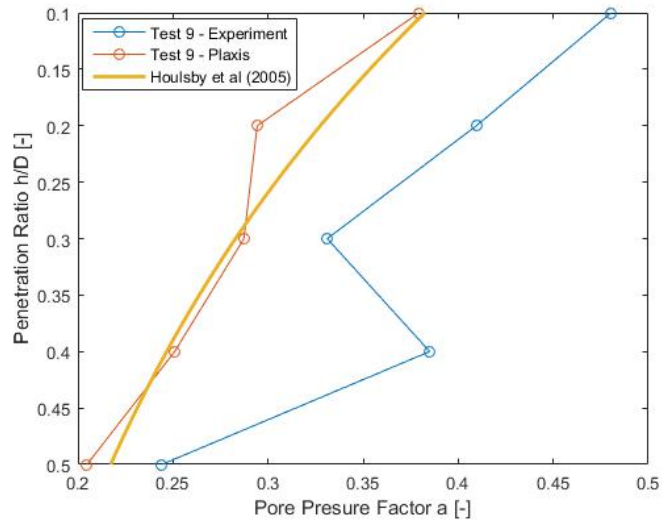


Figure C.43: Pore pressure factor results from experiments and Plaxis, along with Housby and Byrne [2005] solution.

The groundwater flow and the development of it is shown in the following 2 figures. The groundwater flow for a penetration length of 0.1 m is shown in Figure C.44 and for a penetration length of 0.5 m is shown in Figure C.45.

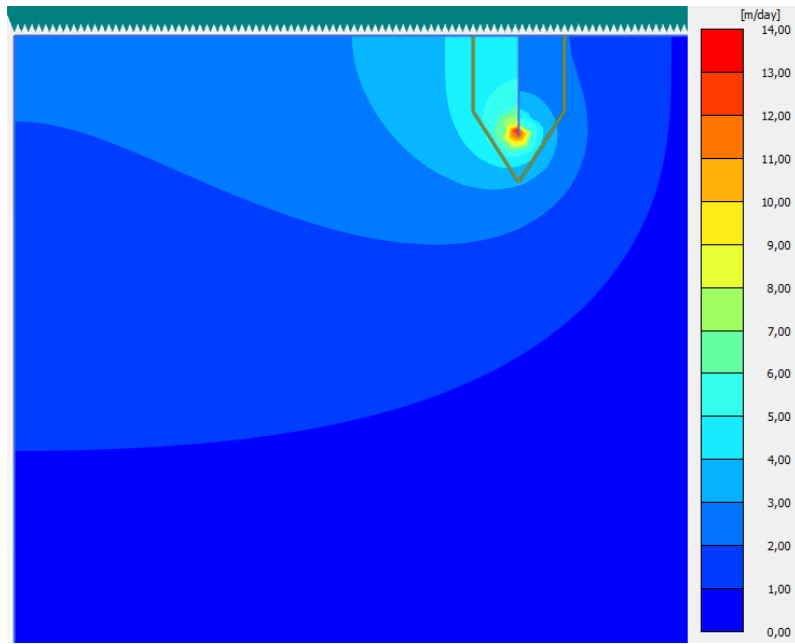


Figure C.44: Groundwater flow for a penetration length of 0.1 m.

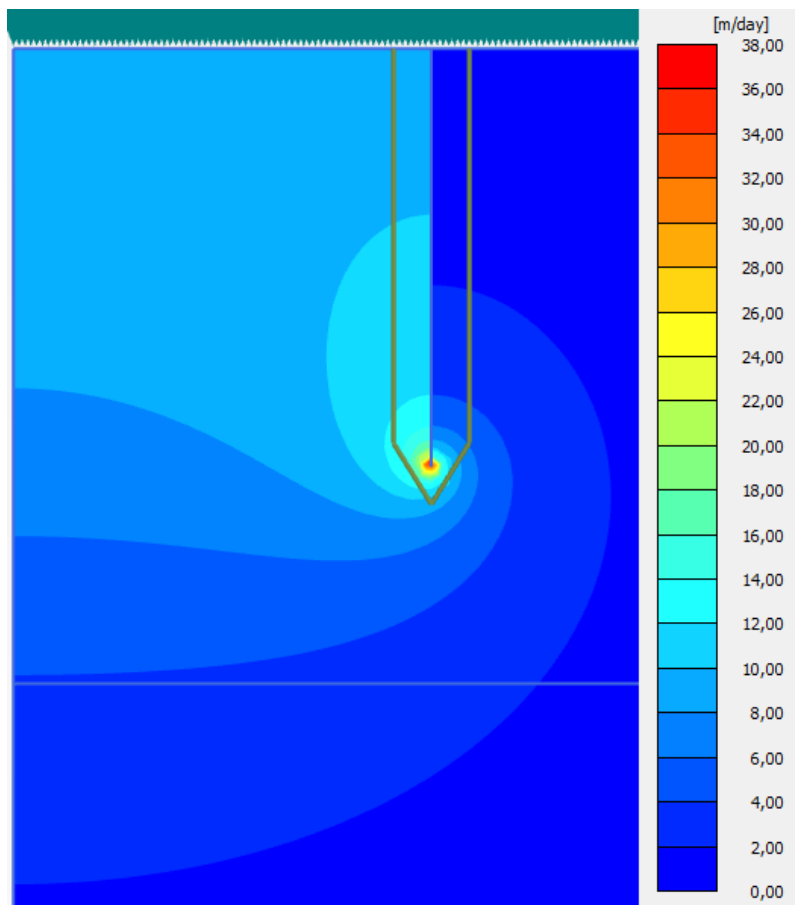


Figure C.45: Groundwater flow for a penetration length of 0.5 m.

Figure C.46 presents results from the numerical calculations for the normalized seepage

length for the exit, using the exit hydraulic gradient with respect to the fitted solutions from equations 4.10 and 4.11. The seepage length exit for the experiment was not possible to calculate since the exit velocity was not measured.

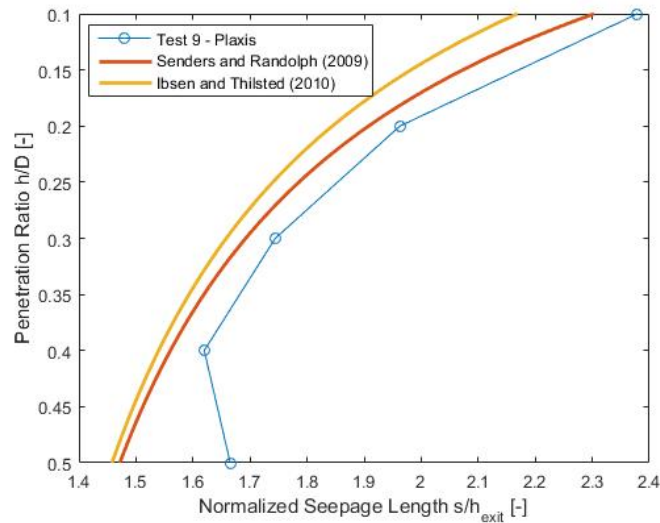


Figure C.46: Normalized seepage length results for the exit hydraulic gradient, compared to the solutions from Ibsen and Thilsted [2010], equation 4.11 and from Senders and Randolph [2009], equation 4.10.

Results for seepage length calculated from the average hydraulic gradient outside are presented in figure C.47.

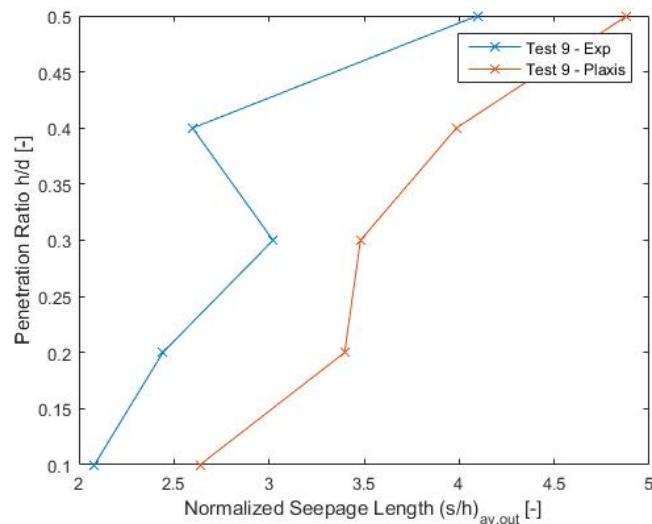


Figure C.47: Normalized seepage length results using the average outside hydraulic gradient.

Results for seepage length calculated from the average hydraulic gradient inside are presented in figure C.48.

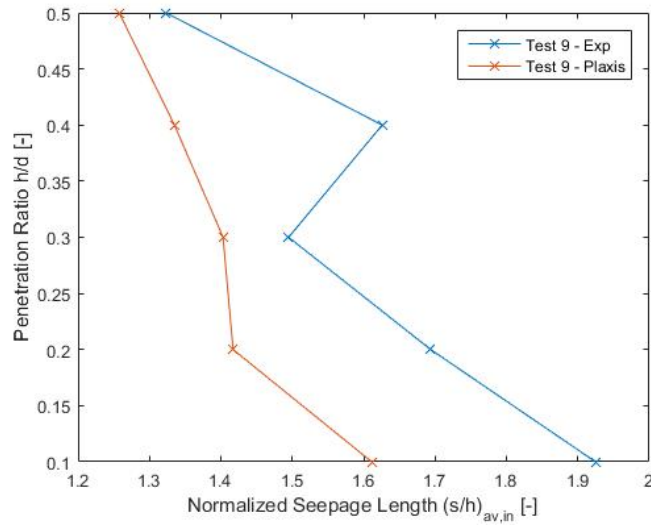


Figure C.48: Normalized seepage length results using the average inside hydraulic gradient.

Results for seepage length calculated from the tip hydraulic gradient are presented in figure C.49.

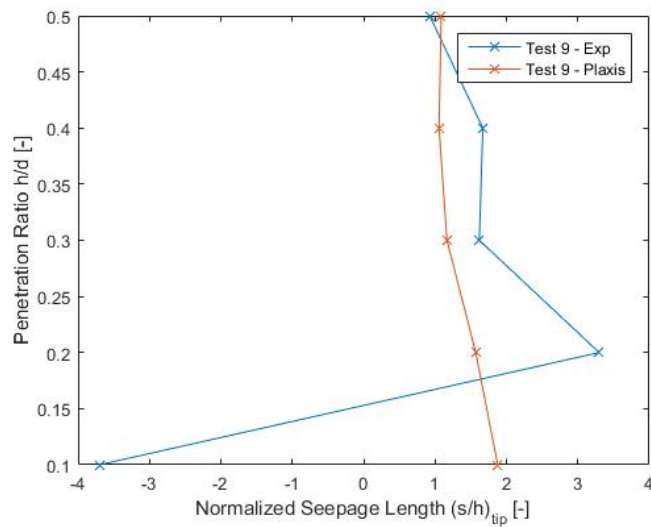


Figure C.49: Normalized seepage length results using the tip hydraulic gradient.

In the following figure, results by Feld [2001], Houlsby and Byrne [2005], Senders and Randolph [2009] and Ibsen and Thilsted [2010] are presented and compared with the numerical model for the normalized critical pressures.

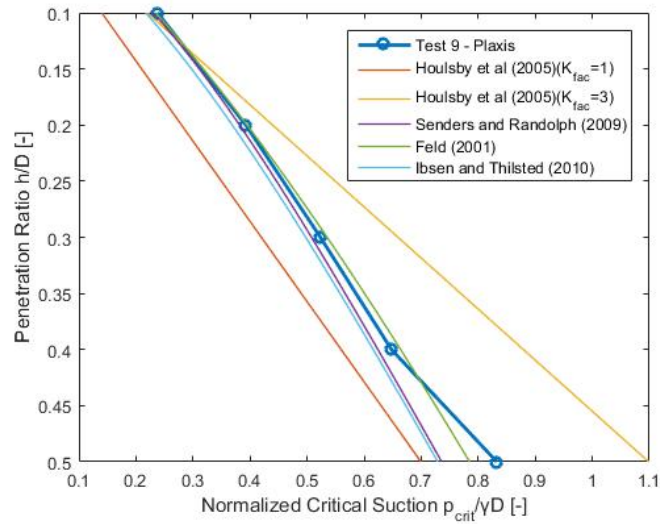


Figure C.50: Normalized critical pressures calculated in Plaxis, in comparison to solution proposed by Feld [2001], Houlsby and Byrne [2005], Senders and Randolph [2009], and Ibsen and Thilsted [2010].

C.2 Uninstallation Test

Results from experiments 5, 6, and 8 are shown in this section. The detailed procedure explained in chapter 4 is based in test number 4.

C.2.1 Test Number 5-Uninstallation with 201 kg

The following table shows the pressure applied and its corresponding hydraulic head for each step of the uninstillation:

Step	Penetration Length	Pressure	Hydraulic Head
1	0.5 m	12.500 kPa	18.75 m
2	0.4 m	7.776 kPa	19.25 m
3	0.3 m	6.152 kPa	19.39 m
4	0.2 m	5.508 kPa	19.45 m

Table C.16: Pressure and hydraulic head used in each step of the uninstillation.

The groundwater head for applied pressure for a penetration length of 0.5 m is shown in Figure C.51.

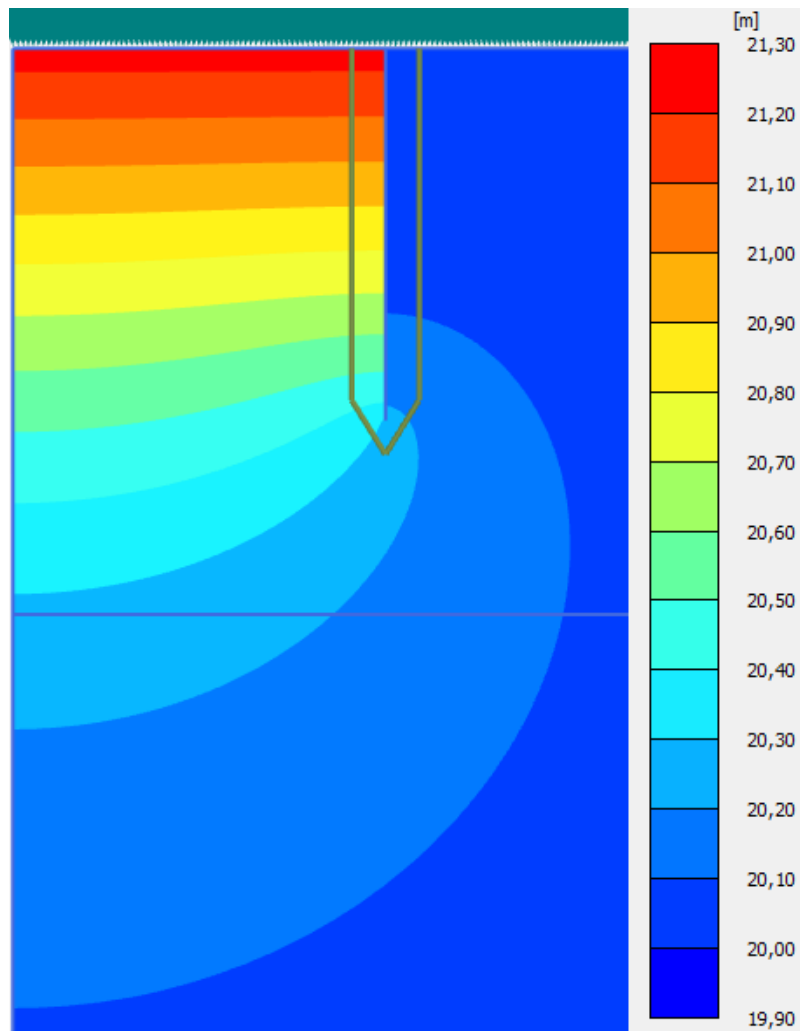


Figure C.51: Groundwater head for applied pressure for a penetration length of 0.5 m.

The groundwater head for applied pressure for a penetration length of 0.2 m when the bucket is uninstalled is shown in Figure C.52.

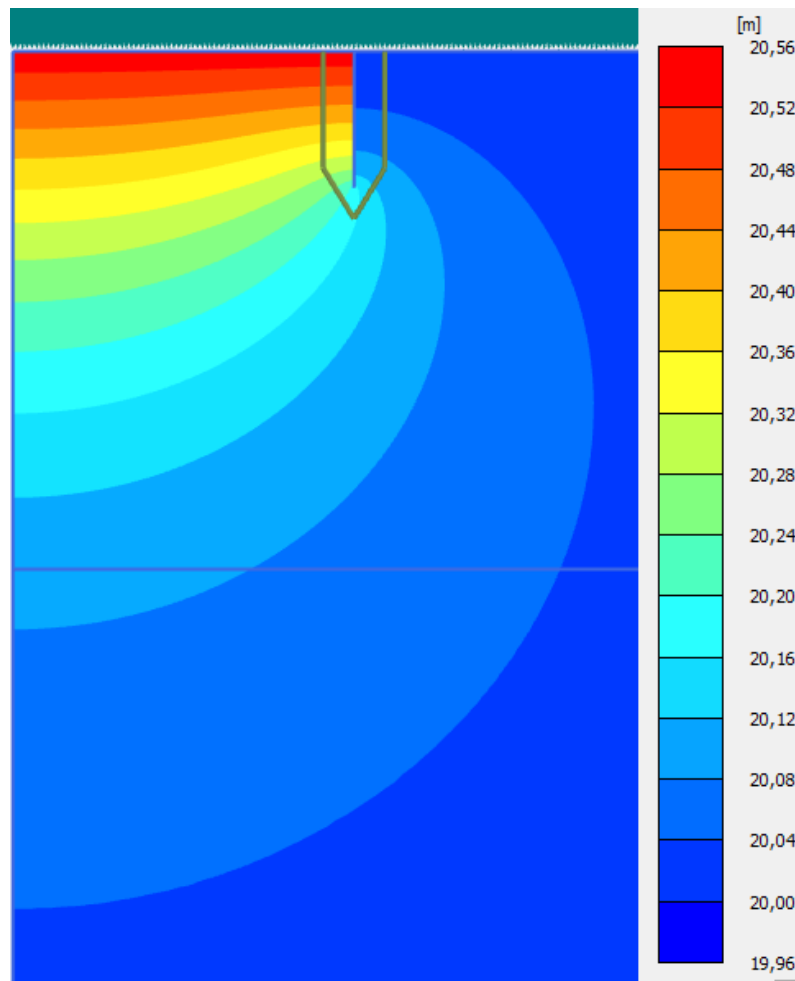


Figure C.52: Groundwater head for applied pressure for a penetration length of 0.2 m.

The groundwater flow and the development of it are shown in the following 2 figures. The groundwater flow for a penetration length of 0.5 m is shown in Figure C.53 and for a penetration length of 0.2 m is shown in Figure C.54.

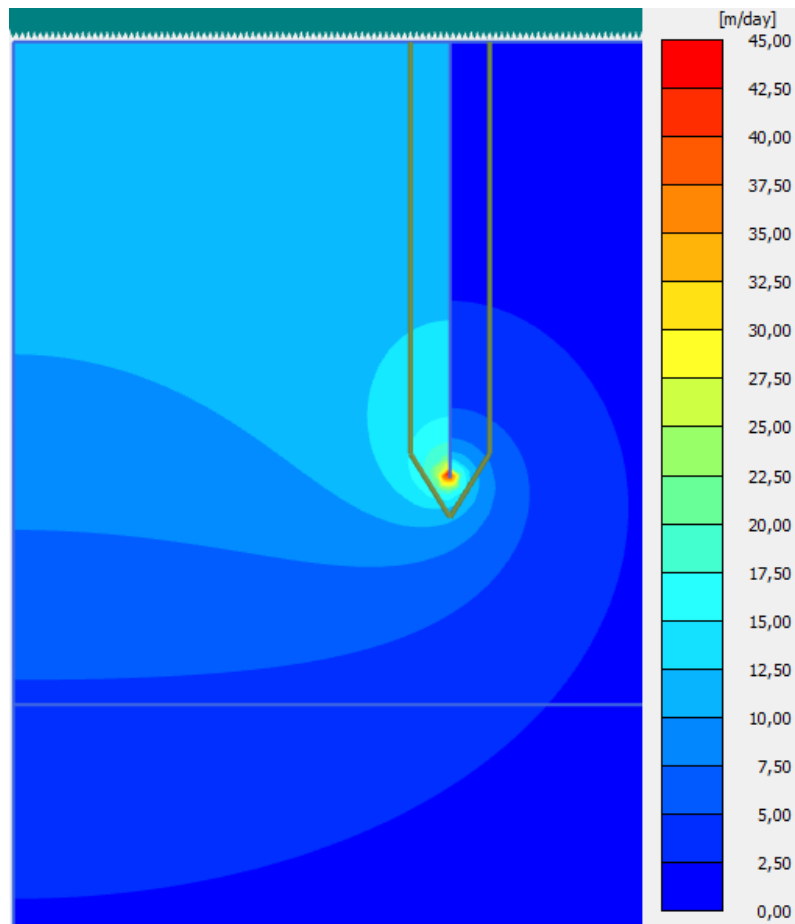


Figure C.53: Groundwater flow for a penetration length of 0.5 m.

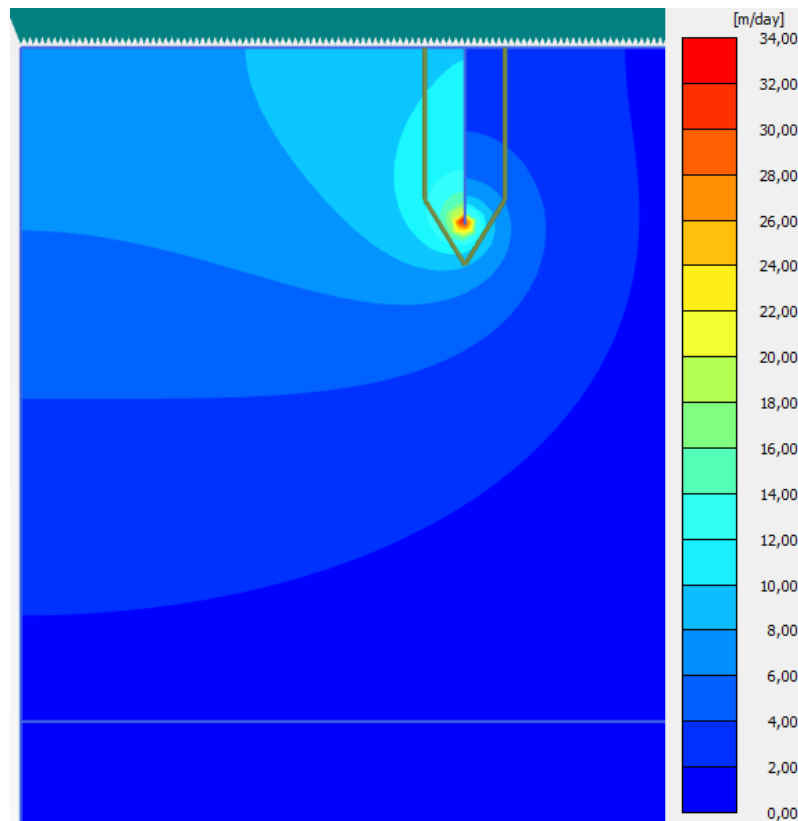


Figure C.54: Groundwater flow for a penetration length of 0.2 m.

Furthermore, Figure C.55 shows the pore pressure factor obtained from the uninstallation procedure for Plaxis, compared to Houlsby and Byrne [2005] solution.

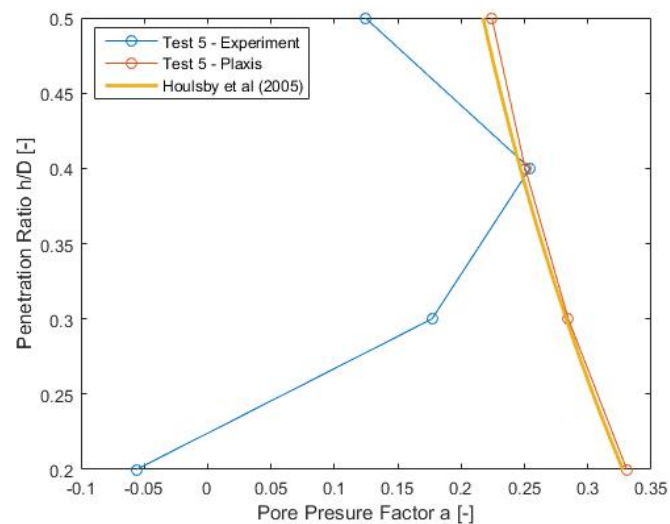


Figure C.55: Pore pressure factor results from uninstallation in Plaxis and results from the experiment, along with Houlsby and Byrne [2005] solution.

Figures C.56 and C.57 illustrate the normalized seepage length during uninstallation for the average hydraulic gradient inside and at the tip, respectively.

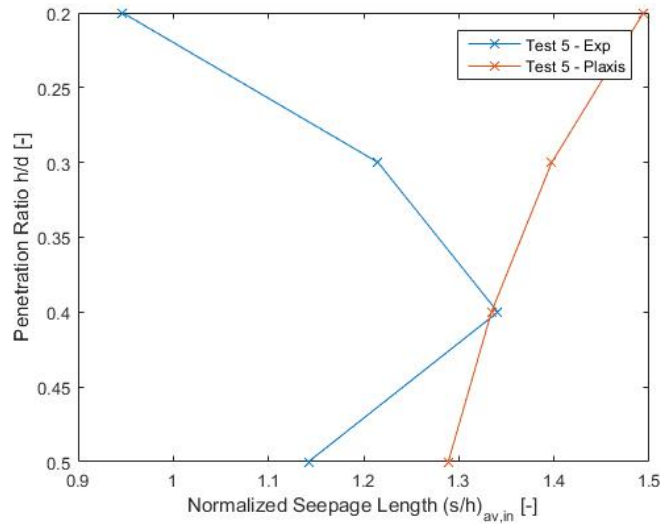


Figure C.56: Normalized seepage length, using the average inside hydraulic gradient.

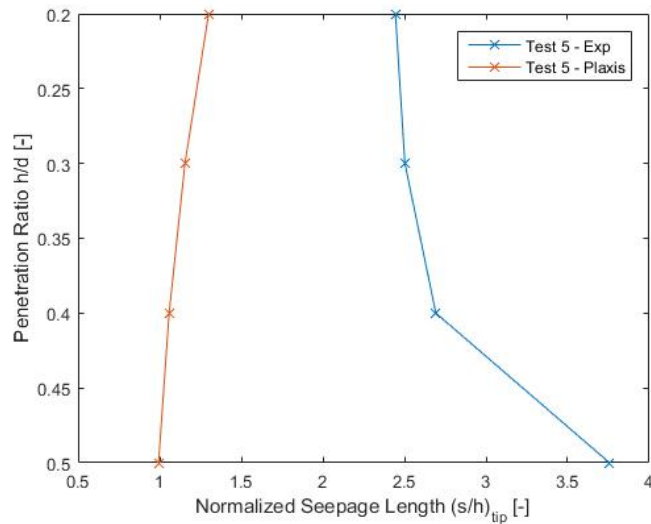


Figure C.57: Normalized seepage length, using the average tip hydraulic gradient.

Finally, as far as the pressure applied for the uninstillation is concerned, Figure C.58 shown it.

C.2.2 Test Number 6-Uninstillation with 402 kg

The following table shows the pressure applied and its corresponding hydraulic head for each step of the uninstillation:

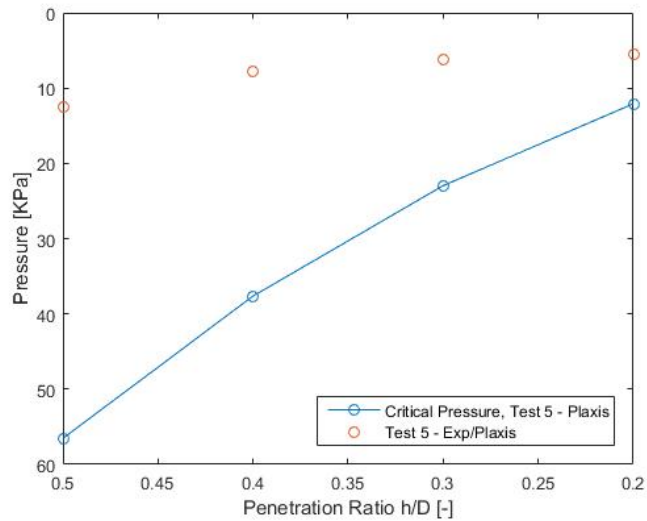


Figure C.58: Critical suction from numerical simulation compared to the real pressure applied.

Step	Penetration Length	Pressure	Hydraulic Head
1	0.5 m	19.55 kPa	18.05 m
2	0.4 m	11.49 kPa	18.85 m
3	0.3 m	9.383 kPa	19.07 m
4	0.2 m	8.039 kPa	19.20 m

Table C.17: Pressure and hydraulic head used in each step of the uninstallation.

The groundwater head for applied pressure for a penetration length of 0.5 m is shown in Figure C.59.

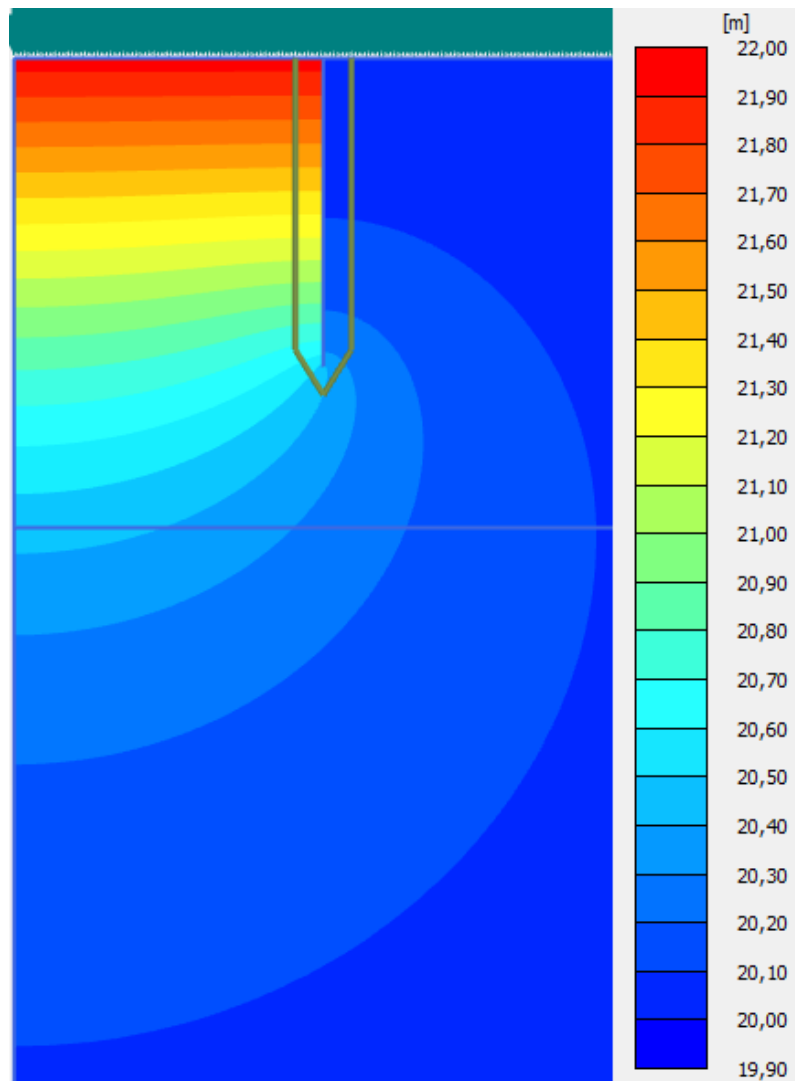


Figure C.59: Groundwater head for applied pressure for a penetration length of 0.5 m.

The groundwater head for applied pressure for a penetration length of 0.2 m when the bucket is uninstalled is shown in Figure C.60.

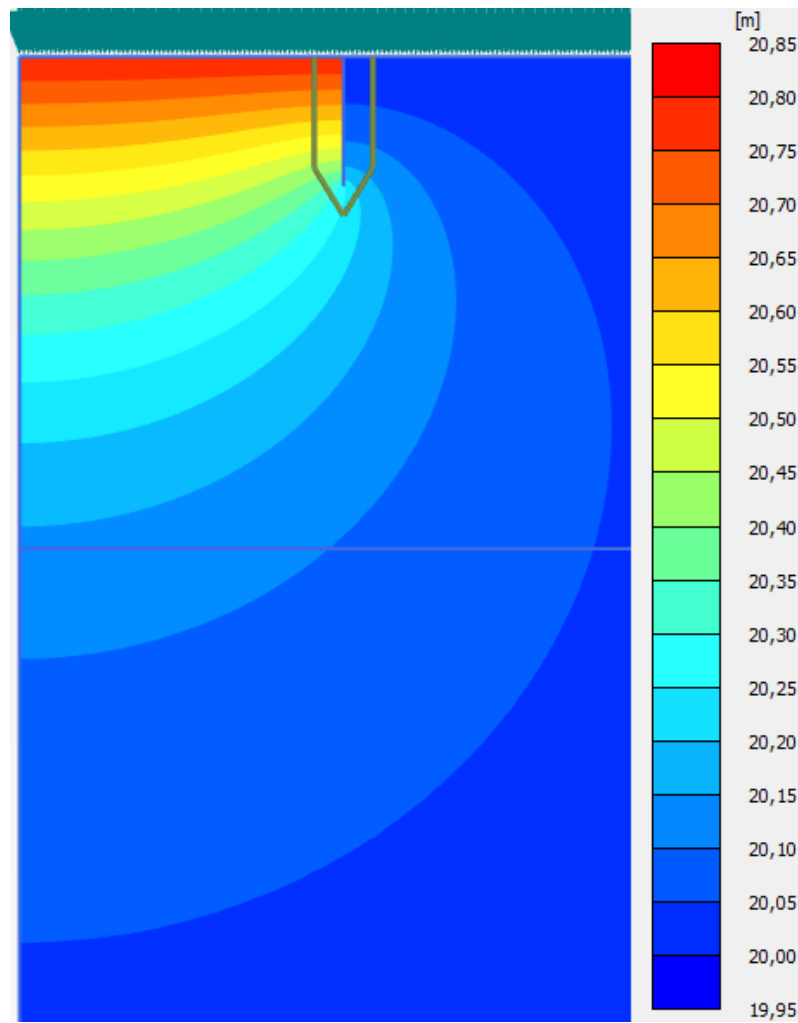


Figure C.60: Groundwater head for applied pressure for a penetration length of 0.2 m.

The groundwater flow and the development of it are shown in the following 2 figures. The groundwater flow for a penetration length of 0.5 m is shown in Figure C.61 and for a penetration length of 0.2 m is shown in Figure C.62.

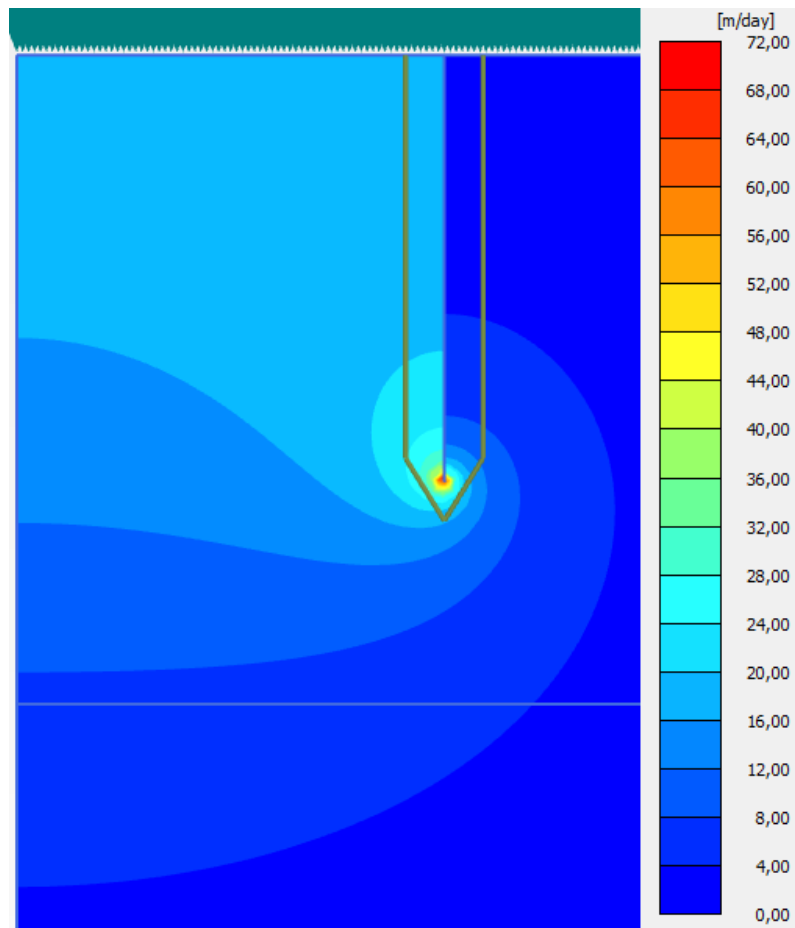


Figure C.61: Groundwater flow for a penetration length of 0.5 m.

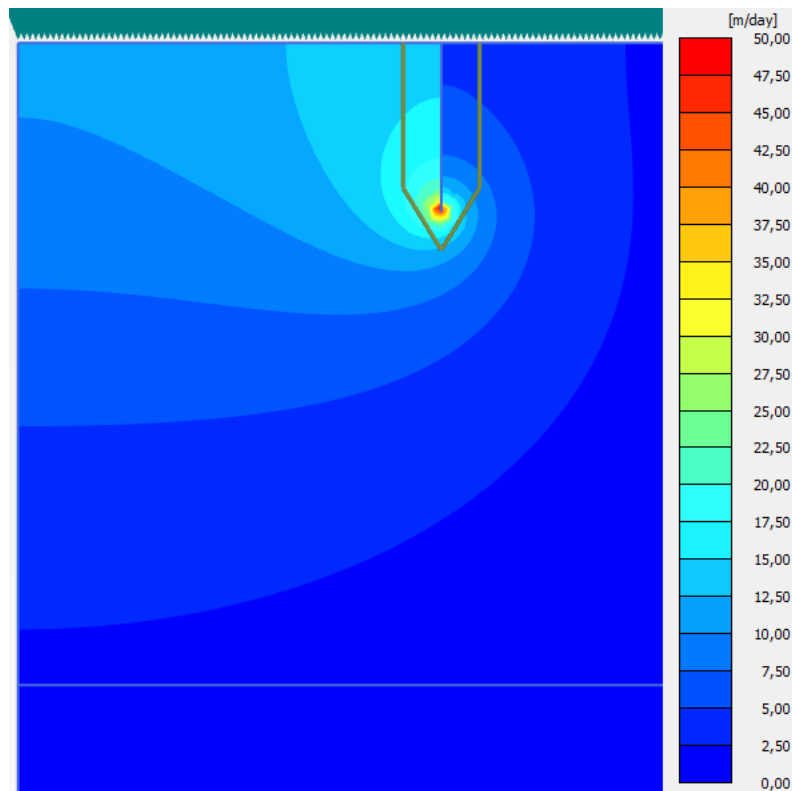


Figure C.62: Groundwater flow for a penetration length of 0.2 m.

Furthermore, Figure C.63 shows the pore pressure factor obtained from the uninstallation procedure for Plaxis, compared to Houlsby and Byrne [2005] solution.

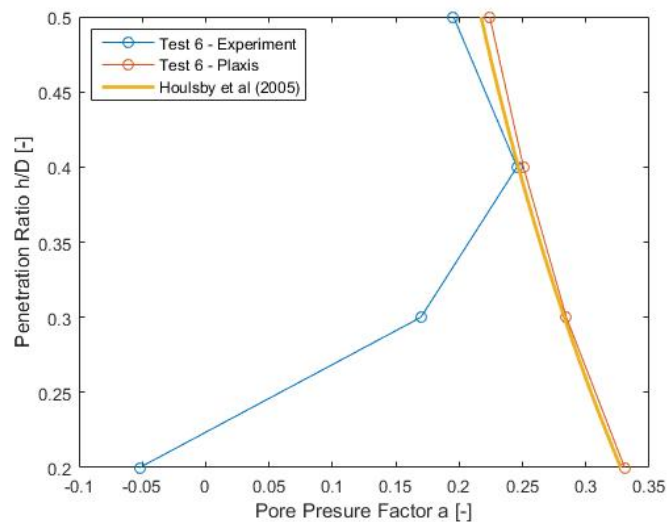


Figure C.63: Pore pressure factor results from uninstallation in Plaxis and results from the experiment, along with Houlsby and Byrne [2005] solution.

Figures C.64 and C.65 illustrate the normalized seepage length during uninstallation for the average hydraulic gradient inside and at the tip, respectively.

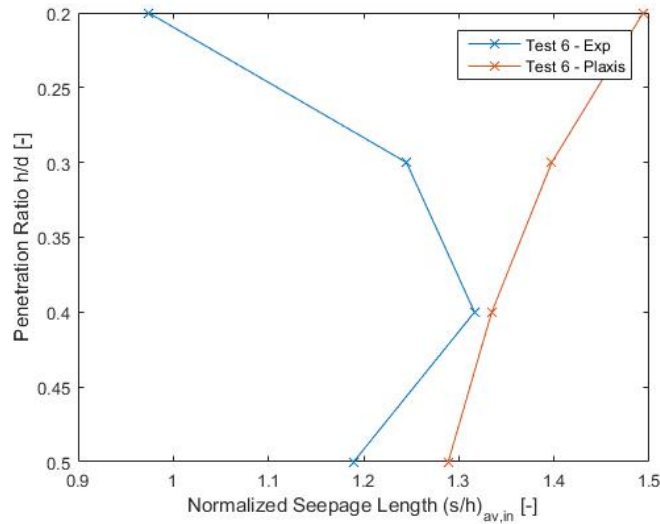


Figure C.64: Normalized seepage length, using the average inside hydraulic gradient.

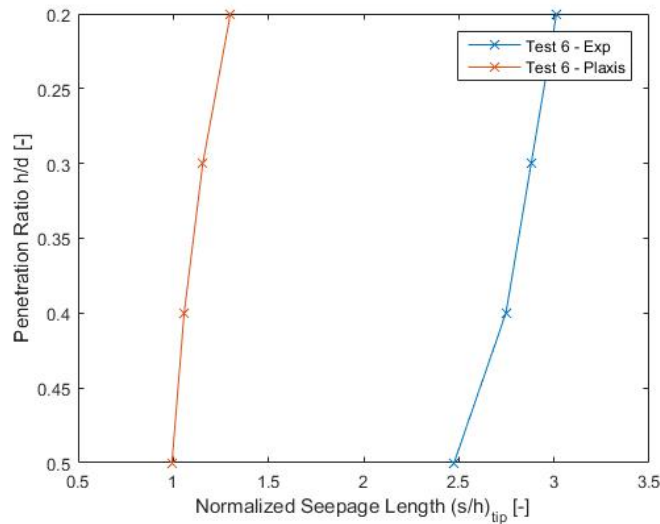


Figure C.65: Normalized seepage length, using the average tip hydraulic gradient.

Finally, as far as the pressure applied for the uninstillation is concerned, Figure C.66 shown it.

C.2.3 Test Number 8-Uninstillation with 302 kg

The following table shows the pressure applied and its corresponding hydraulic head for each step of the uninstillation:

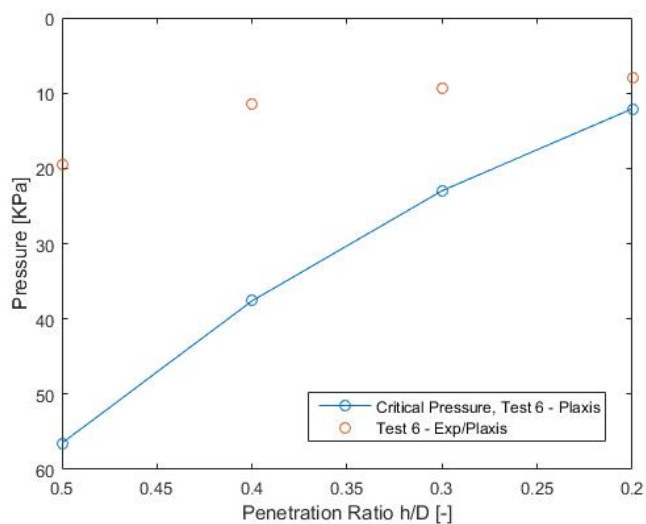


Figure C.66: Critical suction from numerical simulation compared to the real pressure applied.

Step	Penetration Length	Pressure	Hydraulic Head
1	0.5 m	16.560 kPa	18.35 m
2	0.4 m	9.529 kPa	19.05 m
3	0.3 m	7.761 kPa	19.23 m
4	0.2 m	6.455 kPa	19.35 m

Table C.18: Pressure and hydraulic head used in each step of the uninstallation.

The groundwater head for applied pressure for a penetration length of 0.5 m is shown in Figure C.67.

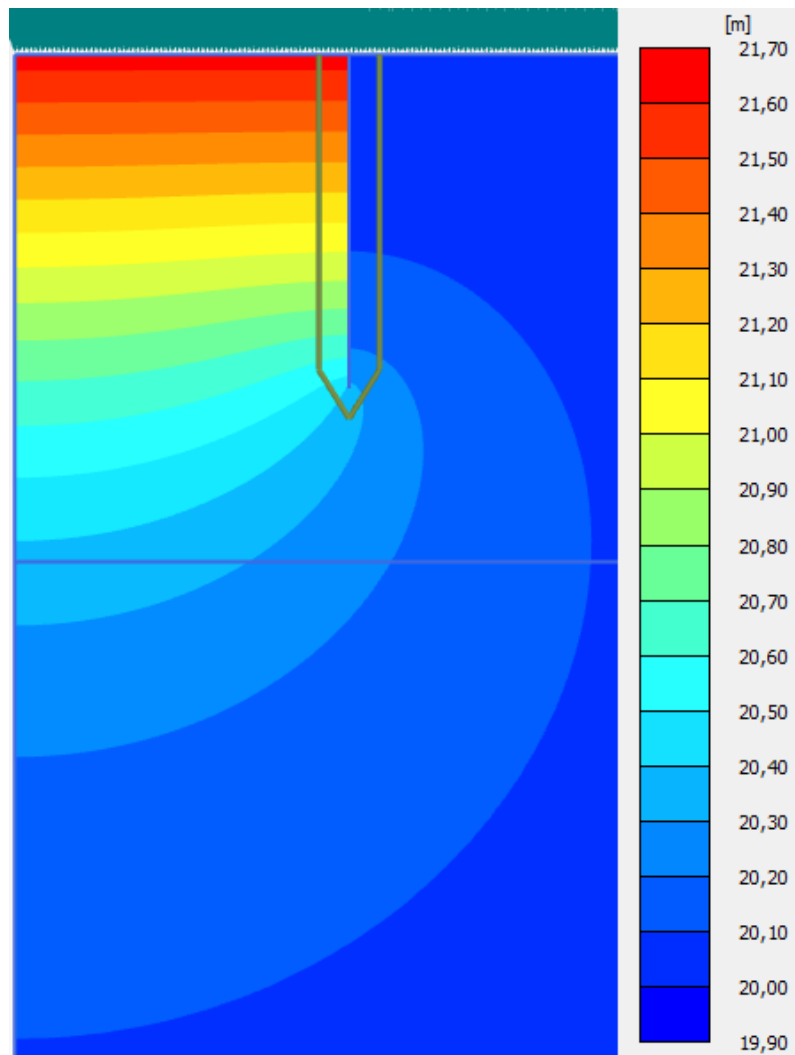


Figure C.67: Groundwater head for applied pressure for a penetration length of 0.5 m.

The groundwater head for applied pressure for a penetration length of 0.2 m when the bucket is uninstalled is shown in Figure C.68.

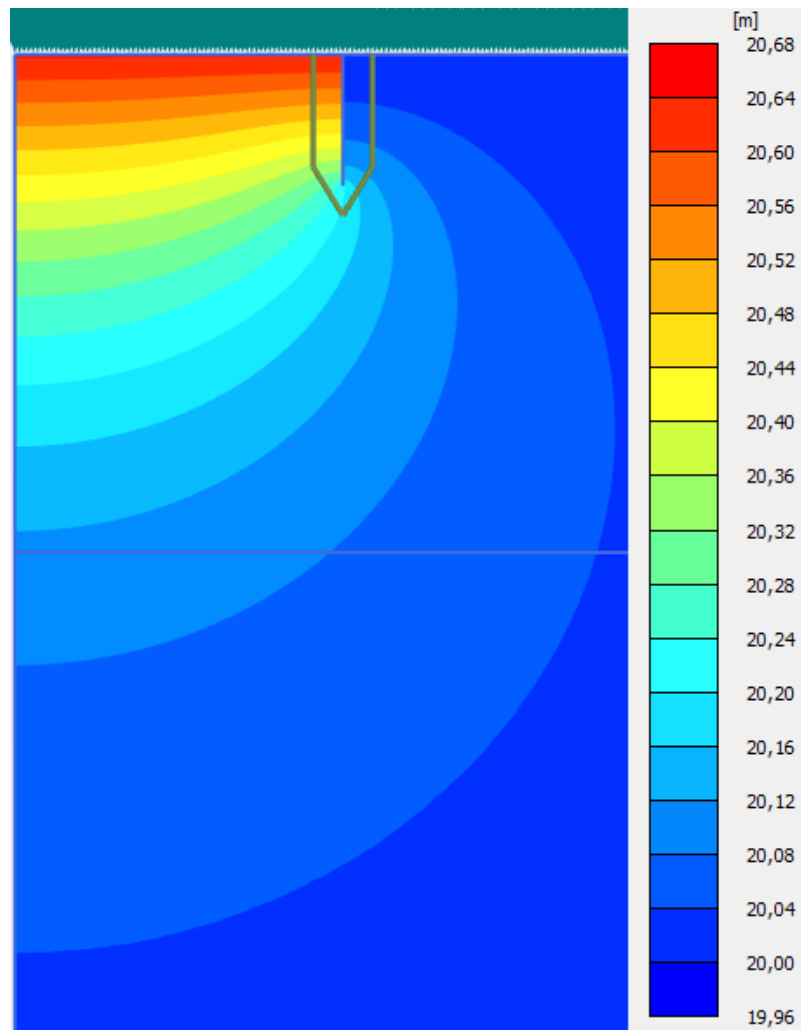


Figure C.68: Groundwater head for applied pressure for a penetration length of 0.2 m.

The groundwater flow and the development of it are shown in the following 2 figures. The groundwater flow for a penetration length of 0.5 m is shown in Figure C.69 and for a penetration length of 0.2 m is shown in Figure C.70.

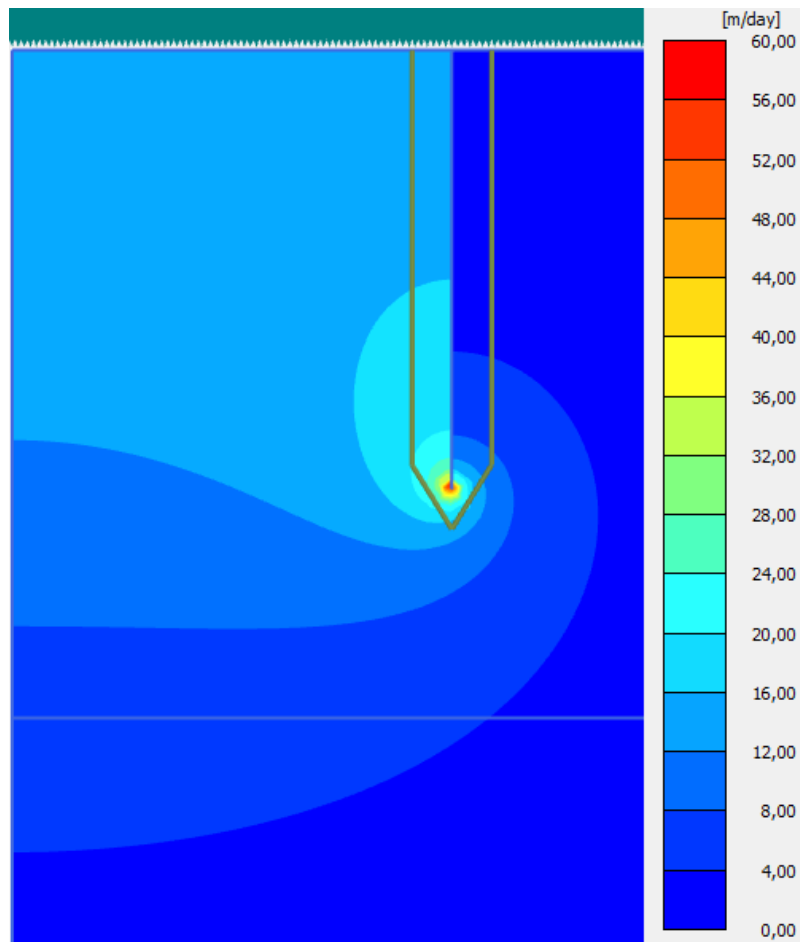


Figure C.69: Groundwater flow for a penetration length of 0.5 m.

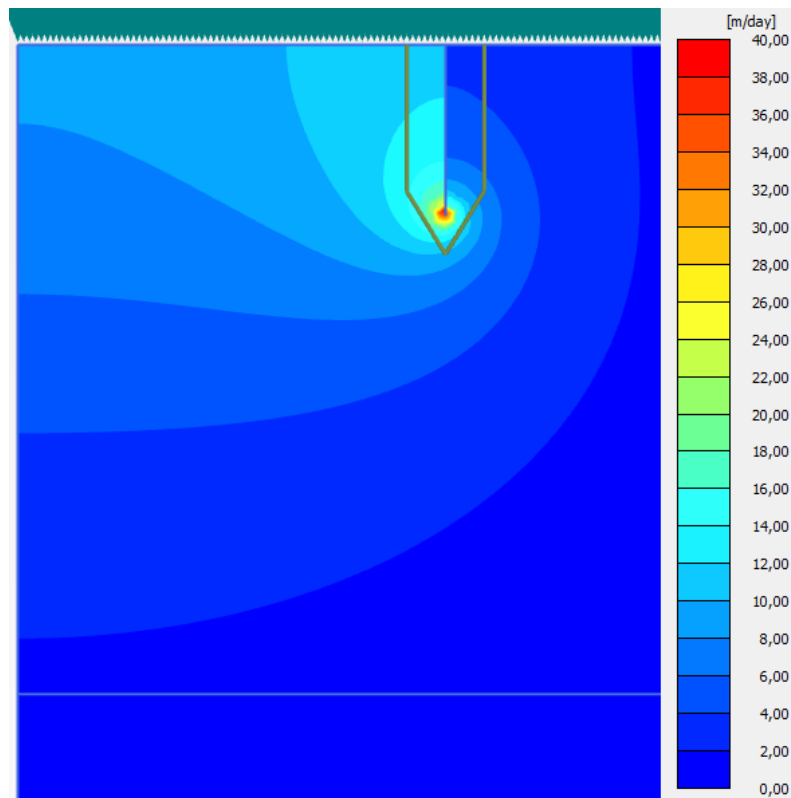


Figure C.70: Groundwater flow for a penetration length of 0.2 m.

Furthermore, Figure C.71 shows the pore pressure factor obtained from the uninstallation procedure for Plaxis, compared to Houlsby and Byrne [2005] solution.

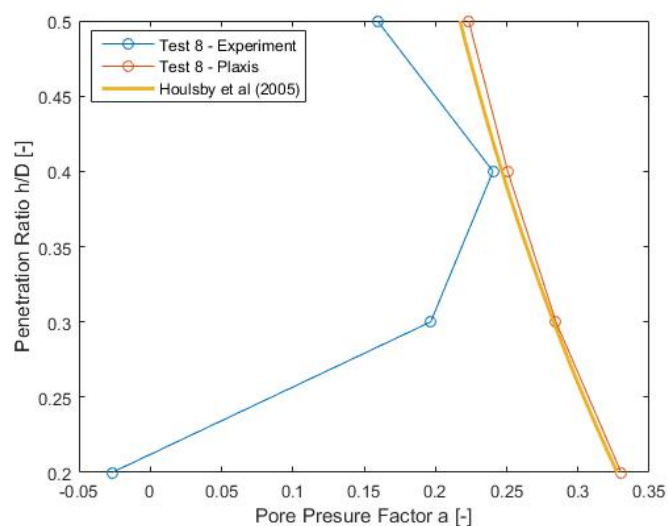


Figure C.71: Pore pressure factor results from uninstallation in Plaxis and results from the experiment, along with Houlsby and Byrne [2005] solution.

Figures C.72 and C.73 illustrate the normalized seepage length during uninstallation for the average hydraulic gradient inside and at the tip, respectively.

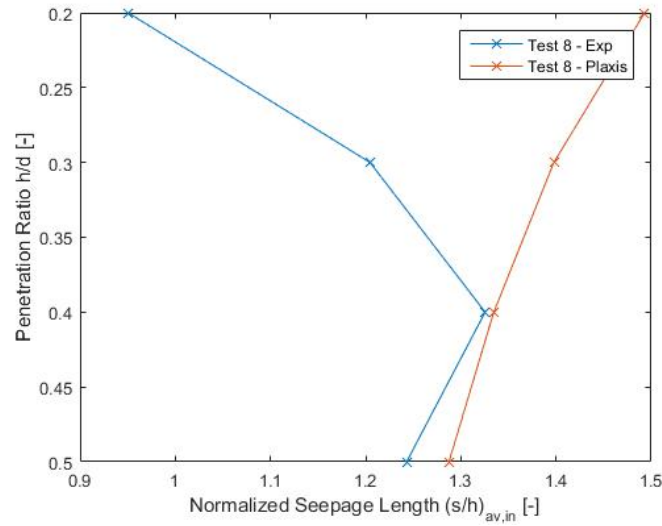


Figure C.72: Normalized seepage length, using the average inside hydraulic gradient.

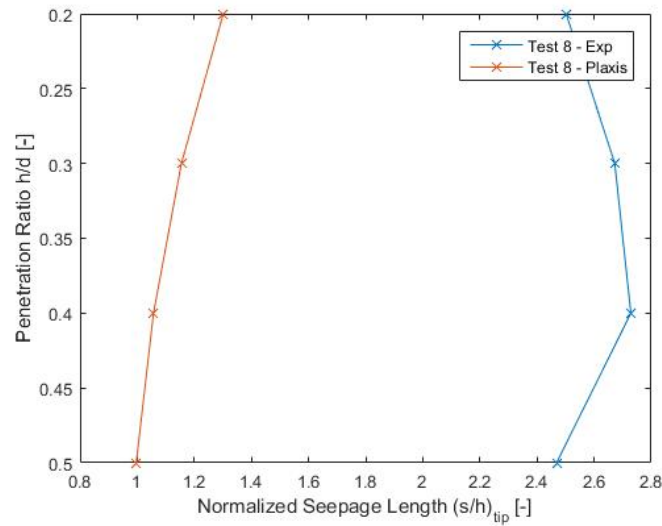


Figure C.73: Normalized seepage length, using the average tip hydraulic gradient.

Finally, as far as the pressure applied for the uninstillation is concerned, Figure C.74 shown it.

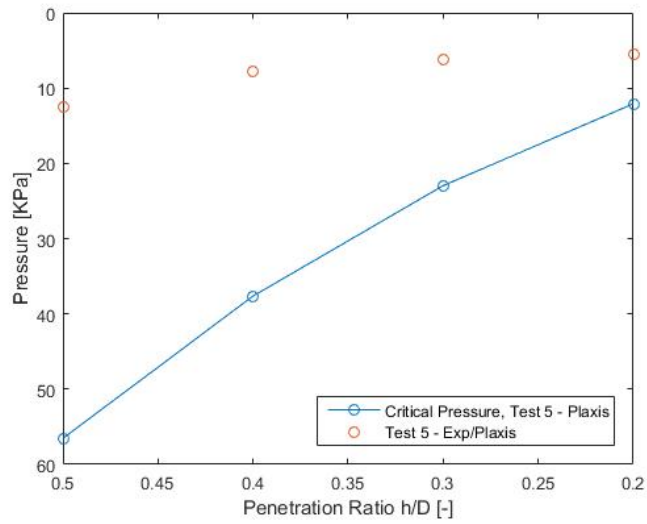


Figure C.74: Critical suction from numerical simulation compared to the real pressure applied.

ATTACHED CD

D

- A *Report* - PDF file and Latex files
- B *Bibliography* - PDF files
- C *Data acquired from the experiments* - Matlab files
- D *Numerical simulations* - PLAXIS 2D files
- E *Numerical Calculations* - Excel files
- F *Empirical coefficient calculations, from Vaitkunaite et al. [2015]* - Matlab files
- G *β factors calculations* - Matlab files